ISSN 2636-8498

Environmental Research & Technology

Year 2023
Volume 6
Number 4

YTU PRESS

www.ert.yildiz.edu.tr

ISSN 2636-8498

Environmental Research & Technology

Volume 6 Number 4 Year 2023

ISSN 2636-8498

Environmental Research & Technology

Volume 6 Number 4 Year 2023

ISSN 2636-8498

Environmental Research & Technology

Volume 6 Number 4 Year 2023

CONTENTS

Research Articles

279 **The evaluation of fibrous disposable facemask for oil sorption and efficient oil/water separation**
Soner KIZIL

288 **The influence of meteorological parameters on $PM_{2.5}$ and PM_{10} values in Ümraniye and Silivri districts of İstanbul**
Hilal ARSLAN, Ali TOLTAR

302 **Long chain fatty acid (LCFA) occurrence in primary and secondary sewage sludge fractions**
Dilek ERDİRENÇELEBİ

308 **Enhancement of the environmental bio-economy by investigating a sustainable cerbera odollam biodiesel at a low heat rejection engine**
Anbazhagan RAMANUJAM, Naveenchandran PANCHACHARAM

317 **Co-digestion potential of different industrial sludge sources and impact on energy recovery**
Melek Şebnem ÇALIŞKAN TEMEL, Çiğdem YANGIN GÖMEÇ

326 **Using chlorella vulgaris as a natural-textile dye**
Tasnim ALMOULKI, Ebru AKKAYA

332 **Optimal route selection using network analysis in terms of time, cost and fuel savings: The case of İskenderun, Türkiye**
Benan YAZICI KARABULUT, Abdullah İzzeddin KARABULUT, Perihan DERİN, Mehmet İrfan YEŞİLNACAR, Gülistan Banu ÇAKMAK

340 **Effect of torrefaction pretreatment on combustion behaviour of different agricultural wastes**
Neslihan Duranay, Melek YILGIN, Ercan AYDOĞMUŞ

347 **The effect of physicochemical properties on paracetamol photodegradation in cuboid bubble column**
Ashwan HAMAD KHALİL, Asawer ALWASİTİ, Jenan ABDULRZAAK, Abbas AL-SHALAL

359 **Investigation of land surface temperature heterogeneity in municipal landfills by satellite images**
Sedat YALÇINKAYA, Fatih DOĞAN

Reviews

371 **Synergies and potential of hybrid solar photovoltaic for enhanced desalination: A review of selected countries**
Dwiprayogo WIBOWO, Raldi Hendrotoro SEPUTRO KOESTOER

383 **How body burden from exposure to endocrine disruptors effects accelerated aging?**
Eunhye SON, Ki Han KWON

Environ Res Tec, Vol. 6, Issue. 4, pp. 279–287, December 2023

Environmental Research and Technology
https://ert.yildiz.edu.tr - https://dergipark.org.tr/tr/pub/ert
DOI: https://doi.org/10.35208/ert.1249400

Environmental Research & Technology

Research Article

The evaluation of fibrous disposable facemask for oil sorption and efficient oil/water separation

Soner KIZIL[*1,2]

[1]*Üsküdar University, Faculty of Engineering and Natural Sciences, İstanbul, Türkiye*
[2]*Institute of Addiction and Forensic Sciences, Üsküdar University, Faculty of Engineering and Natural Sciences, İstanbul, Türkiye*

ARTICLE INFO

Article history
Received: 09 February 2023
Revised: 11 August 2023
Accepted: 05 September 2023

Key words:
Absorbent; Disposable facemask; Oil/water separation

ABSTRACT

During the pandemic period, people have used various personal protective equipment including gloves, facemask and face shields. Among them, disposable facemask plays a critical role to control the spread of COVID-19, that situation lead to occurring huge amount waste materials. Hence, there is urgent need to evaluate and suspend such waste materials from environment. Herein, we have investigated the potential use of disposable facemask as oil sorbent material for efficient oil/water separation due to their hydrophobic/oleophilic character of PP based disposable facemask. Some structural characterization techniques are employed to examine the facemask. A number of tests including absorbency, oil/water separation stability in oils and waters, selective removal of oils in different water medium have been systematically investigated. The outcomes show that waste facemask have great potential in the field of oil-water separation that achieve selectively separate the oil from oily wastewater.

Cite this article as: Soner Kızıl. The evaluation of fibrous disposable facemask for oil sorption and efficient oil/water separation. Environ Res Tec 2023;6(4)279–287.

INTRODUCTION

The COVID-19 virus emerged towards the end of 2019 and has spread all over the world in a very short time. Since the major cause for the transmission of the virus between people was reported as respiratory droplets [1], people all around the world have used different personal protective equipment such as facemasks, face shield, gloves, gown, etc. Among them, Facemasks have been especially introduced as a countermeasure to decelerate the spread of the virus since it can repel the air droplets caused by cough, sneeze, breathe, and can prevent human-to-human transmission of the virus. Subsequently, there were difficulties in the supplement of masks globally for a short period [2]. Fortunately, there is no longer a shortage of facemasks after significant efforts made in the production and supply of masks on a global scale. Not surprisingly, the use of facemasks has increased with the increasing number of COVID-19 cases [3]. Throughout pandemic, facemasks are required in places such as public transport, indoor and crowded environments in most countries and this led to facemasks have become an essential item of everyday life and exploded the numbers of facemasks used. Disposable facemask can be manufactured from different polymer materials such as polyethylene, polypropylene, polyester, polyurethane, polyamide [4]. Therefore, amount of generated waste allied with the use of this personal protective equipment also increased unwittingly and mishandling of this waste led to environmental contamination [5]. Although recommendations on the management of pandemic derived wastes including waste facemasks have been developed and implemented by most administrations, proper management and final destination of this waste is

***Corresponding author.**
*E-mail address: soner.kizil@uskudar.edu.tr

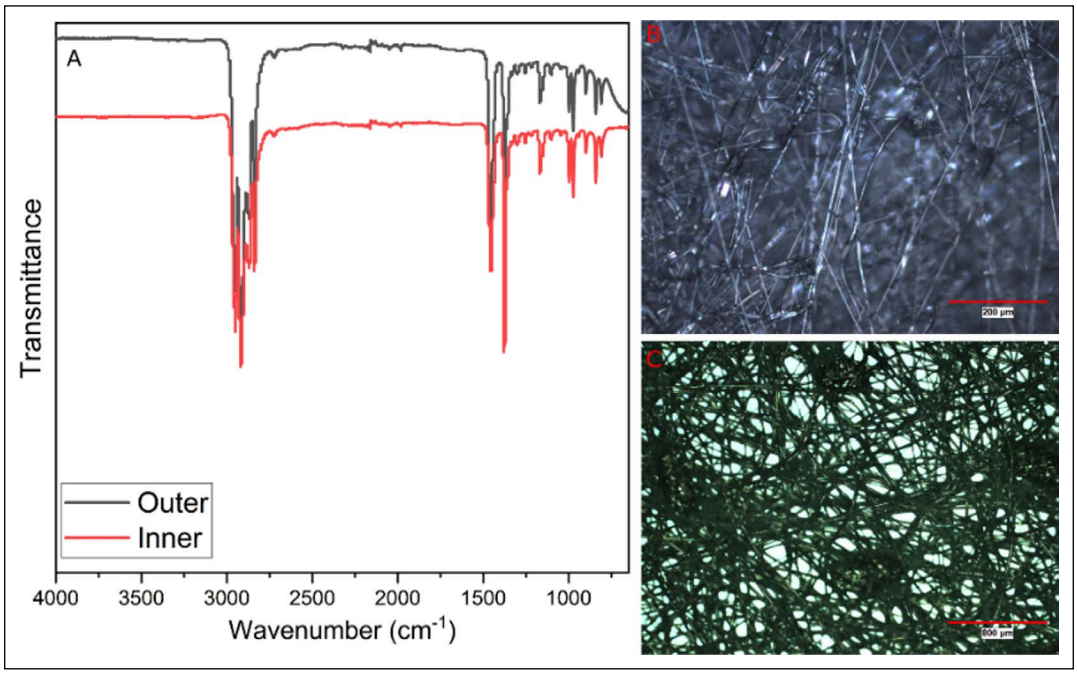

Figure 1. **(a)** FTIR spectra of inner and outer layer of facemask **(b)** Optical microscope image of inner layer **(c)** Optical microscope image of outer layer.

highly dependent on the citizen's awareness and commitment [6]. A mask waste that has not been disposed of properly and has entered the environment has potential threats to the nature. Main concerns arising from these threats are plastic pollution [7], organophosphate esters [8], microplastic release from masks to the aquatic environment [9–11] and leaching of chemicals and nanoparticles [12, 13].

One of the important things that will determine the future of facemask waste is how long the pandemic will last. The effectiveness of existing vaccines against new variants of the virus remains unclear for now, which also extends the estimated time for us to achieve herd immunity [14]. So, as the pandemic continues, it will not be possible to reduce these facemask wastes because it is a necessity. Then, recycling or reuse for different purposes comes into prominence. So far, many studies have been carried out on how to recycle and reuse waste facemasks in order to reduce the waste caused by the pandemic. In one of the studies, the use of waste facemasks in sound insulation has been tried and compared with commercial sound absorbers that currently used in building sector. Acoustic efficiency of waste facemasks was found better than actually used fibrous sound absorbers and it was recommended that it can be used for sound insulation purposes after proper disinfection [15]. The fibril structure of masks is also of interest in the field of construction to increase mechanical strength. It has been revealed that the addition of disposable masks up to 0.2% into the initial mixture increased the strength and quality of the concrete [16]. In another study, it was demonstrated that shredded masks can also be used successfully in road and pavement applications [17]. Rehman and Khalid used shredded facemasks successfully as a fibrous reinforcement additive to increase the mechanical strength of fat clay [18]. Purnomo et. al. reviewed thermochemical conversion technologies for COVID-19 derived medical wastes (CMW) including incineration, carbonization, pyrolysis and gasification. Incineration was found suitable for all types of CMW including waste facemasks but also found most potential harmful to the nature since it releases CO2 and other gases coming from burning process. Moreover, gasification and pyrolysis were evaluated as towardly with regards to environmental impact and efficiency [19]. In another study, pyrolysis of single use facemask was examined to benefit from this waste as an energy source. Fuel range chemicals as 14.7 wt% gasoline-, 18.4 wt% jet fuel-, 34.1 wt% diesel-, and 18.1 wt% motor oil-range hydrocarbons were yielded in this study [20].

As can be seen from the previous paragraph, various recycling and reuse strategies have been developed by utilizing the fibrous structure and carbon-containing nature of waste facemasks. This fibrous structure and hydrophobic nature of the facemasks can also be utilized for the separation of oils, which is an important pollutant for nature. Oil spill is a major threat for all living organism due to its negative effects such as inhibits the penetration of sunlight, make water source undrinkable etc. Water can be polluted because of tanker accidents, natural events, war, and personnel mistakes and so on. To minimize the catastrophic effects of oil spill, effective removal of such pollutions should be paid close attention. So far, a wide range of clean-up methods such as chemical, biological and physical was operated for effective removal of oil from wastewater. Among them, use of absorbents is most promising approach due to its easy to operate, cheap and high selectivity properties [21]. Plenty of absorbents have been utilized for rapid oil spill conditions, mainly categorized as inorganic mineral sor-

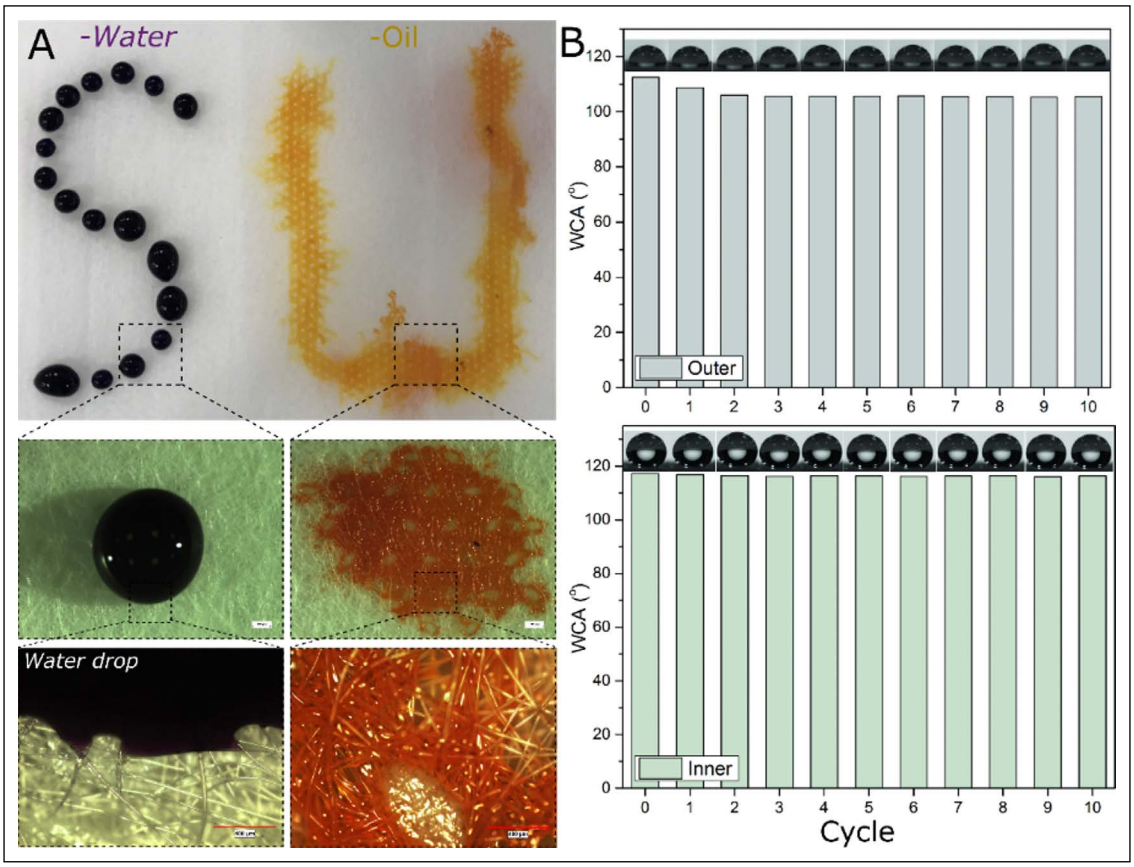

Figure 2. **(a)** The photos of facemask contacted with oil and water **(b)** WCA of inner/outer layer of facemask.

bents such as perlite, clay; organic vegetable sorbents such as straw, kenaf, rice husk, bark; and synthetic sorbents such as polyalkoxysilanes, alkyl acrylates, foams, electrospun fibers, and polypropylene [22–24]. It was well known that ideal sorbent should have some characteristics including high and quick oil absorbency, hydrophobicity, high oil/water selectivity, buoyancy before and after sorption [25]. Among them, use of polypropylene stand out for oil/water separation applications due to their attractive features such as high hydrophobicity and oleophilicity, low water interest, easy to use and low cost [26].

In this study, the use of facemask wastes in oil removal from water was investigated in order to benefit from its polypropylene material and fibrous structure. Since it is not certain when the epidemic will end and thus these wastes will continue to be created, it is very important for sustainability to investigate the potential benefits that can be obtained from these wastes. To the best of our knowledge, there has not been any research for the use of waste facemask as oil sorbent materials. The oil absorbency and oil absorption kinetics are investigated by dipping into different oils and organic liquids and different oil/water medium is explored. Detailed characterizations of the masks were carried out with FTIR, contact angle, microscopic analysis. The outcomes show that waste nonwoven polypropylene facemask have high hydrophobicity, thus have high oil and organic liquids interest and low water absorbency. What's more, they can selectively absorb the oil from different water medium including simulated and subzero water with an almost same performance in organic liquids medium. We think that this study reveals a significant benefit potential in waste facemasks.

MATERIALS AND METHODS

Materials and Chemicals

The oils used in swelling experiments including toluene, hexane and chloroform were purchased from Sigma-Aldrich. Euro diesel was purchased from British Petroleum (BP) and motor oil was obtained from Mobil. Disposable, three-layer surgical single use facemasks providing European Standard EN 14683:2019 were purchased from a local store. It consists of a polypropylene melt-blown non-woven fabric layer sandwiched between two spunbonded fabric layers. Disperse red and Crystal violet, which were used for visualization of oil and water are purchased from Fluka. To get a reliable swelling result, some units of facemask such as ear strap, metallic nose wire are removed. In this study, a clean facemask was used to eliminate the risk of COVID-19 spread and transmission in the laboratory. However, there are many studies in the literature on disinfecting masks describing the methods like ethyl alcohol treatment, vaporized hydrogen peroxide (H_2O_2), dry heat treatment, hot water contamination, moist heat and UV irradiation [27–32]. These methods can be implemented in the further necessary scale-up cases.

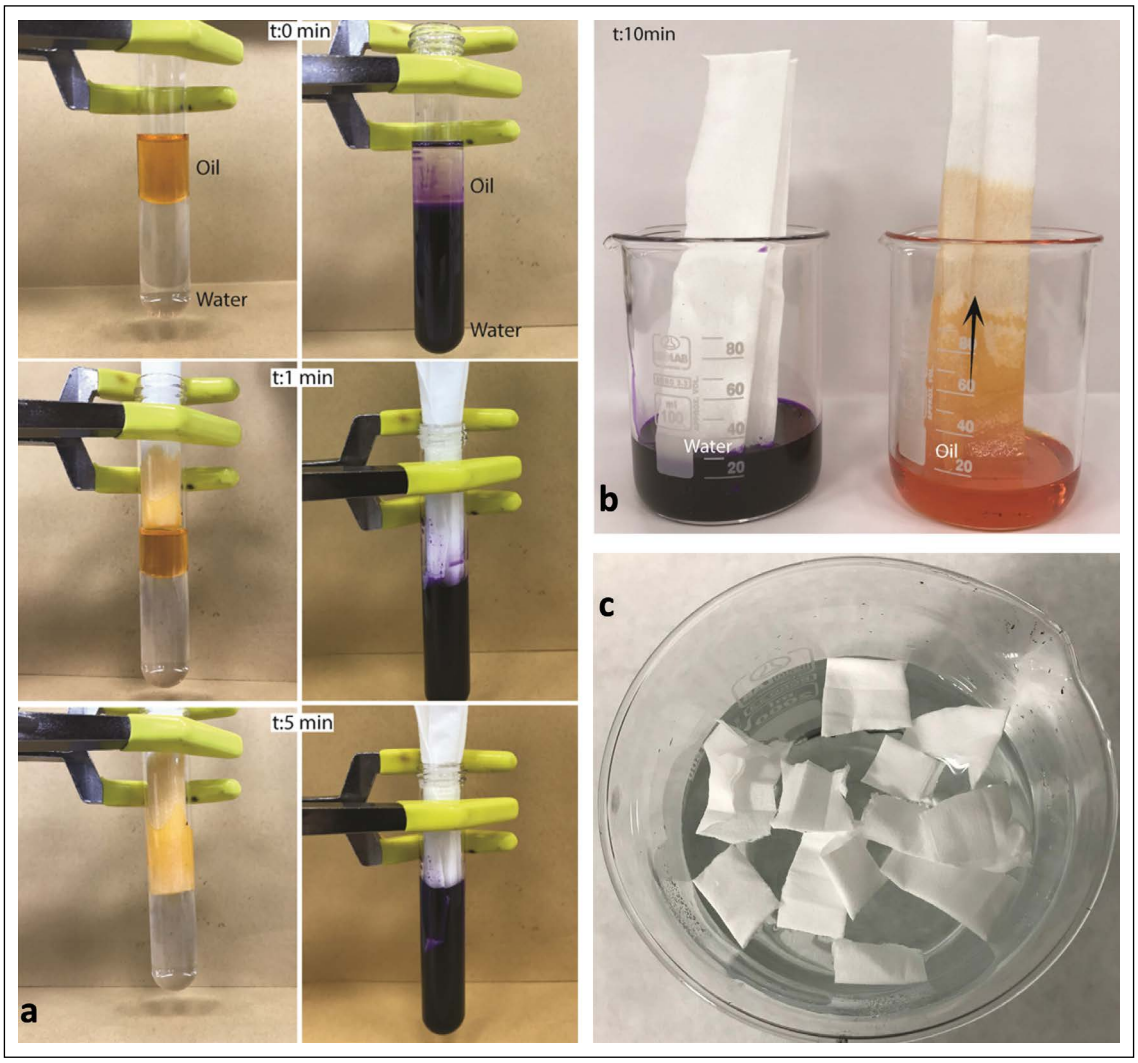

Figure 3. **(a)** Immersion of facemask into the oil/water mixture, **(b)** Wettability of facemask in oil and water, **(c)** Buoyancy of facemask in water medium.

Oil Absorption Experiments

As it mentioned before, to get reliable results and eliminate the risk of COVID-19 spread and transmission by used facemask, clean facemasks were used. Before swelling experiments, facemask is sliced equal parts to provide efficient absorption. For swelling experiments, different aromatic, aliphatic, halogenated solvents, vegetable oil, motor oils and petroleum-based fuel are used.

2x2 cm pieces of facemasks are dipped in various oils and oil absorbency are determined by gravimetric methods. To achieve this, a known amount of facemask was put in a wire mesh basket and immersed in oils. Then, the wire mesh basket was taken out after a certain time and drained for 5 s to remove excess oils and weighed. The oil absorbency was calculated with the following formula (1):

$$(W_c\text{-}W_b\text{-}W_k)*100/W_k \quad (1)$$

where W_b is the weight of wetted empty stainless-steel mesh, W_k and W_c show the dry and swollen facemask materials, respectively.

For oil/water separation tests, toluene is mixed with distiller water, simulated (%3.5 NaCI) water and sub-zero water. For visualize the oil/water separation, the disperse red 1 and crystal violet dyes were used for colorization of toluene and water, respectively.

Instrumental Analyses

Structural analysis of facemask was obtained using Nicolet IS10 Fourier Transform Infrared Spectrometer (FT-IR) with an ATR system, at a resolution of 4 with 128 scans. Water and oil contact angles were determined via Drop shape analysis system (KRÜSS DSA 10-MK2).

RESULTS AND DISCUSSION

Structural Analysis of Facemasks

Single use facemasks contain some other units different than filter such as ear strap and metallic nose wire. In order to investigate the facemask, such units are removed and only filter part are left behind. FTIR is used to characterize the chemical composition of this part. As presented in Figure 1a, the peak at 1365 cm^{-1} are belong to the Symmetric

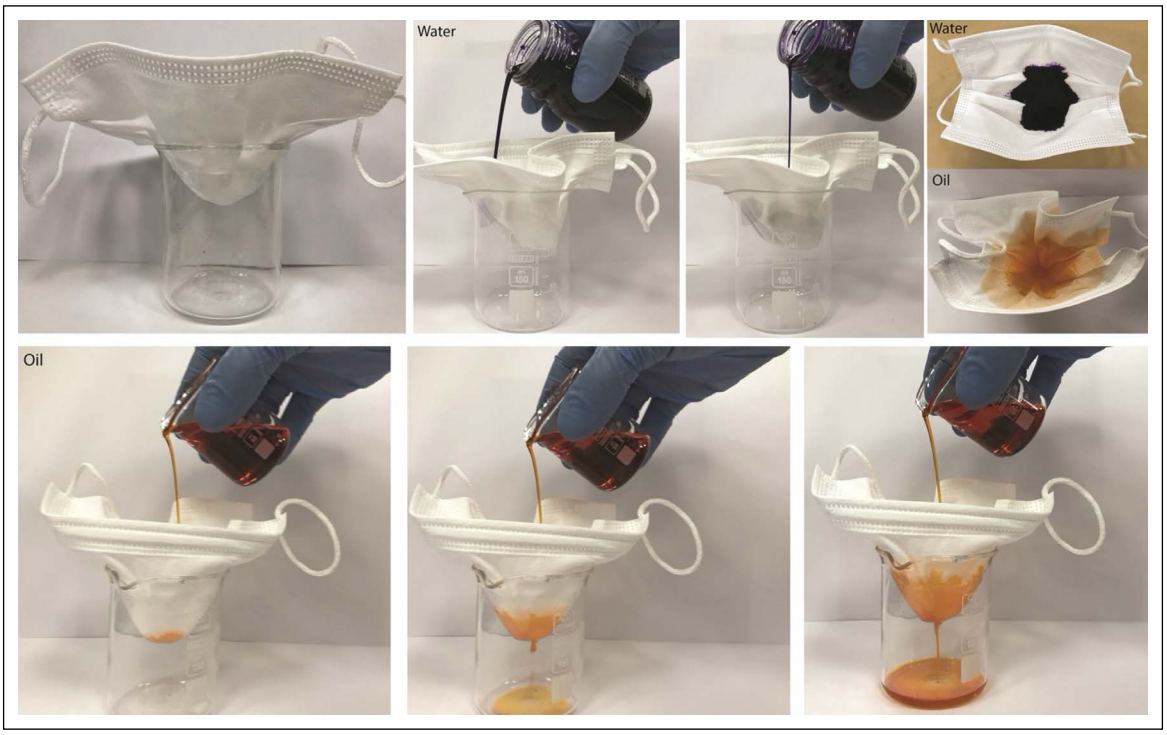

Figure 4. Liquid permeability performance of disposable facemask.

bending vibration mode of $-CH_3$ group, the peaks at 1451, 2827, 2913 cm^{-1} are attributed to attributed to $-CH_2-$ symmetric bending, $-CH_2-$ symmetric stretching and $-CH_2-$ asymmetric stretching, respectively [33]. The observed FTIR peaks fit very well with polypropylene characteristic peaks and these results clearly reveal that the inner and outer filter layer is made up with polypropylene polymer.

Layers of single-use facemask are displayed in Figure 1a. To observe fibrous structure of facemask, the outer and inner layer are disassembled and observed via optical microscopy. Optical microscope images of outer and inner surface are given in Figure 1. All images translucently show that the inner layer is denser than the outer layer.

The facemask exhibited hydrophobic character having a water contact angle of 116±2 ° for inner surface, 107±2 ° for outer surface and oleophilicity with almost 0° oil contact angle for different oils such as dichloromethane, toluene and euro diesel. As the water droplets were placed on inner and outer surface of facemasks, the droplets remained almost stable. However, the oil droplet is swiftly absorbed by facemask, as represented in Figure 2. Moreover, the water droplet is pulled from the surface without leaving any water residue, indicating its excellent water repellent and oil loving character of facemask.

To visualize swelling performance of facemask in oil and water, the disperse red 1 and crystal violet dyes were used for colorization of toluene and water, respectively. When facemask is dipped in mixture, the oil (orange color) is rapidly absorbed and fully swollen in 5 min as given in Figure 3a. As the facemask is dipped in oil/water mixture, no color change on the facemask surface, indicating water (dyed with Crystal Violet) does not penetrate the fibrous structure and does not go up. To detect interest facemask toward the oil and water for longer periods, a part of long piece facemask is immersed for about 5 min. At the end of this, oil is swiftly penetrated through the hydrophobic fibrous structure of facemask; water cannot diffuse the fibrous structure, implying that good candidate for practical applications, represented in Figure 3b. In addition, to observe buoyancy, facemask is pushed via forceps to submerge, but it still keeps floating character on the water surface indicating high interest toward organic liquids and low interest to water as seen in Figure 3c.

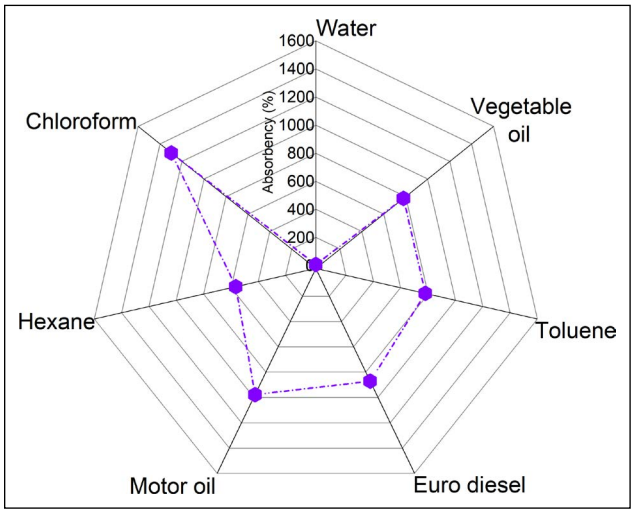

Figure 5. Oil absorbencies of facemask in different oils and water.

For further determination of oil/water interaction of facemasks and observe separation efficiency, waste facemask was placed on the top of a beaker. When water (purple) is

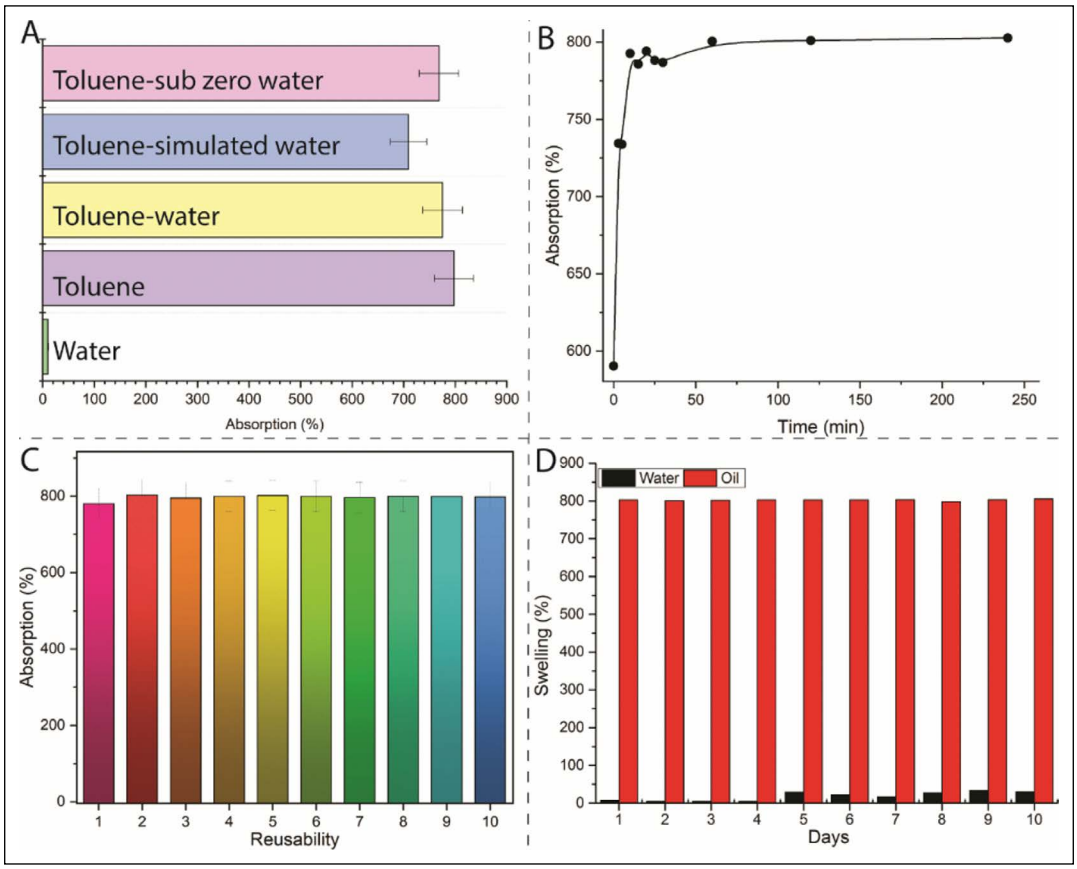

Figure 6. **(a)** Selective removal of oil in different water medium **(b)** Absorption kinetics of facemask in toluene **(c)** Reusability in toluene **(d)** Absorption stability of facemask in oil and water.

poured onto the facemask, water was retained without any water drop is crossed through fibrous structure. The water on the facemask have waited for a while (10 days) and no obvious droplet is seen on the beaker, implying high hydrophobicity and good oil selectivity of fibrous facemask. However, when oil is poured onto the facemask, the oil is immediately absorbed and diffused through the fibrous structure and collected at the bottom of beaker (Fig. 4).

Oil Absorption and Separation Characteristics

Prior to oil absorption experiments, Nose wire and ear strap of single-use facemask are removed and remained part is split into 2x2 cm pieces using scissors. Swelling measurements of fibrous facemask are achieved in different oils including toluene, hexane, chloroform, motor oil, gasoline and calculated according to the formula 1. The maximum oil absorbency of facemask is given in Figure 5. The absorption capacity of facemask for several kinds of oils is in the range between 565%–1300%, depending on their density and viscosity.

For practical applications, some characteristics including high absorbency, reusability, quick absorption feature and selectivity are the main significant performance parameters in the field of oil/water separation. Oil leakage could occur in environments such as sea, lake, drinking water mediums or harsh environments. To simulate the oil absorption behavior toward different conditions, facemask is dipped into oil (toluene is used as a representative solvent)/ lake, oil/distilled water, oil/simulated water and oil/subzero water, seen in Figure 6a. It is clear that facemask exhibited high interest toward oil while low interest is shown into the water. Furthermore, facemask has almost reached their maximum capacity in different water environments including simulated, distillated or subzero waters.

It was shown from the absorption speed given in Figure 6b that it reaches 75% of maximum absorption capacity just in 1 min, reach their maximum absorbency in 3 min and keep swollen form for a long time without release of organic liquids.

Reusability is one another critical parameter for ideal absorbent materials in the field of oil absorbing applications. To detect the reusability performance, facemask is dipped in toluene for 24 h to make sure fully absorption is completed. After that, swollen fibrous mask are allowed to release the oil at room conditions. Then, dry fibrous facemask is again dipped in oil, repeated for 10 times. It can be clearly seen that fibrous facemask can reach their maximum absorbency each absorption test without significance change, seen in Figure 6c. Moreover, swelling performance is investigated to check stability of swollen fibrous facemask for 10 days indicating that facemask keep their fibrous structure and oil absorption features for a long time.

For comparison, different commercial polypropylene materials and other type of polymer materials were used and their properties are given in Table 1. It is clearly seen that waste facemask are competitive with some commercial PP

Table 1. Comparison of some materials as oil sorbents

Materials	Oils	Uptake*	Cycle	Ref.
Commercial pads	Diesel	8 g/g	n.a	[34]
PDMS sponge	Chloroform	1100%	20	[35]
Waste PET sorbents	Machine oil	2.43 g/g	3	[36]
3D PP sponges	Toluene	2100%	#6	[37]
Commercial PP (Mavisorb)	Toluene	11.4 g/g	n.a	[38]
Commercial PP	Diesel	8 g/g	n.a	[39]
Disposable facemask	Chloroform	1300%	10	This work
	Motor oil	977%		
	Euro diesel	871%		
	Toluene	798%		
	Vegetable oil	780%		
	Hexane	565%		

#: Decreasing absorption performance.

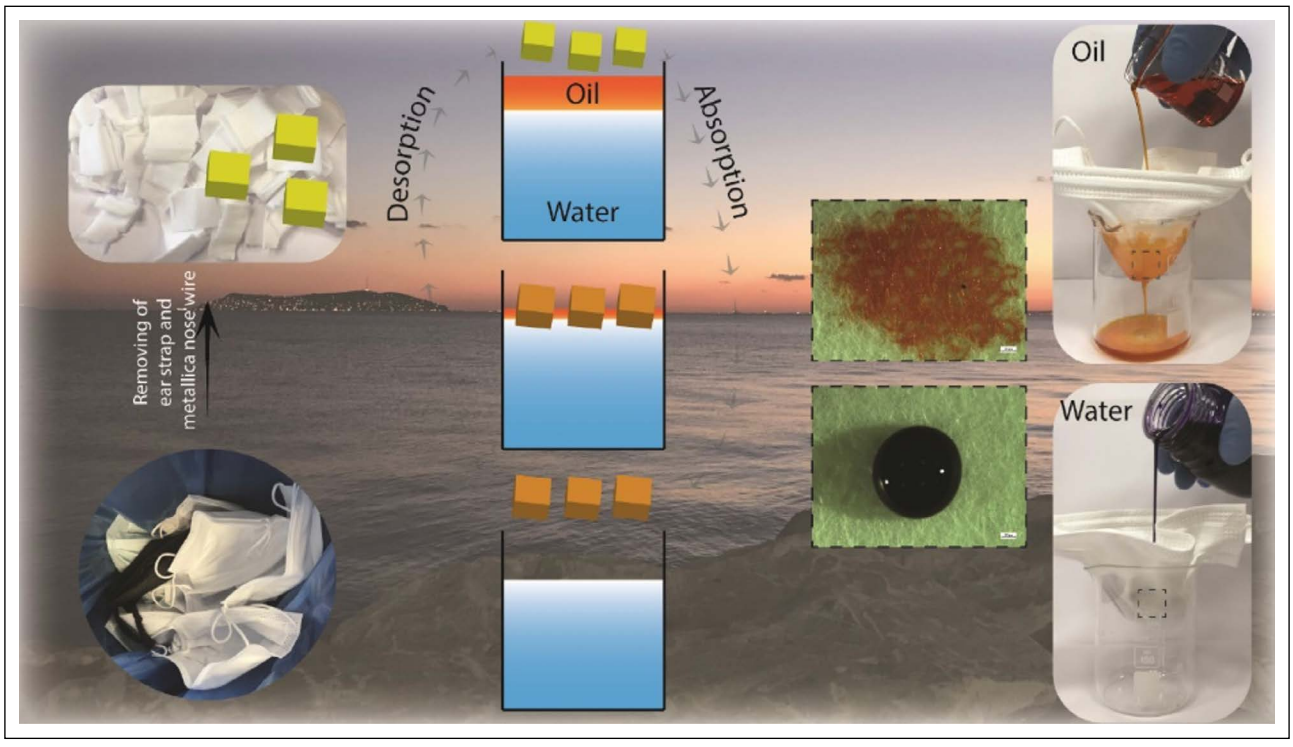

Figure 7. The illustration of disposable facemask for oil/water separation applications.

sorbents. Moreover, facemask could be reused for several times, which make them very favorable for efficient oil absorbent in rapid oil pollution situations.

CONCLUSION

It has been successfully demonstrated that the fibrous structure and hydrophobic character of the disposable facemask, which is the most used protection equipment during the pandemic, can be used in oil-water separation (Fig. 7). Fibrous facemask can absorb a variety of oils in a short time, ranged between 565–1300% depending on the oil types. Moreover, oils in the different water medium such as simulated, lake, seawater and sub-zero water can be effectively separated by fibrous facemask waste, with the same capacity in the oil medium and buoyant before and after oil sorption. Considering the uncertainty of when the Covid-19 pandemic will end and the inevitable necessity of facemask use, we believe that the facemask waste can be evaluated as oil sorbents. The disposable facemask could be collected, sterilized and get packed in the form of booms, pads or rolls. The waste polymeric facemask materials then could be used as collective materials, as the oil spill is occurred in personal mistakes, natural events.

DATA AVAILABILITY STATEMENT

The authors confirm that the data that supports the findings of this study are available within the article. Raw data that support the finding of this study are available from the corresponding author, upon reasonable request.

CONFLICT OF INTEREST

The authors declared no potential conflicts of interest with respect to the research, authorship, and/or publication of this article.

ETHICS

There are no ethical issues with the publication of this manuscript.

REFERENCES

[1] D. Taylor, A. C. Lindsay, and J. P. Halcox, "Aerosol and Surface Stability of SARS-CoV-2 as Compared with SARS-CoV-1," New England Journal of Medicine, Vol. 382(16), pp. 1564–1567, 2020. [CrossRef]

[2] O. O. Fadare, and E. D. Okoffo, "Covid-19 face masks: A potential source of microplastic fibers in the environment," Science of the Total Environment, Vol. 737, Article 140279–140282, 2020. [CrossRef]

[3] S. Sangkham, "Face mask and medical waste disposal during the novel COVID-19 pandemic in Asia," Case Studies in Chemical and Environmental Engineering, Vol. 2, pp. 100052–100060, 2020. [CrossRef]

[4] N. U. Benson, D. E. Bassey, and T. Palanisami, "COVID pollution: impact of COVID-19 pandemic on global plastic waste footprint," Heliyon, Vol. 7(2), pp. e06343–e06351, 2021. [CrossRef]

[5] K. I. Olatayo, P. T. Mativenga, and A. L. Marnewick, "COVID-19 PPE plastic material flows and waste management: Quantification and implications for South Africa," Science of the Total Environment, Vol. 790, pp. 148190–148202, 2021. [CrossRef]

[6] C.S.G. Penteado, and M.A.S. de Castro, "Covid-19 effects on municipal solid waste management: What can effectively be done in the Brazilian scenario?", Resources, Conservation and Recycling, Vol. 164, pp. 105152–105160, 2021. [CrossRef]

[7] M. R. J. Rakib, G. E. De-la-Torre, C. I. Pizarro-Ortega, D. C. Dioses-Salinas, and S. Al-Nahian, "Personal protective equipment (PPE) pollution driven by the COVID-19 pandemic in Cox's Bazar, the longest natural beach in the World," Marine Pollution Bulletin, Vol. 169, Article 112497–112503, 2021. [CrossRef]

[8] J. Fernández-Arribas, T. Moreno, R. Bartrolí, and E. Eljarrat, "COVID-19 face masks: A new source of human and environmental exposure to organophosphate esters," Environment International, Vol. 154, pp. 106654–106661, 2021. [CrossRef]

[9] J. Ammendolia, J. Saturno, A. L. Brooks, S. Jacobs, and J. R. Jambeck, "An emerging source of plastic pollution: Environmental presence of plastic personal protective equipment (PPE) debris related to COVID-19 in a metropolitan city," Environmental Pollution, Vol. 269, pp. 116160–116169, 2021. [CrossRef]

[10] T. A. Aragaw, "Surgical face masks as a potential source for microplastic pollution in the COVID-19 scenario," Marine Pollution Bulletin, Vol. 159, pp. 111517–111523, 2020. [CrossRef]

[11] X. Chen, X. Chen, Q. Liu, Q. Zhao, X. Xiong, and C. Wu, "Used disposable face masks are significant sources of microplastics to environment," Environmental Pollution, Vol. 285, pp. 117485–117490, 2021. [CrossRef]

[12] G. L. Sullivan, J. Delgado-Gallardo, T. M. Watson, and S. Sarp, "An investigation into the leaching of micro and nano particles and chemical pollutants from disposable face masks - linked to the COVID-19 pandemic," Water Research, Vol. 196, pp. 117033–117043, 2021. [CrossRef]

[13] M. Ardusso, A. D. Forero-López, N. S. Buzzi, C. V. Spetter, M. D. Fernández-Severini, "COVID-19 pandemic repercussions on plastic and antiviral polymeric textile causing pollution on beaches and coasts of South America," Science of the Total Environment, Vol. 763, pp. 144365–144376, 2021. [CrossRef]

[14] Mckinsy. "When will the COVID-19 pandemic end?" https://www.mckinsey.com/industries/healthcare-systems-and-services/our-insights/when-will-the-covid-19-pandemic-end Accessed on Nov 09, 2023.

[15] R. Maderuelo-Sanz, P. Acedo-Fuentes, F. J. García-Cobos, F. J. Sánchez-Delgado, M. I. Mota-López, and J. M. Meneses-Rodríguez, "The recycling of surgical face masks as sound porous absorbers: Preliminary evaluation," Science of the Total Environment, Vol. 786 pp. 147461–147469, 2021. [CrossRef]

[16] S. K. Lynch, M. Saberian, J. Li, R. Roychand, and G. Zhang, "Preliminary evaluation of the feasibility of using polypropylene fibres from COVID-19 single-use face masks to improve the mechanical properties of concrete," Journal of Cleaner Production, Vol. 296, pp. 126460–126467, 2021. [CrossRef]

[17] M. Saberian, J. Li, S. K. Lynch, and M. Boroujeni, "Repurposing of COVID-19 single-use face masks for pavements base/subbase," Science of the Total Environment, Vol. 769, pp. 145527–145534, 2021. [CrossRef]

[18] Z. U. Rehman, and U. Khalid, "Reuse of COVID-19 face mask for the amelioration of mechanical properties of fat clay: A novel solution to an emerging waste problem," Science of The Total Environment, Vol. 794, pp. 148746–148762, 2021. [CrossRef]

[19] C. W. Purnomo, W. Kurniawan, and M. Aziz, "Technological review on thermochemical conversion of COVID-19-related medical wastes," Resources, Conservation and Recycling, Vol. 167 pp. 105429–105441, 2021. [CrossRef]

[20] C. Park, H. Choi, K. Y. A. Lin, E. E. Kwon, and J. Lee, "COVID-19 mask waste to energy via thermochemical pathway: Effect of Co-Feeding food waste," Energy, Vol. 230, pp. 120876–120884, 2021. [CrossRef]

[21] J. Ge, H. Y. Zhao, H. W. Zhu, J. Huang, L. A. Shi, and S. H. Yu, "Advanced sorbents for oil-spill cleanup: recent advances and future perspectives," Advanced Materials, Vol. 28, pp. 10459–10490, 2016. [CrossRef]

[22] L. M. T. M. Oliveira, J. Saleem, A. Bazargan, J. L. D. S. Duarte, G. McKay, and L. Meili, "Sorption as a rapidly response for oil spill accidents: A material and mechanistic approach," Journal of Hazardous Materials, Vol. 407, pp. 124842–124861, 2021. [CrossRef]

[23] B. Doshi, M. Sillanpää, and S. Kalliola, "A review of bio-based materials for oil spill treatment," Water Research, Vol. 135, pp. 262–277, 2018. [CrossRef]

[24] S. Kizil, and H. B. Sonmez, "One-pot fabrication of reusable hybrid sorbents for quick removal of oils from wastewater," Journal of Environmental Management, Vol. 261, pp. 109911–109918, 2021. [CrossRef]

[25] S. B. Hammouda, Z. Chen, C. An, and K. Lee, "Recent advances in developing cellulosic sorbent materials for oil spill cleanup: A state-of-the-art review," Journal of Cleaner Production, Vol. 311, pp. 127630–127648, 2021. [CrossRef]

[26] Q. F. Wei, R. R. Mather, A. F. Fotheringham, and R. D. Yang, "Evaluation of nonwoven polypropylene oil sorbents in marine oil-spill recovery," Marine Pollution Bulletin, Vol. 46(3), pp. 780–783, 2003. [CrossRef]

[27] D. Wang, B. C. Sun, J. X. Wang, Y. Y. Zhou, Z. W. Chen, Y. Fang, W. H. Yue, S. M. Liu, K. Y. Liu, X. F. Zeng, G. W. Chu, and J. F. Chen, "Can masks be reused after hot water decontamination during the COVID-19 pandemic?" Engineering, Vol. 6(10), pp. 1115–1121, 2020. [CrossRef]

[28] L. F. L. Begall, C. Wielick, L. Dams, H. Nauwynck, P. F. Demeuldre, A. Napp, J. Laperre, E. Haubruge, and E. Thiry, "The use of germicidal ultraviolet light, vaporised hydrogen peroxide and dry heat to decontaminate face masks and filtering respirators contaminated with an infectious norovirus," Journal of Hospital Infection, Vol. 106(3), pp. 577–584, 2021. [CrossRef]

[29] H. P. Kim, M. S. Jo, C. H. Kim, J. S. Choi, and I. J. Yu, "Re-use of health masks after autoclaving," NanoImpact, Vol. 19, pp. 100231–100236, 2020. [CrossRef]

[30] D. F. Li, J. L. Cadnum, S. N. Redmond, L. D. Jones, B. Pearlmutter, M. F. Haq, and C. J. Donskey, "Steam treatment for rapid decontamination of N95 respirators and medical face masks,"American Journal of Infection Control, Vol. 48, pp. 853–858, 2020. [CrossRef]

[31] N. J. Rowan, J. G. Laffey, "Unlocking the surge in demand for personal and protective equipment (PPE) and improvised face coverings arising from coronavirus disease (COVID-19) pandemic – Implications for efficacy, re-use and sustainable waste management," Science of the Total Environment, Vol. 752, pp. 142259–142276, 2021.

[32] J. C. R. Romero, M. D. C. P. Ferreira, J. A. T. García, and S. C. Castro, "Disposable masks: Disinfection and sterilization for reuse, and non-certified manufacturing, in the face of shortages during the COVID-19 pandemic," Safety Science, Vol. 129, pp. 104830–104840, 2020. [CrossRef]

[33] A. Gopanna, R. N. Mandapati, S. P. Thomas, K. Rajan, and M. Chavali, "Fourier transform infrared spectroscopy (FTIR), Raman spectroscopy and wide-angle X-ray scattering (WAXS) of polypropylene (PP)/cyclic olefin copolymer (COC) blends for qualitative and quantitative analysis," Polymer Bulletin, Vol. 76, pp. 4259–4274, 2018. [CrossRef]

[34] Y. H. Lee, E. J. Lee, G. S. Chang, D. J. Lee, Y. J. Jung, and H. D. Kim, "Comparison of oil sorption capacity and biodegradability of PP, PP/kapok(10/90wt%) blend and commercial(T2COM) oil sorbent pads," Textile Coloration and Finishing, Vol. 26, pp. 151–158, 2014. [CrossRef]

[35] S. J. Choi, T. H. Kwon, H. Im, D. Moon, D. J. Baek, M. L. Seol, J. P. Duarte, and Y. K. Choi, "A polydimethylsiloxane (PDMS) sponge for the selective absorption of oil from water," ACS Appl Mater Interfaces, Vol. 3(12), pp. 4552–4556, 2011. [CrossRef]

[36] E. A. Bukharova, E. A. Tatarintseva, and L. N. Ol'Shanskaya, "Production of polyethylene terephthalate based sorbent and its use for waste and surface water cleaning from oil products," Chemical and Petroleum Engineering, Vol. 50, pp. 595–599, 2015. [CrossRef]

[37] G. Wang, and H. Uyama, "Facile synthesis of flexible macroporous polypropylene sponges for separation of oil and water," Scientific Reports, Vol. 6, pp. 1–6, 2016. [CrossRef]

[38] D. Ceylan, S. Dogu, B. Karacik, S. D. Yakan, O. S. Okay, and O. Okay, "Evaluation of butyl rubber as sorbent material for the removal of oil and polycyclic aromatic hydrocarbons from seawater," Environmental Science and Technology, Vol. 43(10), pp. 3846–3852, 2009. [CrossRef]

[39] H. Zhu, S. Qiu, W. Jiang, D. Wu, and C. Zhang, "Evaluation of electrospun polyvinyl chloride/polystyrene fibers as sorbent materials for oil spill cleanup," Environmental Science and Technology, Vol. 45(10), pp. 4527–4531, 2011. [CrossRef]

Environ Res Tec, Vol. 6, Issue. 4, pp. 288–301, December 2023

Environmental Research and Technology
https://ert.yildiz.edu.tr - https://dergipark.org.tr/tr/pub/ert
DOI: https://doi.org/10.35208/ert.1220649

Research Article

The influence of meteorological parameters on $PM_{2.5}$ and PM_{10} values in Ümraniye and Silivri districts of İstanbul

Hilal ARSLAN*[1], Ali TOLTAR[2]

[1]*Department of Occupational Health and Safety, University of Health Sciences, Hamidiye Faculty of Health Sciences, İstanbul, Türkiye*
[2]*Department of Occupational Health and Safety, İstanbul Gedik University, Institute of Graduate Studies, İstanbul, Türkiye*

ARTICLE INFO

Article history
Received: 18 December 2022
Revised: 15 May 2023
Accepted: 07 September 2023

Key words:
Air quality; Correlation coefficient; İstanbul, Meteorological parameters; Particulate matter

ABSTRACT

In this study, spatiotemporal relationship between $PM_{2.5}$ and PM_{10} concentrations and meteorological parameters were investigated for Silivri and Ümraniye districts in İstanbul for 2014–2020. For this purpose, hourly $PM_{2.5}$ and PM_{10} concentrations values of two air quality monitoring stations and meteorological data (wind speed, wind direction, relative humidity, total precipitation, minimum and maximum temperature) were examined. In all seasons, while PM concentrations were lowest at 06:00 local time (LT), $PM_{2.5}$ and PM_{10} have peak values around 09:00 and 19:00 LT both in Silivri and Ümraniye mainly due to anthropogenic activities such as vehicle exhaust emissions. In daily perspective, highest PM values were observed on Sundays in winter at Silivri. On the other side, peak PM values are shown on Fridays at Ümraniye. It was found that local emission sources during low wind speeds cause the highest $PM_{2.5}$ concentrations during winter months and southerly winds exceeding 8 m/s increase the PM_{10} levels at Silivri and Ümraniye. The statistical analysis showed that $PM_{2.5}$ and PM_{10} concentrations at Silivri were negatively correlated with wind speed with correlation coefficients of -0.56 (winter), -0.47 (autumn), respectively. Wind speed is negatively associated with $PM_{2.5}$ (r=-0.48) and PM_{10} (r=-0.38) in winter season at Ümraniye. In addition to this, relative humidity showed negative relationship with PM10 (r=-0.43)in spring at Silivri, while a positive correlation was found between PM_{10} (r=0.40) and $PM_{2.5}$ (r=0.38) measured in the summer season and the maximum temperature. In addition to the anthropogenic factors (e.g. urbanization, transportation, and industrialization) that decrease air quality of İstanbul, local meteorological variables and atmospheric transport of pollution are observed to be the other factors that contribute to air pollution.

Cite this article as: Arslan H, Toltar A. The influence of meteorological parameters on $PM_{2.5}$ and PM_{10} values in Ümraniye and Silivri districts of İstanbul. Environ Res Tec 2023;6(4)288–301.

INTRODUCTION

Air pollution is one of the most serious environmental concerns, influencing all living things and having severe and fatal health consequences. The main air pollutants are known as particulate matter (PM_{10}<10 μm particles and $PM_{2.5}$<2.5 μm particles), sulfur dioxide (SO_2), carbon monoxide (CO), ground-level ozone (O_3), lead (Pb) and nitrogen dioxide (NO_2). Particularly, particulate matter plays an important role in urban and regional air pollution and causes serious health effects according to the World Health Organization [1]. Many epidemiological studies have shown that exposure to particulate matter is associated with numerous adverse health effects, including respiratory diseases (e.g.

***Corresponding author.**
*E-mail address: hilal.arslan@sbu.edu.tr

asthma, COPD, bronchitis) and cardiovascular diseases [2–8].In addition, the International Agency for Research on Cancer (IARC) included particulate matter in the list of carcinogenic agents in 2013 [9]. Moreover, particulate matter pollution can generate haze, which can lead to airline delays or cancellations, as well as highway closures [10–12].

Nowadays, air pollution is increasing as a result of anthropogenic factors like urbanization, transportation, and industrialization. In addition to these emissions, local [13]and large-scale meteorological factors are also crucial for transport and distribution of air pollution [14, 15]. Furthermore, meteorological factors affect the concentrations and residence times of pollutants in the atmosphere. Even if the amount of pollutants emitted into the atmosphere does not change, pollutant concentrations can change over time. On days with high PM pollution, the effect of meteorological factors (e.g. temperature, wind speed, precipitation, pressure and inversion) is particularly important. Generally, high temperature values increase the concentration of particulate matter, while precipitation reduces these values by removing particulate matter from the atmosphere [16–19]. Wind speed plays an important role for dilution, distribution and transport of particulate matter and reduce air pollution [20–22]. Since wind removes pollutants from their sources, wind patterns also provide information about where pollutants are transported [23, 24]. Some pollutants pollute the air directly when released from the source, while others are formed in the atmosphere as a result of a reaction between two pollutants. This is caused by meteorological factors such as temperature and humidity. Li et al. [25] indicated that PM concentrations have negative correlation with wind speed in most season but found positive correlations with temperature, relative humidity and pressure over Shenyang in China. Li et al. [26] found that the $PM_{2.5}$, PM_{10}, and SO_2 values were significantly associated with precipitation, temperature and wind speed. Ansari et al. [27] investigated the relationship between the $PM_{2.5}$ concentrations and meteorological factors in Iran. They found weak correlations between $PM_{2.5}$ and average temperature and humidity.

Air pollution has become a major issue in Türkiye due to urbanization, which has led to increased unemployment in rural areas, causing migration from rural to urban areas. With the population growth in cities, transportation activities have increased. As a result, the amount of pollutants in cities has increased dramatically. These sources grow mutually, resulting in air pollution, particularly in urban areas. Although association between air pollution and meteorological factors is important, very limited studies have been carried up for Afyon, Bolu, Erzurum, Karabük, Zonguldak [28–32]. Celik and Kadi [29] indicated that PM concentrations have negative correlation with wind speed, humidity and temperature in Karabük. Tecer et al. [31] found high correlation between particulate matter and relative humidity, cloudiness, and lower temperature at episodic events. Sari et al. [33] examined the relationship between the PM_{10}, $PM_{2.5}$, SO_2, CO, O_3, NO, NO_2, NO_x, and CH_4 concentrations and meteorological parameters (temperature, wind speed, wind direction, and relative humidity) in Bursa. They found strong correlations between pollutant concentrations and wind speed.

İstanbul, with its significant population growth, industrial activities, and traffic congestion, is one of Türkiye's most polluted cities. A high concentration of pollutants have been observed in recent years, due to population growth, industrial activities, and the use of low-quality fuel. Air pollution studies in industrial regions and settlements with a high pollutant source type variety and heavy concentration loads aid in the development of solutions to improve air quality.

This study aimed to examine the association between $PM_{2.5}$ and PM_{10} concentrations and meteorological parameters (average temperature, minimum temperature (Tmin), maximum temperature (Tmax), total precipitation, average relative humidity and average wind speed) in, Ümraniye and Silivri for 2014 to 2020.

MATERIALS AND METHOD

Description of Study Area

İstanbul is the major metropolitan city with 16 million population, located in the Marmara region (northwestern Türkiye) [34]. The city is divided into two sides by the Bosphorus and lies in both Europe and Asia. The total area of the city is 5.343 km^2. İstanbul is located at the latitude of 41.15984°N and longitude of 29.07412°E in the northern hemisphere, with an average altitude of 40 m from the sea level. İstanbul's climate is a transition between Mediterranean and Black Sea, with mild winters and hot summers [35]. Seasonal temperature values of Ümraniye district show that the highest average temperature was measured in summer with 23 °C and the lowest average temperature was measured in winter with 6.2 °C. Average temperatures were found as 16.4 °C in the autumn season and 12.9 °C in the spring season. In Silivri district, the highest average temperature was found in summer season as 22.6 °C and the lowest average temperature was found in winter as 5.7 °C. Average temperature was 15.9 °C in autumn and 12.6 °C in spring. When the seasonal precipitation data of Ümraniye is examined, the highest total precipitation was measured as 2179 mm in winter, followed by 1331 mm in autumn, 1000 mm in spring, and 911 mm in summer as the lowest. In Silivri, the highest total precipitation was 1219 mm in winter, followed by 1082 mm in autumn, 960 mm in spring and 807 mm in summer. When the two districts are compared in terms of precipitation, Ümraniye district receives more precipitation than Silivri district. When the wind rose chart of İstanbul province is examined, the prevailing wind direction is found as northeast, and the second dominant wind direction is found as southwest.

In İstanbul, air quality of the city decreases due to anthropogenic activities such as transportation, coal consumption and urban transformation and the environment and public health are adversely affected. Air pollution becomes a chronic problem in İstanbul due to population growth, expansion of city, destruction of nature and encouraging the use of individual vehicles instead of public transportation.

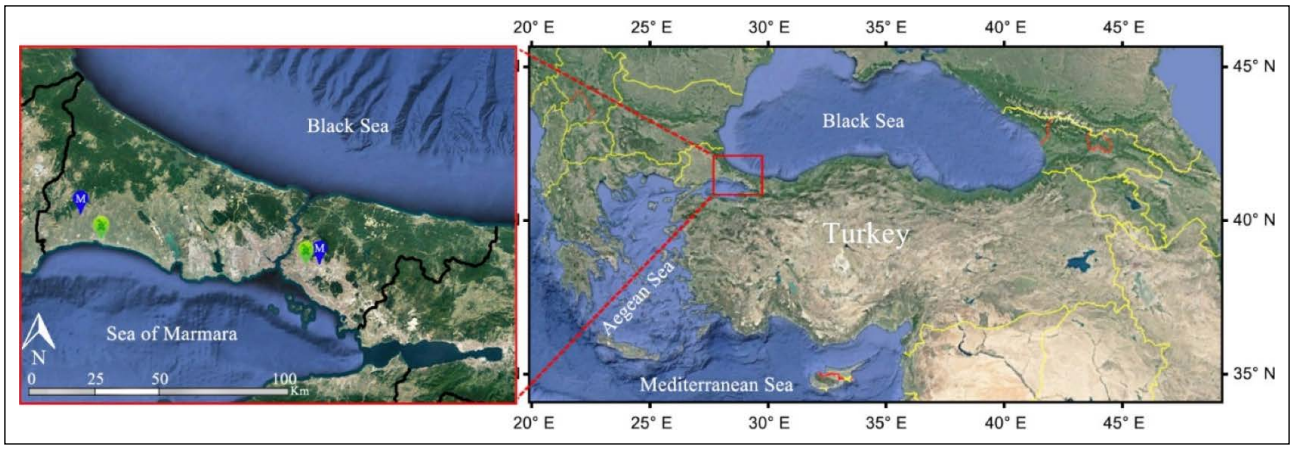

Figure 1. Locations of air quality monitoring stations (green) and meteorological stations (blue) in İstanbul.

Air Quality and Meteorological Data

Marmara Region (MR) is the most developed region of Türkiye. Industry, trade, tourism, and agriculture sectors take an important place compared to other regions. Therefore, MR faces more serious environmental and public health problems than other regions. For this reason, this study is carried out in the province of İstanbul, which is located in the MR, where the population and industrial activities are dense and traffic-related emissions are high. To investigate the relationship between $PM_{2.5}$ and PM_{10} concentration values and meteorological factors in İstanbul, hourly air quality data ($PM_{2.5}$ and PM_{10}) of Silivri and Ümraniye stations between 01/01/2014 and 31/12/2020 were obtained from National Air Quality and Monitoring Network database [36]. Furthermore, hourly wind speed (m/s), direction, temperature, minimum temperature, maximum temperature, total precipitation, relative humidity values of the meteorological stations, which are closest to the air quality stations, are provided by the Turkish State Meteorological Service. Meteorological data used in this study represent the characteristic meteorological properties of the pollutant source area. Missing air quality data are eliminated from the study. Figure 1 shows the locations of air quality monitoring stations and meteorological stations.

In order to preserve the environment and public health, limit values for $PM_{2.5}$ and PM_{10} pollutants have been determined by WHO, EU and various country. 24-hour average limit value of PM_{10} is 45 μg/m³ for WHO and 50 μg/m³ for EU [37, 38]. PM_{10} limit values in Türkiye have been gradually improved and leveled with the European Union regulation no 2008/50/EC starting from 2008. $PM_{2.5}$ is recognized as one of the most harmful air pollutants by the European Union and the World Health Organization. The daily limit values of $PM_{2.5}$ were set as 15 μg/m³ for WHO to protect the public from the health effects of particulate matter. In Türkiye, there is no legal limit value for $PM_{2.5}$ concentrations.

$PM_{2.5}$ and PM_{10} concentrations in the atmosphere vary depending on meteorological parameters (air temperature, wind speed and direction, relative humidity, precipitation, dew point temperature, average pressure, cloud cover and mixing layer). In this study, the effects of hourly wind speed (m/s), wind direction, average temperature, minimum temperature (Tmin), maximum temperature (Tmax), total precipitation and relative humidity on particulate matter values were investigated for Silivri and Ümraniye stations.

Statistical Analysis

Correlation matrix was used to analyze the strength of the association between $PM_{2.5}$ and PM_{10} concentrations and meteorological factors (wind speed, wind direction, temperature, minimum temperature, maximum temperature, total precipitation, relative humidity). All the statistical calculations and graphics were done using R version 3.1.2 [39].

RESULTS AND DISCUSSION

Table 1 shows the statistical information on air pollutants and meteorological parameters from 2014 to 2020 for Silivri station. The annual mean $PM_{2.5}$ and PM_{10} concentrations were calculated as 19.1 μg/m³ and 34.1 μg/m³, respectively.

The descriptive statistics of air pollutant sand meteorological parameters for Ümraniye station were shown in Table 2. The annual mean $PM_{2.5}$ and PM_{10} concentrations at Ümraniye station were both higher than Silivri station as 22.9 μg/m³ and 44.8 μg/m³, respectively.

When hourly PM_{10} values of Silivri station were seasonally analyzed, highest mean PM_{10} concentration was found as 38.6 μg/m³ in spring season followed by 35.5 μg/m³ in winter and 32.6 μg/m³ in autumn. In the spring and autumn months, there is intense dust transport to Türkiye with the effect of the Asiatic characteristics of surface low and it increases the particulate matter concentration [40]. The dry and hot air originating from the surface Asian monsoon low is the primary cause of dust storms during the summer and fall seasons. Arabian dust particles are transported to the region via dry hot air, leading to high levels of PM concentration during dust episodes [15]. The lowest mean value was measured in summer (11.1 μg/m³), similar to other studies [7]. When $PM_{2.5}$ value is examined, the highest average value was recorded in winter with 23.2 μg/m³, followed byspring (20.6 μg/m³), autumn (18.3 μg/m³) and summer (10.3 μg/m³) seasons. Many studies indicate that the con-

Table 1. The statistical information of air pollutants and meteorological parameters in Silivri, 2014–2020

Variables	Mean±SD	Min	P_{25}	P_{50}	P_{75}	Max
Particulate matter (μg/m^3)						
$PM_{2.5}$	19.1±10.2	3.2	12.2	15.9	22.8	80.4
PM_{10}	34.1±18.9	4.8	21.7	29.8	41.5	318.0
Meteorological factors						
Avg. relative humidity (%)	78.3±14.3	15.0	69.0	78.3	89.2	100
Avg. temperature (°C)	14.3±7.2	-7.7	7.2	14.5	21.1	28.2
Total precipitation (mm)	1.7±5.6	28.2	0	0	0.4	98.3
Avg. wind Speed (m/s)	4.1±1.7	1.1	2.7	3.8	5.2	13.1

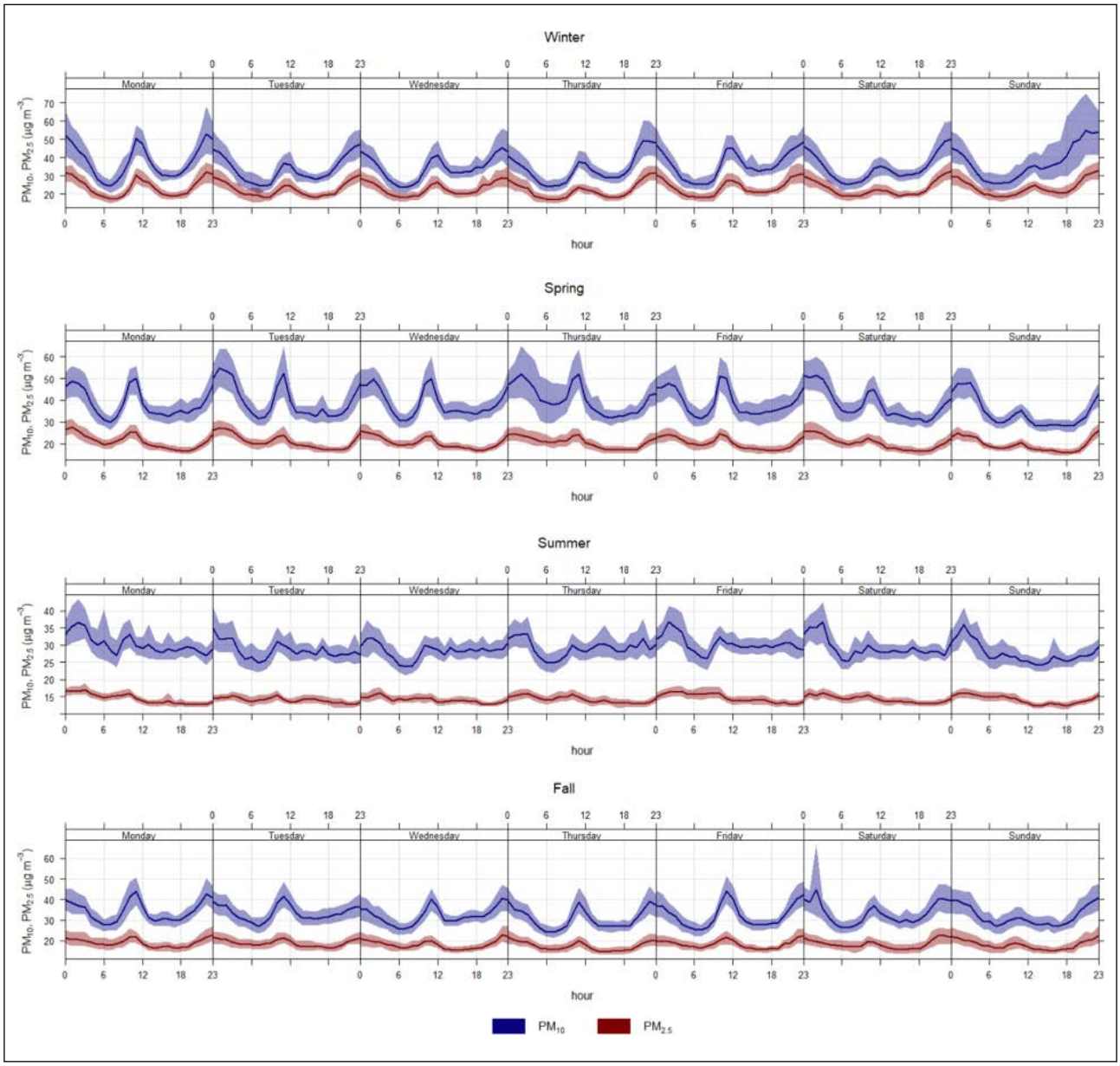

Figure 2. Seasonal variation of PM_{10} and $PM_{2.5}$ concentrations throughout the period 2014–2020 for Silivri Station (the blue lines show the values of PM_{10}, and the red line represents the values of $PM_{2.5}$).

centration of particulate matter is generally high during the winter months [41, 42]. When the hourly PM_{10} and $PM_{2.5}$ concentration variations are examined in Figure 2, the increase and decrease of pollutants show similar characteristics. The highest particulate matter concentration values were measured in winter, depending on local factors such

Table 2. The statistical information of air pollutants and meteorological parameters in Ümraniye, 2014–2020

Variables	Mean±SD	Min	P_{25}	P_{50}	P_{75}	Max
Particulate matter (μg/m³)						
$PM_{2.5}$	22.9±12.5	2.8	14.8	20.1	27.9	88.9
PM_{10}	44.8±24.3	5.7	28.8	39.6	54.8	315.1
Meteorological factors						
Avg. relative humidity (%)	77.4±14.8	3.0	68.7	78.7	88.4	100
Avg. temperature (°C)	14.8±7.3	-5.0	8.9	15.1	21.5	30.6
Total precipitation (mm)	2.2±5.7	0	0	0	1.2	77.5
Avg. wind Speed (m/s)	3.2±1.1	0	2.4	3	3.9	8.8

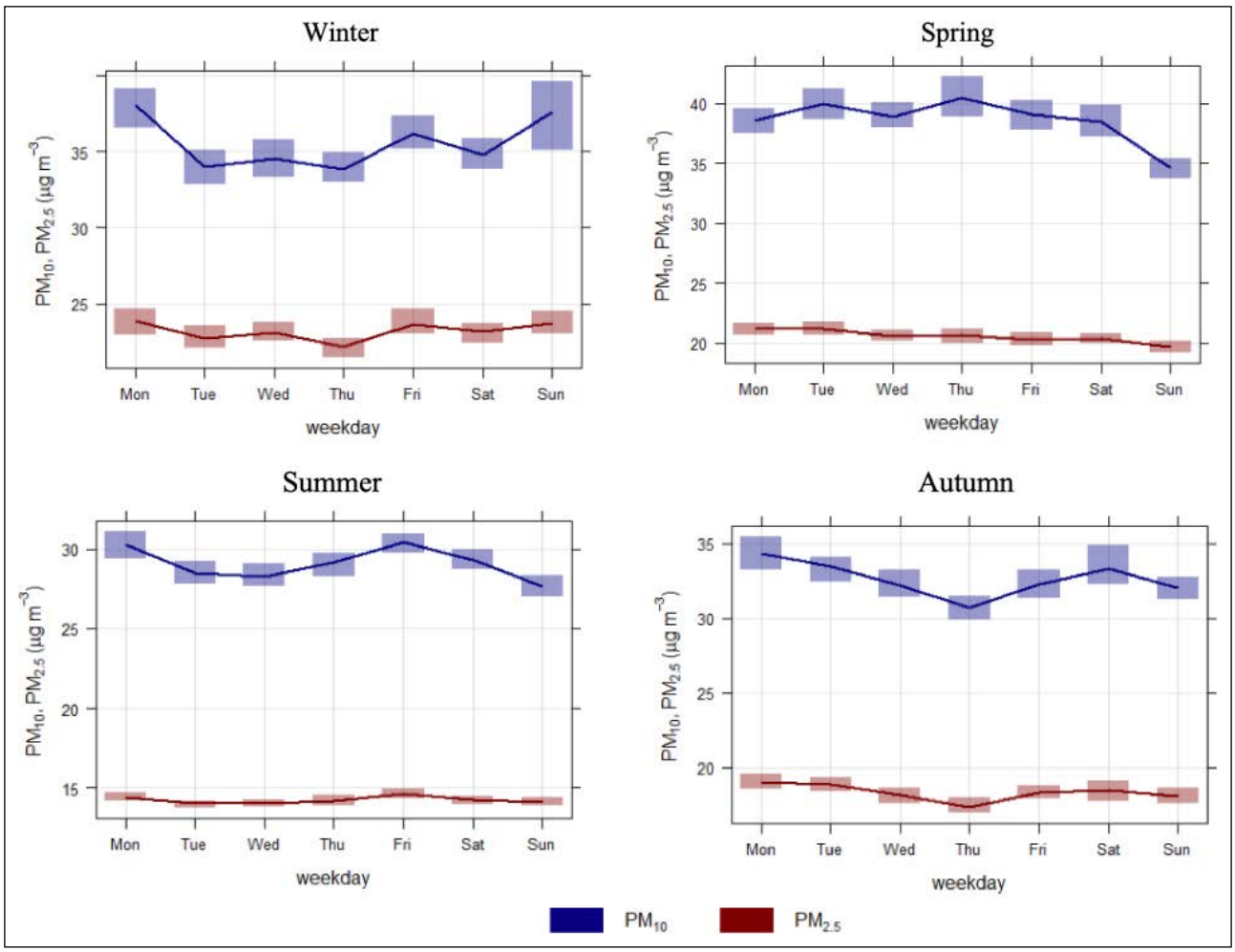

Figure 3. Daily variation of PM_{10} and $PM_{2.5}$ concentrations throughout the period 2014–2020 for Silivri Station (the blue lines show the values of PM_{10}, and the red line represents the values of $PM_{2.5}$).

as domestic warming. When particulate matter concentrations in the winter months were examined, pollutants show increase at noon and also in the evening hours. In the spring season, while the lowest values are recorded at 06:00 in the morning, increases are shown at noon and night hours. Higher pollutant amount was measured on Thursdays compared to other days of the week. The lowest particulate matter values are recorded in summer when PM_{10} and $PM_{2.5}$ values are more uniformly distributed. In autumn, PM_{10} values increase especially at midday (Fig. 2).

When the daily PM_{10} and $PM_{2.5}$ values at Silivri station are analyzed, it is seen that there is an increase in pollution on Sundays and Mondays in winter, Mondays and Fridays in summer, and Mondays and Saturdays in autumn, depending on traffic density (Fig. 3). In the spring season, the lowest particulate matter values were recorded on Sundays and a more uniform distribution is observed on other days.

When the hourly PM_{10} values of Ümraniye station are examined seasonally, the highest average PM_{10} concen-

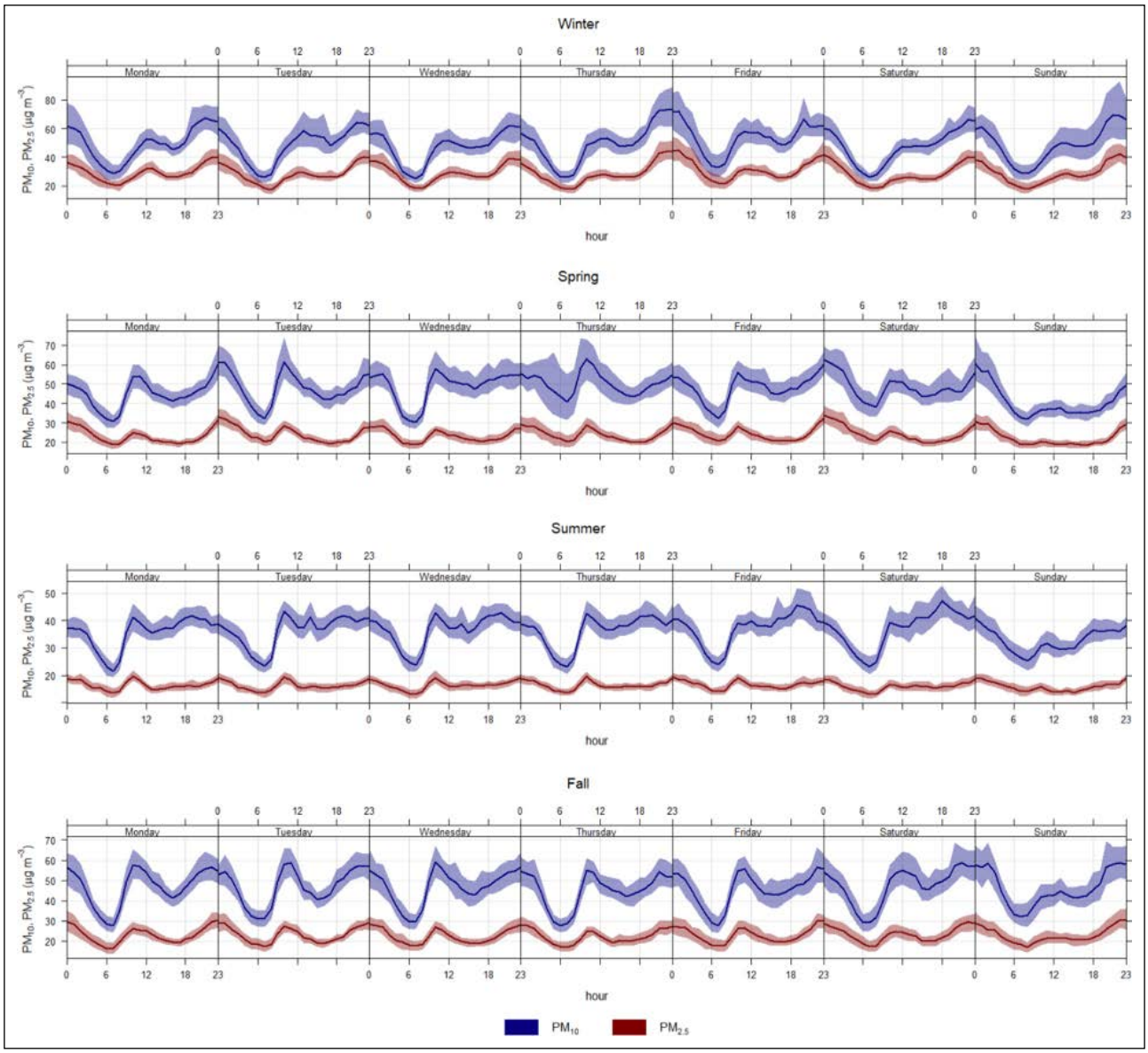

Figure 4. Seasonal variation of PM_{10} and $PM_{2.5}$ concentrations throughout the period 2014–2020 for Umraniye Station (the blue lines show the values of PM_{10}, and the red line represents the values of $PM_{2.5}$).

tration is recorded with 49.4 µg/m³ in winter, followed by 47.2 µg/m³ in spring and 46.5 µg/m³ in autumn. Particularly in the spring months, dust transport occurs and there is a significant increase in the concentration of particulate matter [14, 15, 43]. The lowest average value is measured in summer (40.0 µg/m³). Similar to PM_{10} values, $PM_{2.5}$ values are highest in winter (29.2 µg/m³) and lowest in summer (16.3 µg/m³).

When the hourly values of PM_{10} and $PM_{2.5}$ at Ümraniye station are examined seasonally, decreases in particulate matter values are observed between 00:00–06:00 due to low traffic activity. These values increase with the traffic density between 06:00 and 09:00. There is a similar increase related to traffic in the evening hours. In winter and autumn, pollutant values increase gradually, especially on weekends. The lowest values are measured around 6 am for all seasons (Fig. 4).

When daily PM_{10} and $PM_{2.5}$ values are examinedfor Ümraniye station, PM_{10} and $PM_{2.5}$ values show similar trends. There is a significant increase in traffic-related concentrations especially on Fridays in the winter season (Fig. 5). In the spring season, the highest particulate matter value is recorded on Thursdays, and the lowest value is recorded on Sundays. The lowest values are measured on Sundays in the summer season and on Thursdays in the autumn season (Fig. 5).

The level of particulate matter is higher in Ümraniye district than in Silivri district. Examining Ümraniye Station data with respect to European Union PM_{10} limit value (50 µg/m³) showed that 37% of autumn data, 35% of winter data, 33% of spring data and 15% of summer data exceeded the limit value. On the other hand, in Silivri Station, 22% of spring data, 18% of winter data, 13% of autumn data and 6% of summer data exceeded the limit value.

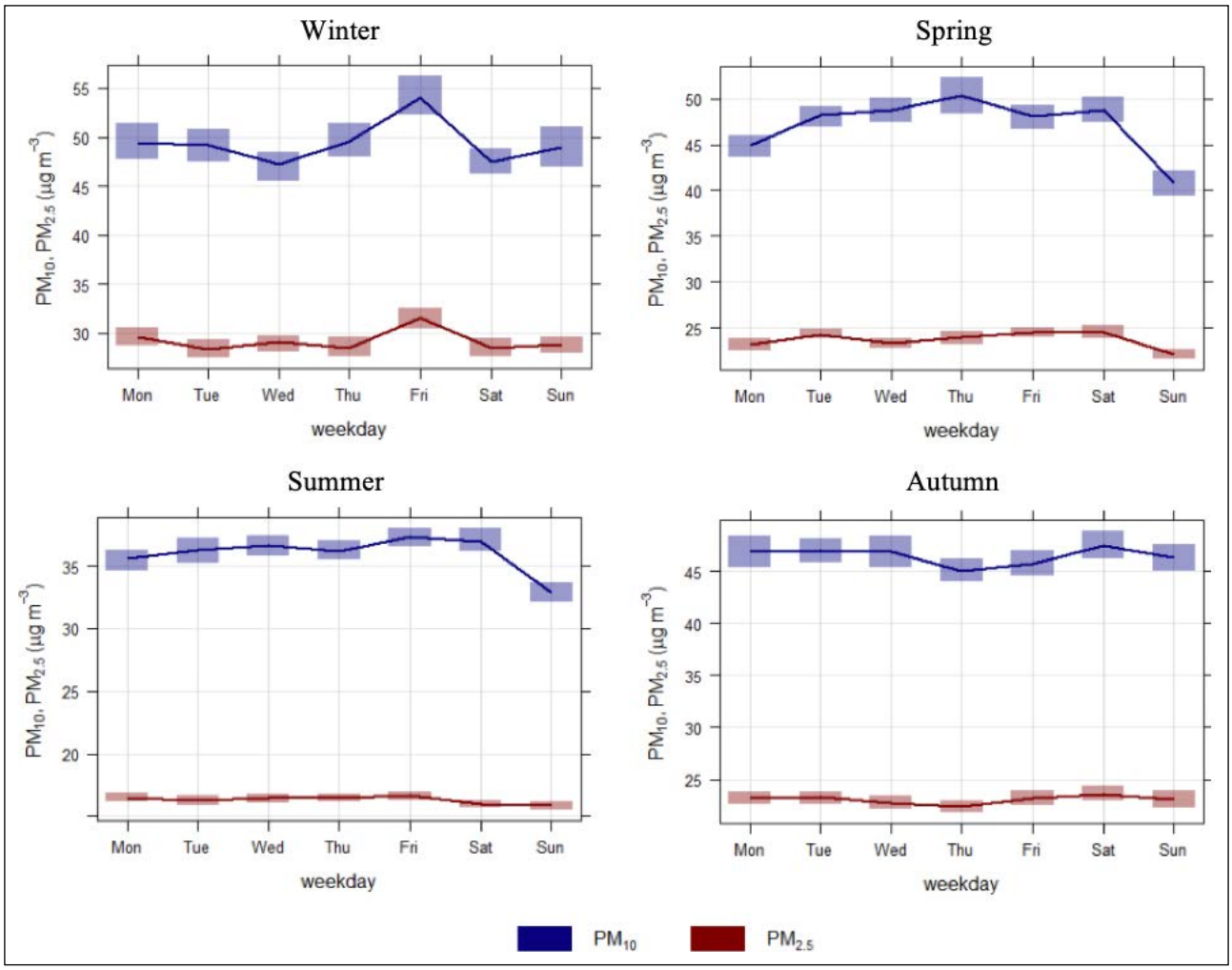

Figure 5. Daily variation of PM_{10} and $PM_{2.5}$ concentrations throughout the period 2014–2020 for Ümraniye Station (the blue lines show the values of PM_{10}, and the red line represents the values of $PM_{2.5}$).

Furthermore, while highest exceedance of limit values occurred in autumn season in Ümraniye Station, in Silivri Station highest exceedance was found in spring season.

In Figure 6, polar plots of PM_{10} and $PM_{2.5}$ are prepared to examine the relationship of pollutant concentrations with wind speed and wind direction. When the polar plots for the $PM_{2.5}$ concentration of Silivri and Ümraniye stations are examined, the highest $PM_{2.5}$ values are measured in winter due to domestic heating, while the lowest values are measured in summer. In winter, when the wind speed is less than 2 m/s, local factors significantly reduce the air quality of the region. In addition, when wind speed increases (2–8 m/s), the $PM_{2.5}$ concentration decreases. This indicates that a decrease in wind speed may restrict the dispersion of particulate matter, resulting in higher concentrations of $PM_{2.5}$. Conversely, an increase in the wind speed can help mitigate the accumulation of particulates, leading to a reduction in $PM_{2.5}$ concentrations. However, as the wind speed continues to escalate, an unexpected resurgence in PM concentration occurs. When the wind speed exceeds 8 m/s, southwestern dust transports increase the amount of particulate matter. In spring, summer and autumn seasons, generally local sources reduce the air quality of Silivri and Ümraniye.

When the polar plots of the PM_{10} values of Silivri and Ümraniye stations are examined, Figure 7 shows that when the wind speed is measured higher than 8 m/s in the winter season, the dust transports from the southwest increase the particulate matter value significantly. Pollution values were measured above the limit value (50 µg/m³) for 221 days in winter months, 213 days in spring months, and 234 days in autumn months due to local sources. When the polar plots of the summer season are examined, it is seen that the northerly transports increase the concentration of particulate matter at the Ümraniye station.

Figure 8 shows multiple correlation charts that are plotted to examine the relationship of PM_{10} and $PM_{2.5}$ values with meteorological factors seasonally. The highest negative correlation at Silivri station was calculated as r=-0.56 between $PM_{2.5}$ and wind speed in winter. In other seasons, correlations were found as r=-0.50 (spring), -0.37 (summer-spring). Wind speed is effective in dilution, dispersion and transport of particulate matter and reduces the concentration of particulate matter in the atmosphere. However, when the wind speed exceeds certain values, it can also reduce the air quality by caus-

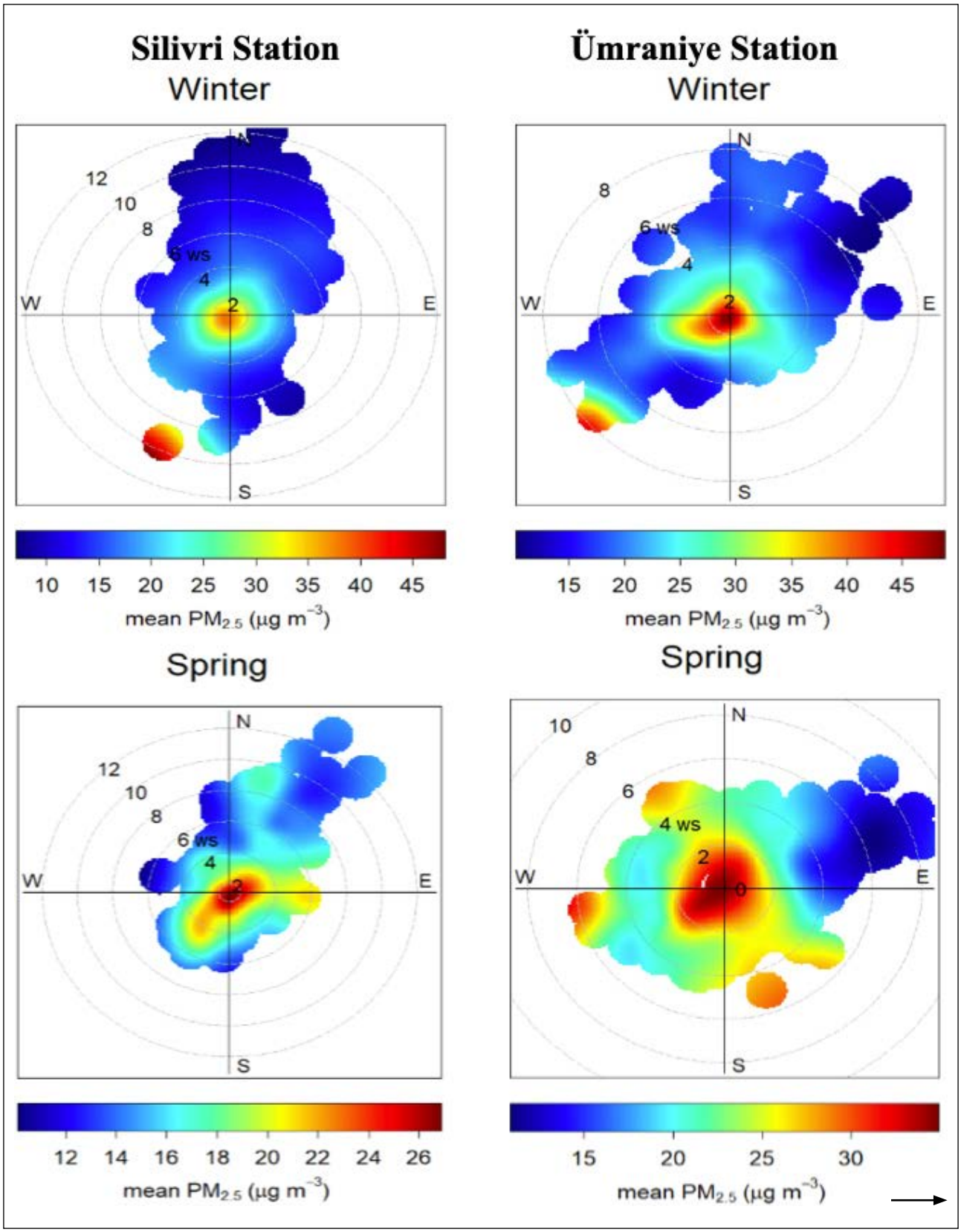

ing dust transport. In addition, a negative correlation (r=-0.43) was found between relative humidity and PM_{10} in the spring season. On the other hand, a positive correlation was found between especially Tmax values and PM_{10} (r=+0.40) and $PM_{2.5}$ (r=+0.38) in summer.

In Ümraniye station, a negative correlation (r=-0.48) was found between $PM_{2.5}$ and wind speed in autumn and winter seasons. The next highest correlation was calculated between PM_{10} and wind speed in winter (r=-0.38) and between $PM_{2.5}$ and wind speed in spring (r=-0.38).

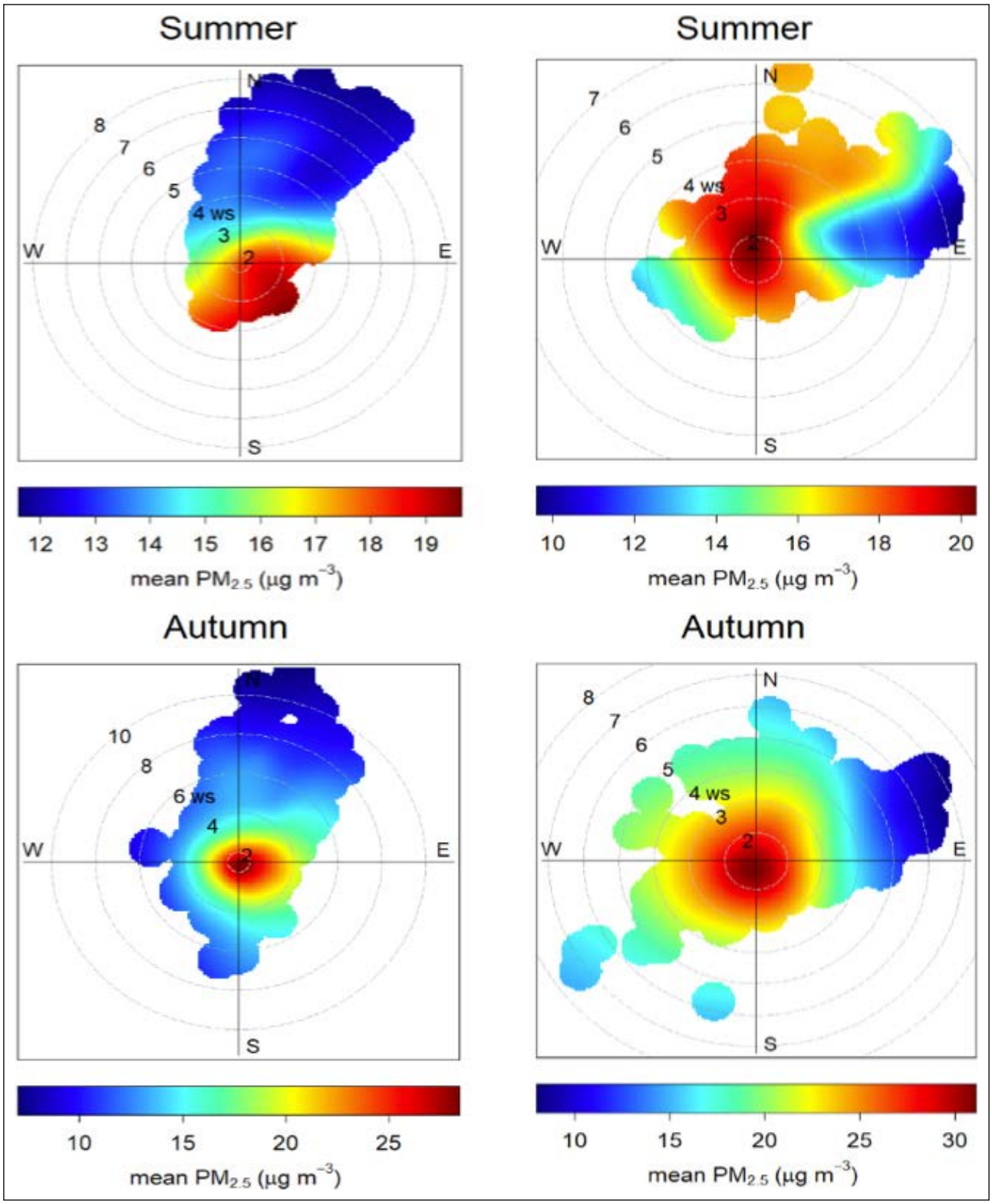

Figure 6. Seasonal polar plots of $PM_{2.5}$ mean concentrations for 2014–2020.

CONCLUSION

In recent years, the air pollutant values measured in İstanbul have risen significantly. The air pollution problem in İstanbul is increasing due to reasons such as population growth,rapid urbanization, vehicle emissions, industrial activities. Industrial and residential areas have various pollutant types and heavy pollutant loads. Air pollution studies carried out in these areas contribute to providing solutions to improve air quality. In this study, relationship between $PM_{2.5}$, PM_{10} and meteorological data (wind speed, wind direction, relative humidity, total precipitation, Tmin, Tmax, temperature) from Silivri and Ümraniye stations in İstanbul were analyzed spatially and temporally for 2014–2020 period.

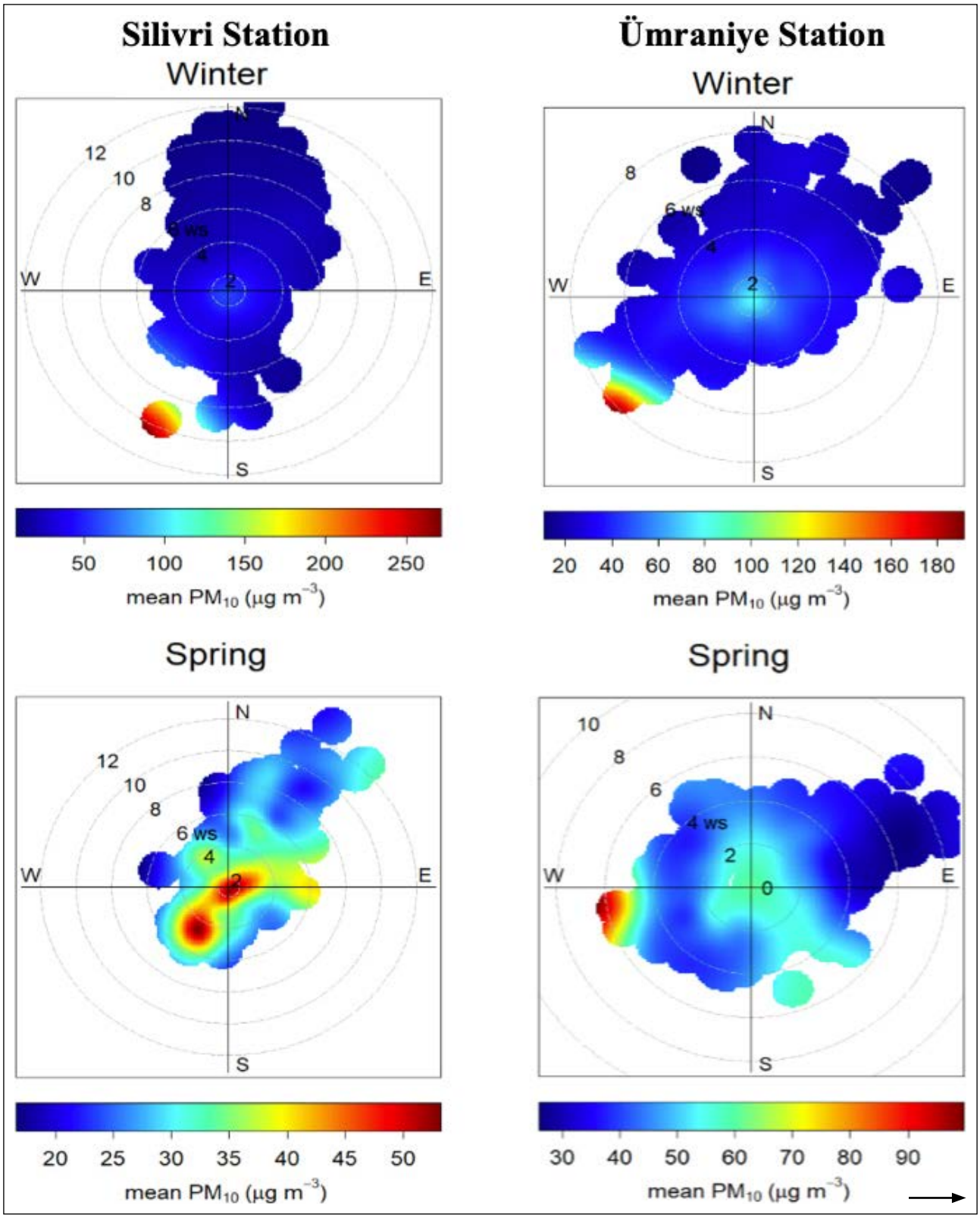

Diurnal analysis data shows that, the particulate matter concentration peaks between 09:00 and 19:00 LT in all seasons due to anthropogenic reasons such as vehicle emissions and residential heating. The highest particulate matter values were measured at Silivri station on Sundays in winter. At Ümraniye station, highest values were measured on Fridays depending on vehicle emissions. $PM_{2.5}$ values increase depending on local sources and low wind speeds. At speeds higher than 8 m/s, southerly winds increase PM_{10} values at Silivri and Ümraniye stations.

When the relationship between meteorological data and particulate matter for Silivri station in winter was examined, negative correlation (r=-0.56) was found,whereas for Ümraniye in winter season the negative correlation

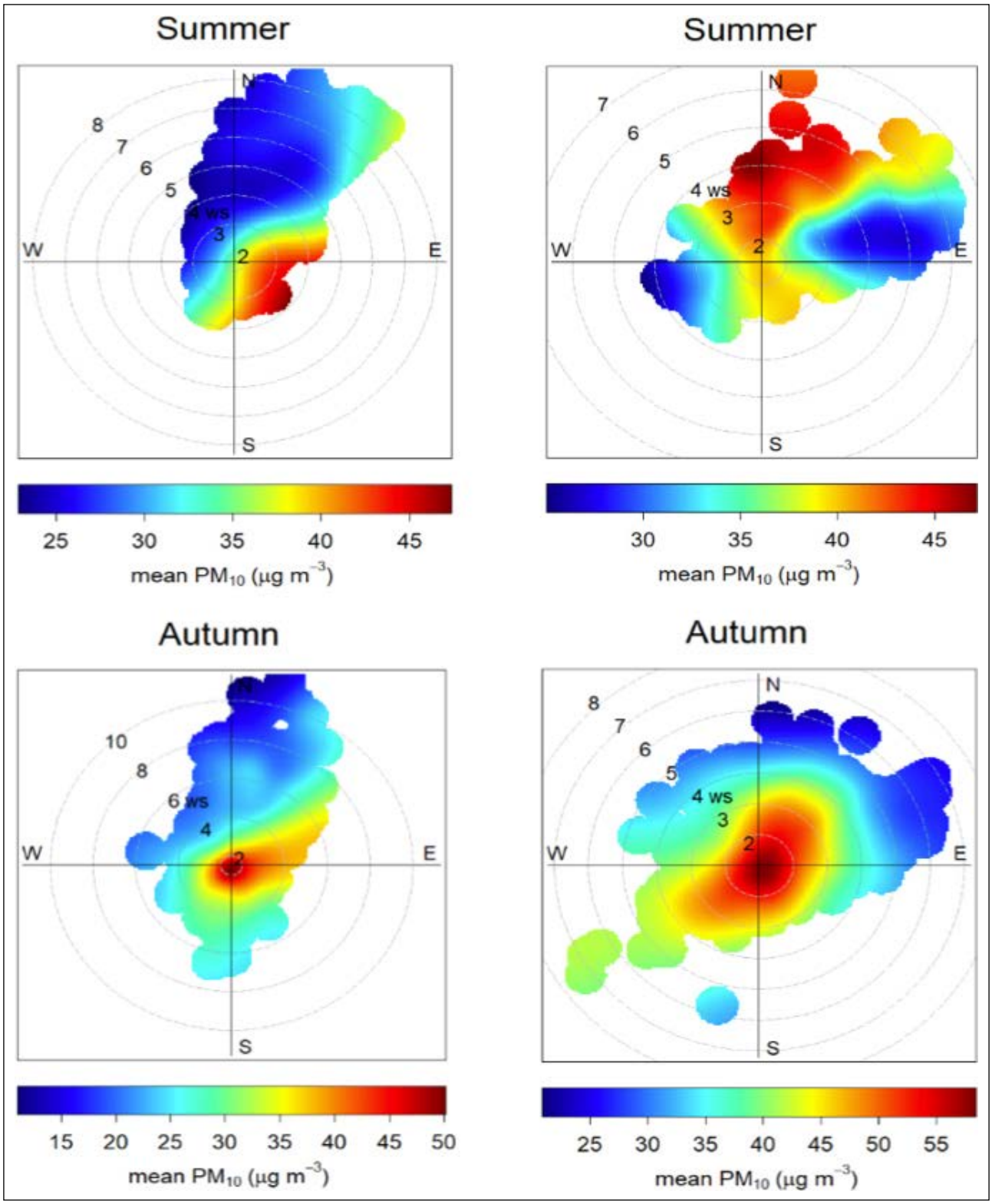

Figure 7. Seasonal polar plots of PM_{10} mean concentrations for 2014–2020.

(r=-0.48) was calculated for $PM_{2.5}$ and significantly weak relationship (r=-0.38) was calculated for PM_{10}. In addition to these, significantly weak correlation (r=-0.43) was found between relative humidity and PM_{10} in Silivri district in spring season. In addition to anthropogenic sources such as industrial activities and residential heating, meteorological factors also affect air quality significantly.

DATA AVAILABILITY STATEMENT

The authors confirm that the data that supports the findings of this study are available within the article. Raw data that support the finding of this study are available from the corresponding author, upon reasonable request.

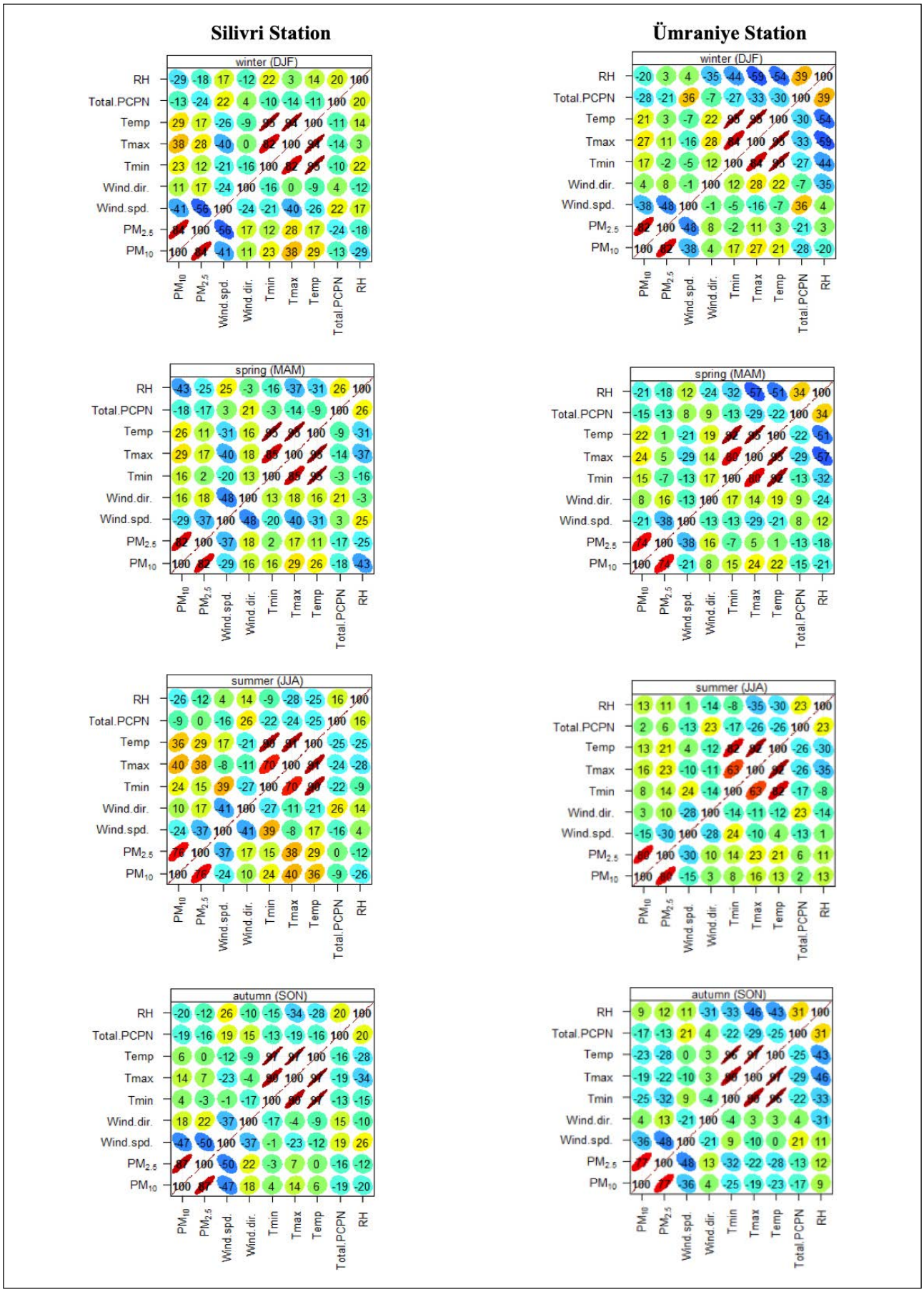

Figure 8. Correlation plots of PM_{10}, $PM_{2.5}$, wind speed, minimum temperature, maximum temperature, total precipitation, relative humidity usingly hourly data from January 2014 to December 2020 in İstanbul.

CONFLICT OF INTEREST

The authors declared no potential conflicts of interest with respect to the research, authorship, and/or publication of this article.

ETHICS

There are no ethical issues with the publication of this manuscript.

REFERENCES

[1] World HealthOrganization (WHO), "Ambient (Outdoor) Air Quality and Health," [Online]. Available: https://www.who.int/news-room/fact-sheets/detail/ambient-(outdoor)-air-quality-and-health. [Accessed: 2022].

[2] Z. Duan, X. Han, Z. Bai, and Y. Yuan, "Fine particulate air pollution and hospitalization for pneumonia: A case-crossover study in Shijiazhuang, China," Air Quality, Atmosphere & Health, Vol. 9(7), pp. 723-733, 2015. [CrossRef]

[3] L. Ding, D. Zhu, D. Peng, and Y. Zhao, "Air pollution and asthma attacks in children: A case–crossover analysis in the city of Chongqing, China," Environmental Pollution, Vol. 220, pp. 3482–353, 2017. [CrossRef]

[4] Y. Hao, G. Zhang, B. Han, X. Xu, N. Feng, Y. Li, W. Wang, H. Kan, Z. Bai, Y. Zhu, W. Au, and Z. Xia, "Prospective evaluation of respiratory health benefits from reduced exposure to airborne particulate matter," International Journal of Environmental Health Research, Vol. 27(2), pp. 126–135, 2017. [CrossRef]

[5] E. J. Jo, W. S. Lee, H. Y. Jo, C. H. Kim, J. S. Eom, J. H. Mok, M. H. Kim, K. Lee, K.U. Kim, M. K. Lee, and H. K. Park, "Effects of particulate matter on respiratory disease and the impact of meteorological factors in Busan, Korea," Respiratory Medicine, Vol. 124, pp. 79–87, 2017. [CrossRef]

[6] X. Xie, Y. Wang, Y. Yang, J. Xu, Y. Zhang, W. Tang, T. Guo, Q. Wang, H. Shen, Y. Zhang, D. Yan, Z. Peng, Y. Chen, Y. He, and X. Ma, "Long-term exposure to fine particulate matter and tachycardia and heart rate: Results from 10 million reproductive-age adults in China," Environmental Pollution, Vol. 242, pp. 1371–1378, 2018. [CrossRef]

[7] H. Baltaci, C. S. A. Ozgen, and B. O. Akkoyunlu, "Background atmospheric conditions of high PM_{10} concentrations in İstanbul, Turkey," Atmospheric Pollution Research, Vol. 11(9), pp. 1524–1534, 2020. [CrossRef]

[8] H. Arslan, H. Baltaci, A. U. Sahin, and B. Onat, "The relationship between air pollutants and respiratory diseases for the western Turkey," Atmospheric Pollution Research, Vol. 13(2), Article 101322, 2022. [CrossRef]

[9] International Agency for Research on Cancer World Health Organization (IARC), "Outdoor Air Pollution a Leading Environmental Cause of Cancer Deaths," No. 221, 2013.

[10] Q. Mu, and S.Q. Zhang, "An evaluation of the economic loss due to the heavy haze during January 2013 in China," Environmental Science, Vol. 33, pp. 2087–2094, 2013.

[11] M. Li, and L. Zhang, "Haze in China: Current and future challenges," Environmental Pollution, Vol. 189, pp. 85–86, 2014. [CrossRef]

[12] X. Hou, B. Zhu, K.R. Kumar, W. Lu, "Inter-annual variability in fine particulate matter pollution over China during 2013–2018: Role of meteorology," Atmospheric Environment, Vol. 214, Article 116842, 2019. [CrossRef]

[13] H. Baltaci, B. O. Akkoyunlu, H. Arslan, O. Yetemen, and E. T. Ozdemir, "The influence of meteorological conditions and atmospheric circulation types on PM_{10} levels in western Turkey," Environmental Monitoring and Assessment, Vol. 191(7),Article 466, 2019. [CrossRef]

[14] H. Baltaci, "Meteorological characteristics of dust storm events in Turkey," Aeolian Research, Vol. 50, Article 100673, 2021. [CrossRef]

[15] H. Baltaci, and Y. Ezber, "Characterization of atmospheric mechanisms that cause the transport of Arabian dust particles to the southeastern region of Turkey," Environmental Science and Pollution Research, Vol. 29, pp.2277–22784, 12021. [CrossRef]

[16] P. Zhang, B. Hong, L. He, F. Cheng, P. Zhao, C. Wei, and Y. Liu, "Temporal and Spatial Simulation of Atmospheric Pollutant $PM_{2.5}$ Changes and Risk Assessment of Population Exposure to Pollution Using Optimization Algorithms of the BackPropagation-Artificial Neural Network Model and GIS," International Journal of Environmental Research and Public Health, Vol. 12(10), pp. 1217–12195, 2015. [CrossRef]

[17] S. Faridi, M. Shamsipour, M. Krzyzanowski, N. Kunzli, H. Amini, F. Azimi, M. Malkawi, F. Momeniha, G. Gholampour, A. Hassanvand, M. S. Hassanvand, N. Naddafi, and K. Naddafi, "Long-term trends and health impact of $PM_{2.5}$ and O_3 in Tehran, Iran, 2006-2015," Environment International, Vol. 114, pp. 37–49, 2018. [CrossRef]

[18] W. F. Ye, Z. Y. Ma, and X. Z. Ha, "Spatial-temporal patterns of $PM_{2.5}$ concentrations for 338 Chinese cities," Science of the Total Environment, Vol. 631-632, pp. 524–533, 2018. [CrossRef]

[19] D. M. Leung, A. P. K. Tai, L. J. Mickley, J. M. Moch, A. van Donkelaar, L. Shen,and R.V. Martin, "Synoptic meteorological modes of variability for fine particulate matter ($PM_{2.5}$) air quality in major metropolitan regions of China," Atmospheric Chemistry and Physics, Vol. 18, pp. 6733–6748, 2018. [CrossRef]

[20] F. Huang, X. Li, C. Wang, Q. Xu, W. Wang, Y. Luo, L. Tao, J. Gao, S. Chen, K. Cao, L. Liu, N. Gao, X. Liu, K. Yang, A. Yan, and X. Guo, "$PM_{2.5}$ Spatiotemporal Variations and the Relationship with Meteorological Factors during 2013-2014 in Beijing, China," PlosOne, Vol. 10(11), Article e0141642, 2015. [CrossRef]

[21] S. Ausati, and J. Amanollahi, "Assessing the accuracy of ANFIS, EEMD-GRNN, PCR, and MLR models in predicting $PM_{2.5}$," Atmospheric Environment, Vol. 142, pp. 465–474, 2016. [CrossRef]

[22] L. Peng, X. Zhao, Y. Tao, S. Mi, J. Huang, and Q. Zhang, "The effects of air pollution and meteorological factors on measles cases in Lanzhou, China," Environmental Science and Pollution Research, Vol. 27, pp. 13524–13533, 2020. [CrossRef]

[23] T. Kindap, "Identifying the trans-boundary transport of air pollutants to the city of İstanbul under specific weather conditions," Water, Air, and Soil Pollution, Vol. 189, pp. 279–289, 2008. [CrossRef]

[24] Y. Lyu, Z. Qu, L. Liu, L. Guo, Y. Yang, X. Hu, Y. Xiong, G. Zhang, M. Zhao, B. Liang, J. Dai, X. Zuo, Q. Jia, H. Zheng, X. Han, S. Zhao, and Q. Liu, "Characterization of dustfall in rural and urban sites during three duststorms in northern China," Aeolian Research, Vol. 28, pp. 29–37, 2010. [CrossRef]

[25] X. Li, Y. Ma, Y. Wang, N. Liu, and Y. Hong, "Temporal and spatial analyses of particulate matter (PM_{10} and $PM_{2.5}$) and its relationship with meteorological parameters over an urban city in northeast China," Atmospheric Research, Vol. 198, pp. 185–193, 2017. [CrossRef]

[26] Z. Li, Y. Wang, Z. Xu, and Y. Cao "Characteristics and sources of atmospheric pollutants in typical inland cities in arid regions of central Asia: A case study of Urumqi city," PLOS ONE, Vol. 16(4), Article e0249563, 2021. [CrossRef]

[27] M. Ansari, and M. H. Ehrampoush, "Meteorological correlates and AirQ+ health risk assessment of ambient fine particulate matter in Tehran, Iran," Environmental Research, Vol. 170, pp. 141–150, 2018. [CrossRef]

[28] E. Oguz, M. D. Kaya, and Y. Nuhoglu, "Interaction between air pollution and meteorological parameters in Erzurum, Turkey," International Journal of Environment and Pollution, Vol. 19(3), Article 292, 2003. [CrossRef]

[29] M. B. Celik, and I. Kadi, "The Relation Between Meteorological Factors and Pollutants Concentrations in Karabük City," Gazi University Journal of Science, Vol. 20(4), pp. 87–95, 2007.

[30] Y. Icaga, and E. Sabah, "Statistical Analysis of Air Pollutants and Meteorological Parameters in Afyon, Turkey," Environmental Modeling Assessment, Vol. 14, pp. 259-266, 2009. [CrossRef]

[31] L. H. Tecer et al., "Effect of meteorological parameters on fine and coarse particulate matter mass concentration in a coal-mining area in Zonguldak, Turkey," Journal of the Air Waste Management Association, Vol. 58(4), pp. 543–552, 2008. [CrossRef]

[32] U. A. Sahin, B. Onat, Ö. Akın, C. Ayvaz, B. Uzun, N. Mangır, M. Doğan, R. M. Harrison, "Temporal variations of atmospheric black carbon and its relation to other pollutants and meteorological factors at an urban traffic site in İstanbul," Atmospheric Pollution Research, Vol. 11(7), pp. 1051–1062, 2020. [CrossRef]

[33] M. F. Sari, Y. Tasdemir, and F. Esen, "Major air pollutants in Bursa, Turkey: their levels, temporal changes, interactions, and sources," Environmental Forensics, Vol. 20(2), pp. 182–195, 2019. [CrossRef]

[34] Turkish Statistical Institute (TUIK), 2021. https://biruni.tuik.gov.tr/medas/

[35] İstanbul Metropolitan Municipality, 2021. https://www.iklim.İstanbul/iklim/

[36] National Air Quality and Monitoring Network database (NAQMS), 2021. http://www.havaizleme.gov.tr/Services/AirQuality

[37] WHO, "WHO global air quality guidelines. Particulate matter ($PM_{2.5}$ and PM_{10}), ozone, nitrogen dioxide, sulfur dioxide and carbon monoxide," World Health Organization, 2021.

[38] European Council, "On Ambient Air Quality and Cleaner Air for Europe 2008/50/EC," Off. J. Eur. Union, vol. 1, pp. 1-44, 2008. https://eur-lex.europa.eu/legal-content/EN/TXT/PDF/?uri=CELEX-:32008L0050&from=en

[39] R Core Team, "A Language and Environment for Statistical Computing," R Foundation for Statistical Computing, Vienna, 2015. http://www.R-project.org/

[40] Turkish State Meteorological Service (TSMS), 2021. https://www.mgm.gov.tr/FILES/arastirma/modeller/toz-tasinimi.pdf

[41] M. Á. García M. L. Sanchez, A. de Ios Rios, and B. Fernandez-Duque, "Analysis of PM_{10} and $PM_{2.5}$ concentrations in an urban atmosphere in Northern Spain," Archives of Environmental Contamination and Toxicology, Vol. 76, pp. 331–345, 2019. [CrossRef]

[42] O. A. Sindosi, G. Markozennas, E. Rizos, and E. Ntzani, "Effects of economic crisis on air quality in Ioannina, Greece," Journal of Environmental Science Health, Part A, Vol. 54(8), pp. 768–781, 2019. [CrossRef]

[43] H. Baltaci, H. Arslan, and B. O. Akkoyunlu, "High PM_{10} source regions and their influence on respiratory diseases in Canakkale, Turkey," International Journal of Environmental Science and Technology, Vol. 19, pp. 797–806, 2022. [CrossRef]

Environ Res Tec, Vol. 6, Issue. 4, pp. 302–307, December 2023

Environmental Research and Technology
https://ert.yildiz.edu.tr - https://dergipark.org.tr/tr/pub/ert
DOI: https://doi.org/10.35208/ert.1244226

Research Article

Long chain fatty acid (LCFA) occurrence in primary and secondary sewage sludge fractions

Dilek ERDİRENÇELEBİ*

Department of Environmental Engineering, Konya Technical University, Konya, Türkiye

ARTICLE INFO

Article history
Received: 29 January 2023
Revised: 15 August 2023
Accepted: 12 September 2023

Key words:
Anaerobic digestion; Inhibition; Long chain fatty acids; Sewage sludge

ABSTRACT

Sewage sludge produced in municipal wastewater treatment plants (WWTPs) is stabilized to produce methane/energy and a final stabilized biosolid suitable for land use using anaerobic digestion (AD) process. Fat, oil, and grease (FOG) matter present in the sewage sludge and their products, long chain fatty acids (LCFA), are not monitored qualitatively and quantitatively for their contribution or inhibition to methane production during the process. AD is designed and operated based on average volatile solid (VS) removal criteria. LCFA can be both present in the sewage sludge and produced as intermediate products during the hydrolysis of FOG. A 1.5-year monitoring of the primary sludge (PS) and secondary sludge (SS) fractions was conducted and evaluated in a timely base in a municipal WWTP. According to the results, the most common and highest presence belonged to palmitate (C16:0) and total LCFA occurred up to 11963 and 927 mg/L in PS and SS, respectively. Detected LCFA species were mostly saturated as laurate, myristate, palmitate, stearate, oleate and elaidate. The level in the mixed sludge feed complied with the inhibitory threshold values neglecting the accumulation in the anaerobic digesters.

Cite this article as: Erdirençelebi D. Long chain fatty acid (LCFA) occurrence in primary and secondary sewage sludge fractions. Environ Res Tec 2023;6(4)302–307.

INTRODUCTION

Sewage sludge produced in municipal wastewater treatment plants (WWTPs) contains fatty matter from both municipal and industrial origins as fat, oil and grease (FOG) and long chain fatty acids (LCFA) accumulated during the treatment of municipal wastewater [1]. LCFA are the products of hydrolysis of FOG and exist in its presence. Oil and grease is a standardized parameter of FOG for wastewater discharges into the sewage collection system due to its clogging effect in the pipeline and toxicity towards the biological treatment units in the end of the sewage system. FOG tends to adsorption on the particulate matter and mostly settles out with the sewage sludge. Organic stabilization of the sewage sludge through anaerobic digestion (AD) converts 40–50% of volatile solids (VS) into methane and CO_2 gas providing a considerable recovery of energy in a 18–25 d of hydraulic retention time (HRT) reducing high operational costs in municipal WWTPs [2, 3]. FOG is converted with a higher yield to methane (1 m^3/kg) compared to proteins (0.63 m^3/kg) and carbohydrates (0.42 m^3/kg), therefore, it is a favorable waste type for AD [1]. Optimum process performance needs to be determined based on process parameters in relation to LCFA threshold values.

LCFA is not a routine pollutant/parameter monitored qualitatively and quantitatively in the sewage sludge fractions and effluent stabilized sludges. They are present in the raw sewage sludge and produced as intermediate products during the anaerobic hydrolysis of FOG. Scum

***Corresponding author.**
*E-mail address: derdirencelebi@ktun.edu.tr

This paper has been presented at Sixth EurAsia Waste Management Symposium (EWMS 2022)/İstanbul, Türkiye / 24–26 October 2022.

formation was related to LCFA as an operational problem in anaerobic digesters [4]. Inhibition was mostly related to high C-number LCFA (>C10) as they accumulated in the sludge due to slow degradation. Inhibition due to oleate (C18:1) started at 0.5 g/L concentration with a higher degree than 50% on the unadapted granular sludge inoculum and palmitate (C16:0) was formed as the main product [5]. The reversibility of the inhibition was obtained in the batch study and revealed that adaptation to LCFA presence by the methanogens was advantageous in the digestion of lipids. A concentration range of 1.154–1.55 g/L for capric acid (C10) was reported as the biocidal threshold value for acetogens and methanogens with no adaptation ability of aceticlastic methanogens [6]. Pereira et al. [7] evidenced irreversibility of the inhibition on methanogens at LCFA concentration of 1–5 g COD-LCFA/g VSS as LCFA were biodegraded. Toxic effect of oleate (C18:1), linoleate (C18:2), palmitate (C16:0), and stearate followed the substrate inhibition pattern [8]. A low concentration range of 40–100 mg LCFA/L reported in the sewage sludge by Quémeneur and Marty was not representative as different types and levels of LCFA can be found depending on the urban activities (local food sector) and industrial wastewater intrusion as substantial sources for FOG/LCFA [9]. The types and concentrations of LCFA vary according to the type of industrial origins. LCFA that was detected at the highest amounts in wastewater and wastes were oleate (C18:1) and linoleate (C18:2) [4]. Oleate, linoleate, palmitate and stearate occurred in the proportions of 37, 13, 27 and 7%, respectively, in the composition of the dairy industry wastewater while other species were present only at the level of 16% in total. Palmitate and stearate were found in high concentrations in slaughterhouse wastewater and stearate in domestic wastewater from vegetable oil. Palmitic, palmitoleic and eicosapentanoic acids were found at a high level in palm and fish oils. As the chain length-C number of LCFA augments their solubility in water decreases and tendency to adsorption on solids/particles increases. In municipal WWTPs, LCFA are adsorbed on to the primary sludge (PS) in the pre-sedimentation unit and secondary (waste biological sludge) sludge (SS) in the biological treatment unit [1]. LCFA concentration is expected to rise through sludge thickening where PS and SS are mixed and thickened to increase the VS content in the feed to anaerobic digesters. The reduction in the methane yield as organic loading rate (OLR) increases without rise in the volatile fatty acids (VFA) was reported as a sign of LCFA accumulation and inhibition in the anaerobic digesters [10, 11].

As sewage sludge is formed mostly in two fractions, the LCFA's qualitative and quantitative contents require investigation and were determined and evaluated in the PS and SS samples collected in a municipal WWTP serving a metropolitan area for a 1.5-year period in this study. The characterization was aimed to indicate seasonal changes and accumulation pattern, and enable a comparison to threshold values for inhibitory effect as well as the difference in contents in the actual sewage sludge samples.

Table 1. Characterization of the sewage sludge samples

Sludge	pH	TS (g/L)	VS (g/L)	Oil and grease (%VS)
PS	6.3–7.0	40–60	25–35	66–75
SS	7.2–8.0	7–10	6–8	29-35

MATERIALS AND METHOD

The samples were taken from the primary settling tank's sludge outlet and the sludge recycle of the biological treatment unit for PS and SS, respectively, from January 2018 to the end of April 2019 in Konya municipal WWTP which served an equivalent population of 1.2 million. The WWTP had an average flow rate of 160000 m^3/d receiving wastewaters both from domestic (major source) and industrial sources (minor source mostly dairy, slaughterhouse and animal husbandry). The suspended solid concentration of the inlet wastewater ranged at 450–650 mg/L. The biological treatment unit consisted of a Bardenpho process with partial nitrogen removal operated at a sludge age between 14–17 d. The samples contained a high level of oil and grease as presented in the Table 1. Standard methods for VS (2540 E) and oil and grease (5520-E soxhlet extraction) were applied to PS and SS samples [12]. PS contained fatty matter at a 70 (+/-5)% of its VS content more than double the level for SS. Drying and esterification procedures were carried out for LCFA analysis in the sludge samples. The sludge drying method was developed by Neves et al. [13] and was applied at 85 °C for 12 h. According to Sönnichsen and Müller, LCFA esterification was carried out on a 20 mg of dry sludge sampled which was weighed and mixed directly with the methanolic HCl, methanol and hexane and the esterification process was performed for 1 h at 100 °C [14]. After the addition of hexane and water, the upper filtrate phase of 1 ml was directed to GC/FID analysis (Shimadzu 17A VP3 and Agilent FFAP 30 m x 0.250 mm x 0.25 μm capillary column). The temperature program started at 100 °C (5 mn) and increased to 240 °C with a rate of 4 °C/mn. The injection mode was 1:2 split. The injector and detector temperature was adjusted to 240 °C. Nitrogen was the carrier gas. F.A.M.E. (Free Acis Methyl ester) Mix, C8 - C22, certified reference material, (ampule of 100 mg (Neat)) from Supelco (CRM18920; Foreign Trade Commodity Code: 38229000000) and Supelco 37 Component FAME Mix TraceCERT® (in dichloromethane (varied conc.), ampule of 1 mL; CRM47885; Foreign Trade Commodity Code: 38229000000) standards were used for the identification and confirmation of the LCFA.

RESULTS AND DISCUSSION

LCFA are low in water solubility as 7.2 and 2.9 mg/L for palmitic and stearic acids, respectively at 20 °C [15]. Unsaturated LCFA are relatively more soluble in water (linoleic acid at 160 mg/L (6.7 °C). This property makes LCFA adsorp onto the particles, raw and microbial cells, and limit their degradation by bacterial species. That is the reason for LCFA

accumulation at a high level onto the PS during the transportation through sewerage systems. Floating particles that escape primary settlers enters the biological treatment units and settle out with the bacterial flocs, undegraded through the activated sludge process. Once fed into the anaerobic digesters, LCFA undergo beta-oxidation releasing H_2 and acetate (and propionate for odd-numbered C-LCFA) at each cleavage stage [16]. Syntrophic acetogens (*Syntrophomonadaceae*) carry out the reaction which proceeds by the H_2 and acetate conversion to methane by hydrogenotrophic and aceticlastic methanogens, respectively, where H_2 utilization is faster and promotes the overall reaction. Acetate conversion is more prone to inhibition due to the responsible archae's sensitivity [17]. Completely mixed reactor configuration such as anaerobic sludge digesters is the advantageous reactor type due to high dilution and HRT to overcome the inhibitory effects of LCFA which will tend to accumulate onto the biomass. The importance of monitoring LCFA in the feed and effluent of ADs lies in the determination of the optimum HRT and OLR that will allow the maximum conversion to methane, especially in the case of thermophilic ADs which are subject to accumulation of VFAs as intermediate products, pH drop and instability due to fastened hydrolysis, higher solubility of LCFA and beta-oxidation resulting in propionate and acetate accumulation [18]. Inhibition by LCFA affects directly acetogens and methanogens but may not be reflected as VFA accumulation but lowered methane production. The amount of LCFA present in the feed sludge needs to be determined especially before the design of the HRT value for thermophilic digesters and any consideration for shortened retention in the ADs.

LCFA species obtained in the raw sludge samples were determined at a very high level in PS samples compared to SS in terms of concentration and number of species (Fig. 1a, b). Total number of 16 species in PS outnumbered 11 of SS also in concentration. Total LCFA occurred up to 11963 and 927 mg/L in PS and SS, respectively. Palmitate was the most common and highest concentration LCFA found in both PS and SS samples reaching 40–55% of the total LCFA concentration. It is likely that high levels of the unsaturated C-18 LCFAs in the FOG material were converted to palmitate as a result of hydrolysis and hydrogen saturation reactions in wastewater and PS samples, and/or use of palm oil dominated the food sector in the metropolitan area. Palmitate was reported as the main product from oleate degradation with a tendency to accumulate on the biomass [19]. Stearate and oleate were second and third, respectively, in the quantity and frequency which were higher in the months of summer compared to other seasons indicating trends in food consumption. Palmitate ranged between 1800–4400 mg/L in PS samples whereas stearate occurred mostly under 1000 mg/L with some peaks reaching 2000 mg/L in the summer months and oleate ranged below 250 mg/L with peaks reaching 1000 mg/L in the summer time. The other common LCFA were myristate (6–11%), palmitoleate (1–9%), elaidate (3–4%), laurate (2–3%), linoleate (1–5%) and pentadecanoate (%1–2). Two heavy LCFAs with C22 and 24 were detected at 1500–2000 mg/L and 500 mg/L occasionally, in the summer months, indicating mineral oil intrusions into the sewage line. Detected LCFA species indicated a high degree of consumption of vegetable oils and animal fat reflecting a current profile resulting from urban activities. Oleate was reported as the most toxic LCFA and palmitate was found accumulated on the cell surface as the first product of its beta-oxidation due to low degradation caused by the inhibited acetogens and methanogens [19]. Saturated species formed the most of the total LCFA indicating an overall slow degradation rate for the subsequent AD.

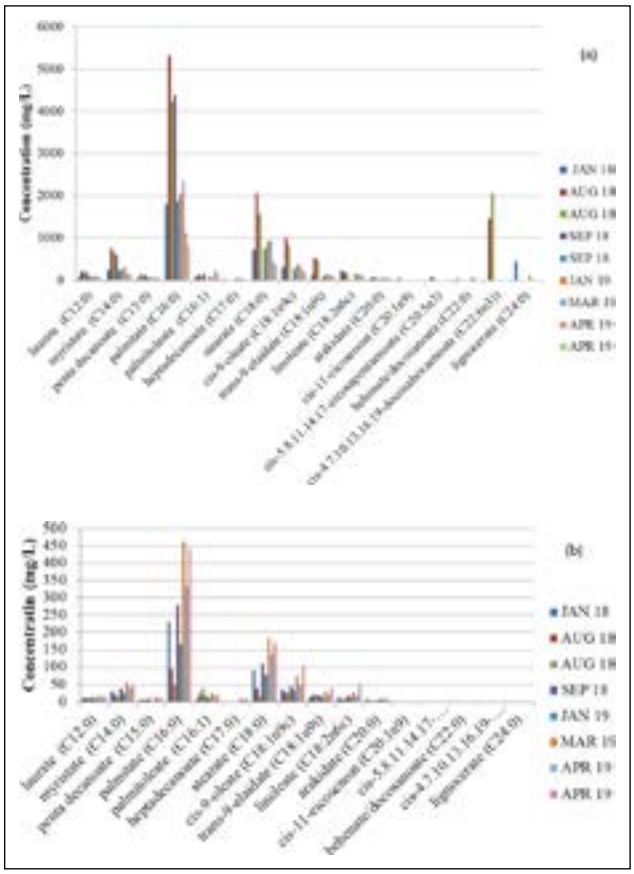

Figure 1. LCFA detected in **(a)** PS and **(b)** SS samples as concentration.

Palmitate, stearate and oleate ranged at 100–450, 80–170 and 44–100 mg/L in SS samples independently from time of the year (Fig. 1b). Palmitate was obtained below 1/10th compared to PS making 26–51% of the total LCFA. All LCFA except palmitoleate were at low concentration ranges in the summer months. Similar percentages were obtained for LCFA except palmitoleate, oleate, elaidate. The descending order in concentration was as palmitate, stearate, oleate, myristate, palmitoleate, elaidate and linoleate (40–57 mg/L), laurate, hepta- and pentadecanoate. The highest number of C was 20 as arachidate at a very low concentration detected occasionally. Total LCFA concentration range (186–927 mg/L) was large but in competence with anaerobic biomass tolerance. The pattern of LCFA occurrence was similar to PS at a lower level in concentration and number and also significant in that LCFA were transported to the biological activated sludge unit in the WWTP. The floating ability of

Table 2. LCFA concentrations (mg/L) calculated in the mixed sludge after thickening

LCFA	Jan 18	Aug 18	Aug 18	Sep 18	Jan 19	Mar 19	Apr 19	Apr 19
Laurate (C12:0)	57	134	131	104	42	60	61	46
Myristate (C14:0)	158	458	400	377	143	188	197	118
Penta decanoate (C15:0)	31	80	66	68	30	41	37	36
Palmitate (C16:0)	1174	3237	2561	2749	1198	1415	1535	844
Palmitoleate (C16:1)	42	82	69	91	4	64	43	140
Heptadecanoate (C17:0)	21				24	31	29	7
Steareta (C18:0)	474	1256	940	48	480	616	624	331
cis-9-oleate (C18:1n9c)	199	617	505	21	165	246	242	186
trans-9-elaidate (C18:1n9t)	83	323	289	11	62	90	91	73
Linoleate (C18:2n6c)	137	120	91	10	6	106	84	97
Arachidate (C20:0)	33	46	39	4	29	28	39	29
cis-11-eicosenoate (C20:1n9)	37							
cis-5.8.11.14.17-eicosapentaenoate (C20:5n3)		47	28					
Behenate/docosanoate (C20:0)	24					30	30	
cis-4.7.10.13.16.19-docosahexaenoate (C22:6n3)		875	1237					
Lignocerate (C24:0)	268					69		
Total	2738	7275	6356	3483	2183	2984	3012	1907

the FOG/LCFA may have been the possible path for their transportation and intrusion into the biological sludge. Another observation was that palmitate's highest presence was opposite as in summer in PS and winter in SS.

When PS and SS are mixed in the sludge thickeners the LCFA concentration sum up to a range of 1907–7275 mg/L for which a conventional dilution rate (1/HRT) of 0.05 (+/- 0.005) complies with the threshold values if their accumulation and synergistic effect in the digester is neglected (Table 2). However, slow degradation of high-C number LCFA will result in accumulation to some degree in the anaerobic digesters. Saturated C16:0 and C14:0 LCFA were reported to accumulate from the degradation of Linoleic acid (C18:2) [20]. Also, individual LCFA concentrations are still higher than reported values in previous inhibition studies on aceticlastic methanogens: linoleic acid (C18:2) that is commonly found in vegetable oils fully deactivated acetate conversion to methane at a 30 mg/L level and IC_{50} was increased up to 137 mg/L for oleic acid after an adaptation was developed on methanogens [20, 21]. Optimization studies on mono- and co-digestion of PS and SS indicated that an optimum OLR allowed a maximum conversion to methane with the highest methane yield outcome, higher OLRs induced an inhibitory effect with the absence of VFA accumulation and temperature increase did not enhance methane yield but VS removal, all outcome in competence with LCFA inhibition being noticeable above a threshold OLR or accumulation degree [10, 11]. As Cavaleiro et al. [22] reported higher degradation rates for unsaturated LCFA and slower rates for saturated LCFA as products, anaerobic digestion of PS and SS necessitated high HRT due to expected slow degradation rates of the products and their efficient conversion to methane. Regarding the lower LCFA content in the SS, higher HRT comes out as a necessity in PS digestion for which mono-digestion may offer a better solution in municipal WWTPs. Alternatively as thermophilic sludge digestion, the profile and level of the LCFA detected especially in PS samples pointed out to a potential hazard in case of a possible conversion to thermophilic operation for which LCFA intolerance was reported at a much higher degree [23, 24]. Oleate was reported less inhibitory than free oleic acid meaning that lower pH than 6.0 presents a toxic environment leading to conversion to free acid forms and necessity for pH or OLR control in thermophilic sludge digestion [23].

CONCLUSIONS

The study reported an actual characterization of LCFA in a long time base in a real-scale municipal WWTP serving a metropolitan area. Total number of LCFA species and maximum concentrations were respectively 16 and 11963 mg/L for PS and 11 and 927 mg/L for SS produced prior to AD. Palmitate was the most common LCFA with the highest concentration found in both PS and SS samples reaching 40–55% of the total LCFA concentration. Palmitate showed the highest presence in summer in PS opposite to SS. Palmitate, stearate and oleate were the most common and high concentration LCFA species. Other LCFA occurred at low concentration ranges especially in the summer months. The results indicated a significant adsorption and accumulation pattern on the PS solids pointing out to both industrial intrusion of FOG and heavy mineral oils banned from discharge and dense social activities such as intense food/restaurant sector having a high usage of vegetable oils and

animal fat in a highly populated metropolitan area. LCFA content consisted mostly of saturated species meaning that slow degradation rates and accumulation in the anaerobic digesters and stabilized sludge should be expected. The concentration levels in PS reflected a seasonal change and were above inhibitory levels for any biological process where a conventional dilution rate (1/HRT) of 0.05 (+/-0.005) complied with the threshold values for mixed sludge if their augmentation in the sludge thickener (with a possible start of anaerobic hydrolysis reaction), synergistic effect and accumulation in the digester were neglected. This emphasized the importance of the dilution degree in the feeding of anaerobic digesters as high HRTs/low OLRs are needed for maximizing the dilution and biodegradation time, thus, biomethanation efficiency, as non-degraded LCFA are prone to be present in the final stabilized biosolid and affect their final disposal method. The future study needs to focus on the accumulation and/or synergistic effects of LCFA and optimization of the operational parameters for mono-digestion of PS and SS in municipal WWTPs. A secondary investigation in the biological unit of the municipal WWTPs not having primary settling units (not producing PS) would enlighten any inhibitory level of LCFA for the activities the activated sludge biomass.

Acknowledgements
The research was financed by the Selçuk University BAP Coordinatorship under the Project number 17401118.

DATA AVAILABILITY STATEMENT

The author confirm that the data that supports the findings of this study are available within the article. Raw data that support the finding of this study are available from the corresponding author, upon reasonable request.

CONFLICT OF INTEREST

The author declared no potential conflicts of interest with respect to the research, authorship, and/or publication of this article.

ETHICS

There are no ethical issues with the publication of this manuscript.

REFERENCES

[1] Water Environment Federation, "Industrial Wastewater Management, Treatment, and Disposal," WEF Manual of Practice No. FD-3, 3rd edition, Alexandria, 2008.

[2] G. Tchobanoglous, F. L. Burton, and H. D. Stensel, "Wastewater engineering: treatment, disposal and reuse," Edited by Metcalf and Eddy. McGraw Hill Press, 2003.

[3] D. Erdirencelebi, and M. Kucukhemek, "Diagnosis of the anaerobic reject water effects on WWTP operational characteristics as a precursor of bulking and foaming," Water Science and Technology, Vol. 71(4), pp. 572–579, 2015. [CrossRef]

[4] M. M. Alves, M. A. Pereira, D. Z. Souza, A. J. Cavaleiro, P. Merjin, H. Smidt, and A. J. M. Stams, "Waste lipids to energy: how to optimize methane production from long-chain fatty acids (LCFA)," Microbial Biotechnology, Vol. 2(5), pp. 538–550, 2009. [CrossRef]

[5] J. Palatsi, R. Affes, B. Fernandez, M. A. Pereira, M. M. Alves, and X. Flotats, "Influence of adsorption and anaerobic granular sludge characteristics on long chain fatty acids inhibition process," Water Research, Vol. 46, pp. 5268–5278, 2012. [CrossRef]

[6] A. Rinzema, M. Boone, K. V. Knippenberg, and G. Lettinga, "Bactericidal effect of long chain fatty acids in anaerobic digestion," Water Environment Research, Vol. 66(1), pp. 40–49, 1994. [CrossRef]

[7] M. A. Pereira, D. Z. Sousa, M. Mota, and M. M. Alves, "Mineralization of LCFA associated with anaerobic sludge: kinetics, enhancement of methanogenic activity, and effect of VFA," Biotechnology Bioengineering, Vol. 88, pp. 502–511, 2004. [CrossRef]

[8] S.-H. Kim, S.-K. Han, and H.-S. Shin, "Kinetics of LCFA inhibition on acetoclastic methanogenesis, propionate degradation and β-oxidation," Journal of Environmental Science and Health, Part A, Vol. A39(4), pp. 1025–1037, 2004. [CrossRef]

[9] M. Quémeneur, and Y. Marty, "Fatty-acids and sterols in domestic wastewaters," Water Research, Vol. 28, pp. 1217–1226, 1994. [CrossRef]

[10] D. Erdirençelebi, and C. Bayhan, "Feasibility and potential of separate anaerobic digestion of municipal sewage sludge fractions," Water SA, Vol. 46(1), pp.123–130, 2020. [CrossRef]

[11] D. Erdirençelebi, and G. M. Ebrahimi, "Enhanced sewage sludge treatment via parallel anaerobic digestion at the upper mesophilic level," Journal of Environmental Management, Vol. 320, Article 115850, 2022. [CrossRef]

[12] American Public Health Association (APHA), "Standard Methods for the Examination of Water and Wastewater (21st ed.)," APHA, AWWA and WEF, Washington, 2005.

[13] L. Neves, M.A. Pereira, M. Mota, and M.M. Alves, "Detection and quantification of long chain fatty acids in liquid and solid samples and its relevance to understand anaerobic digestion of lipids," Bioresource Technology, Vol. 100, pp. 91–96, 2009. [CrossRef]

[14] M. Sönnichsen, and B. W. Müller, "A rapid and quantitative method for total fatty acid analysis of fungi and other biological samples," Lipids, Vol. 34(12), pp. 1347–1349, 1999. [CrossRef]

[15] J. T. Yoke III, "The solubility of calcium soaps," Journal of Physical Chemistry, Vol. 62(6), pp. 753–755, 1958. [CrossRef]

[16] R. H. Abeles, P. A. Frey, and W. P. Jencks, "Biochemistry," Jones and Bartlett Publishers, Boston, 1992.

[17] M. M. Alves, J. A. Mota Vieira, R. M. Álvares Pereira, M. A. Pereira, and M. Mota, "Effects of lipids and oleic acid on biomass development in anaerobic fixed-bed reactors. Part II: oleic acid toxicity and biodegradability," Water Research, Vol. 35(1), pp. 264–270, 2001. [CrossRef]

[18] J. Jiang, L. Li, M. Cui, F. Zhang, Y. Liu, Y. Liu, J. Long, and Y. Guo, "Anaerobic digestion of kitchen waste: The effects of source, concentration, and temperature," Biochemical Engineering Journal, Vol. 135, pp. 91–97, 2018. [CrossRef]

[19] M. A. Pereira, O. C. Pires, M. Mota, and M. M. Alves, "Anaerobic degradation of oleic acid by suspended sludge: identification of palmitic acid as a key intermediate," Water Science and Technology, Vol. 45(10), pp. 139–144, 2002. [CrossRef]

[20] J. A. Lalman, and D. M. Bagley, "Anaerobic degradation and inhibitory effects of linoleic acid," Water Research, Vol. 34(17), pp. 4220–4228, 2000. [CrossRef]

[21] M. M. Alves, J. A. Mota Vieira, R. M. Alvares Pereira, M. A. Pereira, and M. M. Mota, "Effects of lipids and oleic acid on biomass development in anaerobic fixed-bed reactors. part ii: oleic acid toxicity and biodegradability," Water Research, Vol. 35(1), pp. 264–270, 2001. [CrossRef]

[22] A. J. Cavaleiro, D. Z. Sousa, and M. M. Alves, "Methane production from oleate: Assessing the bioaugmentation potential of Syntrophomonas zehnderi," Water Research, Vol. 44, pp. 4940–4947, 2010. [CrossRef]

[23] I. Angelidaki, and B. K. Ahring, "Effects of free long-chain fatty acids on thermophilic anaerobic digestion," Applied Microbiology and Biotechnology, Vol. 37, pp. 808–812, 1992. [CrossRef]

[24] J. Palatsi, J. Illa, F.X. Prenafeta-Boldú, M. Laureni, B. Fernandez, I. Angelidaki, and X. Flotats, "Long-chain fatty acids inhibition and adaptation process in anaerobic thermophilic digestion: Batch tests, microbial community structure and mathematical modelling," Bioresource Technology, Vol. 101, pp. 2243–2251, 2010. [CrossRef]

Environ Res Tec, Vol. 6, Issue. 4, pp. 308–316, December 2023

Environmental Research and Technology
https://ert.yildiz.edu.tr - https://dergipark.org.tr/tr/pub/ert
DOI: https://doi.org/10.35208/ert.1341951

Research Article

Enhancement of the environmental bio-economy by investigating a sustainable cerbera odollam biodiesel at a low heat rejection engine

Anbazhagan RAMANUJAM*, Naveenchandran PANCHACHARAM

Department of Automobile Engineering, Bharath Institute of Higher Education and Research, Chennai, India

ARTICLE INFO

Article history
Received: 12 August 2023
Revised: 09 September 2023
Accepted: 16 September 2023

Key words:
Biodiesel; Bio economy; Diesel engine; Cerbera odollam seed; Nano coating; Low heat rejection engine

ABSTRACT

It is essential to maintain the environment by preserving the ecological balance of the area and keeping an eye on emission regulations. It's common knowledge that fossil fuels are the backbone of the transportation industry. Over time, the atmospheric concentrations of carbon and nitrogen oxides have risen dramatically due to human activities, particularly the burning of fossil fuels at excessive rates. Long-term sustainability may be attainable with the implementation of a bio-based, circular economy. Fears of a future fuel shortage and the negative effects on the environment spurred researchers to search for more sustainable energy sources. Renewability, reduced emissions, biodegradability, and better lubricating characteristics are just some of the reasons why biodiesel is becoming increasingly popular as a viable alternative to petroleum diesel. In this research paper, biodiesel extracted from cerbera odollam seeds was tested for its performance and emission characteristics on a low-heat rejection diesel engine with its piston coated with nano coating. The results were compared with those of a standard diesel engine, BCO25 at coated piston engine enhances break thermal efficiency by over 5.5%, consumes less fuel by 6.4%, reduces CO by 5.9%–10.7%, and reduces UBHC by 4% to 8.5%.

Cite this article as: Ramanujam A, Panchacharam N. Enhancement of the environmental bio-economy by investigating a sustainable cerbera odollam biodiesel at a low heat rejection engine. Environ Res Tec 2023;6(4)308–316.

INTRODUCTION

The preservation of the regional ecological balance and the implementation of vigilant emission controls are considered to be of utmost importance in ensuring environmental protection. The successful transition to a circular bio-economy can be achieved through the incorporation of global inclusiveness in the establishment of an organizational framework. This framework would be responsible for facilitating knowledge sharing, establishing global testing standards, evaluating the demand and supply of bio-based products, and providing support for research and development in biotechnology with the aim of commercialization [1].

The global bio-economy summit provides a definition of bio economy as the utilization of biological resources, implementation of new biological processes, and adherence to sustainable principles to facilitate the creation and provision of goods and services across many economic sectors, all of which are founded on knowledge. This concept elucidates that the bio economy is founded upon two fundamental pillars: resource efficiency and the substitution of fossil fuel-derived feedstock, as well as advancements in the field of biotechnology. Therefore, the bio economy enhances the worth of biomass resources, and an examination of the economic advantages of a specific resources [2, 3].

***Corresponding author.**
*E-mail address: anbazhaganbiher@gmail.com

At now, the majority of biodiesel production in the commercial sector mostly relies on edible oils, notably soybean oil, rapeseed oil, and palm oil, as the primary feedstock for the synthesis of fatty acid methyl esters. Hence, biodiesel is engaged in a competition for scarce land resources with the food business, as both sectors rely on the cultivation of the same oil crops. Consequently, the current practice involves allocating arable land for the cultivation of fuel crops rather than for food production. Consequently, the increased cost of edible oil will result in a higher price for biodiesel, rendering its production economically impractical when compared to petroleum-based diesel fuel. To address this challenge, numerous scholars have initiated investigations into more cost-effective and non-consumable oils as potential substitutes for biodiesel production feedstock [4, 5].

Despite the possibility of exaggerated price hikes in biodiesel and edible oils, the ongoing discourse about the allocation of feedstock production for either food or fuel persists. The practice of converting cooking oil into biodiesel has recently attracted attention and criticism from environmental advocates. The proliferation of edible oil crop plantations, necessary for the large-scale production of biodiesel, is associated with deforestation and ecological degradation [6, 7]. The production of biodiesel from vegetable oil introduces a conundrum in balancing the demands of energy consumption and nutritional requirements. The current situation is characterized by a scarcity of available land, which has led to a competition between the production of biodiesel from edible oil and other land-intensive activities. The aforementioned phenomenon is currently observed in various regions across the globe, wherein extensive areas of land are being utilized for the cultivation of oil crops as a direct response to the increasing need for the production of biodiesel. The utilization of biodiesel derived from edible oils as a substitute for petroleum diesel oil possesses the capacity to deplete the global reserves of edible oils over an extended period of time [8, 9].

Researchers worldwide have conducted numerous studies to explore sustainable and renewable feed stock for the manufacture of biodiesel, aiming to address this discouraging issue. Second-generation biofuels encompass the utilization of waste oil to produce biodiesel. The feedstock utilized in second-generation biofuel production comprises non-edible plant sources, including jatropha, rubber seed, jojoba, tobacco seed, cerbera odollam, neem, candlenut, mahua, karanja, and yellow oleander. In the manufacturing of biodiesel, animal fats such as chicken fat, swine lard, and cattle tallow can also be utilized. In recent years, there has been a growing interest in utilizing waste edible oils, such as used cooking oils, as viable for the creation of biodiesel [10–12].

To effectively address sustainability challenges, it is imperative to establish a bioeconomy that is truly sustainable, rather than simply a bioeconomy. The present state of the bioeconomy continues to heavily depend on non-renewable energy sources and fossil-derived raw materials, such as nitrogen fertilizers, organic chemicals, and polymers, which are primarily derived from petroleum oil and gas. The establishment of a sustainable bioeconomy encompasses more than simply replacing non-renewable fossil resources with renewable alternatives. It necessitates the implementation of sustainable practices in the production of biomass feedstock, the conversion of biomass, and the development of sustainable bio-based products [13, 14].

The implementation of a circular economy that is based on bio-resources has the potential to contribute significantly to the attainment of sustainable development in the long run. This paper outlines five ecological principles that govern the utilization of biomass within a circular bioeconomy. The principles encompassed in this framework involve the conservation and rehabilitation of ecosystems, the avoidance of unnecessary products and the minimization of waste for essential items, the prioritization of biomass resources for basic human needs, the utilization and recycling of by-products from ecosystems, and the adoption of renewable energy sources with a focus on reducing energy consumption. The implementation of these concepts necessitates a comprehensive overhaul of our economic framework, encompassing policy reforms, technological advancements, organizational restructuring, shifts in social conduct, and market dynamics [15, 16].

The potential influence of biofuels on heat and electricity applications is expected to be substantial in the foreseeable future. Despite notable progress in diesel engine technology, the thermal efficiency of a traditional diesel-fueled engine continues to fall short of 35%. The primary cause of this phenomenon can be traced to the dissipation of heat from the engine. For several years, there has been a notable emphasis on the adoption of low heat rejection (LHR) engine technology as a strategy to mitigate heat dissipation from engines [17, 18]. In the study conducted by [19] the NOx emission saw a notable rise during engine running as a result of the synergistic effects of oxygenated biodiesel and ceramic coating applied to the piston crown. The findings indicate that the utilization of a 15% Exhaust Gas Recirculation system with a Thermal Barrier Coating (TBC) Piston in a normal diesel engine fuelled by Rape seed biodiesel leads to a reduction of 3.5% in brake thermal efficiency. Additionally, there is an observed rise of 2.8% in hydrocarbon emissions, 4% in carbon monoxide emissions, 2% in smoke emissions, and 6.2% in nitrogen oxide emissions.

The experiment employed free fatty acid methyl ester biodiesel from discarded frying oil. Biodiesel fuel works in diesel engines without modification since its qualities are comparable to diesel fuel. Thermal barrier coating is yttrium-stabilized zirconia. Experimentally, B20 was the best biodiesel-diesel blend since it possessed diesel-like qualities and reduced emissions. This study used a greaves diesel engine with and without heat barrier coating. In the diesel engine without thermal barrier coating, all biodiesel blends had lower braking power and higher brake specific fuel consumption than diesel fuel across the load range. All biodiesel mixes emit lower HC, CO, and greater CO2 and NOx than diesel [20, 21]. Various types of coatings, such as yttrium-stabilized zirconia, magnesium-stabilized zirconia, and gadolinium zir-

conate, were employed in the experimental procedure involving the utilization of soup nut biodiesel. The performance of biodiesel in terms of engine fuel consumption and emission efficiency was evaluated on a coated engine [22].

Diethyl ether (DEE) on the performance and emissions of a thermal-barrier-coated (TBC) engine running on papaw) and eucalyptus oil mixes. The DEE-adapted CPME30Eu70 mix had 32.2% BTE, while diesel had 31.8%, 1.2% more than at normal operation. Compared to a non-coated CPME30Eu70 engine, DEE lowered BSEC and BSFC by 8.9 and 7.2%, respectively. DEE-CPME30Eu70 reduced nitrogen oxide emissions. After DEE addition, CPME30Eu70's carbon monoxide and hydrocarbon emissions were 0.195% vol. and 38 ppm, 13.3 and 5.1% lower than with a compression ignition engine. DEE enhanced CPME30Eu70's atomization and spray. The CPME30Eu70-powered engine also improved performance and emissions [23, 24]. Ceramic TBCs insulate the base material and safeguard the source at high temperatures. This study examines 500-micron-thick yttrium-stabilized zirconia (YSZ). Plasma-sprayed bond coat. Diesel and mahua biodiesel are tested in a diesel engine under varied loads. This study shows brake thermal efficiency increases with BSFC decrease. The LHR engine emits more NOx but less HC and CO [25].

The main aim of this study is to assess the viability of employing biodiesel derived from Cerbera odollam oil (BCO) as a potential alternative energy source for boiler and industrial fuel applications. In order to address the issues pertaining to the performance and emissions of biodiesel-derived crude oil (BCO) in a diesel engine, the implementation of a thermal barrier coating on the piston head is considered to be of great significance. In this study, the utilization of a zirconia nano-coated piston is examined in the context of a single-cylinder diesel engine as low hear rejection (LHR) engine. The primary objectives of this investigation are to assess the benefits of utilizing the zirconia nano-coated piston in terms of reducing exhaust pollution, enhancing engine performance, and improving fuel consumption efficiency. In this experiment, the biodiesel derived from Cerbera odollam oil was blended with diesel at volume ratios of 25% and 50%. The performance and exhaust emission characteristics of these blends were assessed using the normal and LHR pistons testes at diesel engine.

MATERIAL AND METHODS

The Apocynaceae family includes the tree that is commonly known as the cerbera odollam. The seed of this noxious, fibrous-kernelled fruit contains a substantial quantity of oil. The fruit itself is deadly. Due to the fact that cerbera odollam contains oil that is inedible, this fruit could be considered for use as a source of non-edible feedstock in the manufacturing of biodiesel [26]. The height of these evergreen trees may range from 6 to 15 meters; have dark green, spiraling leaves; and egg-shaped fruits, which are 5 to 10 centimeters in length. The spirals of glossy dark green leaves have an ovoid form. The blooms have a pleasant aroma and have a white, five-lobed tubular corolla that is between 1.2 and 2.0 inches in diameter, with a pink or red throat.

Table 1. Properties of base diesel and biodiesel of cerbera odollam oil

Properties of fuel	Units	Diesel	Biodiesel of cerbera odollam oil
Calorific value	MJ/kg	45.5	38.5
Density	kg/m^3	832	847.9
Kinematics viscosity	mm^2/s	2.82	3.15
Cetane number	-	55	51
Flash point	^{o}C	64	121

Cerberin, a powerful cardiac glycoside, may be found in both the leaves and the fruits, making them very toxic. Extraction of glycosides from the seeds has anti-heart failure activity. There are few cases when the trunk bark or leaves are used as a purgative, however this is only done with extreme care due to its high toxicity. Cerbera odollam, known locally as cerbera odollam, is one of the few oil-producing plants. Cerbera odollam thrives in coastal salt swamps and creeks in south India and along riverbanks in southern and central Sri Lanka, Vietnam, Myanmar, Malaysia. Cambodia, and Madagascar. Malaysian roadside decorative trees are numerous. The plant's toxicity dominated. The plant's oil can be utilized as biodiesel feedstock because decantation can remove the toxin (cerberin). The poison only harms when digested [4, 11]. The oil content derived from the seeds of Cerbera odollam amounts to 54%. The predominant fatty acid found in cerbera odollam oil is oleic acid, accounting for 48.1% of the content. This is followed by palmitic acid at 30.3%, linoleic acid at 17.8%, and stearic acid at 3.8% [27].

The findings pertaining to the characteristics of cerbera odollam methyl esters indicate that the viscosity exhibited a value of around 3.15 mm^2/s, the density was measured at 847.9 kg/m^3, the flash point was determined to be 214 °C, the acid value was found to be 0.4 mg KOH/g, the oxidation stability was observed to be 6.35 hours, the FAME content accounted for 97.77% w/w, and the heating value was calculated to be 40.49 MJ/kg. Upon conducting an analysis of these qualities, it has been determined that there exists a significant potential for the manufacture of biodiesel from this particular seed [11]. Table 1 displays the Properties of Base Diesel and Biodiesel of Cerbera odollam oil.

The thermal barrier coating (TBC) system reduces substrate material heat load and improves thermal efficiency. The TBC system can insulate the piston crown by coating diesel engine pistons. The piston heat load could be reduced by heat lost through the piston. The piston substrate can resist lower temperatures than the covering, which is ceramic-based and strong. Coating also reduces fuel consumption and pollution [19, 28]. The classic double-layer structure thermal barrier coating has a ceramic topcoat and a metallic bond coat. Due to its modest expansion coefficient, the bond coat substance, an intermetallic alloy, helps the ce-

ramic topcoat and substrate adhere. Internal stress between the ceramic covering and substrate is reduced by high-temperature oxidation resistance. The ceramic topcoat may effectively isolate heat in the combustion chamber because it has a lower thermal conductivity than the substrate. Thus, the piston substrate's temperature drops, improving piston reliability. The chamber's thermal efficiency increases as its temperature rises [29].

To enhance thermal efficiency in diesel engines and mitigate heat loss during combustion, the integration of piston heat insulation has been implemented. The significance of ceramic insulation techniques is increasing as the global community seeks more effective methods to comply with emission standards and conserve fuel resources. Ceramics has excellent insulating properties due to their inert nature. In this context, it is worth mentioning that yttrium-stabilized zirconia and alumina are widely utilized as materials for thermal barrier coatings [22, 25].

The process of plasma spraying involves the utilization of metal powder as its primary input material. Coating materials, often in the form of powders, are delivered into a plasma jet, whereby their particles undergo a process of melting and subsequent propulsion towards the target surface for the purpose of coating. The initial step in the deposition process involves the application of a 200-micron thick bond layer, composed of alumina, zirconia, and nickel, onto the aluminium alloy base grain of the piston. The term "bond coat" refers to the initial coating of paint that is applied. A thermal shield was fabricated with a bond coating comprising of alumina, zirconia, and nickel. The application of the bond layer was facilitated by the utilization of plasma spraying technique. Bond coatings have the potential to enhance the adhesion of oxide coatings to various surfaces. The adhesion between the coating and the substrate is a crucial factor in the fabrication of a thermal shield. Subsequently, a layer of zirconia with a thickness of 250 micrometres is applied onto the surface of the piston. The discrete particles of powder possess an approximate diameter of 50 micrometres. The objects are driven at high velocities of the flame, undergoing instantaneous melting and subsequent solidification.

Experimental Details

The necessity of employing a two-step procedure for the synthesis of biodiesel from Cerbera odollam oil can be attributed to its elevated free fatty acid concentration. The acid esterification process was conducted using a molar ratio of 10:1 of methyl alcohol to oil for a duration of 120 minutes. Sulphuric acid, with a concentration of 2%, was employed as the acid catalyst. The speed of the magnetic stirrer was maintained at a constant rate of 500 rpm to mitigate limitations on mass transfer. The objective of this technique was to decrease the acid value of the input oil. After the acid-esterification procedure, a settling period of four hours was provided for the reaction mixture. The cerbera odollam oil that had been esterified was subsequently subjected to the transesterification procedure. Alkali homogeneous catalysts, such as NaOH and KOH, offer several advantages compared

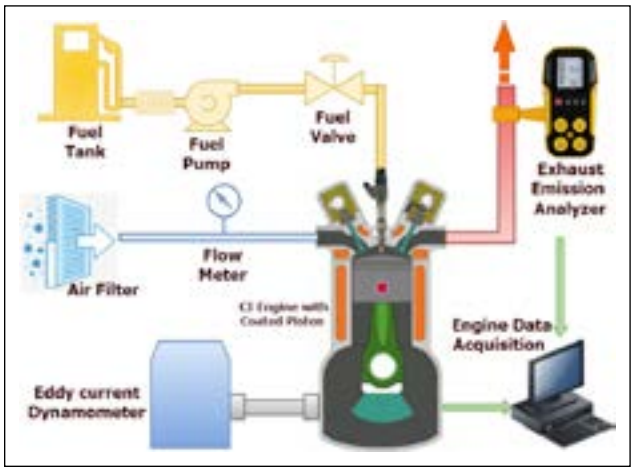

Figure 1. Experimental setup.

to other catalysts. These benefits include the ability to conduct the process at atmospheric pressure, with a very short reaction time of 30–90 minutes, at low temperatures ranging from 40–60 °C. Additionally, the use of alkali homogeneous catalysts is cost-effective and leads to high conversion rates. Upon completion of the procedure, the emergence of two distinct layers becomes apparent. The uppermost stratum consisted of biodiesel, whereas glycerol occupied the lowermost stratum. The glycerol that accumulated at the bottom was extracted, while the biodiesel was afterwards subjected to a purification washing operation, so concluding the transesterification process and yielding pure biodiesel.

An experimental investigation was conducted to evaluate the performance of a diesel fuel blend consisting of Cerbera odollam oil in a single-cylinder, direct-injection, constant-speed engine equipped with a piston coated with a nano material. Figure 1 illustrates the experimental setup. The eddy current dynamometer was utilized to impose a spectrum of loads on the engine, spanning from zero to one hundred percent. The engine power output of 4.4 kW is utilized to its maximum capacity, exerting a force of 1.1 kW on each testing mixture. The adjustment of engine loads can be achieved through hand manipulation with an eddy current dynamometer. In this experimental study, the measurement of airflow was conducted utilizing a calibrated burette, whereas the measurement of fuel flow was carried out using a calibrated aperture situated on an air drum. Table 2 describes the instruments and its details used for the investigation. The researchers also made note of the amount of diesel and biodiesel blends used in the studies of fuel flow. Through the utilization of AVL software, a diverse range of measurements and outcomes were obtained during the operation of the test rig.

Biodiesel of Cerbera odollam oil (BCO), was blended with diesel at different ratios of 25% and 50% on a volume basis as BCO25 and BCO50. Further, the biodiesel tested at low heat rejection engine (LHR) for the same blend as BCO25@LHR and BCO50@LHR. This paper examines the diesel engine performance and emission characteristics of biodiesel blends at uncoated piston and coated piston.

Table 2. Details of test instrumentation

Measurement	Range	Accuracy	Instrument
Load	–	+0.1 kg to −0.1 kg	Load cell
Speed	0–10000 rpm	±10 rpm	Digital tachometer
Fuel quantity	0–50 cm^3	±0.1 cm3	Burette measurement
Carbon monoxide	0 to 20000 ppm	±10 ppm	AVL exhaust gas analyser, NDIR technique
Hydro carbon	0 to 15%	±0.03%	AVL exhaust gas analyser, NDIR technique
Nitrogen oxides	0 to 5000 ppm	±10 ppm	AVL exhaust gas analyser, NDIR technique
Smoke	0–100%	±1 %	AVL smoke meter

RESULTS AND DISCUSSION

Figure 2 displays the brake thermal efficiency (BTE) fluctuation across the engine power for the cerbera odollam blends. BCO25@LHR performed more than 5.5% increase in Break thermal efficiency due to LHR engine's in-cylinder temperatures, combustion efficiency, and ignition timing are all enhanced by the increased vaporization and air-fuel atomization. Also, BCO25@LHR over performed the same fuel by 2 to 6.6% more at break thermal efficiency. In addition to boosting power generation for constrained diesel volume and brake thermal performance, the nano coating also reduces the reject rate in the combustion chamber. The increase in load resulted in a corresponding growth in the brake thermal efficiency due to reduced energy losses. BCO25 and BCO50 have less thermal efficiency by 1.8% and 5.9% compared to base diesel. Furthermore, it was observed that when the blend ratio increased, there was a corresponding decrease in brake thermal efficiency. When biodiesel is used with diesel, it results in an increase in viscosity and a decrease in volatility. The occurrence of incomplete combustion and poor brake thermal efficiency may be attributed to the inadequate spray pattern, resulting in the uneven dispersion of fuel within the combustion chamber. In addition, the low calorific value of cerbera odollam biodiesel played a role in the decrease of brake thermal efficiency [4, 27].

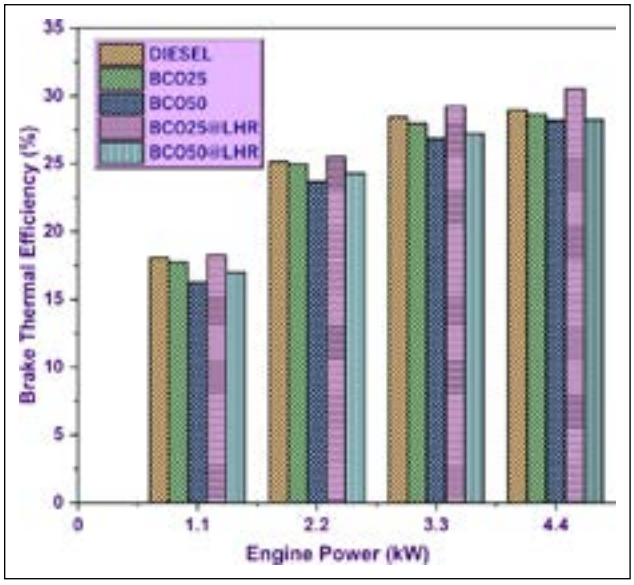

Figure 2. Study of brake thermal efficiency with BCO.

Several factors significantly affect the Specific Fuel Consumption (SFC), which includes the fuel's density, heating value, viscosity and cetane value. The LHR coating on the combustion components reduces the ignition delay time, the engine uses less fuel consumption than a standard diesel engine. BCO25@LHR consumed less fuel by 6.4% compared to base diesel fuel and 3.5% than the same blend at non coated engine. The higher viscosity and density of BCO50 produce poor atomization, leading to a rise in SFC about 6%. In response to varying engine loads, different fuel samples exhibit varying patterns of specific fuel consumption, as seen in Figure 3. The SFC decreases noticeably at mid-range of engine power, and then decreases further as the load increases. Because of an increase in engine power under higher loads and a corresponding decrease in heat dissipation ratios, we observe this phenomenon. Diesel's higher calorific value and lower density result in a lower specific fuel consumption. Because biodiesel has a lower calorific value than conventional diesel, blending it increased the blends' fuel consumption [11, 29].

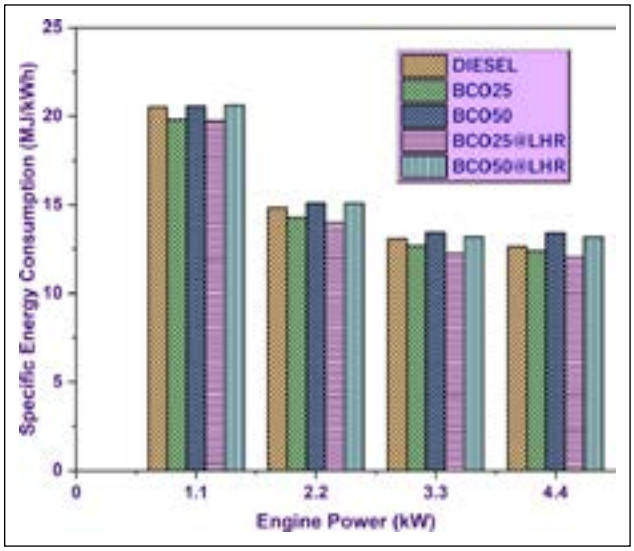

Figure 3. Study of fuel consumption with BCO.

Figure 4 illustrates the range of carbon monoxide (CO) emissions observed across several fuel samples in relation to engine load. CO emissions of the fuel samples exhibit an upward trend until reaching maximum load, with a decline until 2.2kW of engine power. The utilization of

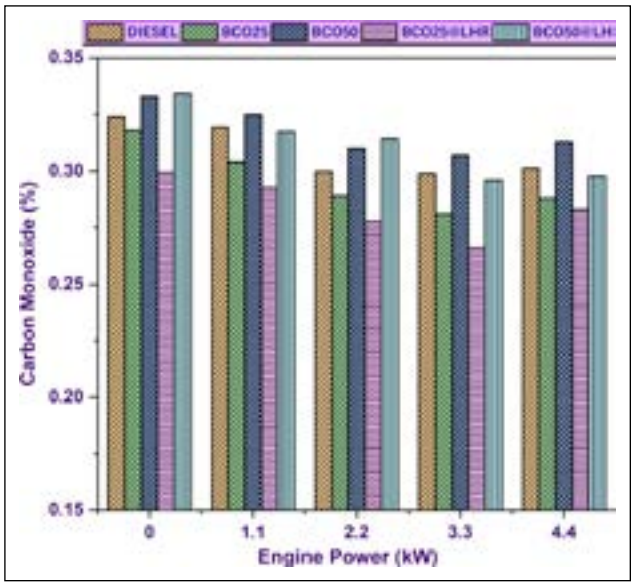

Figure 4. Study of carbon monoxide emissions with BCO.

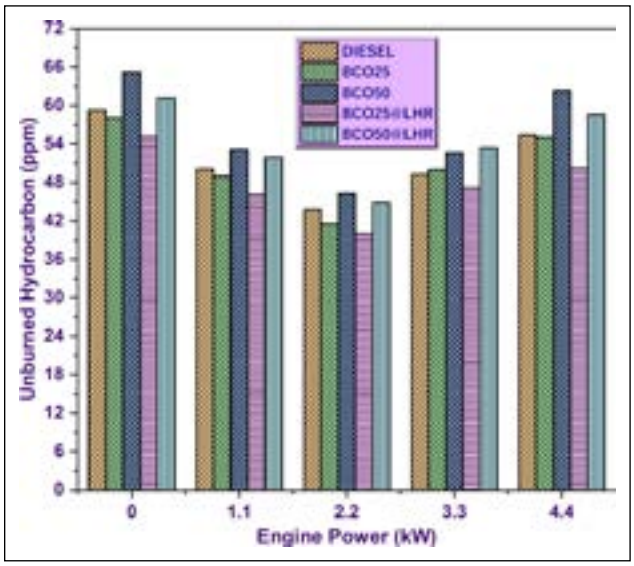

Figure 5. Study of unburned hydrocarbon emissions with BCO.

low loads in engines results in the maintenance of low gas temperatures, hence causing incomplete combustion in the gas phase and subsequently leading to elevated levels of carbon monoxide emissions [30]. An elevated temperature of the gas within the cylinder at load leads to a higher rate of CO oxidation, resulting in reduced emissions of CO. BCO25 blends performed better at different engine loads, with 6 to 10% reduced CO emissions compared to diesel fuel. At BCO25@LHR blends, CO reduced by 5.9% to 10.7% with respect to all loads compared with base fuel. The rationale behind this phenomenon lies in the fact that biodiesel fuels exhibit a greater oxygen content in comparison to conventional diesel fuel. As a result, the oxidation process is enhanced, leading to a reduction in carbon monoxide emissions [9, 31].

Figure 5 illustrates a between the emissions of unburned hydrocarbon (UBHC) and the rise in load across all fuel types. The primary factors contributing to hydrocarbon emissions are inadequate fuel-air mixing, suppression of the oxidation process, and an elevated carbon-to-oxygen ratio. The occurrence of this phenomenon can be attributed to the existence of fuel-rich mixes and a deficiency of oxygen necessary for combustion under increased loads. Moreover, the likelihood of incomplete combustion in an engine increases when additional fuel is introduced to the system [4, 32]. These conditions arise as a result of increased engine loads, leading to a corresponding increase in hydrocarbon emissions. The findings of the study indicate that the utilization of mixed fuels resulted in a reduction of hydrocarbon emissions in comparison to the emissions generated by pure diesel fuel. BCO25 blends performed better at different engine loads, with 5 to 8.5% reduced UBHC emissions compared to diesel fuel. At BCO25@LHR blends, UBHC reduced by 4% to 8.5% with respect to all loads compared with base fuel. The acceleration of soot oxidation at high temperatures is attributed to the elevated oxygen level within the combustion chamber [33].

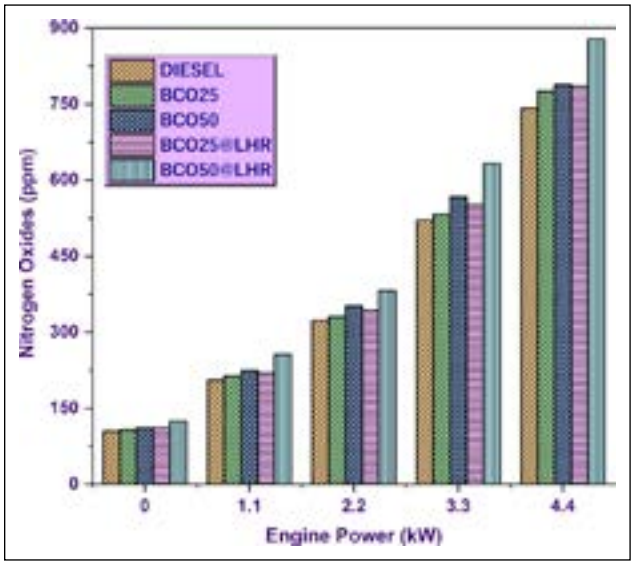

Figure 6. Study of nitrogen oxides emissions with BCO.

The emissions of nitrogen oxides exhibit an upward trend when the operating condition transitions from no load to full load. An observable phenomenon is that an increase in load leads to a corresponding increase in combustion temperature, which subsequently results in elevated levels of nitrogen oxide emissions. The primary generation of NOx occurs within engines due to the increased heat generated during the power stroke. The primary by products generated during the internal combustion process within the cylinder are nitrogen oxides, resulting from the chemical reaction between nitrogen and oxygen [22, 25]. In contrast to diesel fuel, biodiesel exhibits a higher propensity for nitrogen oxide emissions due to its increased oxygen content. Figure 6 illustrates the levels of nitrogen oxide emissions resulting from the combustion of diesel and biodiesel mixtures. BCO25, BCO50 recorded with an increase of 4.6% and 8.8% than the diesel. Whereas at LHR, same blends recorded more than 6% and 18% than the base diesel due to higher combustion temperature. The use

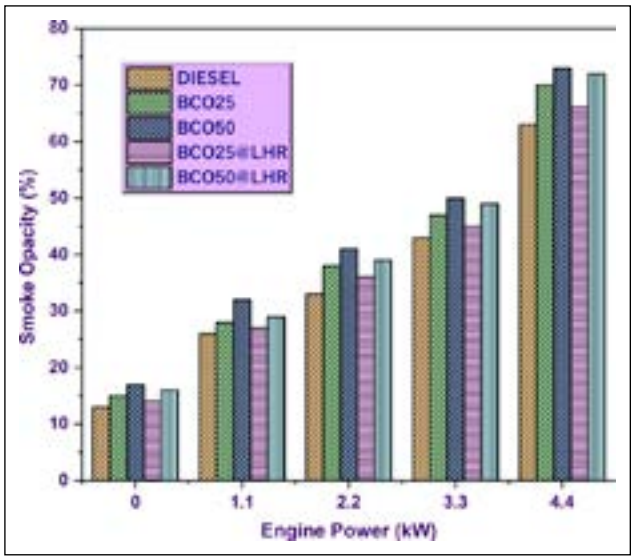

Figure 7. Study of smoke emissions with BCO.

of bio diesel at low heat rejection engine has been found to raise the higher combustion temperature, accelerate the combustion rate, and improve the heat transfer rate, resulting in a reduction in nitrogen oxides emissions [34].

The quick reaction between the hydrogen molecules in the liquid fuel and oxygen results in the production of smoke due to insufficient oxygen to facilitate the complete combustion of the remaining carbon. The qualitative interpretation of this phenomenon pertains to the concentration of particles within the exhaust stream that possess a diameter significant enough to cause scattering of incident light upon interaction. From Figure 7, BCO25, BCO50 recorded the smoke with an increase of 7.1% to 24.2% than the diesel. Whereas at LHR, same blends recorded more than 4% and 14% than the base diesel due to higher combustion temperature. It is conceivable that increased loads may result in a greater number of fuel molecules actively engaging in oxidation reactions. Smoke is generated in the fuel-rich section of the cylinder due to the elevated temperature and pressure resulting from the lack of oxygen. The utilization of biodiesel fuel mixes resulted in a significant reduction in smoke emissions [35]. The rationale behind this phenomenon is in the elevated oxygen level found in biodiesel blends, which consequently enhances the efficiency of oxidation and combustion processes. When the fuel injection pressure is raised, the fuel blends are better atomized, leading to cleaner burning and less smoke. Diesel mix products have bigger shattered droplet sizes due to the presence of LHR engine laminates, which reduces ignition centres and smoke by increasing cylinder temperature [36].

CONCLUSION

Bio economy is the study of the economic benefits of using a certain resource, which raises the value of biomass resources. This study evaluated the efficiency and emissions of diesel fuel made from Cerbera odollam seeds using a low-heat rejection diesel engine with a piston covered with Nano coating. The investigation compared the findings to those of a conventional diesel engine and analysed the most important characteristics, as discussed below.

- BCO25@LHR performed more than 5.5% increase in break thermal efficiency than the base diesel. Also, same blend at LHR over performed the same fuel by 2 to 6.6% more at thermal efficiency.
- BCO25@LHR consumed less fuel by 6.4% compared to base diesel fuel and 3.5% than the same blend at non coated engine. The higher viscosity and density of BCO50 produce poor atomization, leading to a rise in SFC about 6%.
- At varying engine loads, BCO25 blends outperformed diesel fuel while emitting 6-10% less CO. BCO25@LHR blends reduced CO by 5.9%-10.7% relative to base diesel across all loads.
- BCO25 blends performed better at different engine loads, with 5 to 8.5% reduced UBHC emissions compared to diesel fuel. At BCO25@LHR blends, UBHC reduced by 4% to 8.5% with respect to all loads compared with base fuel.
- NOx was found to be higher in the BCO25 and BCO50 than in the diesel, by 4.6% and 8.8%, respectively. However, the same blends showed increases of 6% and 18% over the standard diesel at LHR.
- The smoke was shown to increase the BCO25 and BCO50 values by 7.1% to 24.2% compared to the diesel. On the other hand, greater combustion temperatures at LHR led to higher readings for the identical blends, exceeding the base diesel by between 4 and 14 percent.

This idea clarifies that the bio economy is built in large part on maximizing resource efficiency and substituting feedstock not produced from fossil fuels. The diversification of the energy portfolio has the potential to reduce dependence on fossil fuels, particularly for countries that have a high reliance on oil imports. They have the potential to facilitate the formation of new markets and job possibilities for farmers, rural communities, and biofuel enterprises. Furthermore, these technologies provide the capability to reduce energy costs and improve energy accessibility in geographically remote or socioeconomically weak regions. The biodiesel extracted from Cerbera odollam seeds' performance and emission characteristics on a low-heat rejection diesel engine were able to meet the needs to achieve the bio economy.

DATA AVAILABILITY STATEMENT

The authors confirm that the data that supports the findings of this study are available within the article. Raw data that support the finding of this study are available from the corresponding author, upon reasonable request.

CONFLICT OF INTEREST

The authors declared no potential conflicts of interest with respect to the research, authorship, and/or publication of this article.

ETHICS

There are no ethical issues with the publication of this manuscript.

REFERENCES

[1] D. Nagarajan, D.-J. Lee, and J.-S. Chang, "Chapter 22 - Circular bioeconomy approaches for sustainability and carbon mitigation in microalgal biorefinery," S. Varjani, A. Pandey, T. Bhaskar, S. V. Mohan, and D. C. W. Tsang, (Eds.), Biofuels, Biochemicals, Elsevier, pp. 557–598, 2022. [CrossRef]

[2] Y. Lokko, M. Heijde, K. Schebesta, P. Scholtès, M. Van Montagu, and M. Giacca, "Biotechnology and the bioeconomy—Towards inclusive and sustainable industrial development," New Biotechnology, Vol. 40, pp. 5–10, 2018. [CrossRef]

[3] World Business Council for Sustainable Development, "Circular Bioeconomy," World Business Council for Sustainable Development, pp. 73, 2020.

[4] J. Kansedo, K. T. Lee, and S. Bhatia, "Cerbera odollam (sea mango) oil as a promising non-edible feedstock for biodiesel production," Fuel, Vol. 88(6), pp. 1148–1150, 2009. [CrossRef]

[5] J. Thamilarasan, V. Ravikumar, S. P. Raj Yadav, J. Yarlagadda, A. Kumar, S. Ramasubramanian, … B. Y. Asres, "Sustainability improvement of ethanol blended gasoline fuelled spark ignition engine by nanoparticles," Journal of Nanomaterials, Vol. 2022, Article 7793947. [CrossRef]

[6] J. Senthil Kumar, S. Ganesan, S. Sivasaravanan, S. Padmanabhan, L. Krishnan, and V. C. Aniruthan, "Effects of nano additives in engine emission characteristics using blends of lemon balm oil with diesel," IOP Conference Series: Materials Science and Engineering, Vol. 197(1), Article 012022. [CrossRef]

[7] V. Hariram, S. Seralathan, M. Rajasekaran, M. Dinesh Kumar, and S. Padmanabhan, "Effect of metallic nano-additives on combustion performance and emissions of DI CI engine fuelled with palm-kernel methyl ester," International Journal of Vehicle Structures and Systems, Vol. 9(2), pp. 103–109, 2017. [CrossRef]

[8] S. Ganesan, S. Padmanabhan, S. Mahalingam, and C. Shanjeevi, "Environmental impact of VCR diesel engine characteristics using blends of cottonseed oil with nano additives," Energy Sources, Part A: Recovery, Utilization, and Environmental Effects, Vol. 42(6), pp. 761–772, 2020. [CrossRef]

[9] V. S. Shaisundaram, M. Chandrasekaran, M. Shanmugam, S. Padmanabhan, R. Muraliraja, and L. Karikalan, "Investigation of Momordica charantia seed biodiesel with cerium oxide nanoparticle on CI engine," International Journal of Ambient Energy, Vol. 42(14), pp. 1615–1619, 2021. [CrossRef]

[10] A. P. Venkatesh, S. Padmanabhan, G. V. Rajveer, K. Yuvaja, and M. Muniyappan, "Effect of fuel injection pressure on the performance and emission analysis of Mahua Methyl ester in a single cylinder diesel engine," International Journal of Ambient Energy, Vol. 43(1), pp. 1556–1560, 2022. [CrossRef]

[11] Khairil, A. Rizki, Iskandar, Jalaluddin, A. S. Silitonga, H. H. Masjuki, and T.M.I. Mahlia"The potential biodiesel production from Cerbera odollam oil (Bintaro) in Aceh," MATEC Web Conferences, Vol. 159, Article 01049, 2018. [CrossRef]

[12] S. Padmanabhan, T. Vinod Kumar, M. Chandrasekaran, and S. Ganesan, "Investigation of Sapindus seed biodiesel with nano additive on single cylinder diesel engine," International Journal of Ambient Energy, Vol. 41(10), pp. 1106–1109, 2020.

[13] D. D'Amato, N. Droste, B. Allen, M. Kettunen, K. Lähtinen, J. Korhonen, ... A. Toppinen, "Green, circular, bio economy: A comparative analysis of sustainability avenues," Journal of Cleaner Production, Vol. 168, pp. 716–734, 2017. [CrossRef]

[14] P. Stegmann, M. Londo, and M. Junginger, "The circular bioeconomy: Its elements and role in European bioeconomy clusters," Resources, Conservation & Recycling: X, Vol. 6, Article 100029, 2020. [CrossRef]

[15] A. Muscat et al., "Principles, drivers and opportunities of a circular bioeconomy," Nat. Food, vol. 2, no. 8, pp. 561–566, 2021. [CrossRef]

[16] V. L. Mangesh, E. M. de Olde, R. Ripoll-Bosch, H. H. E. Van Zanten, T. A. P. Metze, C. J. A. M. Termeer, M. K. van Ittersum, and I. J. M. de Boer., "Green energy: Hydroprocessing waste polypropylene to produce transport fuel," Journal of Cleaner Production, Vol. 276, Article 124200, 2020. [CrossRef]

[17] K. K. Pandey, and S. Murugan, "A review of bio-fuelled LHR engines," International Journal of Ambient Energy, Vol. 43(1), pp. 2486–2509, 2022. [CrossRef]

[18] K. K. Pandey, and M. S., "Thermal and experimental analyses of thermal barrier coated pistons," International Journal of Modelling and Simulation, pp. 1–19, Preprint, 2023. doi: 10.1080/02286203.2023.2176676. [CrossRef]

[19] H. Tarigonda, V. Reddy Gangula, P. Ratnaraju, R. R. Doddipalli, and R. L. Krupakaran, "Effect of TBC, turbocharger and EGR on the performance of diesel engine using biodiesel," SAE Technical Paper 2022-28-0558, 2022. [CrossRef]

[20] V. Sankar, M. Ramachandran, G. Thampi, and M. K. Jayaraj, "Combined effects of thermal barrier coating and blending of diesel fuel with biodiesel in diesel engines," Materials Today Proceedings, Vol. 11(3), pp. 903–911, 2019. [CrossRef]

[21] S. Padmanabhan, K. Giridharan, B. Stalin , V. Elango, J. Vairamuthu, P. Sureshkumar, L. T. Jule, and R. Krishnaraj. "Sustainability and environmental impact of ethanol and oxyhydrogen addition on nanocoated gasoline engine," Bioinorganic Chemistry and Applications, Vol. 2022, Article 1936415, 2022. [CrossRef]

[22] C. Karthikeyan, K. L. Harikrishna, and N. Nallusamy, "Experimental investigation of TBC coated piston with various blends of biodiesel," Environmental Progress & Sustainable Energy, Vol. 42(4), Article e14065, 2023. [CrossRef]

[23] P. Murugesan, P. V. Elumalai, D. Balasubramanian, S. Padmanabhan, N. Murugunachippan, Asif Afzal, P. Sharma, K. Kiran, J. S. Femilda Josephin, E. G. Varuvel , T. T. Le, T. Hai Truong, "Exploration of low heat rejection engine characteristics powered with carbon nanotubes-added waste plastic pyrolysis oil," Process Safety and Environmental Protection, Vol. 176, pp. 1101–1119, 2023. [CrossRef]

[24] E. P. Venkatesan, P. Murugesan, S. Rajendran, P. Sekar, P. A. Remigious, and R. B. Durai Chinna, "Experimental studies on thermal-barrier-coated engine fuelled by a blend of eucalyptus oil and DEE," ACS Omega, Vol. 7(50), pp. 46391–46401, 2022. [CrossRef]

[25] R. Rajesh, C. V. B. Reddy, and B. D. Prasad, "Experimental investigation of YSZ coated piston crown on performance and emission features of LHR diesel engine with mahua Biodiesel," IOP Conference Series: Materials Science and Engineering, Vol. 998, Article 012054, 2020. [CrossRef]

[26] J. Lie, M. B. Rizkiana, F. E. Soetaredjo, Y.-H. Ju, and S. Ismadji, "Production of biodiesel from sea mango (Cerbera odollam) seed using in situ subcritical methanol–water under a non-catalytic process," International Journal of Industrial Chemistry, Vol. 9(1), pp. 53–59, 2018. [CrossRef]

[27] S. S. Dhillon, and K. T. Tan, "Optimization of biodiesel production via methyl acetate reaction from cerbera odollam," Advanced Energy Resources, Vol. 4(4), pp. 325–337, 2016. [CrossRef]

[28] S. Padmanabhan, C. Joel, L. Joel, O. Y. Reddy, K. G. D. S. Harsha, and S. Ganesan, "Evaluation of waste plastic pyrolysis oil performance with diethyl ether additive on insulated piston diesel engine," Nature Environment and Pollution Technology, Vol. 20(5), pp. 2079–2086, 2021. [CrossRef]

[29] Z. Shu, J. Deng, Z. Qian, C. Fei, S. Zhu, Y. Du, and K. Zhou, "Thermal analysis of mullite coated piston used in a diesel engine," Coatings, Vol. 12(9), Article 1302, 2022. [CrossRef]

[30] M. A. J. Selvam, R. Arunraj, T. M. Inbamalar, V. Kannagi, and S. Padmanabhan, "Exploration of performance and emission characteristics of soybean biodiesel blends on CI engine," in AIP Conference Proceedings, Vol. 2492, 2023. [CrossRef]

[31] S. Ganesan, S. Padmanabhan, J. Hemanandh, and S. P. Venkatesan, "Influence of substrate temperature on coated engine piston head using multi-response optimisation techniques," International Journal of Ambient Energy, Vol. 43(1), pp. 610–617, 2022. [CrossRef]

[32] M. Bhargavi, T. Vinod Kumar, R. Ali Azmath Shaik, S. Kishore Kanna, and S. Padmanabhan, "Effective utilization and optimization of waste plastic oil with ethanol additive in diesel engine using full factorial design," Materials Today: Proceedings, Vol. 52, pp. 930–936, 2022. [CrossRef]

[33] P. Sambandam, P. Murugesan, M. I. Shajahan, B. Sethuraman, and H. A. Hussein, "Sustainability and environmental impact of hydroxy addition on a light-duty generator powered with an ethanol gasoline blend," Journal of Renewable Energy and Environment, Vol. 9(2), pp. 82–92, 2022. [CrossRef]

[34] V. L. Mangesh, S. Padmanabhan, P. Tamizhdurai, and A. Ramesh, "Experimental investigation to identify the type of waste plastic pyrolysis oil suitable for conversion to diesel engine fuel," Journal of Cleaner Production, Vol. 246, Article 2020. [CrossRef]

[35] S. Ramkumar, M. Parthasarathy, and S. Padmanabhan, "Performance optimization of HCCI engine fueled with Tamanu methyl ether," The International Journal of Vehicle Structures and Systems, Vol. 11(2), pp. 149–153, 2019. [CrossRef]

[36] S. Padmanabhan, K. Karthikeyan, K. K. Nagachandrika, K. Giridharan, and G. Chakravarthi, "Evaluation and optimization of plastic pyrolysis blends performance on diesel engine with ethanol additive using full factorial design," The International Journal of Vehicle Structures and Systems, Vol. 14(3), pp. 348–355, 2022. [CrossRef]

Environ Res Tec, Vol. 6, Issue. 4, pp. 317–325, December 2023

Environmental Research and Technology
https://ert.yildiz.edu.tr - https://dergipark.org.tr/tr/pub/ert
DOI: https://doi.org/10.35208/ert.1225752

Research Article

Co-digestion potential of different industrial sludge sources and impact on energy recovery

Melek Şebnem ÇALIŞKAN TEMEL, Çiğdem YANGIN GÖMEÇ*

Department of Environmental Engineering, İstanbul Technical University, İstanbul, Türkiye

ARTICLE INFO

Article history
Received: 28 December 2022
Revised: 01 September 2023
Accepted: 21 September 2023

Key words:
Anaerobic digestion; Biogas yield; Food industry; Heavy metals; Textile industry

ABSTRACT

Co-digestion potential of the wastewater treatment sludges produced at two industries with different characteristics was investigated in anaerobic batch reactors operated at mesophilic (35±2 °C) condition. The sludge sources selected were from a food industry producing edible oil and from a textile industry producing woven fabric. Reactor performance was evaluated by the conventional parameters as well as by monitoring the biogas production during co-digestion of both industrial sludges at equal mixing proportions. Results indicated that both of these sludge sources had substantial biogas production potential with a cumulative biogas yield more than 425 mL/g-VSS_{fed} whereas it was about 5-fold lower only for the food sludge. On the other hand, chemical oxygen demand (COD) removal reached to about 90% during co-digestion with a well recovery of pH value and alkalinity concentration for sufficient buffering at the end of incubation. Therefore, by the combination of different industrial sludges through co-digestion; higher digestion performance and improved methane yield could be achieved due to better balanced substrate and nutrients. Regarding the initial heavy metals in the supernatant phase of the mixed sludge; iron (Fe), zinc (Zn), nickel (Ni), aluminum (Al), and manganese (Mn) could be removed from 56% to 80% while no apparent removals were observed in cadmium (Cd) and lead (Pb) at the end of operation. Hence, these potential toxic pollutants in the digestate should be taken into consideration while deciding the most appropriate resource recovery and ultimate disposal methods.

Cite this article as: Çalışkan Temel MŞ, Yangın Gömeç Ç. Co-digestion potential of different industrial sludge sources and impact on energy recovery. Environ Res Tec 2023;6(4)317–325.

INTRODUCTION

It has been still a major challenge to treat the wastewaters produced at several industries owing to their different characteristics that depend on the raw materials used during the production stage. Hence, most industries are required to construct their own treatment plants due to the complexity of these wastewaters which can be problematic to be treated in municipal wastewater treatment plants (WWTPs). Wastewaters from food industries producing edible oil are generally rich in chemical oxygen demand (COD), total dissolved and suspended solids, oil and grease, fats, and phosphate that cause high organic and inorganic loading rates in bioreactors. Besides, if discharged to receiving water bodies without subjected to any treatment, wastewater from edible oil production would lead to rapid de-oxygenation and irreversible damage to aquatic life [1, 2]. On the other hand, wastewaters of textile industries mostly contain various parameters characterized by high strength pollutants such as COD, suspended solids, color, toxicity, and

***Corresponding author.**
*E-mail address: yanginci@itu.edu.tr

This paper has been presented at Sixth EurAsia Waste Management Symposium (EWMS 2022)/İstanbul, Türkiye / 24–26 October 2022.

turbidity due to the usage of a wide range of chemicals and dyes during textile processing which severely threaten the soil and receiving waters [3, 4]. Therefore, the reduction at the source and application of the most efficient methods of treatment should be the major focus of industrial sectors. Additionally, sludge produced in the industrial WWTPs remains a challenge for many industries due to inefficient and limited waste management strategies especially in developing countries Additionally, sludge produced in the industrial WWTPs remains a challenge for many industries due to inefficient and limited waste management strategies especially in developing countries. For example, huge amounts of wastewater, organic solid waste and inorganic residues are generated in the processing and refining oilseed for the production of edible oil. Instead of producing economically valuable products or generating energy from these wastes, residues, and by-products; most edible oil industries prefer landfilling for the ultimate disposal of the produced sludge. However, conversion of waste to energy as a form of resource recovery should be the preferable route for managing the organic wastes from all industrial facilities [5, 6].

In this context, since industrial waste sludges are generally well-known with their high COD and total solids (TS) contents, they become very suitable for anaerobic digestion (AD) processes that have been widely applied for volume reduction and biogas generation with low operating cost [7]. However, fluctuations in organic loading rate (OLR), heterogeneity of wastes, or the presence of the inhibitors can result in unstable processes. Besides, initial substrate characteristics such as C/N ratio, pH value, etc. could make some feedstocks not suitable for AD technology which has been used extensively for converting organic compounds to biomethane -especially co-digestion of appropriate biological industrial sludges with other waste sources- for achieving a sustainable industrial sludge management [8]. Hence, the combination of different wastes through co-digestion has been recommended in recent years. Compared to mono-digestion (i.e., with only one substrate), co-digestion provides the simultaneous digestion of two or more feedstocks and it has been indicated to be beneficial for its economic viability, improved biogas yields, and its ability to prevent some of the operating problems due to imbalanced nutrients, existence of heavy metals, toxic materials, or recalcitrant compounds [9]. According to Alrawashdeh [10], co-digestion of the olive mill wastes with sewage sludge was recommended to improve biogas generation due to a better nutrient balance. On the other hand, heavy metals can be found in olive mill waste in high concentrations and it was reported that substrate biodegradability was enhanced by co-digestion [11]. Kumar et al. [12] also recommended co-digestion of textile sludge (aerobic waste sludge) with manure at equal ratios with a biogas production of ca. 525 mL/g-TS_{added} while no obvious biogas production occurred when only textile sludge was digested.

Stabilized sludge by anaerobic digestion contains organic matter and other substances needed by plants for growth, e.g., nitrogen, phosphorus, potassium, calcium and magnesium, and thus it can be used in agriculture as fertilizer or soil conditioner. However, the content of heavy metals detectable in soils may cause toxicity which makes them as the most important limitation in the use of sludge for agricultural purpose. Because, the application of stabilized sludge onto soils could affect the potential availability of heavy metals which are found in several forms in the soil such as solid phases, free ions in soil solution, soluble organic-mineral complexes, or adsorbed on colloidal particles. Hence, soils can store and accumulate heavy metals to some extent owing to their adsorption capacity. The most unwanted heavy metals in stabilized sludge that are highly toxic for the living organisms are cadmium, chromium, nickel, lead, and mercury [13–17]. Since acidification of soils leads to an increase in solubility and absorption rate of heavy metals; pH plays the main role for the fate of the metal compounds in the environment. According to the study by Babel and del Mundo Dacera [13]; the heavy metals could be dissolved and could exist in solution when acid was added to the sludge through the process of exchanging the protons (from the acid) by solubilization of heavy metals in sludge. On the other hand, it was also reported that solids content also had an impact on the solubilization rate of the heavy metals. The metal removal efficiency during bacterial leaching of heavy metals from anaerobically digested sludge decreased with an increase in solids concentration of sludge. Hence generally, lower pH and lower solid content favored metal solubilization for anaerobically digested sludge [13, 14]. Accordingly, if the soil has strong acidification potential; the release of heavy metals bonded with oxides of manganese, aluminum and iron as well as other minerals increases. Among the metals, cadmium had the highest mobility (i.e., at a pH value of 6.5) with chromium and phosphorus whereas zinc was up to 60% bonded by the oxides of manganese and iron [14]. The inhibiting level and toxic effect of Fe, Ni, Pb, Zn, Cu, and Cr on the digestion process were investigated in previous studies and it was reported that adding some of the heavy metals not only decreased the efficiency of biogas production but also affected the COD and solid reduction [11, 18]. Moreover, heavy metals toxicity was observed in the following order: Cu > Ni > Pb > Cr > Zn > Fe in a previous study by Alrawashdeh et al. [11]. Regarding the ultimate disposal of the industrial stabilized sludge as the by-product of the sludge digestion process, heavy metal content can make composting, land application, sanitary landfilling, and incineration options not suitable [19]. In case of land application as the ultimate disposal method, the major inorganic constituents in sludge (Fe, Al, Ca, or P), as well as the characteristics of the soil (i.e., the sludge is laid on) have strong impact on the mobility of heavy metals as organic matter decays. Besides, each heavy metal has different characteristics (with exchangeable, adsorbed and organically-bound fractions) independent of sludge type and they are likely to be mobile to some degree once applied onto land and mobilization of metals may result from dissolution of the carbonate fractions of Cd, Pb, and Ni or oxidation of the sulfide fraction of Cu [13].

Hence, the aims of this study were to investigate mesophilic anaerobic co-digestion potential of two sludge sources from food and textile industries while presenting the impact on reactor performance and biogas recovery as well as to assess the change in the concentrations of heavy metals during the digestion period.

MATERIALS AND METHODS

Sludge Samples and Inoculum Used

The food and textile sludge samples with respective TS contents of 8.5% (volatile content of ~89%) and 0.5% (volatile content of ~45%) were supplied by a food industry producing edible oil and by a textile industry producing woven fabric, finishing cotton and mixed fiber woven cloth both located in Lüleburgaz/Kırklareli/Türkiye. The food sludge (FdS) was provided from the decanter unit –where the mixed biological and chemical sludges are thickened- of the existing WWTP of the investigated industry. The textile sludge (TxtS) used as the substrate was the biological sludge from the extended air activated sludge system provided before the thickener unit of the existing WWTP treating the wastewater produced from several units (e.g., desizing, bleaching, mercerization, drying, dyeing, washing, etc.) of the investigated industry. Raw sludge samples from the food and textile industry indicated the following characteristics, respectively: pH 4.20 and 7.11, alkalinity 2725 and 1075 mg $CaCO_3$/L, 85565 and 2730 mg tCOD/L, 84078 and 4415 mg TS/L, 786 and 11 mg TP/L, 0.054 and 3.31 mg NH_4^+-N/L. Heavy metals in raw sludge samples from the food and textile industry indicated the following concentrations, respectively: 1370 and 21 mg Al/L; 1.66 and 6.1 mg Cu/L; <0.001 and <0.001 mg Cd/L; 0.12 and 0.1 mg Cr/L; 91.5 and 14.6 mg Fe/L; 1.3 and 0.3 mg Mn/L; 0.164 and 0.121 mg Ni/L; <0.010 and 0.095 mg Pb/L; 11 and 0.59 mg Zn/L. Moreover, the FdS was rich in oil and grease with about 13900 mg/L. The inoculum was obtained from a mesophilic anaerobic digester treating the sewage sludge produced at a municipal WWTP (İstanbul, Türkiye) with TS content of about 6.6%.

Batch Reactors and Operating Conditions

The assays were carried out in two sets (i.e., Set I and Set II) at mesophilic condition (35±2 °C) in 1 L glass bottles which were used as reactors with a working volume of 700 mL. Each flask was run with the same inoculum in a 1:6 ratio ($v_{inoculum}/v_{substrate}$). Moreover, co-digestion of food and textile sludges was applied at equal mixing proportions of 1:1 (v/v). During set-up of the batch study, the reactors were configured only for co-digestion at Set I as FdS+TxtS (1:1) (300 + 300 = 600 mL) + inoculum (100 mL) whereas for mono- and co-digestion at Set II as follows: (i) FdS (600 mL) + inoculum (100 mL); (ii) TxtS (600 mL) + inoculum (100 mL); (iii) FdS+TxtS (1:1) (300 + 300 = 600 mL) + inoculum (100 mL). The flasks were also designed to be opened at different operating periods (i.e., for Set I at the 5th, 26th, 41st, and last day whereas for Set II at the 7th, 16th, 30th, 47th, and last day) to conduct experimental analyses during hydrolysis, acidogenesis and methanogenesis phases. Initial samples were immediately taken for t=0 d analyses. Since the FdS used in this study was acidic with a pH of 4.2, the pH of the flasks including FdS was adjusted to 7.0 with 1.0 N NaOH during set-up. In order to measure the methane production of only the inoculum, the inoculum was also incubated without the addition of substrates. After the addition of the sludge samples; each bottle was closed tightly and sealed with a cap and a rubber septum. Then, the headspace of each reactor was flushed with the gas mixture of 80% N_2 and 20% CO_2 for 2 minutes to establish anaerobic conditions inside the reactors. The reactors were then kept in an incubator at 35±2 °C and operated as batch systems while they were shaken manually once a day during the incubation period. The experimental set-up was done minimum in triplicates and average biogas values were calculated.

Analytical Procedure

The solids, COD, and alkalinity were determined according to Standard Methods [20]. Total COD (tCOD) and soluble COD (sCOD) experiments were conducted according to dichromate open-reflux method. For sCOD experiments, the samples were filtered through 0.45 µm syringe PVDF filters. After addition of dichromate and acid solutions; samples were kept at 150 °C for 2 hours and COD concentrations were measured by behr TRS 300 control device. The pH measurement was done using a pH meter (Hach Lange HQ/40 D model) and alkalinity measurement was done by titrating with 0.02 N H_2SO_4 acid solution till the pH dropped down to 4.5. Total phosphorus (TP) concentration of the samples was measured by the Thermo ICP-OES Spectrophotometer (iCAP 6300 Duo) according to the same procedure as explained below for the determination of heavy metals.

For the measurement of heavy metals (iron, Fe; zinc, Zn; nickel, Ni; aluminum, Al; manganese, Mn; cadmium, Cd; lead, Pb; copper, Cu; and chromium, Cr), the samples were prepared according to the EPA 200.7 method in the liquid (i.e., supernatant of the digestate) and in the solid (i.e., digested sludge) phases which were taken from the batch sets during the study [21]. For heavy metal analysis in the digested sludge, samples were oven-dried at 50 °C and then crushed into pieces. A homogeneous sample with an amount of 0.4 g (±0.1) was put into a microwave vessel for acid extraction (i.e., respectively with 9 and 3 mL of nitric and hydrochloric acid). Then, the samples were burned at 160 °C, allowed to cool down to room temperature, quantitatively transferred to a volumetric flask, diluted to 50 mL with distilled water, and mixed thoroughly. The concentrations of all investigated heavy metals were measured by the Thermo ICP-OES Spectrophotometer.

The biogas generation was measured using a manometer (Lutron PM 9107 model) before being released from each flask by an injection needle. The measured biogas values were then converted from pressure unit (mbar) to volume unit (mL) under the standard conditions (0 °C and 1 atm). During the study, biogas production at the headspace of

Table 1. Initial substrate characteristics in the batch sets

Parameter	Unit	Set I	Set II		
		Co-digestion	Mono-digestion		Co-digestion
		[FdS+TxtS (1:1)]	[FdS]	[TxtS]	[FdS+TxtS (1:1)]
tCOD	mg/L	12,331±5[a]	16,300±77	261±33	8682±77
sCOD	mg/L	2417±10	10,035±42	110±2	4805±69
pH[b]	–	7.0	7.0	7.65	7.0
Alkalinity	mg/L	1705	2725	1075	1625
TSS	mg/L	21,742±330	56,398±429	5779±159	26,818±152
VSS	mg/L	16,924±384	47,425±250	3322±14	22,099±142

a: Average±Standard deviation; b: Initial pH was adjusted to 7.0 with 1.0 N NaOH in the reactors with FdS.

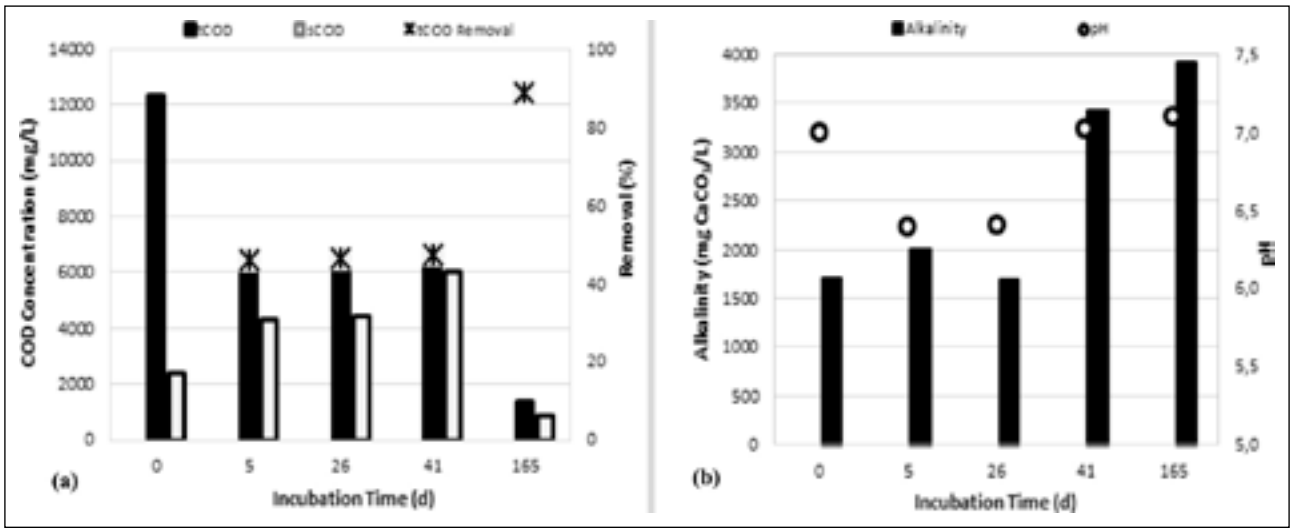

Figure 1. Profile of **(a)** COD; **(b)** pH and alkalinity during anaerobic co-digestion during Set I [FdS+TxtS (1:1)].

each flask was monitored daily till the last incubation day (i.e., until daily biogas productions ceased in the bioreactors and cumulative biogas volume reached to a constant value).

RESULTS AND DISCUSSION

In this study, the potential of using anaerobic co-digestion of two different sludge sources (i.e., from textile and food industries) was tested at equal mixing proportions compared to mono-digestion of single industrial sludge and the initial substrate characteristics are presented in Table 1.

Results of Set I revealed that tCOD removal reached about 90% during co-digestion with a pH value higher than 7.0 at the end of the digestion period. The tCOD profile is shown in Figure 1a whereas pH and alkalinity profile is shown in Figure 1b during anaerobic co-digestion of the investigated industrial sludge sources at equal ratios in Set I. Although the pH value at 41-d reactor indicated about 7.0 in Set I, the pH value was still lower than 7.0 at 47-d reactor in Set II co-digesting both sludge samples. On the other hand, the pH values were 6.57 and 7.24 in the reactors digesting only FdS and TxtS, respectively. This showed the significance of co-digestion, especially of the FdS. However, although digestion performance could not be monitored between the 47th and last days of operation; respective pH values were of 7.28, 7.95, and 7.66 in the reactors with FdS, TxtS, and (FdS + TxtS) at the end of incubation. Also, TP concentration was substantially removed in the liquid part with more than 50% (i.e., from 366 mg/L to 180 mg/L) after digestion. On the other hand, regarding the initial heavy metals concentrations in the liquid phase (i.e., supernatant of the digestate) of the mixed sludge; iron (Fe), zinc (Zn), nickel (Ni), aluminum (Al), and manganese (Mn) could be removed from 56% to 80% while no apparent removals were observed in cadmium (Cd) and lead (Pb) at the end of operation for both sets. Although heavy metals except copper (Cu) and chromium (Cr) indicated compatible profile in both sets; no apparent reduction in Cu and Cr concentrations was observed in the Set I (Table 2) whereas final concentrations of these heavy metals were determined lower compared to the initial values in the Set II [22].

Accordingly, Fe, Zn, Ni, Al, and Mn were reduced from 32% to 77% and from 55% to 99% in the FdS and TxtS digestates with 53% and 28% TP removals, respectively. The biogenic sulfides produced result in insoluble complexes with heavy metals and then precipitated. Since the main removal

mechanisms of heavy metals from digestate/liquid phase are precipitation and adsorption onto sludge; bicarbonate and phosphate in bioreactor, and biogenic sulfides that might be produced under sulfate reducing conditions might favor their removal [23]. On the other hand, the heavy metals present in the sludge can be dissolved and then exist in solution in the case of acid addition with the exchange of the protons (from the acid) by solubilization of heavy metals in sludge. Hence, one of the most important factors affecting the solubilization of metals in sludge is pH and metals solubilization increases with lower pH values. In a study by Aktaş [24], the metal removal mechanisms are listed as follows: (i) a metabolism-independent process (passive uptake) through ion-exchange phenomena, (ii) complexation with negatively charged groups, and (iii) adsorption and precipitation by extracellular polymeric substances (EPS).

In this study, respective heavy metal concentrations in raw food sludge and textile sludge were measured as 1370 and 21 mg Al/L; 1.66 and 6.1 mg Cu/L; <0.001 and <0.001 mg Cd/L; 0.12 and 0.1 mg Cr/L; 91.5 and 14.6 mg Fe/L; 1.3 and 0.3 mg Mn/L; 0.164 and 0.121 mg Ni/L; <0.010 and 0.095 mg Pb/L; 11 and 0.59 mg Zn/L. Xiao et al. [25] also reported that Cu, Ni, Zn and Cr were the detected heavy metals in the effluents of food industry. Textile industries, on the other hand, are known as the facilities discharging a large amount of heavy metal due to the fact that these metals might be naturally present in textiles. Moreover, heavy metals might penetrate into textile fibers as a result of production and dyeing processes; protective agents used during storage; the wide usage of chemicals, colorants, and other additives (e.g., caustic soda, sodium carbonate, etc.) during the manufacturing processes. For example, Cr, Ni, Zn, Pb, Cu, and Cd are used for the production of colour pigments in textile dyes. Besides, different heavy metals such as Co, Cu, and Cr are found within the dye chromophores used in textile industry [26]. According to Kaur et al. [27], the heavy metal contents of a textile industry effluent were measured in the order of Co > Cd > Pb > Zn > Cr > Cu with respective concentrations 1.69, 1.33, 0.14, 0.13, 0.06, and 0.03 mg/L. Hence, the content of heavy metals in sludge might be different according to the source of wastewater, the sludge treatment process, the geography, industrial characteristics, and the economic welfare of the city as described in Xiao et al. [25] who also reported higher levels of heavy metals in municipal sludge which were collected from regions with higher industrial facilities.

Although heavy metals can be stimulatory, they might be inhibitory, or even toxic for biochemical reactions. Accordingly, the industrial sludge that contains considerable amount of heavy metals should be avoided for any biogas production through AD. Especially, heavy metals have the potential to affect anaerobic microorganisms including methanogens depending on their concentrations which might cause reduction in the performance of biological metal removal and in biogas generation as well [23, 24, 28]. Regarding the inhibitory effect of the four heavy metals investigated by Altaş [24], the IC50 values (i.e., the concentrations that cause a 50% reduction in the cumulative methane production over a fixed period of exposure time), were found to be as Zn=7.5 mg/L, Cr=27 mg/L, Ni=35 mg/L, and Cd=36 mg/L when glucose was used as the carbon source. For the 50% inhibiting concentration of Cu^{2+} to acetoclastic and hydrogenotrophic methanogens was reported by Karri et al. [23] as about 21 and 9.0 mg/L, respectively whereas the activity of an acetate-degrading methanogenic enrichment culture was inhibited by 50% at about 67 mg Pb/L. According to Table 2 in this particular study; Zn, Cr, Ni, and Cd in the initial combined sludge sample were measured far below aforementioned IC50 values indicating the inhibitory effect on methane-producing anaerobic sludge. The effects of some metals on methane production from food waste were also investigated by Zhang et al. [29] who reported that biogas generation was substantially dependent on the supplementation of Fe, Co, Mo, Ni elements; however, excessive Fe and Ni addition (i.e., 1000 and 50 mg/L, respectively) indicated toxicity to methanogens. They also reported the optimal dosages for Fe as 100 mg/L and for Ni as 5 mg/L which indicated the highest methane yield (504 mL/g VS_{added}) with an increment of about 36% compared to the control reactor in the absence of these metals. Hence, according to Table 2; Fe was measured as about 70 mg/L in the initial combined sludge sample which was again below that toxic concentration reported by Zhang et al. [29]. Abdel-Shafy and Mansour [28] also reported that the presence of heavy metals during AD decreased the efficiency of the biological process, gas production and volatile organic matter removal and even methanogenic bacteria inhibition was observed. It was reported that this inhibition was due to accumulation of organic acid intermediates which was dependent on heavy metals. The toxicity of the investigated metals was obtained in the following order: Hg < Cd < Cr (III); hence, the presence of these toxic heavy metals in organic waste should be avoided or controlled during AD. Abdel-Shafy and Mansour [28] defined inhibitory level of a heavy metal as that caused a radical decrease in the gas production. On the other hand, they defined toxic limits as the concentration at which total gas production was reduced by 60% from control reactor. Results indicated inhibiting concentrations as 125, 170, and 775 mg/L whereas toxic

Table 2. Change in heavy metals concentrations in the liquid phase during anaerobic co-digestion in Set I [FdS+TxtS (1:1)]

Heavy metal	Initial (mg/L)	Final (mg/L)	Reduction (%)
Iron (Fe)	69.64	14.03	80
Nickel (Ni)	1.410	0.320	77
Manganese (Mn)	2.140	0.737	65
Zinc (Zn)	13.62	5.182	62
Aluminum (Al)	663.2	289.2	56
Copper (Cu)	2.124	2.018	5
Chromium (Cr)	0.748	0.747	–
Cadmium (Cd)	0.002	<0.002	–
Lead (Pb)	0.095	0.167	–

limit values as >250, >340, and >1550 mg/L for Hg, Cd, and Cr (III), respectively. In Kadam et al. [30], IC50 values for some heavy metals during methanogenesis were presented. Accordingly, they reported that for Cr, Zn, Ni, Cd, Cu, Pb, and Co; IC50 values were about 15, 16, 400, 8, 13, 67, and 0.8 mg/L, respectively. They also reported optimum values of Zn, Cd, Fe, Ni, and Cu for an effective AD as 5.0, 0.1, 0–1000, 0.8–4.0, and 5.0–30 mg/L, respectively.

In this context, many studies reported large differences in the inhibitory concentrations of metals which might be due to some factors such as the change in; the biofilm structure, the precipitation and adsorption of soluble metals, EPS concentration of sludge, and the dense distribution at the outer layer of the inoculum sludge especially in granular form. Even the variations in the sludge characteristics might have significant effect on the inhibitory concentrations of heavy metals on anaerobic microorganisms [24].

Since, heavy metals are commonly found in stabilized sludge, there has been an increased concern about its direct re-use in agriculture as fertilizer due to the limitation of the heavy metal concentration according to regulations in recent years. Hence, source control of industrial discharges is required by; (i) controlling the processes and materials used during the production stage at the facilities, (ii) removal and controlled disposal of hazardous constituents before reaching to the waste stream, (iii) separation of highly contaminated industrial effluents from the domestic wastewater, and (iv) pretreatment before municipal collection system [13]. It was reported that the share of industrial effluents has been still increasing in the overall mass of sewage sludge which also leads to high heavy metal content with the most toxic ones as cadmium, lead, arsenic and mercury. Heavy metals occur in different forms and can be absorbed by clay minerals, hydrated iron oxides and organic matter. Heavy metals also appear in the form of inorganic compounds (e.g., oxides, phosphates, carbonates, sulphates, sulphides). When the metals occur in a soluble and exchangeable form, they are released to the environment most easily (nickel, cadmium). However, when the metals are found in bonded form (i.e., with carbonates, phosphates, sulphides and oxides of manganese, iron, chromium and zinc) they are less easily released to the environment. On the other hand, heavy metals can prevent iron metabolism, whereas iron can prevent from absorption and transportation of other components, e.g. phosphorus [14]. According to chemical speciation of heavy metals in anaerobically digested sludges; Cd, Cr, Cu, Pb, Mn, Ni, and Zn seem to predominate in the following forms: Cd in carbonate and residual forms; Cr in organic and residual forms; Cu in residual and organic forms; Pb in carbonate and organic forms; Mn mostly in organically bound form; Ni in carbonate and residual forms; and Zn mostly in organically bound form. Among the heavy metals, Cu changed most easily into its chemical (i.e., sulfide precipitated) form which increased as AD continued further. Besides, when compared to the chemical forms of Zn and Ni before and after the AD process; the degree of Cu stabilization was higher [13].

Babel and del Mundo Dacera [13] already emphasized the importance of the removal of some heavy metals from especially agro-industrial sludge to levels below the regulatory standards of that country to make the sludge suitable for land application and to be used in agriculture. They reported that removals attained for the metals were 30% for Cu, 59% for Mn and 39% for Ni, for anaerobically digested sludge. In this particular study, compared to initial raw sludge samples; all the investigated heavy metals concentrations except cadmium indicated a positive change (i.e. the increases were between 11% in nickel and 52% in lead) in the final digested sludge samples taken from the co-digester (with food and textile sludge sources). For example in Set I, the results of the heavy metals in the solid phase of the combined sludge sample were as follows (rounded values in mg/kg): 17000 for Al; 85 for Cu; <1.25 for Cd; 37 for Cr; 3000 for Fe; 54 for Mn; 30 for Ni; 5.1 for Pb; and 290 for Zn. On the other hand in Set II; the results of Al and Fe in the solid phase of the FdS and TxtS samples were respectively as follows (rounded values in mg/kg): 23000 and 4160; and 3600 and 4530 whereas the results of other investigated heavy metals in the solid phase of the FdS, TxtS, and the combined sludge samples were respectively as follows (rounded values in mg/kg): 74, 280, 158 for Cu; <1.25, <1.25, <1.25 for Cd; 32, 113, 59 for Cr; 56, 127, 96 for Mn; 28, 135, 60 for Ni; 4.6, 13.5, 12.7 for Pb; and 305, 698, 502 for Zn [21]. Nevertheless, the measured heavy metals in the solid phase of the digested sludge did not exceed the permissible level specified in the related regulation of Türkiye [31]. Because, according to Annex I-B Limit Values (mg/kg DS); heavy metals concentrations must not exceed the following values (mg/kg): 1000, Cu; 10, Cd; 1000, Cr; 300, Ni; 750, Pb; and 2500, Zn [31]. However, the mercury and pathogen contents should be also below the limit values in order to assure their usage by laying on soil for agricultural purposes.

Kadam et al. [30] also studied permissible values of some heavy metals to be used as fertilizer in Eropean Union (EU). Accordingly, the permissible values for Zn, Cd, Ni, and Cu metals were reported as 200, 1.0, 50, and 100 mg/kg, respectively. Kaur et al. [27] also investigated the contents of some heavy metals in the soil of the agricultural field collected from the neighborhood of textile industries. They reported that Cd, Cr, Co, Cu, Pb, and Zn were detected as 1.33, 16.43, 214.60, 13.63, 57.33, and 92.52 mg/kg, respectively.

In another study by Xiao et al. [25], distribution characteristics of typical heavy metals in sludge from WWTPs in China was investigated. Moreover, the variation in sludge composition containing wastewaters from different facilities from metallurgical, chemical, food and metal industry was evaluated. Accordingly, heavy metal levels were in the order of Zn > Cu > Cr > Ni > Pb > As > Hg > Cd, ranging from 154 to 2970 mg/kg, 28 to 1150 mg/kg, 10 to 136 mg/kg, 9 to 262 mg/kg, 0 to 79 mg/kg, 12.1 to 41.6 mg/kg, 0.67 to 19.50 mg/kg and 0.21 to 2.77 mg/kg, respectively. Besides, according to the typical heavy metal distribution in sludge; Hg, Zn and Cu were apparently affected by the

degree of industrial intensity, while the distribution in Ni, Cd, Pb, As and Cr were more even. Regarding the sludge with wastewater from the food industry; Cu, Ni, Zn and Cr content in sludge increased significantly whereas Ni and Zn content in sludge with wastewater from the printing and dyeing industry increased at a great extent. Hence, it was concluded that the heavy metal content in sludge may vary and can be affected by several factors mainly the source of wastewater [25].

In this study, biogas productions were also monitored during the incubation period of both sets except the lockdown periods due to pandemic situation. Daily and cumulative biogas production during co-digestion of FdS and TxtS in Set I, during mono-digestion of FdS in Set II, and during co-digestion of FdS and TxtS in Set II are illustrated in Figure 2a–c, respectively. According to the biogas results, both sludge sources used in this study had substantial biogas production potential when anaerobically digested together (i.e., at least 325 and 425 mL/g-VSS_{fed} in Set I and Set II, respectively); however, each industrial sludge alone had much lower biogas production (i.e., at least 80 mL/g-VSS_{fed} for FdS in Set II). In the reactor digesting only TxtS indicated about 50 mL cumulative biogas result in Set II. Hence, the results from this study showed that co-digestion not only reduced the environmental pollution and health risks from the selected industries but also recovered useful energy [22].

In conclusion, co-digestion proposed a sustainable management method for the sludge produced at the WWTPs of appropriate industries. Moreover, since majority of industrial sludges are generated in much smaller quantities; it is considered that co-digestion would also provide potential of using the available anaerobic digesters of the industries producing higher amounts of sludge in adjacent areas [8].

CONCLUSIONS

Results revealed that both of the sludge sources from food and textile industries had substantial biogas production potential during anaerobic co-digestion at mesophilic condition. Accordingly, the cumulative biogas yield was observed more than 425 mL/g-VSS_{fed} for the FdS and TxtS at equal mixing proportions whereas it was about 5-fold lower only for the FdS. Hence, co-digestion yielded a higher amount of biogas compared to mono-digestion where single industrial sludge was digested. Next to the improved biogas yields; results showed better process performance in terms of total COD removal which was about 50% and 90% at the 41st and last days of operation respectively with a well recovery of pH and sufficient buffering capacity in the batch assays. On the other hand, respective total COD removals were 84% and 36% when FdS and TxtS were digested alone. Besides, heavy metals (aluminum, iron, manganese, nickel, and zinc) was substantially reduced from 56% to 80% with more than 50% TP removal in the liquid supernatant of the digestate after co-digestion. These heavy metals were reduced from 32% to 77% and from 55% to 99% in the liquid

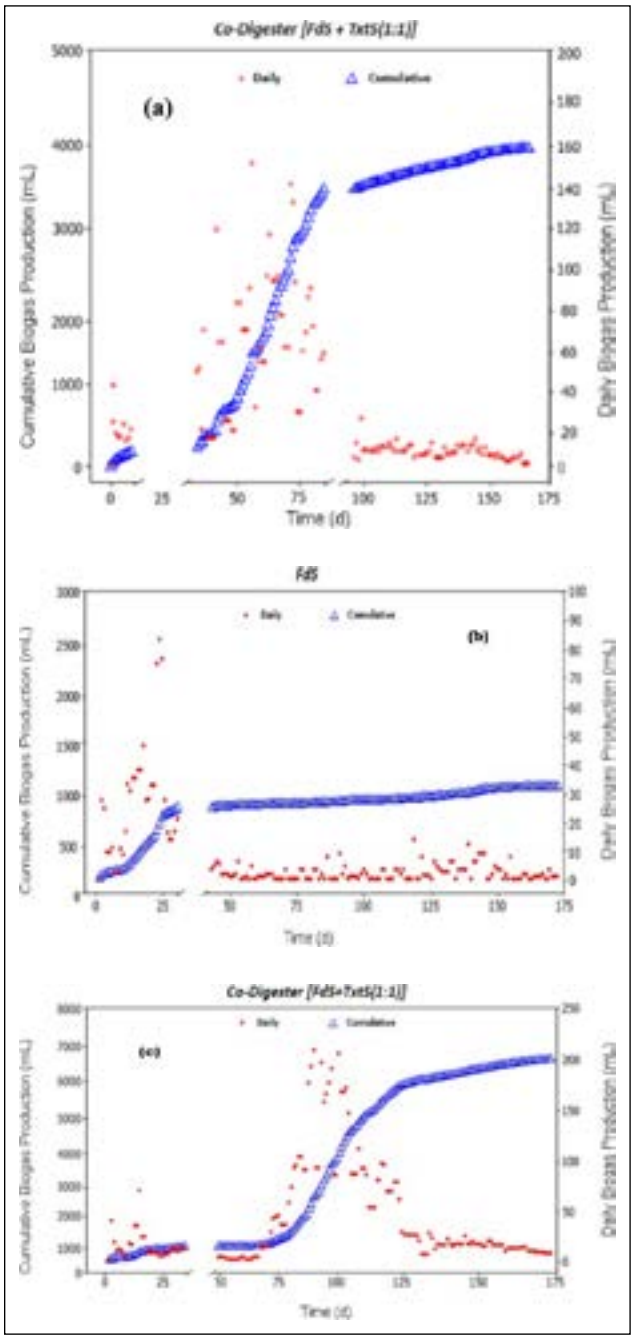

Figure 2. Daily and cumulative biogas production during anaerobic; **(a)** co-digestion in Set I [FdS+TxtS (1:1)], **(b)** mono-digestion in Set II [FdS], and **(c)** co-digestion in Set II [FdS+TxtS (1:1)].

phases of the FdS and TxtS digestates with 53% and 28% TP removals, respectively. On the other hand, the content of the investigated heavy metals in the solid phase of the digested sludge samples did not exceed the permissible level specified in the related regulations of Türkiye for their usage by laying on soil for agricultural purposes. However, this conclusion should be confirmed by the fact that the mercury and pathogen contents were also below the limit values. Therefore, the use of digested sludge for non-agricultural purposes and land reclamation would essentially be a better alternative.

Acknowledgements
The authors are grateful to Pelin Gürler, Gülcan Gül and Buket Yavuz for their help during the lab study.

DATA AVAILABILITY STATEMENT

The authors confirm that the data that supports the findings of this study are available within the article. Raw data that support the finding of this study are available from the corresponding author, upon reasonable request.

CONFLICT OF INTEREST

The authors declared no potential conflicts of interest with respect to the research, authorship, and/or publication of this article.

ETHICS

There are no ethical issues with the publication of this manuscript.

REFERENCES

[1] C. Rashama, G. Ijoma, and T. Matambo, "Biogas generation from by-products of edible oil processing: a review of opportunities, challenges and strategies," Biomass Conversion and Biorefinery, Vol. 9, pp. 803–826, 2019. [CrossRef]

[2] Z. S. Lee, S. Y. Chin, J. W. Lim, T. Witoon, and C. K. Cheng, "Treatment technologies of palm oil mill effluent (POME) and olive mill wastewater (OMW): A brief Review," Environmental Technology & Innovation, Vol. 15, Article 100377, 2019. [CrossRef]

[3] R. Katal, H. Zare, S. O. Rastegar, P. Mavaddat, and G. N. Darzi, "Removal of dye and chemical oxygen demand (COD) reduction from textile industrial wastewater using hybrid bioreactors," Environmental Engineering and Management Journal, Vol. 13, pp. 43–50, 2014. [CrossRef]

[4] K. Sarayu, and S. Sandhya, "Current technologies for biological treatment of textile wastewater--a review," Applied Biochemistry and Biotechnology, Vol. 167, pp. 645–661, 2012. [CrossRef]

[5] W. I. Ngoie, O. O. Oyekola, D. Ikhu-Omoregbe, and P. J. Welz, "Valorisation of edible oil wastewater sludge: Bioethanol and biodiesel production," Waste and Biomass Valorization, Vol. 11, pp. 2431–2440, 2020. [CrossRef]

[6] C. Yangin-Gomec, E. Yarsur, and O.Y. Ozcan, "Energy recovery during anaerobic treatment of lignocellulosic wastewater with dynamic modeling and simulation results," Biomass Conversion and Biorefinery, Vol. 13, pp. 9227–9236, 2021. [CrossRef]

[7] J.N. Meegoda, B. Li, K. Patel, and L.B. Wang, "A review of the processes, parameters, and optimization of anaerobic digestion," International Journal of Environmental Research and Public Health, Vol. 15, Article 2224, 2018. [CrossRef]

[8] H. A. Bahçeci, S. L. Sanin, and F. D. Sanin, "Co-digestion potential of industrial sludges with municipal sludge," Waste and Biomass Valorization, Vol. 12, pp. 5437–5449, 2021. [CrossRef]

[9] A. Rabii, S. Aldin, Y. Dahman, and E. Elbeshbishy, "A review on anaerobic co-digestion with a focus on the microbial populations and the effect of multi-stage digester configuration," Energies, Vol. 12, Article 1106, 2019. [CrossRef]

[10] K. Al bkoor Alrawashdeh, "Improving anaerobic co-digestion of sewage sludge with thermal dried olive mill wastewater," Waste Biomass Valorization, Vol. 10, pp. 2113–2119, 2018. [CrossRef]

[11] K.A. Alrawashdeh, E. Gul, Q. Yang, H. Yang, P. Bartocci, and F. Fantozzi, "Effect of heavy metals in the performance of anaerobic digestion of olive mill waste," Processes, Vol. 8, Article 1146, 2020. [CrossRef]

[12] P. Kumar, S. Samuchiwal, and A. Malik, "Anaerobic digestion of textile industries wastes for biogas production," Biomass Conversion and Biorefinery, Vol. 10, pp. 715–724, 2020. [CrossRef]

[13] S. Babel, and D. del Mundo Dacera, "Heavy metal removal from contaminated sludge for land application: A review," Waste Management, Vol. 26, pp. 988–1004, 2006. [CrossRef]

[14] J. K. Milik, R. Pasela, M. Lachowicz, and M. Chalamoński, "The concentration of trace elements in sewage sludge from wastewater treatment plant in Gniewino," Journal of Ecological Engineering, Vol. 18, pp. 118–124, 2017. [CrossRef]

[15] H. Morita, and H. Tsuboi, "Basic investigation on the chemical forms of heavy metals in a sewage treatment plant," Water Science and Technology, Vol. 42, pp. 159–165, 2000. [CrossRef]

[16] B. Bayraklı, O. Dengiz, M. A. Özyazıcı, Y. Koç, E. Kesim, and F. Türkmen, "Assessment of heavy metal concentrations and behavior in cultivated soils under humid-subhumid environmental condition of the Black Sea region," Geoderma Regional, Vol. 32, Article e00593, 2023. [CrossRef]

[17] B. Zhang, X. Zhou, X. Ren, X. Hu, and B. Ji, "Recent research on municipal sludge as soil fertilizer in China: a review," Water, Air, & Soil Pollution, Vol. 234, Article 119, 2023. [CrossRef]

[18] N. Quang-Minh, B. Duy-Cam, P. Thao, D. Van-Huong, N. Thi-Nham, N. Minh-Viet, T. Thien-Hien, and D. Quang-Trung, "Investigation of heavy metal effects on the anaerobic co-digestion process of waste activated sludge and septic tank sludge," International Journal of Chemical Engineering, Vol. 2019, Article 5138060, 2019. [CrossRef]

[19] İ. Öztürk, İ., and Ç. Yangın-Gömeç, Çamurların İşlenmesi, Arıtılması ve Uzaklaştırılması, İ. Öztürk, Ed. Atıksu Mühendisliği, Bölüm 9, İstanbul, Türkiye: İSKİ, pp. 341–416, 2017. [Turkish]

[20] American Public Health Association. Standard Methods for the Examination of Water and Wastewater, 21st Ed., American Public Health Association (APHA) Press, Washington, United States, 2005.

[21] U.S. EPA. 1994. "Method 200.7: Determination of Metals and Trace Elements in Water and Wastes by Inductively Coupled Plasma-Atomic Emission Spec-

trometry," Revision 4.4. Cincinnati, OH. https://www.epa.gov/esam/method-2007-determination-metals-and-trace-elements-water-and-wastes-inductively-coupled Accessed on Nov 10, 2023.

[22] M.Ş. Çalışkan-Temel, "Anaerobic Co-Digestion of Industrial Wastewater Sludges: An Investigation on Heavy Metal Contents and Energy Recovery," Master thesis, Istanbul Technical University, 2022.

[23] S. Karri, R. Sierra-Alvarez, and J. A. Field, "Toxicity of copper to acetoclastic and hydrogenotrophic activities of methanogens and sulfate reducers in anaerobic sludge," Chemosphere, Vol. 62, pp. 121–127, 2006. [CrossRef]

[24] L. Altaş, "Inhibitory effect of heavy metals on methane-producing anaerobic granular sludge," Journal of Hazardous Materials, Vol. 162, pp. 1551–1556, 2009. [CrossRef]

[25] D. Xiao, H. Li, Y. Wang, G. Wen, and C. Wang, "Distribution characteristics of typical heavy metals in sludge from wastewater plants in Jiangsu Province (China) and their potential risks," Water, Vol. 15, Article 313, 2023. [CrossRef]

[26] R. Türksoy, G. Terzioglu, and İ. E. Yalçın, Ö. Türksoy, and G. Demir, "Removal of heavy metals from textile industry wastewater," Frontiers in Life Sciences and Related Technologies, Vol. 2, pp. 44–50, 2021. [CrossRef]

[27] J. Kaur, S. S. Bhatti, S. A. Bhat, A. K. Nagpal, V. Kaur, and J. K. Katnoria, "Evaluating potential ecological risks of heavy metals of textile effluents and soil samples in vicinity of textile industries," Soil System, Vol. 5, Article 63, 2021. [CrossRef]

[28] H. I. Abdel-Shafy, and M. S. M. Mansour, "Biogas production as affected by heavy metals in the anaerobic digestion of sludge," Egyptian Journal of Petroleum, Vol. 23, pp. 409–417, 2014. [CrossRef]

[29] W. Zhang, L. Zhang, and A. Li, "Enhanced anaerobic digestion of food waste by trace metal elements supplementation and reduced metals dosage by green chelating agent [S, S]-EDDS via improving metals bioavailability," Water Research, Vol. 84, pp. 266–277, 2015. [CrossRef]

[30] R. Kadam, K. Khanthong, H. Jang, J. Lee, and J. Park, "Occurrence, fate, and implications of heavy metals during anaerobic digestion: A review," Energies, Vol. 15, Article 8618, 2022. [CrossRef]

[31] Official Gazette. Regulation on the Usage of Domestic and Municipal Treatment Sludge in Soil, Republic of Turkiye Ministry of Environment and Forestry, Official Gazette, No: 27661, Date: 03/08/2010.

Environ Res Tec, Vol. 6, Issue. 4, pp. 326–331, December 2023

Environmental Research and Technology
https://ert.yildiz.edu.tr - https://dergipark.org.tr/tr/pub/ert
DOI: https://doi.org/10.35208/ert.1264338

Environmental Research & Technology

Research Article

Using chlorella vulgaris as a natural-textile dye

Tasnim ALMOULKI*, Ebru AKKAYA

Department of Environmental Engineering, Yıldız Technical University, İstanbul, Türkiye

ARTICLE INFO

Article history
Received: 17 March 2023
Revised: 19 June 2023
Accepted: 21 September 2023

Key words:
Algae; Dyestuff; Textile.

ABSTRACT

The applications of algae are becoming more popular day by day. From biofuels to nutrients, cosmetics, pharmaceuticals, and most recently ink and textile dyes. Due to algae's high lipid content that works best as a substitute for petroleum-based products, and because it is carbon negative and eco-friendly, algae-based dyes can present a transitional solution to the environmental damages caused by the dyeing phases in the textile industry. Researchers have investigated the types, methods, applications, and efficiency of various algae species and types of dyes to serve in various coloring and printing applications. In this paper, we present the possibility of using microalgae as a natural dye for the textile industry. The microalgae studied were mixed species dominated by Chlorella Vulgaris. Pigments were extracted by acetone to create the natural dye which was used on a 100% cotton fabric using basic dying methods. A light-fastness test was subsequently performed, and the results indicated that the algae-colored fabric gained a value similar to those usually obtained with natural dyes.

Cite this article as: Almoulki T, Akkaya E. Using chlorella vulgaris as a natural-textile dye. Environ Res Tec 2023;6(4)326–331.

INTRODUCTION

With the growing awareness on the environmental damages caused by industrialization, and the increase in legislations that support carbon negative production and puts more limits on the use of harmful material or unmanaged waste disposal, researchers have become more interested in finding natural alternatives to synthetic material in almost every industry. In the textile industry, the dyeing stage represents the most dangerous to the environment due to the presence and high consumption of chemicals in each step and the difficulty to treat the resulted waste.

Natural dyes have proven to be successful substitutes for synthetic dyes in terms of color and quality. Only to produce such dyes, a large demand for landscape, water, and time is required; resulting in a challenge to withdraw conventional products in preference of natural alternatives. Dyes may be defined as substances that, when applied to a substrate, provide color by a process that alters, at least temporarily, any crystal structure of the colored substances [1, 2]. It is estimated that over 10.000 different dyes and pigments are used industrially, and over 7 x 10^5 tons of synthetic dyes are produced annually worldwide [3].

In recent years, significant interest has been developed in the commercial utilization of algae [4] due to its reliance on carbon dioxide and sunlight to grow, and because of its short growth rate and little need of landscape, in addition to its wide range of species that are majorly high in lipids, fatty acids, proteins, polysaccharides, and pigments [5]. Algae contains a broad range of photosynthetic pigments. Three main classes of photosynthetic pigments are: chlorophylls, carotenoids (xanthophylls and carotenes) and phycobilins.

***Corresponding author.**
*E-mail address: tasnim.almoulki1@std.yildiz.edu.tr

This paper has been presented at Sixth EurAsia Waste Management Symposium (EWMS 2022)/İstanbul, Türkiye / 24–26 October 2022.

Table 1. Different color constituents in algae [20]

	Colored constituents in algae constituents (Major)	Category
Green algae	Chlorophyll b	Chlorophyta
Euglenoids	Chlorophyll b	Euglenophyta
Brown algae	Chlorophyll c l, c2 and fucoxanthin	Phaeophyta
Yellow-brown or golden-brown algae	Chlorophyll c l, c2 and fucoxanthin	Chrysophyta
Dinoflagellates	Chlorophyll c2, peridinn	Pyrrophyta
Cryptomonads	Chlorophyll 2, phycobillins	Cryptophyta
Red algae	Phycoerythrin, phycocyanin	Rhodophyta
Blue-green algae	Phycoerythrin, phycocyanin	Cyanophyta

Different algal groups are classified based on predominant pigments, such as chlorophyll b in green algae [6], fucoxanthin, and carotenoids in brown algae [7], and β-carotene and zeaxanthin in red algae [8]. Furthermore, acetone extraction is considered the most effective and ecofriendly approach for efficient extraction of natural dyes [9].

This research points out some of the basic methods of extraction of algal dyes and their potential to serve the textile industry by dyeing a natural fabric.

Textile Dyes

Before diving into the overall process, it is important to gain some background on the dyeing phase in the textile industry. As the coloring of fabrics is considered one of the key factors in the successful trading of textile products [10]. The current dyeing methods have been used for a long time which differ according to the desired fiber, print or color, and product quality such as water repelling, antistatic protection, fire retardants etc. In order to result with a colored fabric, it generally goes through three steps, preparation or pretreatment, dyeing and finishing [10, 11]. However, it is known that no dye can be applied to all existing fibers, and no fiber can be dyed by all known dyes [12].

By the main use of synthetic dyes, the textile industry has posed serious environmental risks with the generated wastewater that can be very difficult to treat and resist in nature for many years. Various types of synthetic dyes and chemicals are characterized by a very high pH and salinity values [13]. A percentage of 54% of the dye effluents in the world are produced by textile industries [14]. It's estimated that 17–20% of industrial water pollution is solely caused by the textile industry according to The World Bank [15].

The main materials used in producing synthetic dyes are coal tar and petroleum, which have negative impacts on the environment. The reason synthetic dyes are still favorable is because natural dyes usually cost higher because of the tedious extraction of colorants from raw materials, the low color value and long dyeing time. In addition, some natural dyes are fugitive and can need mordants to enhance their fastness characteristics. Natural dyes also work best with natural, not synthetic, fabrics [16].

Algae Dyes

Algae can be considered as microscopic plants that are invisible to the naked eye, but when grown in water with sufficient nutrients, changes the color of water to green, brown, red, or blue depending on the microalgae species [17]. Of the total of 200.000 to 800.000 species of algae, only tens of thousands are listed in the literature [18]. Algae is known to have high lipid content that ranges from 50 to 80 % in biomass [19] and contains photosynthetic pigments [20]. For high-yielding varieties, the oil content in the dry matter of algae can reach up to 50–60% [21]. Table 1 shows the color constituents in algae.

Its pigments have been successfully used in food dyes, cosmetics, and pharmaceutical industries. Algae dyes for the textile industry can be produced similarly by the same pigments. Considering algae's fast growth rate, variety of colors, main reliance on sunlight and carbon dioxide to grow, and availability worldwide, it can serve as the best source of natural dyes [22].

For the aforementioned reasons, this study was performed to prove the possibility of using microalgae as an ecofriendly alternative to synthetic dyes.

MATERIALS AND METHODS

The process of creating algal-based dyes goes through three main stages: Biomass Production, Pigment Extraction, and Dyeing. Each stage will be explained in further detail as follows.

Biomass Production

In this study, firstly, Chlorella Vulgaris microalgae species obtained from a strain of international collection at Yildiz Technical University's Environmental Engineering Laboratory were dominantly grown in a mixed-algae culture with a synthetic nutrient medium. Bold's Basal Medium (BBM) was used as the freshwater-synthetic culture medium. BBM medium consists of the nutrients given in Table 2. According to Nichols and Bold, 1965 [23].

The stock solutions used in the preparation of the BBM were prepared in corresponding volumes of balloon flasks covered with aluminum foil, each solution is then completed with pure water, mixed for 30 minutes, and finally set in the autoclave for 120 °C 20 minutes for sterilization [23].

Table 2. Chemicals used in the preparation of the BBM culture media [23]

Stock solution number	Name of chemical	Formula	Weight (g)	Distilled water (ml)
1	Di potassium hydrogen orthophosphate	K_2HPO_4	1.875	250
2	Potassium dihydrogen orthophosphate	KH_2PO	4.375	250
3	Magnesium sulfate	$MgSO_4.7H_2O$	1.875	250
4	Sodium nitrate	$NaNO_3$	6.250	250
5	Calcium chloride	$CaCl_2.2H_2O$	0.625	250
6	Sodium chloride	NaCI	0.625	250
7	Tetrasodium EDTA	EDTA-Na_4	5.000	100
	Potassium hydroxide	KOH	3.100	
8	Ferrous sulfate	$FeSO_4.7H_2O$	0.498	100
	Sulfuric acid (1 mL=1.84 g)	H_2SO_4	0.184 g	
9*	Boric acid	H_3BO_3	1.142	100
10	Zinc sulfate	$ZnSO_4.7H_2O$	0.353	25
11	Manganese chloride	$MnCl_2.4H_2O$	0.058	25
12	Copper sulfate	$CuSO_4.5H_2O$	0.063	25
13	Cobalt nitrate	$Co(NO_3)_2.6H_2O$	0.020	25
14	Sodium molybdate	$Na_2MoO_4.2H_2O$	0.048	25

*: Should be heated at 50–60 °C to dissolve. All chemicals should be weighed with aluminum foil.

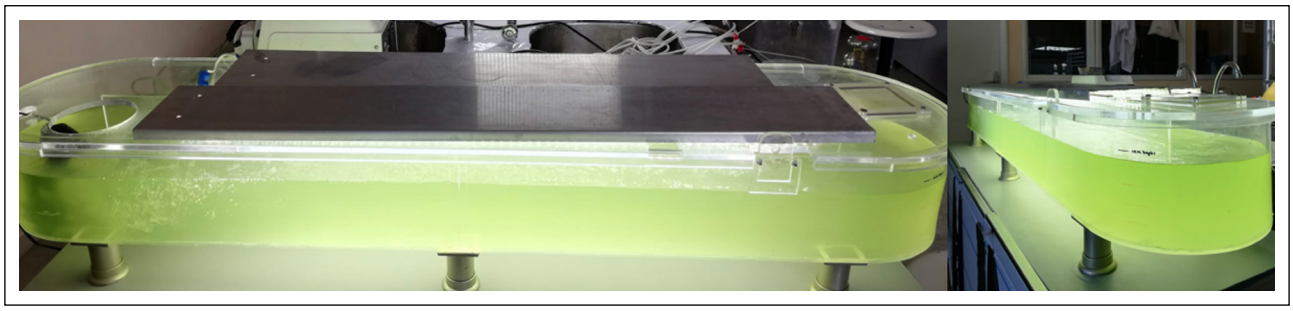

Figure 1. Microalgae production and growth processes in the bioreactor.

This process was repeated numerous times in order to fill the algae bioreactor that had a 50-liters volume in total, extra volumes were also made for the smaller algae samples that were constantly under control and required addition of BBM every week.

For the growth processes, available mixed-microalgae culture dominated by Chlorella Vulgaris were combined with sufficient amounts of media in the bioreactor as shown in Figure 1 for large production.

The growth rate and species were constantly monitored by measuring the Suspended Solid Matter's SSM concentration daily, and detecting the species under the microscope, the growth of algae in the bioreactor over time can be shown in Figure 2.

Following the daily measurements, and when the Suspended Solid Matter's SSM concentration reached approximately 0,5 mg/L, the samples were concentrated by a centrifuging machine to begin the drying phase.

Pigment Extraction

In the drying phase, semi-liquid biomass was obtained from microalgae species, which were concentrated by centrifuging at 4000 RPM for 10 minutes in the ROTO-FIX 32. This biomass was spread on a tray and placed in an oven to dry at 40˚C for 6 hours.

Afterwards, the obtained dry biomass was crushed in a mortar as in Figure 3 to create a fine powder of algae.

Soxhlet extraction was applied as the pigment extraction method from the microalgae powder. In this method, 5 gr of dry biomass' pigment was extracted using acetone as a solvent, and then the solvent was collected with a rotary evaporator [4]. Following the extraction process, the colored supernatant part was separated from the biomass wastes by filtration and/or centrifuging. After the separated supernatant was concentrated, it was stored for use in the dyeing process.

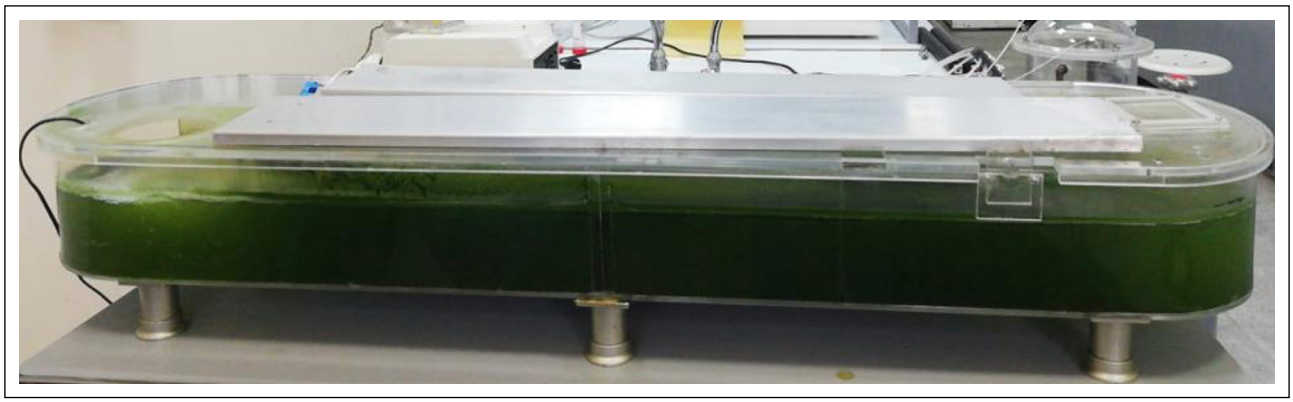

Figure 2. Biomass production.

Figure 3. Crushing of dried biomass in a mortar.

Coloring Process

The dyeing or coloring process experiment was carried out by using acetone for pigment extraction, with a pH 8.4, and 10 gr of %100 cotton fiber, the fiber was heated under 55 °C and set in a mixer for around 1 hour. This method was modified and adapted from the European Sea Colors Project [24]. The mordanting process to fix the dye to the product was not performed, as mordanting was disregarded in this study.

Since chlorophyl is the photosynthetic pigment found in the plant cell's chloroplast with its specific form chlorophyll-a, also a general photosynthetic pigment that plays an important role in photosynthesis [25], the amount of pigment extracted from the microalgae biomass was measured spectrophotometrically depending on the amount of chlorophyll-a presented on the fabrics.

Light Fastness Analysis

The color quality of the dyed fabric was determined by light fastness analysis carried out according to the ISO 105 B02 1994 method, through service procurement.

RESULTS AND DISCUSSION

Obtained Species

As previously mentioned, mixed microalgae culture dominated by Chlorella Vulgaris was used in the bioreactor and was monitored daily using a light microscope.

Figure 4 shows images of mixed species of microalgae obtained from the microscope.

The image shows Chlorella Vulgaris, Nannochloropsis, and traces of Spirulina.

Light Fastness

When exposed to sunlight, dyed fabrics can fade or change color over time. The durability of color on such materials against light is called light fastness [26]. Light fastness measurements are interpreted with the standard dyed blue scale made on 8 wools and separated according to their fastness. The dyed wool scale, along with the tested fabric, which are both exposed to light for the same amount of time, consist of 1–8 points for 8 appropriate standardly dyed samples for

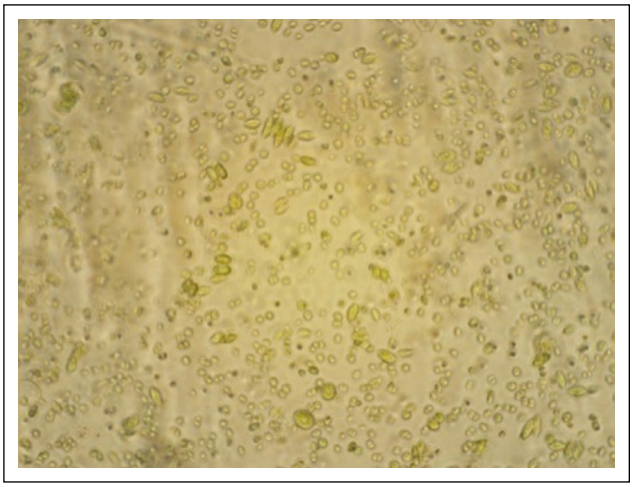

Figure 4. Mixed species under the light microscope.

Figure 5. Dyeing results of using an algae pigment.

light fastness. Number '1' indicates low light fastness whereas number '8' indicates high fastness [26]. Nearly all natural dyes have a lightfastness below British Standard (BS) grade 5 and most have a fastness below 4 [27].

Figure 5 shows the resulting light-green color of dyeing the cotton fabric. The sample gained a result of "2", which is in the range of 1–8 and deemed normal for usual organic dyes. This result was given by a private laboratory in İstanbul, Türkiye.

CONCLUSION

According to this study, the rich content of chlorophyll in microalgae gives it a high potential to be used as a natural dye resource. Although terrestrial plants can provide abundant amounts of chlorophyll, microalgae are much faster to grow, and require less resources and land to produce. Nevertheless, more research is required for the best methods of application of natural dyes in order to achieve similar quality to synthetic dyes.

The future of algae-based dyes is very promising as they are carbon negative and very safe to produce. The study showed preliminary results of successful coloring of fabric using pigments extracted from microalgae, nonetheless, further research on optimum algae species, variety of colors, and color fastness should be done.

Acknowledgements
The authors would like to express their sincere appreciation to Gülnaz Kımıldar, Sümeyye Yaşar, Prof. Dr. Mehmet Sinan Bilgili, Prof. Dr. Burcu Yılmaz and Research Assistant Umut Metin.

FUNDING

This work has been supported by TÜBİTAK 2209-B Project's Coordination Unit under project number 1139B412100508.

DATA AVAILABILITY STATEMENT

The authors confirm that the data that supports the findings of this study are available within the article. Raw data that support the finding of this study are available from the corresponding author, upon reasonable request.

CONFLICT OF INTEREST

The authors declared no potential conflicts of interest with respect to the research, authorship, and/or publication of this article.

ETHICS

There are no ethical issues with the publication of this manuscript.

REFERENCES

[1] S. I. Kroschwitz and A. Seidel, "Kirk-othmer encyclopedia of chemical technology," 5th ed., Wiley-Interscience, 2004.

[2] A. Bafana, S. Sivanesan, and T. Chakrabarti, "Azo dyes: Past, present and the future," Environmental Reviews, Vol. 19, 2011. [CrossRef]

[3] M. Hanafi, and N. Sapawe, "A review on the water problem associate with organic pollutants derived from phenol, methyl orange, and remazol brilliant blue dyes," Materials Today: Proceedings, Vol. 31(1), pp. A141–A150, 2020. [CrossRef]

[4] S. Mona, M. Yazhini, P. F. Shaukat, S. C. Sekarenthiran, and S. Maya, "Extraction of algal pigments and their suitability as natural dyes," Journal of Algal Biomass Utilization, Vol. 10(2), pp. 1–8, 2019.

[5] D. B. Stengel, S. Connan, and Z. A. Popper, "Algal chemo diversity and bioactivity: Sources of natural variability and implications for commercial application," Biotechnology Advances, Vol. 29(5), pp. 483–501, 2011. [CrossRef]

[6] E. M. El-Khatib, N. F. Ali, and R. S. R. El-Mohamedy, "Enhancing dyeing of wool fibers with colorant pigment extracted from green algae," Journal of Chemical and Pharmaceutical Research, Vol. 8(2), pp. 614–619, 2016.

[7] E. Susanto, A. S. Fahmi, T. Agustini, S. Rosyadi, and A. D. Wardani, "Effects of different heat processing on fucoxanthin, antioxidant activity and colour of indonesian brown seaweeds," IOP Conference Series: Earth and Environmental Science, Vol. 55, Article 012063, 2017. [CrossRef]

[8] N. Schubert, E. G. Mendoza, and I. P. Ruiz, “Carotenoid Composition of Marine Red Algae,” Journal of Phycology, Vol. 16(11), Article 426, 2006.
[9] I. Michalak and K. Chojnacka, “Algae as production systems of bioactive compounds,” Engineering in Life Sciences, Vol 15(2), pp. 160–176, 2014. [CrossRef]
[10] D. Chequer, F. Maria, G. A. R. Oliveira, E. Raquel A. Ferraz, J. Carvalho, M. V. B. Zanoni, and D. P. Oliveira, “Eco-friendly textile dyeing and finishing," in M. Günay (Eds.), Textile dyes: Dyeing process and environmental Impact, InTech, Chapter 6, 2013.
[11] T. A. Khattab, M. S. Abdelrahman, and M. Rehan, “Textile dyeing industry: environmental impacts and remediation,” Environmental Science Pollution Research International, Vol. 27(4), pp. 3803–3818, 2020. [CrossRef]
[12] M. Alcantara and D. Daltin, "A química do processamento têxtil," Química Nova, Vol. 19(3), pp. 320–330, 1996.
[13] M. Dilaver, S. M. Hocaoğlu, G. Soydemir, M. Dursun, B. Keskinler, İ. Koyuncu, and M. Ağtaş, “Hot wastewater recovery by using ceramic membrane ultrafiltration and its reusability in textile industry,” Journal of Cleaner Production, Vol. 171, pp. 220–233, 2018. [CrossRef]
[14] S. Samsami, M. Mohamadizaniani, M. H. Sarrafzadeh, E. R. Rene, and M. Firoozbahr, “Recent advances in the treatment of dye-containing wastewater from textile industries: Overview and perspectives,” Process Safety and Environmental Protection, Vol. 143, pp. 138–163, 2020. [CrossRef]
[15] R. Kant, “Textile dyeing industry an environmental hazard,” Natural Science, Vol. 4(1), pp. 22–26, 2012. [CrossRef]
[16] P. S. Vankar, “Chemistry of natural dyes,” Resonance, 2000. https://www.ias.ac.in/public/Volumes/reso/005/10/0073-0080.pdf Accessed on March 23, 2023.
[17] S. Hemming, A. Sapounas, and W. Voogt, “Algenteelt Systemen voor de tuinbouw: Integratie,” Wageningen UR, 2012.
[18] H. Wolkers, M. Barbosa, D. M. Kleinegris, R. Bosma, and R. H. Wijffels, “Microalgae: the green gold of the future,” Wageningen UR, 2011.
[19] X. Wang, Y. Zhang, C. Xia, A. Alqahtani, A. Sharma, and A. Pugazhendhi, “A review on optimistic biorefinery products: Biofuel and bioproducts from algae biomass,”Fuel, vol. 338, Article 127378, 2023. [CrossRef]
[20] N. Sekar, "Dyes from algae," Colourage, 2016.
[21] J. T. Agata, E. Wołejko, M. D. Ernazarovna, A. Glowacka, G. Sokolowska, and U. Wydro, “Using, Algae for biofuel production: A review," Energies, Vol. 16(4), Article 1758, 2023. [CrossRef]
[22] M. Azeem1, N. Iqbal, R. A. Mir, S. Adeel, F. Batool, A. A. Khan, and S. Gul, “Harnessing natural colorants from algal species for fabric dyeing: A sustainable eco-friendly approach for textile processing,” Journal of Applied Phycology, Vol. 31, pp. 3941–3948, 2019. [CrossRef]
[23] N. H. Wayne, and H. C. Bold, "Trichosarcina Polymorpha Gen. et Sp. Nov,” Wiley, 1965.
[24] Sea Colors, Layman’s Report, 2016.: https://webgate.ec.europa.eu/life/publicWebsite/index.cfm?fuseaction=search.dspPage&n_proj_id=5017#read-more Accessed on March 23, 2023.
[25] M. Fathi, S. Meshkini, and R. Nadiri, “The effect of extracted salt from urmia lake on the growth, βeta- carotene and chlorophyll a content of halophilic alga chlorella sp.,” Turkish Journal of Fisheries and Aquatic Sciences, Vol. 13(2), pp. 233–240, 2013. [CrossRef]
[26] T.C. Millî Eğitim Bakanlığı Tekstil Teknolojisi, “Renk Haslığı Testleri (Mekanik),” 1. basım. T.C. Millî Eğitim Bakanlığı, 2015.
[27] T. Padfield, and S. Landi, “The light-fastness of the natural dyes,” Studies in Conservation Vol. 11(4), pp. 181–196, 1966. [CrossRef]

Environ Res Tec, Vol. 6, Issue. 4, pp. 332–339, December 2023

Environmental Research and Technology
https://ert.yildiz.edu.tr - https://dergipark.org.tr/tr/pub/ert
DOI: https://doi.org/10.35208/ert.1244755

Environmental Research & Technology

Research Article

Optimal route selection using network analysis in terms of time, cost and fuel savings: The case of İskenderun, Türkiye

Benan YAZICI KARABULUT[1], Abdullah İzzeddin KARABULUT[2], Perihan DERİN[2], Mehmet İrfan YEŞİLNACAR[*1], Gülistan Banu ÇAKMAK[3]

[1]Department of Environmental Engineering, Harran University, Şanlıurfa, Türkiye
[2]Graduate School of Natural and Applied Sciences, Harran University, Remote Sensing and Geographic Information Systems, Şanlıurfa, Türkiye
[3]Graduate School of Natural and Applied Sciences, Harran University, Şanlıurfa, Türkiye

ARTICLE INFO

Article history
Received: 30 January 2023
Revised: 22 September 2023
Accepted: 28 September 2023

Key words:
GIS; Municipal Solid Waste Management; Route; Solid Waste Collection; Solid Waste

ABSTRACT

Solid waste generation has increased significantly as a result of increasing population and living standards. In this context, variables such as waste classification, amount produced, collection and transportation status, disposal method, socioeconomic status of the region include important stages in system planning. It is important to optimize these variables, waste collection route, time, cost, environmental impacts and examine the current situation. The cost of collection and processing accounts for roughly 65–80% of the total cost of the solid waste management system managed by local governments. Therefore, by optimization studies, the trash collection-transport route can significantly reduce this rate. Depreciation and fuel expenditures can be significantly reduced as a result of improvements in operational costs. Denizciler neighborhood was selected as an example of all district characteristics within the study's scope when the socio-economic, demographic, and topographic conditions of the Iskenderun district of Hatay province were evaluated. The ESRI ARCGIS software's tools have been used to test the optimization path. A 421-meter shorter route was discovered using network analysis. Considering the current route, which is 14340 meters long, a 3% improvement has been achieved with the analysis made. Garbage collection was done using the newly developed route in the study's final section. As a result, the viability of the network analysis enhancement has been evaluated in practice, and it has been discovered that time and fuel savings are realized in terms of cost.

Cite this article as: Yazıcı Karabulut B, Karabulut Aİ, Derin P, Yeşilnacar Mİ, Çakma GB. Optimal route selection using network analysis in terms of time, cost and fuel savings: The case of İskenderun, Türkiye. Environ Res Tec 2023;6(4)332–339.

INTRODUCTION

One of the most important environmental problems that directly affect human life and cause harmful effects is solid waste. As the population shows a constantly increasing trend around the world, it is inevitable that consumption should follow this rising trend together with the population. As a result, solid waste production is increasing day by day. As of 2020, according to the data of the Turkish Statistical Institute, the population of our country has been

***Corresponding author.**
*E-mail address: mirfan@harran.edu.tr

This paper has been presented at Sixth EurAsia Waste Management Symposium (EWMS 2022)/İstanbul, Türkiye / 24–26 October 2022.

determined as 83 million 614 thousand 362 people. While around 32.3 million tons of urban solid waste is produced annually in our country, an average of 1.13 kg of solid waste is produced per person per day [1]. With the increase in population, the investment costs for the collection of solid wastes have increased.

Solid waste management is a major concern for local governments worldwide, not only because of its environmental impact, but also because waste collection services are one of the highest expenditures of municipalities in low-income countries [2]. Typically, collection costs represent 80-90% and 50-80% of the municipal solid waste management budget in low-income and middle-income countries, respectively [3]. Waste collection and transport alone accounts for approximately 50-70% of the total cost of the system. Optimum location and number of transfer stations are required for an economical and efficient collection system [4]. In particular, solid waste collection and transport activities account for approximately 50% to 70% of total solid waste management costs. Total collection costs represent 0.5% to 2.5% of per capita income for developing countries [5]. Therefore, solid waste collection and transportation is a costly business. Improvements to be made in solid waste collection routes will have a positive impact on the collection cost. In a study by İrdemez et al. [6], the process of municipal solid waste collection and transport systems in Palandöken district of Erzurum province was examined in all aspects. Studies on the characterization, amount and projection of municipal solid wastes have been carried out, and a route optimization study has been carried out by using Google earth program to determine the most suitable routes. Minimum cost systems have been developed for effective, efficient and regular collection and transport of wastes.

It is essential to design efficient and simple transport routes for collection and recovery systems (including the processing capacity of distribution points and recycling stations, disposal and transport times, staffing arrangement, etc.), based on the principles of maintaining minimum cost and hygiene standards [7]. The traditional approach to waste collection creates a fleet of trucks that collect/transfer waste from individual/common bins to treatment/disposal facilities. This is a very costly process that accounts for more than 60% of total waste management expenditure due to fees, fuel consumption, maintenance and depreciation. A study developed a GIS-based smart collection model for waste collection route in the United Arab Emirates. In this way, it was found that the system reduced the cost of waste collection by 19% compared to the traditional scenario [8]. In this context, it is possible to use a geographic information system (GIS) as a strategy to optimize collection times and reduce costs on routes [9]. The most common optimization goals are; It includes waste collection path optimization by reducing the route length, time optimization, cost optimization and environmental effects [10].

Collection and transportation of solid waste constitutes the majority of solid waste management. In the literature, it is possible to reach optimization studies with the integration of different disciplines such as environment, geomatics and industrial engineering.

In the study, an optimization study was conducted to increase the efficiency of solid waste collection in Greece. ArcGIS network analysis was used for optimization. Within the scope of the study, two different experiments were conducted. The first set of experiments (S1) dealt with collection vehicle route optimization and the second set of experiments (S2) dealt with container reallocation and route optimization. In both cases, savings were observed compared to the current operation. According to the results of the optimization study, 3% improvement in collection time for S1 and 17% improvement for S2; 5.5% improvement for S1 and 12.5% improvement for S2 in terms of distance traveled [11]. In the study [12], optimization was performed for solid waste collection and transportation operations in Safakes, Tunisia. In the optimization process using ArcGIS Network network analysis, 3 sets of experiments were created.

GIS was used [13] domestic solid waste collection and transportation works in Şanlıurfa, Suruç Municipality. With this study, it was aimed to minimize the solid waste collection and transportation process costs. It has been seen that the obtained data contributed greatly to the cost of the studies using GIS.

In the study conducted [14] the solid waste collection route optimization of Diyarbakır province, Kayapınar district, Barış neighborhood was discussed. For this study, the ant colony, which is one of the artificial intelligence samples, and the performance of genetic algorithms and GIS software were used in coordination. As a result of the study in question, different results were obtained with each method. The Ant Colony Algorithm provided the most efficient result in numerical terms, with an improvement of approximately 41%.

The Denizciler neighborhood in the İskenderun county of Hatay was chosen as a representative neighborhood for the study, and the neighborhood's current waste collection system was examined. The solid waste collection route was then attempted to be optimized using GIS. The ArcGIS solution was able to reduce the total distance by 3% as a result of the optimization research conducted to optimize using these methods. Therefore, this work will be further developed to combine various flexible computing techniques in terms of time, money and a sustainable environment.

MATERIALS AND METHODS

Study Area

To route optimization, İskenderun district, which is the most developed district in terms of industry and urbanization, was selected from 15 districts in Hatay province. The population of Iskenderun is 250 thousand 964 according to 2020 Turkish Statistical Institute data [1]. There are 45

Figure 1. Location map of the study area.

neighborhoods in Iskenderun district (Fig. 1). Denizciler neighborhood one of the neighborhoods by the sea, has a surface area of 2 million 921 thousand 200 square meters and a population of 24 thousand 617 people. The slope of the elevation profile of Denizciler neighborhood, which is one of the densely populated neighborhoods, is 15% and has an average slope of 5.7%. According to the geometric standards of the highways, the Denizciler neighborhood topographic structure (5.7%) can be considered flat. The daily waste amount was calculated as approximately 28 tons and 10,000 tons per year.

Geographic Information System and Network Analysis Tool

Geographic Information System (GIS) "designed to solve complex planning and management problems; It can be defined as the system of hardware, software and methods that enable the coverage, management, processing, analysis, modeling, and display of the data whose position in the space is determined [15–17]. Environmental management, municipal activities, transportation, health, tourism, education, agriculture, trade, defense, and security systems, etc. It has a wide usage area [15]. Network analyst tool, which is one of the GIS analyzes, was used. With the network analysis tool, many analyzes can be performed such as creating a single or multi-modal network dataset, determining the best route using a network dataset, creating a model for route analysis, transporting several orders with a vehicle fleet, network analysis using traffic data, and optimal location allocation [18, 19].

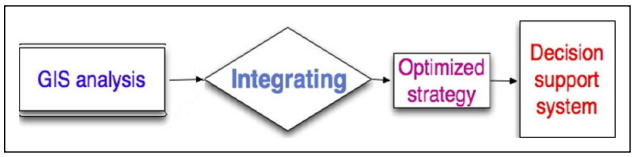

Figure 2. Optimization implementation stages.

The primary purpose of adopting GIS in solid waste management is to reduce cost and time (feasibility) and also to help planners make better decisions when designing solid waste management. From a technical point of view, geographic information systems are an up-to-date tool for modeling and optimizing service routes for which a better scenario can be proposed [19].

Methodology

The road map of Denizciler neighborhood was obtained from the Planning and Project Directorate of Iskenderun Municipality and converted into ".shp" format supported by Esri ArcGIS software from Geographic Information System applications. The coordinate data of the points where the Solid Waste containers are located were determined in the field study with the help of Iskenderun Solid Waste Association and Envitec personnel, and the coordinates of the locations of these points were transferred to Esri ArcGIS 10.8 software.

Esri ArcGIS 10.8 software was used within the scope of Denizciler neighborhood solid waste collection route optimization (Fig. 2). To be transferred to the GIS software, Denizciler neighborhood road map coordinates obtained from the Planning and Project Directorate of Iskenderun Municipality were converted to the "TUREF_TM39" coordinate system by adding direction limitation, speed limit and time limit. As a result of the field work carried out with the officials of Envitech company, which is authorized by the Iskenderun Municipality for the collection of neighborhoods in Denizciler neighborhood, the solid waste container points were recorded by GPS. This program records the coordinate data of garbage collection vehicles instantly. As a result of this study, after the locations of the containers were marked on the map, the network topology of Denizciler neighborhood was created. There are 202 solid waste collection containers available in Denizciler neighborhood. Network structure and container points of Denizciler neighborhood is shown in Figure 3.

RESULTS AND DISCUSSION

Examination of the Current Route

To determine the route and container points in Denizciler neighborhood, field work was carried out by getting on the garbage collection vehicle in the company of Envitec personnel. The garbage collection process, which started at 6:45 in the morning from Dutlu Bahçe Site in Denizciler neighborhood, took 5 hours and a total distance of 14340 meters was measured. This process is carried out regularly at the same time every day of the week. The neighborhood where the fieldwork was carried out has streets and avenues that can be considered regular.

Figure 3. Network structure and container points of Denizciler neighborhood.

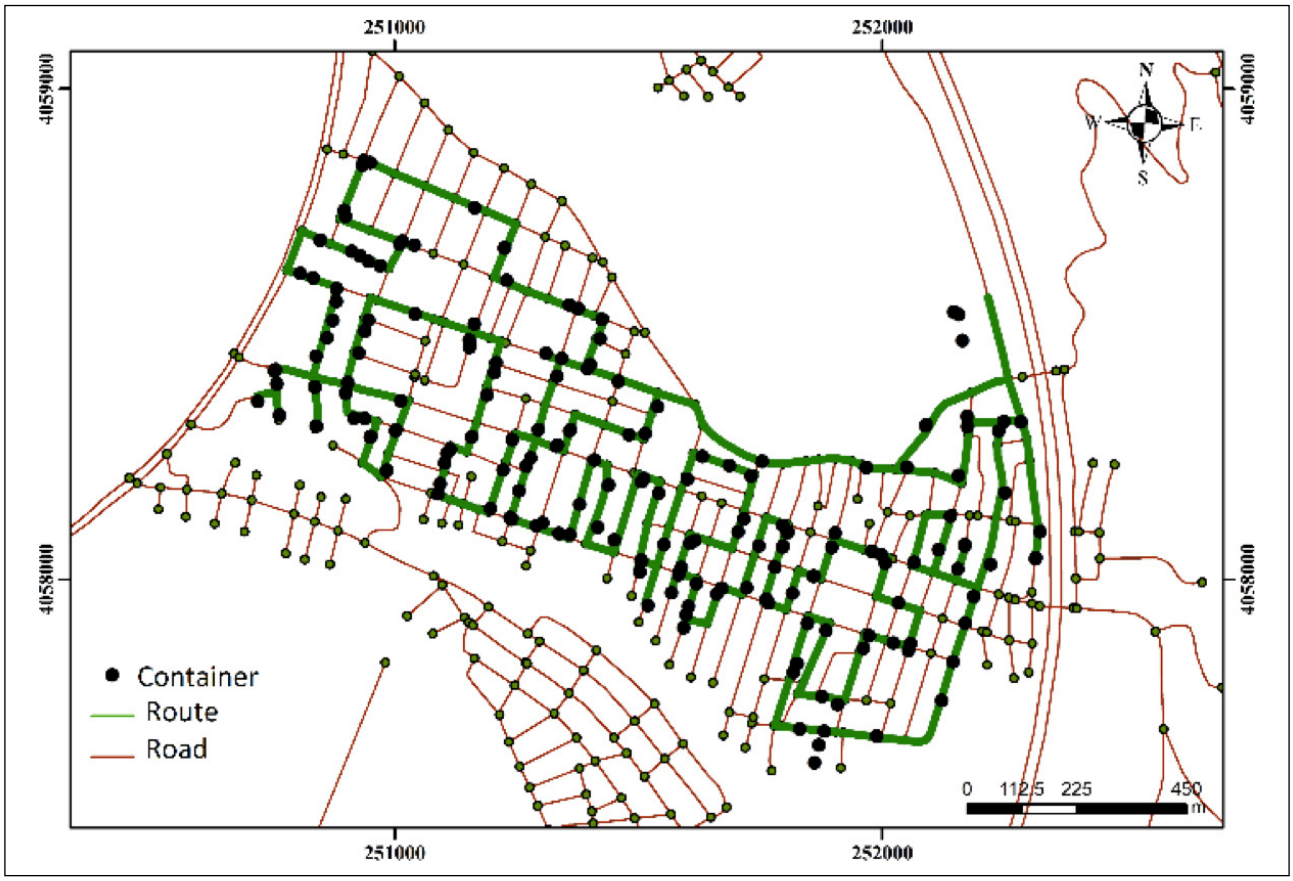

Figure 4. Road route optimization as a result of network analysis.

Figure 5. Route ranking of container points because of network analysis.

Denizciler Neighborhood Solid Waste Collection and Route Optimization Data

The physical and logical structures of networks are explained by topology. In this context, the ways in which the components that make up the networks come together with each other, the ways to be followed and the appropriate usage patterns are within the scope of the topology. The combination of parts connected by different forms creates networks. These interconnected lines are explained by network analysis. Connecting parts such as street, road, main road, avenue is within the scope of network analysis. The connection states of the networks are determined by the topological relationships explained by the nodes.

The coordinate data of Denizciler neighborhood solid waste container points were transferred the ArcGIS software, and the optimum route was obtained with Network Analysis. Route For optimization, the ArcGIS software has been tested with various tools in the software. As a result of the route optimization with network analysis, 13919 meters distance was measured (Fig. 4). Network The analysis has been obtained 421 meters shorter route. 14340 meters in length available Considering the route, a significant improvement was obtained with the analysis (Fig. 5).

A lot of research has been done to find suitable targets in waste optimization. Prabhakaran et al. [20], route optimization was performed with ArcGIS network analysis for domestic solid waste collection. The determined region was studied by dividing it into two. It was observed that the distance traveled to collect solid waste was reduced by 25% as a result of optimization. In a study by Gümüş et al. [21], it was aimed to minimize the transport cost by organizing the collection routes of the recycling facility wastes belonging to Alanya Municipality. As a result of the study, it was found that the proposed vehicle routing problem (ARP) model shortened the transport distance and provided a monthly vehicle fuel saving of approximately 12%. Sanjeevi et al. [12] an optimization study was carried out using ArcGIS application in Chennai, one of the major metropolitan cities in the southeast of India. After developing a spatial database for the whole of Chennai with 200 nodes, 13 solid waste transfer stations were identified through optimization studies using ArcGIS. This optimization process has reduced the distance traveled by 9.93%. In the study conducted by Ağaçsapan (2016) [22] Geographic Information Systems (GIS) were used in the selection of the waste transfer stations in Eskişehir province. The characteristics of the area where the wastes are managed, which differ according to the characteristics of the environment in which they are produced, are taken into consideration. In this context, GIS application was used in the sustainable realization of waste management and in determining the most suitable area for the environment and human health in line with the data available while determining the field of activity.

Table 1 shows the number of containers and the distances between them at the stops on the route formed as a result

Table 1. The mathematical model of the routes in the study

Container sorting and cumulus distance					
Container 1	0,00	Container 69	5283,18	Container 137	9234,30
Container 2	2,32	Container 70	5283,18	Container 138	9266,86
Container 3	54,48	Container 71	5348,67	Container 139	9407,69
Container 4	482,39	Container 72	5404,11	Container 140	9557,90
Container 5	533,97	Container 73	5450,73	Container 141	9592,25
Container 6	542,37	Container 74	5520,92	Container 142	9654,29
Container 7	911,68	Container 75	5549,84	Container 143	9724,80
Container 8	914,01	Container 76	5664,76	Container 144	9744,61
Container 9	1043,54	Container 77	5693,42	Container 145	9744,99
Container 10	1180,24	Container 78	5792,03	Container 146	9796,78
Container 11	1302,72	Container 79	5839,97	Container 147	9819,75
Container 12	1323,62	Container 80	5898,60	Container 148	9880,66
Container 13	1410,96	Container 81	5970,41	Container 149	9882,89
Container 14	1410,96	Container 82	6122,35	Container 150	9998,98
Container 15	1536,14	Container 83	6250,26	Container 151	10000,08
Container 16	1683,24	Container 84	6391,68	Container 152	10080,36
Container 17	1809,36	Container 85	6418,71	Container 153	10082,77
Container 18	1859,17	Container 86	6419,01	Container 154	10163,93
Container 19	1861,20	Container 87	6566,03	Container 155	10373,64
Container 20	2030,29	Container 88	6621,48	Container 156	10373,80
Container 21	2108,43	Container 89	6624,76	Container 157	10453,55
Container 22	2262,60	Container 90	6779,53	Container 158	10453,73
Container 23	2429,67	Container 91	6907,86	Container 159	10731,88
Container 24	2480,97	Container 92	6992,75	Container 160	10818,21
Container 25	2555,02	Container 93	6994,07	Container 161	10878,36
Container 26	2628,69	Container 94	7059,24	Container 162	10904,45
Container 27	2628,69	Container 95	7157,80	Container 163	10907,24
Container 28	2819,53	Container 96	7222,61	Container 164	11031,52
Container 29	2937,00	Container 97	7251,82	Container 165	11075,84
Container 30	2953,02	Container 98	7253,24	Container 166	11112,67
Container 31	2959,32	Container 99	7301,74	Container 167	11152,14
Container 32	3005,28	Container 100	7320,25	Container 168	11152,55
Container 33	3178,26	Container 101	7391,94	Container 169	11176,75
Container 34	3196,48	Container 102	7397,37	Container 170	11233,28
Container 35	3197,11	Container 103	7402,47	Container 171	11260,76
Container 36	3282,36	Container 104	7465,32	Container 172	11415,08
Container 37	3357,68	Container 105	7518,19	Container 173	11415,69
Container 38	3550,77	Container 106	7536,84	Container 174	11415,69
Container 39	3583,86	Container 107	7619,79	Container 175	11415,69
Container 40	3710,01	Container 108	7621,66	Container 176	11484,31
Container 41	3747,15	Container 109	7677,90	Container 177	11503,09
Container 42	3799,22	Container 110	7680,95	Container 178	11523,38
Container 43	3839,58	Container 111	7830,91	Container 179	11549,51
Container 44	3854,50	Container 112	7873,56	Container 180	11634,15
Container 45	3985,87	Container 113	7934,88	Container 181	11634,67
Container 46	4104,89	Container 114	8053,36	Container 182	11642,19
Container 47	4132,22	Container 115	8123,04	Container 183	11669,34
Container 48	4152,31	Container 116	8123,04	Container 184	11822,24
Container 49	4251,30	Container 117	8213,68	Container 185	11851,66
Container 50	4281,30	Container 118	8249,74	Container 186	11952,14
Container 51	4393,48	Container 119	8287,74	Container 187	11977,17
Container 52	4395,15	Container 120	8403,53	Container 188	11993,51
Container 53	4474,92	Container 121	8480,55	Container 189	12241,43
Container 54	4548,93	Container 122	8544,45	Container 190	12385,91
Container 55	4566,20	Container 123	8627,07	Container 191	12386,77
Container 56	4633,45	Container 124	8744,54	Container 192	12477,94
Container 57	4677,76	Container 125	8773,72	Container 193	12615,59
Container 58	4680,11	Container 126	8774,93	Container 194	12635,68
Container 59	4732,75	Container 127	8817,38	Container 195	12687,97
Container 60	4754,66	Container 128	8837,49	Container 196	12746,05
Container 61	4756,87	Container 129	8847,17	Container 197	12803,50
Container 62	4877,12	Container 130	8919,77	Container 198	13241,93
Container 63	4965,49	Container 131	8921,40	Container 199	13242,00
Container 64	5024,18	Container 132	9012,18	Container 200	13474,38
Container 65	5044,97	Container 133	9060,69	Container 201	13475,12
Container 66	5163,31	Container 134	9081,95	Container 202	13880,02
Container 67	5189,61	Container 135	9218,80	Container 203	13919,04
Container 68	5234,00	Container 136	9222,08		

Table 2. Comparison of route optimization data

Data	Current route	Route optimization	New route	Net gain
Time	5 hours	4 hours 42 minute	4 hours 47 minute	0.13 minute
Distance	14340 m.	13919 m.	14000 m.	340 m.

of the Route Optimization model. Before starting the study, an interview was held with the relevant municipality personnel in the study area. As a result of this meeting, it was learned that 1 vehicle in the study area is sufficient for solid waste collection. Therefore, the capacity of vehicle was not taken into account in the route optimization that constitutes the method of this study.

Comparison of Route Optimization Data

Route optimization with network analysis calculated the current route as 4 hours 42 minutes and 13919 meters. Solid waste collection was carried out by applying the route formed as a result of route optimization in the GIS. With the use of the re-determined route after reflecting these data on the field, the time to reach the last point of the solid waste collection vehicle, which started from the first container, was 4 hours and 47 minutes, and the total distance was measured as 14000 meters (Table 2). As a result of the optimization study, a real gain of 18 minutes and 340 meters emerged. This daily time and distance gain for the solid waste collection vehicle operating every day of the week will be 126 minutes and 2380 meters per week, 540 minutes and 10200 meters per month, 6570 minutes and 124100 meters per year.

It was evaluated that the difference between the time and distance obtained by network analysis and Route Optimization and the time and distance obtained by reflecting these data to the field is due to the arbitrary relocation of containers, the containers are not full and the traffic situation in dead-end streets may vary.

CONCLUSIONS

The fieldwork, which was initiated from Denizciler neighborhood Dutlu Bahçe Sitesi at 06:45 in the morning to examine the current route, lasted 5 hours and a total of 14340 meters of road was measured. As a result of the optimization study, a real gain of 18 minutes and 340 meters emerged. This daily time and distance gain for the solid waste collection vehicle operating every day of the week will be 126 minutes and 2380 meters per week, 540 minutes and 10200 meters per month, 6570 minutes and 124100 meters per year. The labor force gain that will occur because of the shortening of the existing route will lead to an increase in productivity for the company. On the other hand, efficiency in fuel consumption will increase as solid waste collection vehicles travel less distance. As another result of this situation, exhaust gas emission will decrease, and it will have less impact on environmental pollution. Since the depreciation shares of vehicles on a yearly basis will decrease, maintenance and repair costs will also decrease.

Acknowledgements

This study was financially supported by Harran University Scientific Projects Research Coordinator (HUBAP) under grant no. 21233.

DATA AVAILABILITY STATEMENT

The authors confirm that the data that supports the findings of this study are available within the article. Raw data that support the finding of this study are available from the corresponding author, upon reasonable request.

CONFLICT OF INTEREST

The authors declared no potential conflicts of interest with respect to the research, authorship, and/or publication of this article.

ETHICS

There are no ethical issues with the publication of this manuscript.

REFERENCES

[1] Turkish Statistical Institute, "Turkish Statistical Institute," https://www.tuik.gov.tr/. Accessed on Feb. 16, 2021.

[2] L. Guibrunet, "What is 'informal' in informal waste management? Insights from the case of waste collection in the Tepito neighbourhood, Mexico City," Waste Management, Vol. 86, pp. 13–22, 2019. [CrossRef]

[3] S. Das, and B. K. Bhattacharyya, "Optimization of municipal solid waste collection and transportation routes," Waste Management, Vol. 43, pp. 9–18, 2015. [CrossRef]

[4] P. Rathore, and S. P. Sarmah, "Modeling transfer station locations considering source separation of solid waste in urban centers: A case study of Bilaspur city, India," Journal of Cleaner Production, Vol. 211, pp. 44–60, 2019. [CrossRef]

[5] C. Blazquez, and G. Paredes-Belmar, "Network design of a household waste collection system: A case study of the commune of Renca in Santiago, Chile," Waste Management, Vol. 116, pp. 179–189, 2020. [CrossRef]

[6] Ş. İrdemez, M. Yıldırım, S. Kul, F. E. Torun, and Z. Bingül, "Erzurum-Palandöken katı atık toplama-taşıma sisteminin cbs destekli optimizasyonu," Kent Akademisi, Vol. 14(3), pp. 687–704, 2021. [Turkish] [CrossRef]

[7] C. X. Lou, J. Shuai, L. Luo, and H. Li, "Optimal transportation planning of classified domestic garbage based on map distance," Journal of Environmental Management, Vol. 254, Article 109781, 2020. [CrossRef]

[8] M. Abdallah, M. Adghim, M. Maraqa, and E. Aldahab, "Simulation and optimization of dynamic waste collection routes," Waste Management & Research, Vol. 37(8), pp. 793–802, 2019. [CrossRef]

[9] A. Exposito-Marquez, C. Exposito-Izquierdo, J. Brito-Santana, and J. A. Moreno-Pérez, "Greedy randomized adaptive search procedure to design waste collection routes in La Palma," Computers & Industrial Engineering, Vol. 137, Article 106047, 2019. [CrossRef]

[10] M. A. Hannan, M. H. Lipu, M. Akhtar, R. A. Begum, M. A. Al Mamun, A. Hussain, and H. Basri, "Solid waste collection optimization objectives, constraints, modeling approaches, and their challenges toward achieving sustainable development goals," Journal of Cleaner Production, Vol. 277, Article 123557, 2020. [CrossRef]

[11] S. Chalkias, and K. Lasaridi, "GIS based model for the optimisation of municipal solid waste collection: the case study of Nikea, Athens, Greece," Wseas Transactions on Environment and Development, pp. 640–650, 2009.

[12] V. Sanjeevi, and P. Shahabudeen, "Optimal routing for efficient municipal solid waste transportation by using Arc GIS application in Chennai, India," Sage Journals, Vol. 34(1), pp. 11–21, 2016. [CrossRef]

[13] M. E. Çakır, A. Demir-Yetiş, M. İ. Yeşilnacar, and M. Ulukavak, "Determination of the optimum routes and performing of the spatial distribution maps for solid waste using GIS: A case of study from Suruç (Şanlıurfa)," BEU Journal of Science, Vol. 8(2), pp. 595–603, 2019. [CrossRef]

[14] H. Pamukçu, "Optimization of solid waste collection route: The example of Kayapinar (Diyarbakir) county," Master thesis. Harran University Graduate School of Natural and Applied Sciences, Sanlıurfa, Türkiye, 2022. [Turkish]

[15] G. Töreyen, İ. Özdemir, and T. Kurt, "ArcGIS 10 desktop application document," Sinan Ofset, Ankara, 2011.

[16] A. İ. Karabulut, B. Yazici-Karabulut, P. Derin, M. I. Yesilnacar, and M. A. Cullu, "Landfill siting for municipal solid waste using remote sensing and geographic information system integrated analytic hierarchy process and simple additive weighting methods from the point of view of a fast-growing metropolitan area in GAP area of Turkey," Environmental Science and Pollution Research, Vol. 29, pp. 4044–4061, 2022. [CrossRef]

[17] A. I. Karabulut, S. Benek, and F. Ernst, "Geodesign yöntemi kullanılarak sürdürülebilir kentsel büyüme analizi: Eyyübiye ilçe merkezinden (Şanlıurfa) bir örnek çalışma," Coğrafya Dergisi, Vol. 42, pp. 251–269, 2021. [Turkish] [CrossRef]

[18] O. Rızvanoğlu, S. Kaya, M. Ulukavak, and M. İ. Yeşilnacar, "Optimization of municipal solid waste collection and transportation routes, through linear programming and geographic information system: a case study from Şanlıurfa, Turkey," Environmental Monitoring Assessment, Vol. 192, Article 9, 2020.

[19] E. M. Asefa, K. B. Barasa, and D. A. Mengistu, "Application of geographic information system in solid waste management," IntechOpen, 2022.

[20] S. Prabhakaran, K. Sindhu, R. Akash, V. Arunkumar, L. Krishna, and D. Manikandan, "Route optimization for municipal solid waste collection using Arc GIS Network," Analyst Journal of Advanced Research in Dynamical and Control Systems, Vol. 9(2), pp. 392–398, 2017.

[21] M. Gümüş, E. H. Özder, E. Hatınoğlu, and A. Uçar, "Geri dönüşüm atıklarının toplanmasında rota optimizasyonu: Alanya ilçesinde bir uygulama," Journal of Turkish Operations Management, Vol. 6(1), pp. 1102–1112, 2022.

[22] B. Ağaçsapan, "Katı atık yönetiminde coğrafi bilgi sistemleri: Eskişehir ili atık aktarma istasyonları için yer seçimi örneklemi," Anadolu University, Graduate School of Natural and Applied Sciences, Master Thesis, Eskişehir, pp. 192, 2016. [Turkish]

Environ Res Tec, Vol. 6, Issue. 4, pp. 340–346, December 2023

Environmental Research and Technology
https://ert.yildiz.edu.tr - https://dergipark.org.tr/tr/pub/ert
DOI: https://doi.org/10.35208/ert.1233807

Environmental Research & Technology

Research Article

Effect of torrefaction pretreatment on combustion behaviour of different agricultural wastes

Neslihan DURANAY*, Melek YILGIN, Ercan AYDOĞMUŞ

Department of Chemical Engineering, Fırat University Faculty of Science and Letters, Elazığ, Türkiye

ARTICLE INFO

Article history
Received: 13 January 2023
Revised: 18 September 2023
Accepted: 10 October 2023

Key words:
Agricultural waste; Combustion; Energy recovery; Torrefaction

ABSTRACT

In this study, which was carried out to investigate the effect of the torrefaction process on the combustion behaviour of agricultural wastes, almond hulls and shells, olive seeds and corn stalks were used. The samples, dried in a laboratory atmosphere, were torrified at 300±5 °C for 41 minutes. The change in fuel properties was determined by making proximate analyses of the solid product obtained after the process and compared with the raw sample. The effects of the torrefaction process on the combustion behaviour of agricultural wastes of different structures were investigated by burning the 1±0.15 g weighted raw and torrefied samples at 700 °C furnace initial temperature in a fixed bed system. Biochars containing higher fixed carbon were obtained with the torrefaction process applied to agricultural waste, and it was determined that this caused biochars to burn more efficiently and for a longer time than raw biomass. As a result, it was determined that biochar with better properties was produced by the torrefaction process applied to agricultural wastes and it was suitable for burning in solid fuel combustion systems. Thus, biochar obtained will both contribute to the country's economy and add value to agricultural wastes that cause problems during storage, transportation, loading into the burning system, and combustion.

Cite this article as: Duranay N, Yılgın M, Aydoğmuş E. Effect of torrefaction pretreatment on combustion behaviour of different agricultural wastes. Environ Res Tec 2023;6(4)340–346.

INTRODUCTION

The increase in greenhouse gas emissions, caused by the burning of fossil fuels, and the resulting increase in global average temperatures, has become a very important problem with its impact on human health, the environment, and climate conditions. The fundamental cause of this is the overuse of fossil fuels. When setting the goals for 2030, it was underlined by the United Nations that providing eco-friendly and green energy was one of the top priorities. Using green energy will help reduce over-reliance on fossil fuels and create an eco-friendly environment. Additionally, studies have shown that conventional energy sources (such as coal and fossil fuels) tend to run out, so it is necessary to investigate alternatives to ensure that customers have access to energy at all times [1]. Hydro, geothermal, tidal, solar, wind and biomass energy are examples of current renewable energy sources. One source of renewable energy, biomass, has dependable and promising qualities. This is due to the abundance of biomasses in both woody (forest wood) and non-woody forms (agricultural). In terms of primary energy sources, biomass ranks fourth behind oil, coal, and natural gas [2, 3].

***Corresponding author.**
*E-mail address: nduranay@firat.edu.tr

This paper has been presented at Sixth EurAsia Waste Management Symposium (EWMS 2022)/İstanbul, Türkiye / 24–26 October 2022.

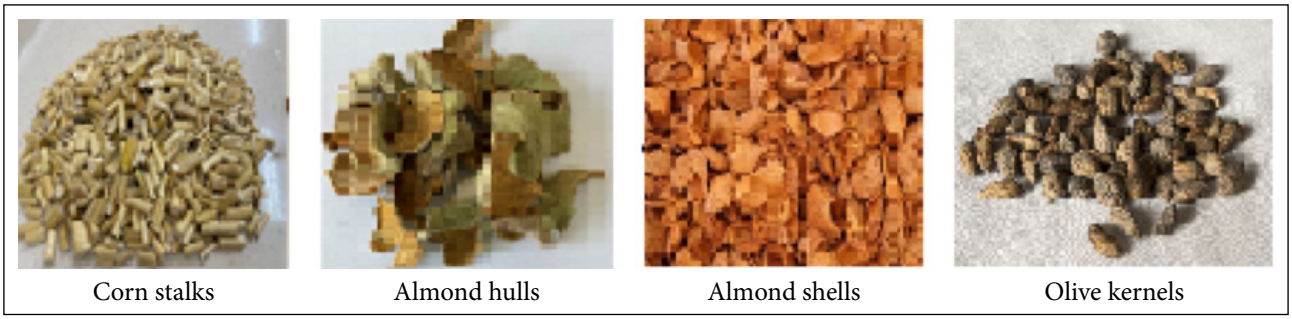

Figure 1. Agricultural waste samples.

Agricultural biomass is defined as energy crops grown and residues/wastes from agricultural production (such as straw, vineyard pruning waste, and vegetable and fruit production waste). It is thought that the residues obtained from agricultural activities will soon be one of the most important energy sources. It is reported in the literature that the annual agricultural waste produced globally is approximately 2000 billion tons [1]. This waste is mostly formed in regions with intensive agricultural activities. Usually, these wastes are dumped in the fields or burned [4]. Conversion of these wastes into usable energy will make an important contribution to the protection of the environment. For agricultural wastes to be used effectively and efficiently in energy production, pre-treatment is required. These processes are carried out to reduce problems such as low calorific value and bulk density, high moisture content, transportation, and storage, which limit the use of agricultural waste as a direct fuel. Various processes are applied to eliminate the disadvantages of biomass to be used in energy production. These are thermal, physical, biological, and mechanical processes [4, 5]. Thermal processes are generally the process of heating biomass in an inert or oxygen-deficient environment. Examples of heat treatment are gasification, pyrolysis, carbonization, and torrefaction [5]. These methods differ in operating temperatures. Torrefaction is a thermal pretreatment technique that operates at temperatures as low as 200–300 °C, usually under inert conditions and at a heating rate not exceeding 50 °C/min. Waste recycling by torrefaction is an important alternative for the sustainable management of both waste and energy and improves the undesirable properties of agricultural wastes that hinder their thermal treatment. As a result of this process; a hydrophobic solid with increased energy density is produced that can be easily ground, processed, and transported. Unlike conventional pyrolysis coal, which is characterized by an energy efficiency of 55–65%, torrefied solid typically retains 90% of the initial energy contained in the main fuel and is suitable for combustion, co-combustion, and gasification applications [1, 6, 7].

In this study, the effect of torrefaction applied to agricultural wastes of different structures on solid fuel combustion stages such as ignition, volatile matter and carbon combustion periods was investigated. For this purpose, almond shells and shells, corn stalks, and olive kernels were used as agricultural waste.

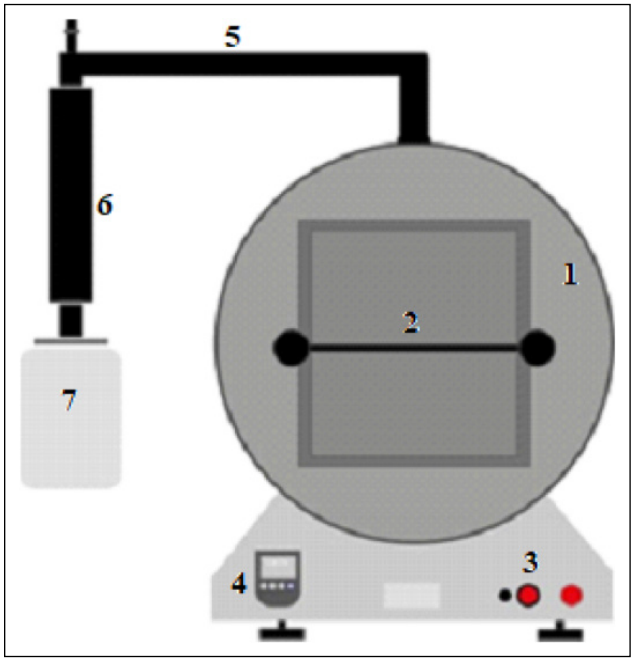

Figure 2. Torrefaction system: 1- Cylindrical tube furnace 2- Furnace cover 3- On/off button 4- PID control system 5- Gas and condensable liquid product output system 6- Double condenser 7- Liquid product container.

MATERIALS AND METHODS

Preparation of Samples

In the experiments, corn stalks, almond hulls, almond shells and olive kernel residues were used as agricultural waste (Fig. 1). Corn stalks, almond hulls and almond shells were obtained from producers in Elazığ, while olive kernels were obtained from producers in İzmir. The samples were dried in the laboratory atmosphere. Some of the dried samples were cut down (e.g., corn stalk) and ground shredded for use in the proximate analysis.

Torrefaction Experiments

Torrefaction experiments were performed in a laboratory-scale torrefaction system given in Figure 2. The torrefaction system consists of a PID-controlled, 40 cm outer diameter and 30 cm long cylindrical tube furnace (18 cm x 18 cm x 20cm inner volume) and a double condenser for collecting the liquid product. In condensers, cooling was done with water. After the system was prepared, 10 g of biomass

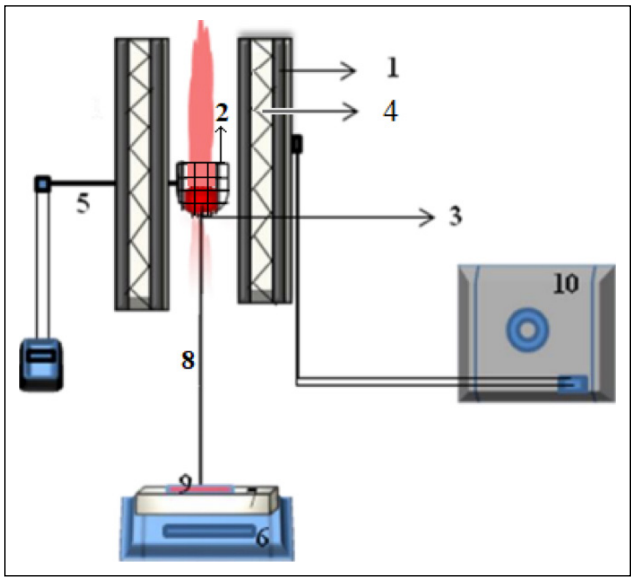

Figure 3. Combustion system: 1-Refractory brick 2-Wire mesh basket 3-Burning pellet 4-Heating elements 5-Thermocouple 6-Top balance 7-Support plate 8-Basket rod 9-Mirro 10.Voltage transformer.

sample was placed in the furnace and heated to the operating temperature with a heating rate of 10 °C/min. When the operating temperature reached 300±5°C, it was torrefied at constant temperature for 41 minutes (working temperature and residence time were determined by preliminary experiments and response surface methodology (RSM)).

The torrefaction process was carried out in volatile matter atmosphere released from the biomass as a result of heating, without passing air or inert gas through the system. At the end of the residence time, the heating was stopped and the system was cooled for 30 minutes. The biochar samples removed from the furnace and completely cooled were weighed and the solid product yield was calculated according to Equation 1. The liquid+gas product yield was calculated from the difference according to Equation 2. Here, m_{bc} and m_{raw} denote the weights of biochar and raw biomass, respectively.

$$\text{Solid product yield (\%)} = \frac{m_{bc}}{m_{raw}} \times 100 \quad (1)$$

$$\text{Liquid+Gas yield (\%)} = 100 - \text{Solid product yield (\%)} \quad (2)$$

Proximate Analysis

Proximate analysis, in which the volatile matter and ash ratios were determined, was performed in the muffle furnace according to ASTM D 1782–84 standards [8]. Proximate analysis was performed on both the original sample and the torrefacted samples (-100 mesh particle size).

The moisture content of the samples was determined in a Mettler LJ16 moisture analyzer (0.01% sensitivity), by keeping them at 105 °C for 2 hours.

For volatile matter analysis, approximately 1 g of the sample was put into the crucible brought to constant weight. The lid of the crucible was closed and put into the muffle furnace (preheated to 950 °C). After the crucible was kept in the furnace for 7 minutes, the covered crucibles were removed and left to cool in the desiccator for 1 hour and then weighed. The volatile matter content of the sample was calculated using Equation 3.

$$\textit{Volatile matter (\%w/w)} = \frac{m_{cs} - m_{cs,950\,°C}}{m_{cs} - m_c} \times 100 \quad (3)$$

Here, m_c, m_{cs} and $m_{cs,950oC}$ are the weights of the crucible, the sample with the crucible, and the sample with the crucible after 950 °C, respectively.

After determining the volatile matter content to determine the ash content, the open crucibles containing the samples were kept in a muffle furnace heated to 750 °C for 6 hours. The crucibles removed from the furnace were cooled in a desiccator for one hour before being weighed. The ash content of the sample was calculated using Equation 2.

$$\textit{Ash (\%w/w)} = \frac{m_{cs,750\,°C} - m_c}{m_{cs} - m_c} \times 100 \quad (4)$$

Here, m_c, m_{cs} and $m_{cs,750oC}$ are the weights of the crucible, the sample with the crucible, and the sample with the crucible after 750 °C, respectively.

To check the accuracy of the experimental data, the analyses were repeated several times. Results of parallel studies with deviations of less than ±5% were averaged.

Combustion Experiments

The effects of the torrefaction process on the combustion behaviour of agricultural wastes were investigated by burning the 1g±0.15 weighted samples of the raw and torrefied biomass particles at the starting temperature of the furnace at 700 °C in the fixed bed system.

The setup depicted in Figure 3 was used for combustion studies. It is made of a vertically grooved refractory chamber with an interior diameter of 35 mm, an outside diameter of 82 mm, and a height of 122 mm that holds electrical heating elements. The chamber's top was closed with a round refractory material. A 30 mm diameter stainless steel mesh basket is placed vertically in the chamber, attached to the upper end of a 1.4 mm diameter and 250 mm long stainless steel rod. The lower end of the rod was placed on a scale with a 1 mg precision while being fastened to a square stainless steel plate. The combustion behaviour of the sample in the chamber was observed with the help of a mirror. Heating of the chamber was accomplished using a variable output voltage transformer and temperature control using a NiCr thermocouple placed just above the basket in the chamber. Before the experiments were carried out, the chamber was first heated up to the operating temperature with transformer control. The sample was then thrown into the basket, the time recording was started and the initial weight of the sample was read. The mass of the samples was recorded at 5s intervals during the volatiles and char burning periods. At the same time, the onset and disappearance times of the volatile flame and the extinction times of the glowing char were also observed with the mirror and recorded. Volatile matter and carbon combustion rates were calculated according to Equation 5 using the corresponding mass loss curves.

$$R = \frac{1}{W_o} \times \frac{dW}{dt} \quad (5)$$

Table 1. Torrefaction yield (300±5 °C for 41 min.)

Sample	Solid %	Liquid and gas %
Almond hull	53.4	46.6
Almond shell	80.8	19.3
Olive kernel	78.4	21.7
Corn stalk	43.7	56.4

Wo is the volatile matter or fixed carbon amounts of the sample determined by proximate analysis and dW/dt is the slope calculated from the graph for the volatile matter or carbon combustion period. Experimental data are given as the average result of at least three experiments.

RESULTS AND DISCUSSIONS

Torrefaction Results

In Table 1, the product distribution of agricultural wastes that were torrefaction treated is given. It was determined that hard woody wastes such as almond shells and olive kernels had higher solid product yields. It was observed that the solid product yields of almond hull and corn stalk, which are more flexible and fibrous, were lower. This result shows that the torrefaction yield depends on the type of biomass. It was determined that harder agricultural wastes were more difficult to decompose when thermal treatment was applied, and therefore the amount of solid product was high, while the fibrous biomass was broken down faster when thermal treatment was applied, and more liquid + gaseous products were obtained. This is because the compounds forming the lignocellulosic structure have different decomposition temperatures. It has been stated that hemicellulose, which forms the lignocellulosic structure, decomposes in the temperature range of 225–325 °C, cellulose at 305–375 °C, and lignin at 280–500 °C [9].

When the biomass is heated, hemicellulose starts to decompose first and the amount of liquid and gas product increases as the amount of hemicellulose in the structure of the biomass increases.

Proximate analysis results of raw and torrefied biomass are given in Table 2. As a result of the applied torrefaction process of all samples, it was determined that while the volatile matter amount decreased, the ash and fixed carbon amounts increased. It was determined that the volatile matter amount of almond shell and olive kernel with a high solid product yield decreased by 9% and the fixed carbon amount increased in the range of 30–55% after the torrefaction process.

As a result, it can be said that the volatile components of agricultural wastes, which have a harder (woody) structure, are slowly separated from the biomass during the torrefaction process and the volatile compounds remaining in the biochar increase the solid product yield. On the other hand, it was determined that the volatile matter contents of corn stalk and almond hull (which yields low solids) decreased by 42% and 32%, respectively, and the fixed carbon contents increased by 309% and 96%, respectively. The results of the proximate analysis show that the structure of the raw biomass affects the composition of the products formed after torrefaction. As a result, it is estimated that the corn stalk is fibrous and decomposes faster as a result of thermal treatment, and therefore the hemicellulose content is higher than the other samples. When these separated compounds reach a certain concentration around the fuel, they ignite with the effect of oxygen in the environment. This time, until the flame appears, is called the ignition time.

Table 2. Proximate analysis data of raw and torrefied samples

Sample	Volatile matter %	Ash %	Fixed carbon %*
Almond hull	76	6.5	17.5
Torrefied almond hull	52	13.7	34.3
Almond shell	85	0.3	14.7
Torrefied almond shell	77	0.4	22.6
Olive kernel	80	1.0	19.0
Torrefied olive kernel	73	1.7	25.3
Corn stalk	85	4.2	10.8
Torrefied corn stalk	49	6.8	44.2

*: Determined from the difference.

Combustion Results

The combustion times of raw and torrefied biomasses determined in the fixed bed combustion system at 700 °C are given in Table 3. It was determined that the combustion times of the four biomass increased after the torrefaction process, although they had different structures. When the fuel is heated, first moisture and then low molecular weight compounds begin to separate.

It was determined that the critical ignition concentration was reached later and the ignition times increased because the volatile matter ratio decreased after the torrefaction process [10, 11]. The time from the appearance of the flame to its disappearance is defined as the volatile matter combustion time. With the spread of volatile compounds around the heated particle, the hydrocarbon concentration increases, and the visible flame volatile combustion event occurs [12, 13]. Volatile matter burning time was also found to be longer in torrefied biomass. This result shows that there is less volatile matter on the surface of the biochar and the volatile compounds remaining in the interior are released slowly from the biochar. This is in agreement with the proximate analysis data. Because the volatile matter burning time around the sample (the period during which the visible flame is observed) depends on the hydrocarbon concentration [13, 14].

The time required for carbon combustion is calculated as the interval between the disappearance of the visible volatile flame and the fading of the burning char. It was determined that the carbon burning period of the torrefied samples was longer and more stable.

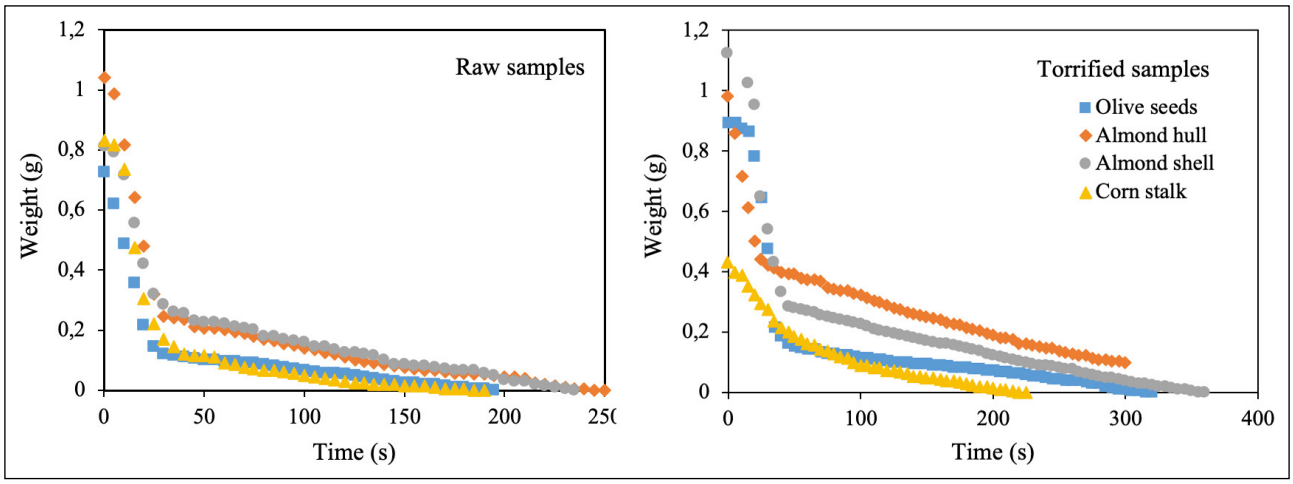

Figure 4. Mass loss curves of raw and torrefied samples.

Table 3. Combustion times of raw and torrefied biomass (700 °C)

Sample	Ignition (flame onset) time (s)	Volatile combustion (flame) time (s)	Carbon combustion time (s)
Almond hull	3.3	29.6	180.1
Torrefied almond hull	5.2	36.2	325.1
Almond shell	5.0	12.5	141.1
Torrefied almond shell	11.5	52.0	385.5
Olive kernel	3.1	29.2	180.2
Torrefied olive kernel	11.0	46.2	381.0
Corn stalk	5.0	26.7	111.2
Torrefied corn stalk	2.4	11.8	208.0

Table 4. Combustion rates of raw and torrefied biomass (70 °C)

Sample	Volatiles combustion rate $(s^{-1})x10^3$	R^2	Carbon combustion rate $(s^{-1})x10^3$	R^2
Almond hull	33.2	93	5.8	98
Torrefied almond hull	21.2	76	4.5	99
Almond shell	26.8	89	5.7	99
Torrefied almond shell	15.6	80	3.5	99
Olive kernel	34.3	95	5.9	99
Torrefied olive kernel	23.2	88	3.3	97
Corn stalk	35.4	95	10.0	94
Torrefied corn stalk	22.8	91	6.9	92

Mass loss curves of raw and torrefied samples during combustion are illustrated in Figure 4 for four samples. All these curves have two distinct regions recognized as volatiles and char combustion periods with different slopes from which respective volatiles and carbon combustion rates can be estimated. Volatile matter combustion and carbon combustion period are seen in both graphs. Although the carbon burning period of the raw samples was close to each other, it was determined that the torrified samples behaved differently in the carbon burning periods.

Numerical values of volatile matter combustion rates represented by the slopes of the first regions of mass loss curves for raw and torrefied samples are given in Table 4. The magnitudes of the correlation coefficients (R^2) for linear fit indicate that the results are acceptable. It was determined that the volatile matter burning rates of the torrefied samples were lower than the raw samples. This result explains the increased volatile burning time after torrefaction. The obtained data show that the volatile compounds near the surface are separated from the biomass during torrefaction and when the biochar formed is burned, the volatile com-

pounds remaining in the interior leave the particle more slowly and for a longer time. In this case, it can be said that the energy of the volatile matter, which constitutes 50–75% of biochar, can be utilized in a more controlled manner during combustion than raw biomass

The carbon combustion rates calculated from the second part of the mass loss curves are also given in Table 4. It is seen that the correlation coefficients (R^2) showing linear fit in the carbon combustion period are quite high and the results are acceptable. It was determined that the carbon of the biochar obtained after torrefaction burned more slowly and for a long time [15]. This is expected behaviour. Because the times required to burn coals practically depend on the rate of combustion and the amount of carbon, as well as the type and relative amounts of other components and their morphology [8]. As a result, it was determined that the biochar obtained after torrefaction burns more slowly and for a longer time under the same conditions when compared to raw biomass [16].

CONCLUSIONS

The results on the effect of the torrefaction process applied to agricultural wastes of different structures on the combustion behaviour of the wastes lead to the following conclusions.

It was determined that while the volatile matter ratio decreased with the applied torrefaction process, the ash and fixed carbon content increased. Proximate analysis data show that the structure of the raw biomass (woody or fibrous) affects the composition (volatile matter and fixed carbon amounts) of the biochar formed after the applied torrefaction process.

Although agriculture wastes have different structures, it was determined that the four biomasses burned more stable and longer after the torrefaction process.

The obtained results showed that biochar with better properties than raw biomass was produced by the torrefaction process applied to agricultural wastes and it is suitable for burning in solid fuel combustion systems. The solid product (biochar) obtained will both contribute to the country's economy and add value to agricultural wastes that cause problems during storage, transportation, loading into the burning system and combustion.

Acknowledgements
We would like to thank Prof. Dr. Dursun Pehlivan, whose knowledge and experience we have benefited from in experimental and theoretical studies. We would also like to thank the Head of Department Prof. Dr. Filiz Kar for her support in the Chemical Engineering Laboratory.

DATA AVAILABILITY STATEMENT

The authors confirm that the data that supports the findings of this study are available within the article. Raw data that support the finding of this study are available from the corresponding author, upon reasonable request.

CONFLICT OF INTEREST

The authors declared no potential conflicts of interest with respect to the research, authorship, and/or publication of this article.

ETHICS

There are no ethical issues with the publication of this manuscript.

REFERENCES

[1] S. E Ibitoye, T. C. Jen, R. M. Mahamood, and E. T. Akinlabi, "Improving the combustion properties of corncob biomass via torrefaction for solid fuel applications," Journal of Composites Science, Vol. 5(10),Article 260, 2021. [CrossRef]

[2] X. Chen, H. Zhang, Y. Song, and R. Xiao, "Prediction of product distribution and bio-oil heating value of biomass fast pyrolysis," Chemical Engineering and Processing-Process Intensification, Vol. 130, pp. 36–42, 2018. [CrossRef]

[3] H. Haykiri-Acma, S. Yaman, S. Kucukbayrak, "Combustion characteristics of torrefied biomass materials to generate power," in 2016 IEEE Smart Energy Grid Engineering (SEGE), pp. 226–230,2016. [CrossRef]

[4] N. D. Duranay, and G. Akkuş, "Solid fuel production with torrefaction from vineyard pruning waste," Biomass Conversion and Biorefinery, Vol. 11(6), pp. 2335–2346, 2021. [CrossRef]

[5] W. H. Chen, J. Peng, and X. T. Bi, "A state-of-the-art review of biomass torrefaction, densification and applications," Renewable and Sustainable Energy Reviews, Vol. 44, pp. 847–866, 2015. [CrossRef]

[6] R. K. Singh, A. Sarkar, and J. P. Chakraborty, "Effect of torrefaction on the physicochemical properties of eucalyptus derived biofuels: estimation of kinetic parameters and optimizing torrefaction using response surface methodology (RSM)," Energy, Vol. 198, Article 117369, 2020. [CrossRef]

[7] Y. P. Rago, F. X. Collard, J. F. Görgens, D. Surroop, and R. Mohee, "Torrefaction of biomass and plastic from municipal solid waste streams and their blends: Evaluation of interactive effects," Fuel, Vol. 277, Article 118089, 2020. [CrossRef]

[8] A. T. Conag, J. E. R. Villahermosa, L. K. Cabatingan, and A. W. Go, "Energy densification of sugarcane leaves through torrefaction under minimized oxidative atmosphere," Energy for Sustainable Development, Vol. 42, pp. 160-169, 2018. [CrossRef]

[9] M. J. Prins, K. J. Ptasinski, and F. J. Janssen, "Torrefaction of wood: Part 1. Weight loss kinetics," Journal of Analytical and Applied Pyrolysis, Vol. 77(1), pp. 28–34, 2006. [CrossRef]

[10] N. Vorobiev, A. Becker, H. Kruggel-Emden, A. Panahi, Y. A. Levendis, and M. Schiemann, "Particle shape and Stefan flow effects on the burning rate of torrefied biomass," Fuel, Vol. 210, pp. 107–120,

2017. [CrossRef]
[11] F. S. Akinrinola, N. Ikechukwu, L. I. Darvell, J. M. Jones, and A. Williams, "The potential use of torrefied Nigerian biomass for combustion applications," Journal of the Energy Institute, Vol. 93(4), pp. 1726–1736, 2020. [CrossRef]
[12] M. Yılgın, N. Duranay, and D. Pehlivan, "Torrefaction and combustion behaviour of beech wood pellets," Journal of Thermal Analysis and Calorimetry, Vol. 138(1), pp. 819–826, 2019. [CrossRef]
[13] J. Riaza, J. Gibbins, and H. Chalmers, "Ignition and combustion of single particles of coal and biomass," Fuel, Vol. 202, pp. 650-655, 2017. [CrossRef]
[14] G. Özer, N. And Duranay, "Bağ Budama Atığına Uygulanan İnert ve Oksidatif Torrefaksiyon İşleminin Karşılaştırılması," Fırat Üniversitesi Mühendislik Bilimleri Dergisi, vol. 35(2), pp. 461–471, 2023. [Turkish] [CrossRef]
[15] Y. Niu, Y. Lv, Y. Lei, S. Liu, Y. Liang, and D. Wang, "Biomass torrefaction: properties, applications, challenges, and economy," Renewable Sustainable Energy Reviews, vol. 115, p. 109395, 2019. [CrossRef]
[16] W. H. Chen, S. W. Du, C. H. Tsai, and Z. Y. Wang, "Torrefied biomasses in a drop tube furnace to evaluate their utility in blast furnaces," Bioresource Technology, Vol. 111, pp. 433–438, 2012. [CrossRef]

Environ Res Tec, Vol. 6, Issue. 4, pp. 347–358, December 2023

Environmental Research and Technology
https://ert.yildiz.edu.tr - https://dergipark.org.tr/tr/pub/ert
DOI: https://doi.org/10.35208/ert.1337407

Research Article

The effect of physicochemical properties on paracetamol photodegradation in cuboid bubble column

Ashwan HAMAD KHALİL, Asawer ALWASİTİ*, Jenan ABDULRZAAK, Abbas AL-SHALAL

Department of Chemical Engineering, University of Technology, Baghdad, Iraq

ARTICLE INFO

Article history
Received: 04 August 2023
Revised: 03 October 2023
Accepted: 10 October 2023

Key words:
Pharmaceuticals; Photocatalyst; Response surface modeling; Titanium oxide

ABSTRACT

Paracetamol is one of the most anthropogenic micropollutants, and their removal from the environment often requires a specialized method of remediation. In this study, a photocatalyst technique aided with air bubbles was used to degrade the pharmaceutical pollutant paracetamol (PCT) from the water via the COD test and HPLC analysis under different operating conditions. The experiments were carried out in a semi-batch rectangular bubble column with dimensions of 1500 mm height, 30 mm depth, and 200 mm width under UV light. Titanium oxide (TiO_2) was used as a source of catalyst. The effect of operating conditions of pH (3–10), air flow rate (0–2) L/min, salinity of solution represented by NaCl concentration (0–1000) mg/L, and 240 min irradiation time on the paracetamol removal were studied. The Box–Behnken design was adopted to study the individual effects of pH (A), air flow rate (B), and salinity (C) and their interactive effects. From the experimental and regression data, a second-order polynomial regression model is predicted, and the variance analysis of the regressions shows that the linear terms (A and B), and all quadratic terms (A, B, and C) have significant effects on the removal percentage of COD. According to numerical optimization, the greatest %COD removal is 76.7 in the process conditions of 5.3 pH, 1L/min, and 269 mg/L of NaCl. The experimental results show that the maximum %COD removal was 78% at pH=7, 1L/min, and 0mg/L of NaCl. HPLC analysis shows 91.2% of paracetamol degradation.

Cite this article as: Hamad Khalil A, Alwasiti A, Abdulrzaak J, Al-Shalal A. The effect of physicochemical properties on paracetamol photodegradation in cuboid bubble column. Environ Res Tec 2023;6(4)347–358.

INTRODUCTION

Due to the increase in the world's human population and industrial development, water pollution has been an alarming issue globally. The pollutants in the water come from the effluent of industries (e.g., the textile industry, paper industry, the pharmaceutical industry, etc.) and domestic pollutants (e.g., pharmaceuticals, pesticides, detergents, etc.) [1, 2]. Pharmaceutical pollutants can be considered among the pollutants that are largely present in wastewater due to the diversity of their sources, whether they are from factories or household pollutants. Due to its high value and low volume in wastewater, it has become the focus of researchers' attention. Since 2000, many researchers [3–6] published research demonstrating the prevalence of pharmaceuticals in aquatic habitats. This has sparked significant issues about the lack of understanding about the possible consequences of pharmaceutical chemicals and their metabolites on human and aquatic creatures, even though they exist in little trace amounts [7, 8]. One of the widely used pharmaceutical drugs is paracetamol (commonly known as acetaminophen) [9–12]. Parac-

***Corresponding author.**
*E-mail address: asawer.a.alwasiti@uotechnology.edu.iq

etamol residues and metabolites have been found in waterbodies all over the world [13, 14]. At therapeutic doses, paracetamol is safe; but, at higher concentrations, it may undergo an oxidative transition to N-acetyl-p-benzoquinone imine (NAPQI) [15]. This toxic chemical causes liver necrosis as well as an uncommon skin condition [16]. On therapeutic usage, around 58–68% of paracetamol and its metabolite are eliminated from the body [17]. These percentages are discharged into the water in general, which leads to pollution.

In recent years, new technologies for paracetamol degradation in wastewater have been developed, like electrocoagulation [18], non-thermal Plasma [19], ozonation and H_2O_2/ UV system [20–22], chlorination treatment [23], and Fenton process [24]. Among those processes, the chemical process that deals with photocatalysts such as TiO_2, ZnO, etc. can dismantle the industrial wastewater [25].

Heterogeneous photocatalysis with titanium photocatalyst is a rapidly growing technology for removing refractory and toxic organic pollutants from water, such as dyes, pesticides, petroleum contaminates and pharmaceuticals [26–32] The efficacy of these environmentally friendly photochemical wastewater treatment technologies is related to the in situ creation of aggressively oxidizing hydroxyl radicals (•OH), which oxidize a wide spectrum of organic contaminants found in water and wastewaters [33, 34].

Titanium dioxide is one of the most promising semiconductors for photocatalytic pollution removal since various organic compounds may be reduced to tiny pieces or mineralized in water at room temperature and pressure [35, 36]. The following reactions have been identified as occurring when TiO_2 interacts with light [37]:

$$TiO_2 + h\nu \rightarrow e^-_{CB} + h^+_{VB} \quad (1)$$

$$e^-_{CB} + O_2 + H^+ \rightarrow HO_2^{\cdot} \quad (2)$$

$$e^-_{CB} + HO_2^{\cdot} + H^+ \rightarrow H_2O_2 \quad (3)$$

$$2e^-_{CB} + O_2 + 2H^+ \rightarrow H_2O_2 \quad (4)$$

$$h^+_{VB} + H_2O \rightarrow HO^{\cdot} + H^+ \quad (5)$$

$$2HO^{\cdot} \rightarrow H_2O_2 \quad (6)$$

$$H_2O_2 + h\nu \rightarrow 2HO^{\cdot} \quad (7)$$

$$H_2O_2 + e^-_{CB} + H^+ \rightarrow HO^{\cdot} + H_2O \quad (8)$$

Several operational factors such as solution pH, metal loading, catalyst dose, starting concentration, light wavelength, and salinity influenced the photocatalytic destruction of the organic pollutants process [38]. According to published research [39, 40], the existence of inorganic salts can reduce or enhance photocatalytic efficacy depending on their composition, concentration, and solution pH. There has been no extensive research on saline wastewater with salinities ranging from 500 to 2,000 mg/L utilizing photocatalytic oxidation techniques. Hence, such a study will be beneficial in giving the knowledge required for the treatment of saline wastewater. Although many researchers have examined the elimination of pharmaceutical waste using photocatalysts, the need to optimize this process is currently being investigated. As a result, unlike previous research, this work intends to increase process efficiency by employing air bubbles in a cuboid bubble column. Therefore, the novelty of the work is to investigate the effectiveness of air bubbles in the degradation of paracetamol in a UV-photo catalyst using a cuboid bubble column, where it was done at air flow rates (0–2) L/min and pH variables (3–10) and salinity (0–1000) mg/L through R.S.M. Their individual and interactive effects towards the COD removal and HPLC analysis are examined.

MATERIALS AND METHODS

Materials

The materials used for this experiment include: Titanium dioxide (TiO_2) (United States, Nanoparticles 10–30 nm Anatase), pharmaceutical (paracetamol, Samaraa SDI/ Iraq), Hydrochloric acid (99% purity, AUSTRIA) and sodium hydroxide (98% purity, India) (to adjust the pH of the wastewater), and sodium chloride (India).

Experimental Methods

The photocatalytic process experiments were conducted by batch and semi-batch systems. The batch system is a 1liter beaker agitated by a magnetic stirrer (Shanghai, China, HS-12) In this process, titanium dioxide is added to the previously prepared solution (0.5 g/liter), and then it is irradiated by UV light for four hours. During this period, a sample is drawn every 1 hour. This process is repeated with different pH values (3, 7, 9) and for different salinity values. The samples that were withdrawn every 1 hour are collected and the chemical oxygen demand (COD) is measured.

The semi-batch system consists of a rectangular glass column (200 mm wide, 30 mm deep, 1500 mm high, and 6 mm thick). Air bubbles enter from the bottom of the column through a gas distributor, placed in the middle of the column bottom plate, which consists of 21 needles with a 5 mm square and 1mm inner diameter. The air is compressed using a gas compressor and a flow meter was used to control the flow rate, as shown in Figure 1. The bubble column was irradiated by a tube-type (60 cm length) UV-C lamp (T5 (G5), W=12 m^2, 220V sterilizer Philippines tube, wavelength 253.7 nm) carried by a sterile tube with a distance of 150 mm. The bubble column and the UV lamp were covered with aluminum foil to avoid the interference of UV light.

The wastewater solution was prepared by adding 300 mg of ground paracetamol in a beaker of 1 liter of distilled water and left on the stirrer for 5 minutes. Then 0.5 mg of TiO_2 is treated with distilled water using an ultrasonic device for 20 minutes. The homogenate mixture was added to the wastewater solution.

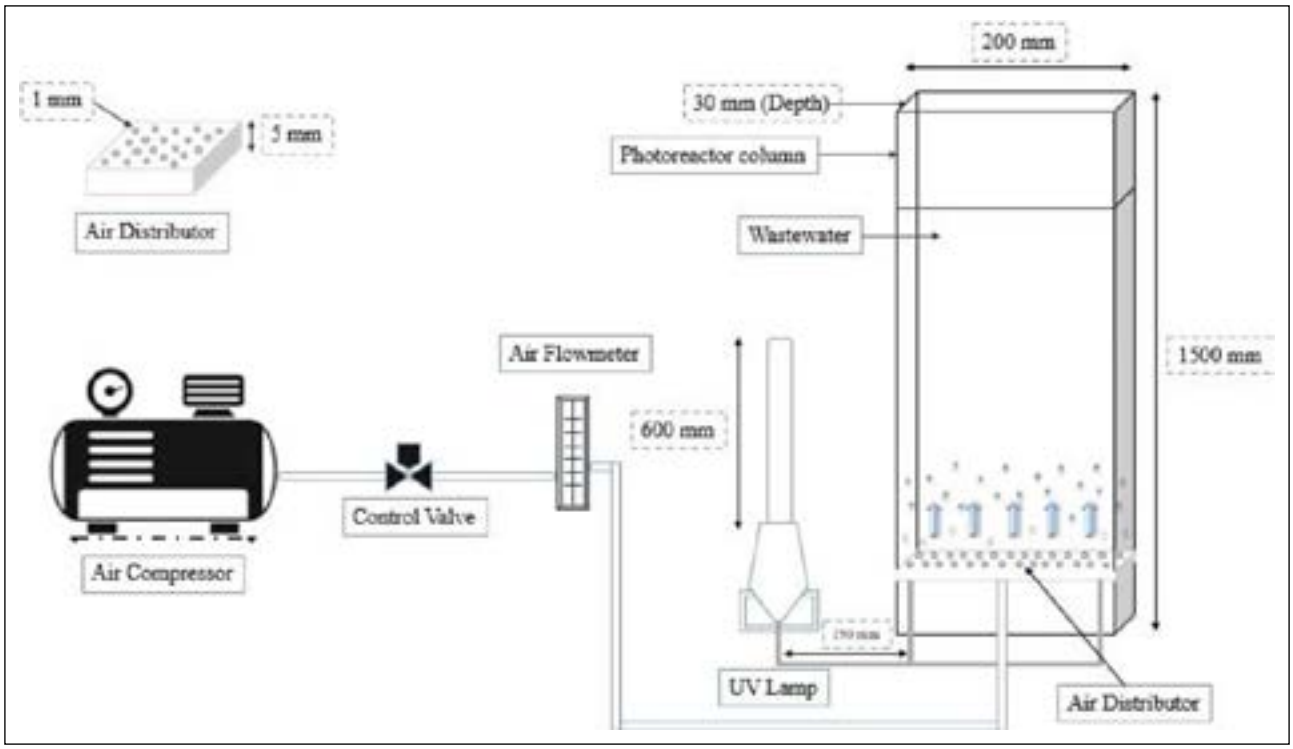

Figure 1. The schematic apparatus.

Table 1. The actual and coded values of the Box-Behnken design variables

	Factors	Coded and actual value		
		-1	0	+1
A	pH	3	7	10
B	Air Flow Rate, L/min	0	1	2
C	Salinity (NaCl concentration) mg/L	0	500	1000

The pH of the solution was changed to (3, 7, and 10) by adding HCl for the acidic medium and (NaOH) for the basic media. After, the solution was added to the bubble column and air bubbles were through in at rates of (1 and 2 L/min). The solution was exposed to ultraviolet radiation for (60, 120, 180, and 240) min. The effect of the salinity parameter was studied by adding two concentrations (500 and 1000) mg/L of sodium chloride to the prepared solution and reading the electrical conductivity of the two cases in the batch system and the semi-batch system.

The efficiency of the proposed removal method was investigated by measuring the chemical oxygen demand (COD) on samples for each irradiation time.

Experimental Design Parameters

The Box-Behnken method was employed in the statistical design of trials to investigate the individual and combined impacts of operational conditions (independent variables) on paracetamol degradation. The following steps were taken to complete the design: (i) experiment design utilizing a statistical model, (ii) response prediction, and (iii) building a mathematical model, calculating the coefficients, and then examining the model's applicability. pH of the solution, concentration of salt, and airflow rate are the three independent variables considered. The independent variables were tested at 3–10, concentrations of 0–1000 mg/L, and 0–3 L/min, respectively. For the design of the experimental run (DoE) matrix, a Box Behnken method with three factors was employed with three levels. Table 1 shows the actual levels and coded levels of each component. There were 17 randomized experimental runs in all, including 12 factorial points and 5 center points. The removal efficiency of COD, after 240 minutes of photocatalytic reaction, was chosen as the response.

A second-order polynomial model to describe the response surface was obtained by multiple regression techniques using Design Expert software. The mathematical expression of the dependent variable (response) on the independent variables was equivalent to a quadratic polynomial.

$$\mathbf{R\%}=+b_0-b_1A+b_2B+b_3C+b_4AB+b_5AC+b_6BC+b_7A^2+b_8B^2+b_{10}C^2 \quad (9)$$

In which that R% is the removal efficiency of COD and (b_o-b_{10}) are variable coefficients.

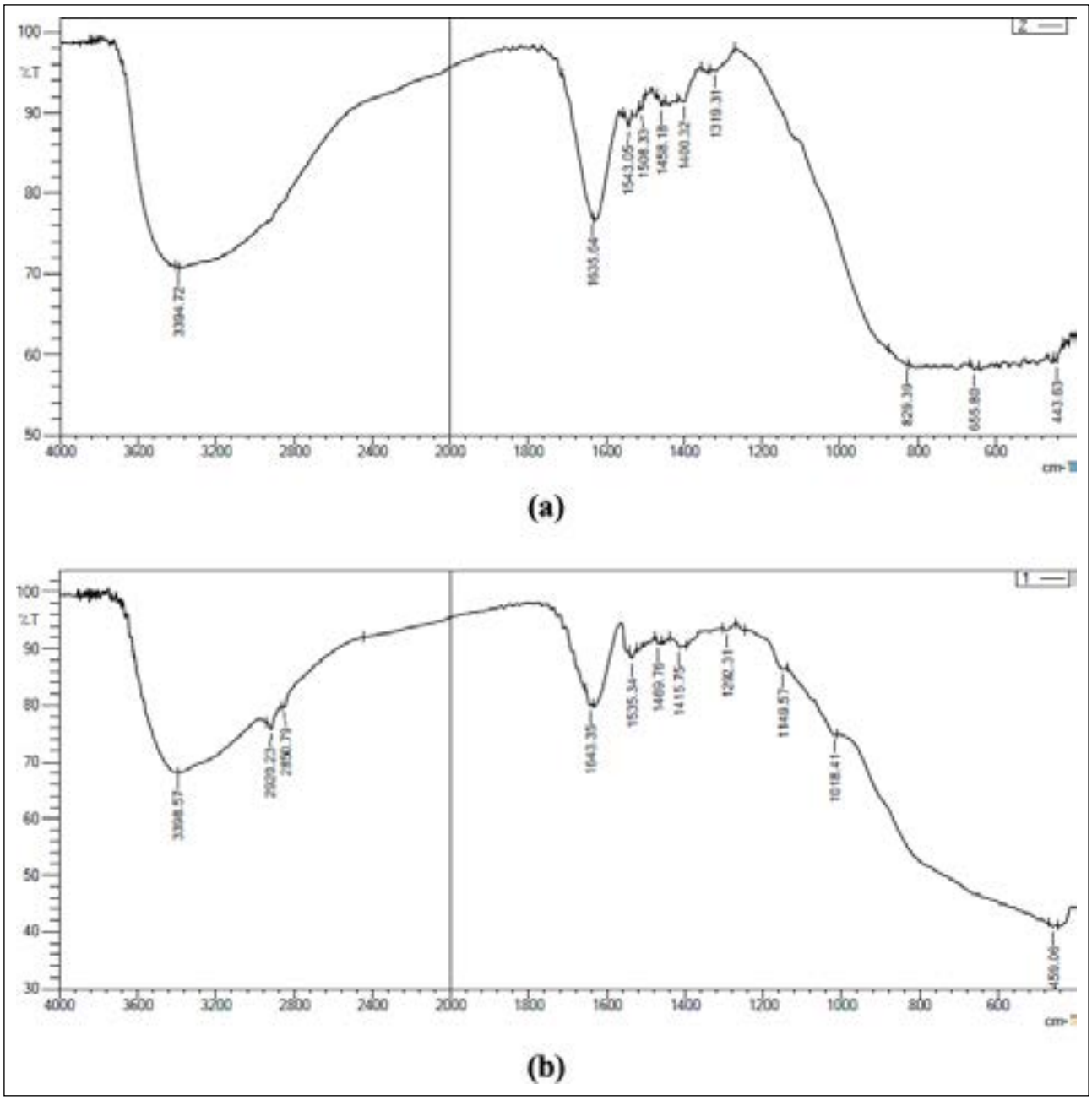

Figure 2. FTIR test of TiO_2, **(a)** before test, **(b)** after test (240 min).

RESULTS AND DISCUSSION

FTIR Characterization

FTIR is used to determine the functional groups and chemical structures of TiO_2 particles. As shown in Figures 2a, b, tests were carried out on TiO_2 powder before and after the photocatalytic process. The FTIR spectra were conducted in the 4000–400 cm^{-1} range.

In Figure 2a the broadband from 1000 to 400 cm^{-1} showed peaks (443.63, 655.80, 829.39) cm^{-1}. This region is ascribed to the Ti–O stretching and Ti–O–Ti bridging stretching mode and those peaks indicate that the powder is a mixture of anatase and rutile. After 240 minutes of work the FTIR test shows peaks (495.06 and 1018.41) cm^{-1}. This indicates that titanium is still effective after the photocatalyst process. The spectra showed the peaks (1319.31 to 1543.05) cm^{-1} in Figure 2a indicating the presence of carboxyl (C=O) and methylene groups. Those peaks gradually decreased to (1292.31 to 1535.34) cm^{-1} after 4 hours of work as shown in Figure 2b. The peak at the (1635.64 cm^{-1}) in Figure 2a. is due to the amide group, this value lightly increased to 1643.35 cm^{-1} after the process, this is due to the degradation process of PMA that can result in some amide group. The peaks observed in Figure 2b, 2920.23 cm^{-1} and 2850.79 cm^{-1}, were due to the bending vibrations of the alkane (C–H) groups, which can appear during PMA degradation. Those peaks are not available in Figure 2a [28].

The peak observed at 3394.76 cm^{-1}, in Figure 2a is due to the stretching vibration of the O–H group, while in Figure 2b after 4 hours of photocatalyst process, the peaks identi-

Table 2. The Experimental run

Run	Factors						Response	
	pH		Air flow rate, L/min		NaCl concentration (mg/L)		%COD removal	
	Coded	Actual	Coded	Actual	Coded	Actual	Experimental	Predicted
1	-1	3	-1	0	0	500	38	43.55
2	0	7	0	1	0	500	76	76
3	+1	10	-1	0	0	500	13	16.89
4	+1	10	0	1	-1	0	26	25.7
5	0	7	-1	0	+1	1000	66	59.71
6	0	7	0	1	0	500	76	76
7	+1	10	0	1	+1	1000	27	30.3
8	-1	3	0	1	-1	0	54	51.15
9	0	7	-1	0	-1	0	55	51.85
10	0	7	0	1	0	500	76	76
11	0	7	+1	2	+1	1000	37	40.15
12	0	7	0	1	0	500	76	76
13	+1	10	+1	2	0	500	17	10.11
14	-1	3	0	1	+1	1000	46	45.85
15	0	7	0	1	0	500	76	76
16	0	7	+1	2	-1	0	41	47.29
17	-1	3	+1	2	0	500	27	24.45

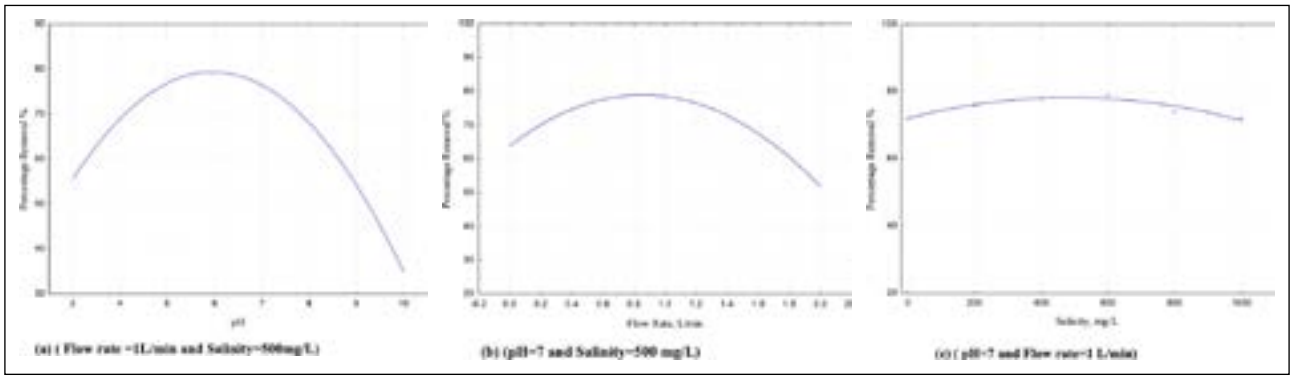

Figure 3. The 2D response surface plots.

fied at 3398.57 cm^{-1}, as shown in Figure 2b, indicating no change between them. Those peaks are the strong broad corresponding to the hydroxyl group's symmetric and asymmetric stretching vibrations due to water molecules. is related to the O–H stretching mode of the hydroxyl group, indicating the presence of moisture in the sample [34].

Response Surface Methodology

The impact of operational variables such as pH, salinity, and flow rate on photocatalytic paracetamol degradation was examined. To evaluate the individual and interaction impacts of these factors, a photocatalytic experimental design by CCD was used, followed by response surface analysis. Table 2 presents the experimental runs collected by Box-Behnken and the removal efficiency obtained in the experimental runs. The degradation effectiveness ranged from 18% to 76%.

The Response Surface Plots

The response surface plots of COD removal are shown in Figure 3. Figure 3a shows that increasing the pH and increasing the flow rate resulted in enhanced removal efficiency into the maximum point, after that the removal efficiency decreased. At acidic and alkaline pH, degradation efficiency is law, however, degradation efficiency increased at near-neutral pH.

The PZC condition is one in which the surface charge of TiO_2 is zero or neutral and its pH ranges from 4:5 to 7:0, depending on the catalysts used. TiO_2 used in this work, has a pH value at the isoelectric point approximately equal to 7, according to previous research [41].

The above results can be attributed to the effect of cations or anions in the solution, the paracetamol distribution, and

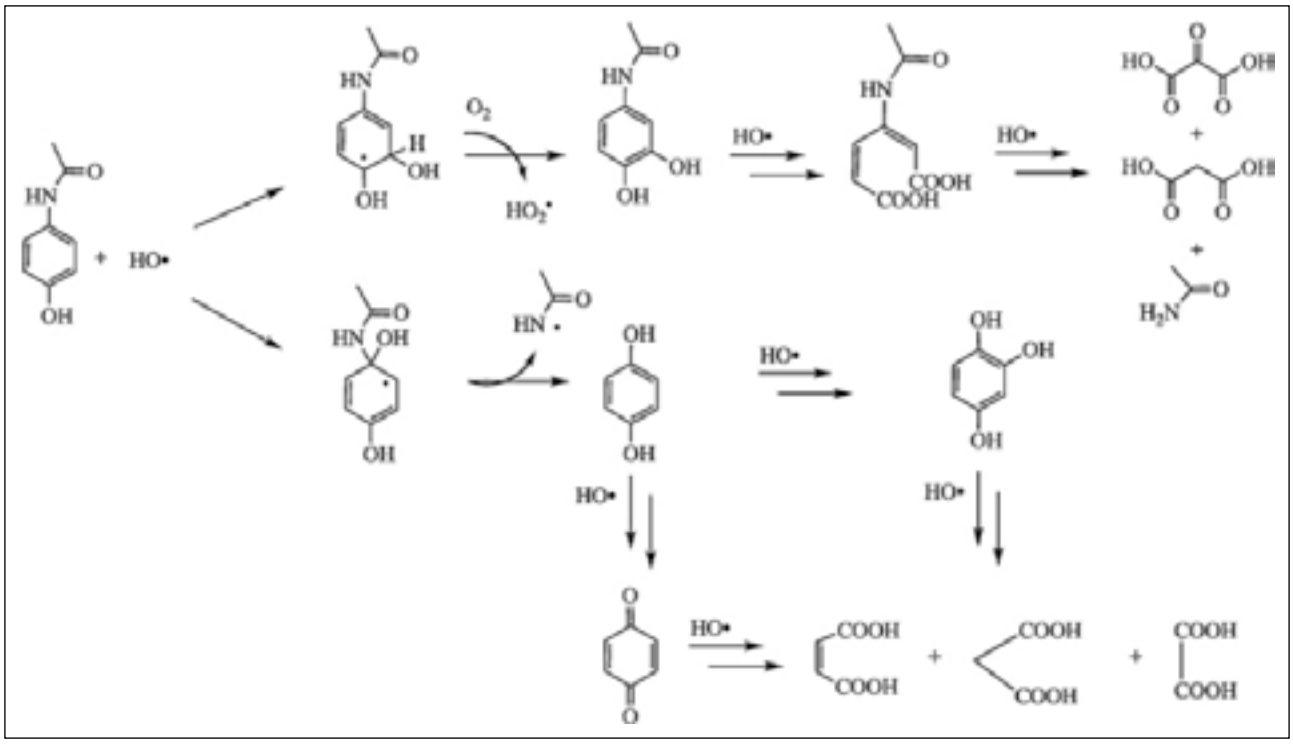

Figure 4. Paracetamol oxidation mechanism [43].

Table 3. The fit summary

Source	Sequential p-value	Std. Dev.	Adjusted R^2	Predicted R^2	
Linear	0.713	23.8	-0.112	-0.423	
2FI	0.982	26.91	-0.422	-1.637	
Quadratic	**<0.0001**	**5.58**	**0.938**	**0.572**	**Suggested**
Cubic		0	1		Aliased

the state of the TiO_2 surface according to the pH values on the photodegradation efficiency. Paracetamol tends to exist as anions in alkaline solutions (with higher pH values=9). Because of their high solubility in solution, such anions will not be considerably adsorbed. As a result, the electrostatic attraction between the TiO_2 surface (pHPZC=7) and paracetamol (pKa=10) increases [10], which is negatively charged at pH values, inhibiting paracetamol adsorption. As a result, paracetamol degrades more slowly in alkaline solutions. In acidic and natural solutions, paracetamol has a nonionic form and positively charged titanium dioxide causing low solubility in water, which increases adsorption on the TiO_2 surface and causes paracetamol breakdown. This result, however, disagrees with that obtained by [42], who determined that the optimal paracetamol degradation occurs at pH=9 and is not preferred to operate in acidic environments. This might be due to a variation in catalyst type as well as other operating circumstances.

The effect of the air bubbles on paracetamol degradation in the range of 0 to 2 L/min is shown in Figures 3b. The figures show that introducing air bubbles caused an increase in COD removal efficiency. The removal rate of COD at pH 7 was increased by 25% more than that using the batch process at pH=7. The same effect of air bubbles is shown at pH =3 and pH=10, in which the COD removal efficiency was 54% and 26% respectively. The same trend is shown with different salinity concentrations of solution.

The impact of air bubbles may be explained by two factors. The first is that inserting air bubbles increases the molecules' diffusivity of paracetamol to the TiO_2 active sites owing to the turbulent flow, which increases the degradation rate. The second reason is that the airflow rate acts as a promoter by supplying the system with molecules of oxygen via the air bubbles. These oxygen molecules interact with the free electrons generated by UV light at the catalyst surface's active sites, Figure 4. According to the figure, the degradation of paracetamol during the photocatalytic process leads to the formation of byproducts at the beginning of the degradation, which are aromatic compounds, and at the end, carboxylic acids are formed. There are two most common paths for the degradation process, which are either getting rid of the –NH-CO-CH_3 group and then forming hydroquinone and 1,2,4-trihydroxy benzene and carboxylic acids, (2) or elimination of the CO-CH_3 group and then forming 4-aminophenol and 4-nitrophenol, before forming hydroquinone and 1,2,4-trihydroxy benzene and carboxyl-

Table 4. The ANOVA analysis of the quadratic model

Source	Sum of Squares	df	Mean Square	F-value	p-value	
Model	7929.86	9	881.1	28.29	0.0001	significant
A-pH	840.5	1	840.5	26.99	0.0013	
B-Flow Rate	331.51	1	331.51	10.64	0.0138	
C-Salinity	0.2475	1	0.2475	0.0079	0.9315	
AB	38.23	1	38.23	1.23	0.3045	
AC	24.75	1	24.75	0.7946	0.4023	
BC	56.25	1	56.25	1.81	0.2209	
A^2	4630.3	1	4630.3	148.66	<0.0001	
B^2	1747.96	1	1747.96	56.12	0.0001	
C^2	145.33	1	145.33	4.67	0.0676	
Residual	218.03	7	31.15			
Lack of Fit	218.03	3	72.68			
Pure Error	0	4	0			
Cor Total	8147.88	16				

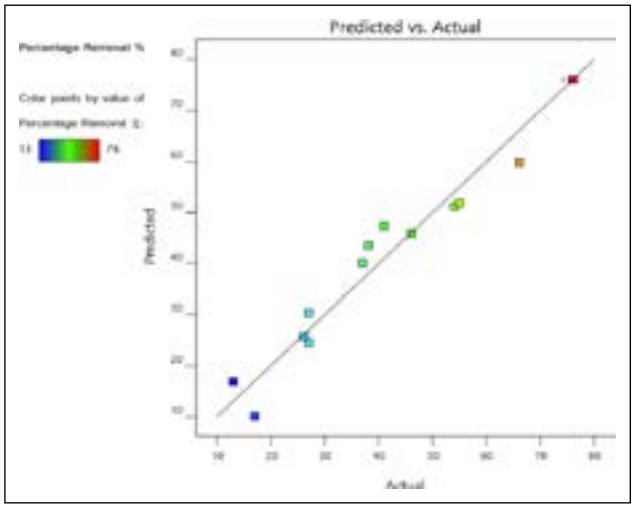

Figure 5. The experimental values vs. the predicted values.

ic acids. As a result of the suggested degradation process, more hydroxyl radicals are produced.

However, raising the flow rate to 2L/min reduces COD removal efficiency. This behavior may be linked to the increased flow rate, which causes the gas bubbles to merge, resulting in the development of huge bubbles and causing the bubble column to work in a heterogeneous pattern. The interaction between the nanoparticle and the UV will be reduced as a result of this heterogeneous pattern [43].

The effect of salinity is shown in Figure 3c. It is observed that there is little interaction effect between salinity, pH, and flow rate indicating salinity has little significant effect on the COD removal efficiency for all examined values of pH and air flow rate.

The prohibiting effect on the paracetamol degradation with the presence of some inorganic salts can be caused by several reasons [43–48]: (i) a decrease in light absorption by the photocatalyst caused by ions such as (Fe^{3+}), which act as an inner filter; (ii) an increase in recombination of h+ and e; (iii) the capturing of (•OH) radicals or other oxidizing species; and (iv) adsorption competition with the reactant at the catalyst surface.

In this research NaCl was used as a source of salinity, the presence of Cl ions can cause many side reactions which can have positive and negative effects on paracetamol degradation. Chloride ions can be electrolyzed to produce chlorins, as shown in equations 10–12 [49], which can affect H_2O_2 amounts (equations 13–14). The Scavenging of the hydroxyl radicals by chloride results in the creation of active chlorine reactive species ($Cl^{\bullet}$ (E_0=2.4 V) and $Cl_2^{\bullet-}$ (E_0=2.0 V)) that can efficiently react with many organic compounds. Cycling between chloride, chlorine, chlorine radicals, and dichlorine radicals can have an impact on PCT degradation (equations 14–19).

$$2Cl^- \rightarrow 2e^- + Cl_2 \quad (10)$$

$$Cl_2 + H_2O \rightarrow HOCl + Cl^- + H^+ \quad (11)$$

$$Cl_2 + H_2O_2 \rightarrow 2H^+ + O_2 + 2Cl^- \quad (12)$$

$$ClO^- + H_2O_2 \rightarrow H_2O + O_2 + Cl^- \quad (13)$$

$$Cl^- + HO^{\cdot} \rightarrow Cl^{\cdot} + OH^- \quad (14)$$

$$HO^{\cdot} + Cl^- \rightarrow ClOH^- \qquad k = 4.3 \times 10^9 \ M^{-1} \ s^{-1} \quad (15)$$

$$Cl^- + Cl^{\cdot} \rightarrow Cl_2^- \qquad k = 2.1 \times 10^{10} \ M^{-1} \ s^{-1} \quad (16)$$

$$Cl_2^- + Cl_2^- \rightarrow Cl_2 + 2Cl^- \quad k = 6.3 \times 10^8 \ M^{-1} \ s^{-1} \quad (17)$$

$$Cl_2^- + Cl^{\cdot} \rightarrow Cl_2 + Cl^- \quad k = 2.1 \times 10^9 \ M^{-1} \ s^{-1} \quad (18)$$

$$Cl^{\cdot} + Cl^{\cdot} \rightarrow Cl_2 \qquad k = 8.8 \times 10^7 \ M^{-1} \ s^{-1} \quad (19)$$

Model Fitting and Validation

Analysis of variance (ANOVA) was used to determine the model's significance, the statistically significant factors, and

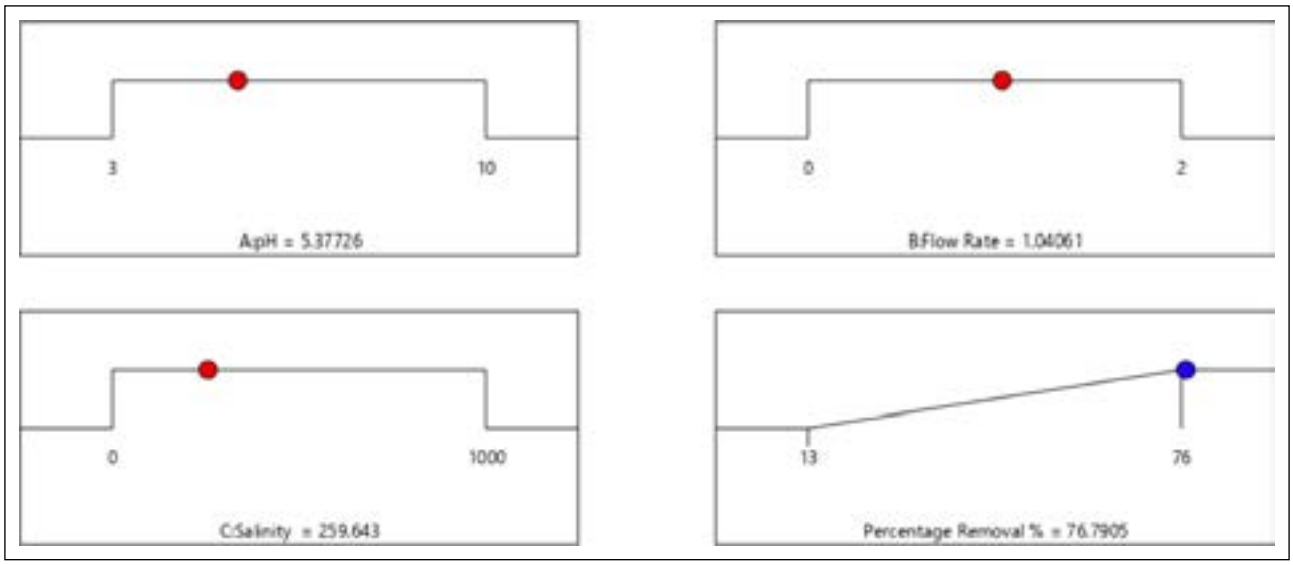

Figure 6. The optimization results.

appropriateness. The predicted and adjusted R^2 values were used to select the best model for the computational study as shown in Table 3. The best model—second-order polynomial regression was chosen for its highest values of R^2. The response of COD removal% is related to the input factors via the following equation.

$$R\% = = -33.2 + 31.6A + 32.3B + 0.021C + 0.878AB + 0.0014AC - 0.007BC - 2.77A^2 - 20.37B^2 - 0.000023C^2 \quad (20)$$

The experimental values vs. the predicted values of % COD removal obtained by the RSM model are shown in Figure 5. This is the most crucial graph in the diagnostic instrument. It enables the detection of a value or set of values that cannot be easily anticipated by the model. The 45-degree line should divide the data points evenly. In this model, the points are fairly near the diagonal line. The little discrepancy between actual and anticipated values demonstrates a high connection between them. The results reveal that the experimental values and the quadratic model correspond well.

Table 4 shows the performance of the ANOVA test of the predicted model. The p-value is the ANOVA coefficient used to assess the significance of the source to the response in the quadratic regression, with a p-value of less than 0.05 being statistically significant. In general, there are three categories of terms: first order (A, B, and C), two-way interaction (AB, AC, and BC), and pure quadratic (A^2, B^2, and C^2). According to the analytical results in Table 4, the linear terms A and B are significant, with p-values of 0.0013 and 0.013, respectively. The pure quadratic terms A and B are also significant terms. The quadratic term C is likewise important, although it has a lower p-value of 0.067. The table shows that the interaction terms have a higher p-value (>0.05, terms that were not statistically significant). Based on the F-values of the variables, the order of factors that impact the effectiveness of removal is as follows: pH (A), air flow rate (B), and salinity(C).

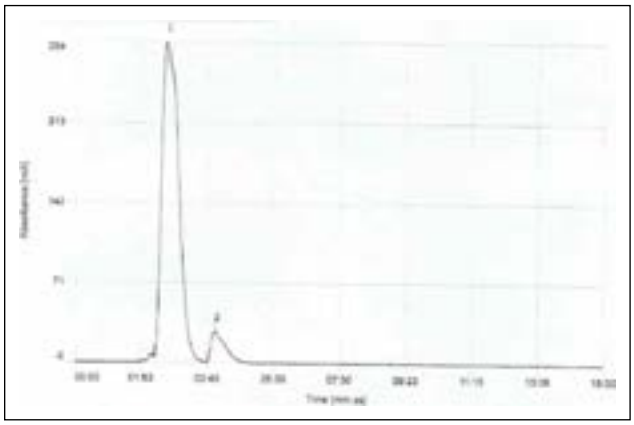

Figure 7. HPLC analysis of the treated sample (after 240 min. of photocatalysis).

The Optimization Result

The primary objective of the RSM study is to establish the optimal values of the variables to get the maximum value of paracetamol degradation based on experimental data modeling. Numerical optimization using the models generated in the study explores the design space for factor configurations that fulfill the goals. The optimal condition is the one chosen based on attractiveness, as represented in the diagram below Figure 6 (pH 5.3, flow rate 1 L/ min, and salinity 259 mg/L) to get maximum removal efficiency 76.7%).

HPLC analysis

For quantitative analysis and estimation of the paracetamol concentration in the unknown sample, different concentrations of the standard substance (5, 10, 25, 50, and 100) ppm were prepared to draw the calibration curve through the straight-line equation shown. The equation of the straight line is shown by drawing between the concentration and area of the peak, and the equation is as follows:

$$\lambda = 0.0054\ X + 2.4457 \quad (21)$$

Table 5. A comparison with other references

Treatment method	Type of wastewater	Condition	Removal effectiveness	References
Electrocoagulation	Real wastewater	pH = 6, electrolyte concentration 2.0 gL^{-1}, and current density 272.72 Am^{-1}	TOC 66% COD 62 5%	[18]
Electrocoagulation	Synthetic wastewater	pH 4, interelectrode distance 2 cm, electrolyte concentration 1.5 gL^{-1} and current density 272.72 Am^{-1}	TOC 63.2% COD 60.8%	[18]
Oxidation of paracetamol by TiO_2/UV	Synthetic wastewater	0.1 g L-1 of TiO_2	90% of paracetamol in 160 minutes	[43]
Photocatalytic degradation using TiO_2 P25 and TiO_2/ cellulosic fiber	Synthetic wastewater	298 K, 0.4 g L^{-1}(TiO_2-P25), pH= 2.5–11.0 under UV light. TiO_2/cellulosic fiber mode combined with solar light	90% of 2.65×10^{-4}M paracetamol was degraded under UV irradiation.	[42]
Photo-Fenton	Synthetic wastewater	hydrogen peroxide (H_2O_2) activation with a copper-based metal-organic	95% of paracetamol was degraded in 60 min.	[50]
Photocatalysis	Synthetic wastewater	photocatalyst consisting of titanium dioxide (TiO_2) and activated carbon (AC)	95% of the Paracetamol photodegradation	[51]
Photocatalysis	Synthetic wastewater	experiments were conducted at pH=7, Flow rate 1 L/min	COD 78%, and 91.2% of paracetamol was degraded	Present study

Where λ represents the concentration value and X represents the peak area.

The analysis of HPLC Analysis done for the solution test with 300 ppm of paracetamol concentration treated at the best condition, which gives higher values of COD removal efficiency, pH 7, flow rate 1L/min, and UV irradiation time 240 minutes. The chromatogram of paracetamol after treatment is shown in Figure 7. The paracetamol standard peak was shown after 2.3 min with the area of the peak of 4435.3 and this represents 26.4 ppm of paracetamol concentration. Hence, at these operating conditions, it may be presumed that complete degradation of paracetamol (91.2%) was observed. Comparing this result with other workers, the obtained results are in agreement with other workers, as shown in Table 4.

CONCLUSIONS

Photocatalysts process aided with air bubbles and UV light was applied to assess the degradation of paracetamol via the COD test and HPLC analysis under different operating conditions of pH, flow rate, and salinity. Surface Response methodology was used to predict the operating values as well as the optimum conditions. The results show that the COD removal percentage was well predicted by the quadratic equation calculated statistically by the Box-Benhken method indicated by the R^2 value (0.938). The results show that all three factors could affect pollutant adsorption on the photocatalyst surface. The effect of pH is partially attributed to its influence on pollutant adsorption on the photocatalyst surface and the electrostatic repulsion between the TiO_2 surface and paracetamol. Indeed, the results show that greater removal efficiency of COD occurs with the presence of air bubbles at 1 L/min. This is caused by two reasons, the first enhancing the diffusion and mobility of Paracetamol molecules towards the active sites of the catalyst. The second is enhancing the generation of active (•OH). The salinity of the solution showed little significant prohibiting effect compared with the other two variables. Moreover, the p-values predicted by the Box- Benhken method showed that the single and quadratic terms of the variables have a significant effect. However, the effect between the variables (AB, AC, and BC) is negligible. According to the numerical optimization, the maximum % COD removal is 76.7 in the process conditions of 5.3 pH, 1 L/min, and 269 mg/L of NaCl. The experimental results show that the maximum % COD removal was 78% at pH=7, 1 L/min, and 0 mg/L of NaCl. The highest paracetamol degradation was 91.2% using HPLC analysis when pH=7 and flow rate 1 L/min and after 240 minutes.

Acknowledgements
The authors would like to thank the Chemical Engineering Department – University of Technology for supporting in completing this work.

DATA AVAILABILITY STATEMENT

The author confirm that the data that supports the findings of this study are available within the article. Raw data that support the finding of this study are available from the corresponding author, upon reasonable request.

CONFLICT OF INTEREST

The author declared no potential conflicts of interest with respect to the research, authorship, and/or publication of this article.

ETHICS

There are no ethical issues with the publication of this manuscript.

REFERENCES

[1] C. Gadipelly, A. Pérez-González, G. D. Yadav, I. Ortiz, R. Ibáñez, V. K. Rathod, and K. V. Marathe, "Pharmaceutical industry wastewater: Review of the technologies for water treatment and reuse," Industrial & Engineering Chemistry Research, Vol. 53(29), pp. 11571–11592, 2018. [CrossRef]

[2] A. R. Ribeiro, O. C. Nunes, M. F. R. Pereira, and A. M. T. Silva, "An overview of the advanced oxidation processes applied for the treatment of water pollutants defined in the recently launched directive 2013/39/EU," Environment International, Vol. 75, pp. 33–51. [CrossRef]

[3] T. Heberer, "Tracking Persistent Pharmaceutical Residues from Municipal Sewage to Drinking Water," Journal of Hydrology, Vol. 266(3–4), pp. 175–189, 2002. [CrossRef]

[4] C. Tixier, H. P. Singer, S. Oellers, and S. R. Müller, "Occurrence and fate of carbamazepine, clofibric acid, diclofenac, ıbuprofen, ketoprofen, and naproxen in surface waters," Environmental Science & Technology, Vol. 37(6), pp. 1061–1068, 2003. [CrossRef]

[5] K. Fent, A. A. Weston, and D. Caminada, "Ecotoxicology of human pharmaceuticals," Aquatic Toxicology, Vol. 76(2), pp. 122–159, 2006. [CrossRef]

[6] C. Miège, J. M. Choubert, L. Ribeiro, M. Eusèbe, and M. Coquery, "Fate of pharmaceuticals and personal care products in wastewater treatment plants—conception of a database and first results," Environmental Pollution, 157(5), pp. 1721–1726, 2008. [CrossRef]

[7] K. Kümmerer, "The presence of pharmaceuticals in the environment due to human use-present knowledge and future challenges," Journal of Environmental Management, Vol. 90(8), pp. 2354–2366, 2009. [CrossRef]

[8] S. Mompelat, B. Le Bot, and O. Thomas, "Occurrence and fate of pharmaceutical products and by-products, from resource to drinking water," Environment International, Vol. 35(5), pp. 803–814, 2009. [CrossRef]

[9] I. M. Sebastine, and R. J. Wakeman, "Consumption and environmental hazards of pharmaceutical substances in the UK," Process Safety Environmental Protection, Vol. 81(B4), pp. 229–235, 2003. [CrossRef]

[10] L. Yang, L. E. Yu, and M. B. Ray, "Degradation of paracetamol in aqueous solutions by TiO2 photocatalysis," Water Research, Vol. 42(13), pp. 3480–3488, 2008. [CrossRef]

[11] B. C. Lourenção, R. A. Medeiros, R. C. Rocha-Filho, L. H. Mazo, and O. Fatibello-Filho, "Simultaneous voltammetric determination of paracetamol and caffeine in pharmaceutical formulations using a boron-doped diamond electrode," Talanta, Vol. 78(3), pp. 748–752, 2009. [CrossRef]

[12] M. Solé, J. P. Shaw, P. E. Frickers, J. W. Readman, and T. H. Hutchinson, "Effects on feeding rate and biomarker responses of marine mussels experimentally exposed to propranolol and acetaminophen," Analytical and Bioanalytical Chemistry, Vol. 96, pp. 649–656, 2010. [CrossRef]

[13] K. H. Langford, and K. V. Thomas, "Determination of pharmaceutical compounds in hospital effluents and their contribution to wastewater treatment works," Environment International, Vol. 35(5), pp. 766–770, 2009. [CrossRef]

[14] P. J. Phillips, S. G. Smith, D. W. Kolpin, S. D. Zaugg, H. T. Buxton, E. T. Furlong, K. Esposito, and B. Stinson, "Pharmaceutical formulation facilities as sources of opioids and other pharmaceuticals to wastewater treatment plant effluents," Environmental Science & Technology, Vol. 44(13), pp. 4910–4916, 2010. [CrossRef]

[15] J. J. Xu, B. S. Hendriks, J. Zhao, and D. Graaf, "Multiple effects of acetaminophen and p38 inhibitors: towards pathway toxicology," FEBS Letters, Vol. 582, pp. 1276–1282, 2008. [CrossRef]

[16] A. Carabin, P. Drogui, and D. Robert, "Photo-degradation of carbamazepine using TiO2 suspended photocatalysts," Journal of Taiwan Institute of Chemical Engineers, Vol. 54, pp. 109–117. [CrossRef]

[17] N. Muir, J. D. Nichols, M. R. Stillings, and J. Sykes, "Comparative bioavailability of aspirin and paracetamol following single dose administration of soluble and plain tablets," Current Medical Research Opinion, Vol. 13(9), pp. 491–500, 1997. [CrossRef]

[18] J. Wang, and S. Wang, "Removal of pharmaceuticals and personal care products (PPCPs) from wastewater: a review," Journal of Environmental Management, Vol. 182, pp. 620–640, 2016. [CrossRef]

[19] M. Chen, F. Zhang, C. Cui, X. Liao, J. Chen, J. Rong, and D. Yu, "Treatment of wastewater from paracetamol factory by using non-thermal plasma and active carbon," 2011 International Conference on Materials for Renewable Energy & Environment, 2011. [CrossRef]

[20] U. Nielsen, C. Hastrup, M. M. Klausen, B. M. Pedersen, G. H. Kristensen, J. L. C. Jansen, S. N. Bak, and J. Tuerk, "Removal of APIs and bacteria from hospital wastewater by MBR plus O3, O3 + H2O2, PAC or ClO2," Water Science and Technology, Vol. 67, pp. 854–862, 2013. [CrossRef]

[21] M. Mameri, N. Debbache, M. E. M. Benacherine, N. Seraghni, and T. Sehili, "Heterogeneous photodegradation of paracetamol using Goethite/H2O2 and Goethite/oxalic acid systems under artificial and natural light," Journal of Photochemistry and Photobiology A: Chemistry, Vol. 315, pp. 129–137, 2016. [CrossRef]

[22] M. E. M. Benacherine, N. Debbache, I. Ghoul, and Y. Mameri, "Heterogeneous photoinduced degradation of amoxicillin by Goethite under artificial and natural irradiation," Journal of Photochemistry and Photobiology A: Chemistry, Vol. 335, pp. 70–77, 2017. [CrossRef]

[23] H. Al Qarni, P. Collier, J. O'Keeffe, and J. Akunna, "Investigating the removal of some pharmaceutical compounds in hospital wastewater treatment plants operating in Saudi Arabia," Environmental Science and Pollution Research, Vol. 23, pp. 13003–11301, 2016. [CrossRef]

[24] F. G. Dalgic, I. Turkdogan, K. Yetilmezsoy, and E. Kocak, "Treatment of real paracetamol wastewater by fenton process," Chemical Industry and Chemical Engineering, Vol. 23, pp. 23–29. [CrossRef]

[25] C. M. Lee, P. Palaniandy, N. Q. Zaman, and M. N. Adlan, "Pharmaceutical removal from synthetic wastewater using heterogeneous – photocatalyst," Applied Mechanics and Materials, Vol. 802, Article 507, 2015. [CrossRef]

[26] J. P. Scott, and D. F. Ollis, "Integration of chemical and biological oxidation processes for water treatment," Environ. Program, Vol. 14, pp. 88– 103, 1995. [CrossRef]

[27] I. K. Konstantinou, and T. A. Albanis, "TiO2-assisted photocatalytic degradation of azo dyes in aqueous solution: kinetic and mechanistic investigations – a review," Applied Catalysis B: Environmental, Vol. 49, pp. 1–14, 2004. [CrossRef]

[28] M. A. Al-Nuaim, A. A. Al-Wasiti, Z. Y. Shnain, and A. K. AL-Shalal, "The combined effect of bubble and photo catalysis technology in btex removal from produced water," https://ejournal.undip.ac.id/ Accessed on Nov 02, 2023. [CrossRef]

[29] N. E. Mousa, S. S. Mohammed, Z. Y. Shnain, M. F. Abid, A. A. Alwasiti, and K. A. Sukkar, "Catalytic photodegradation of cyclic sulfur compounds in a model fuel using a bench-scale falling-film reactor ırradiated by a visible light," Bulletin of Chemical Reaction Engineering & Catalysis, Vol. 17(4), pp. 755–767, 2022. [CrossRef]

[30] H. Shemer, Y. K. Kunukcu, and K. G. Linden, "Degradation of the pharmaceutical metronidazole via UV, Fenton and photo-Fenton processes," Chemosphere, Vol. 63, pp. 269–276, 2005. [CrossRef]

[31] S. A. Abdulrahman, S. S. Ibraheem, and Z. Y. Shnain, "An overview of wastewater treatment using combined heterogeneous photocatalysis and membrane distillation," Chimica Techno Acta, Vol. 10(1), Article 10114, 2023. [CrossRef]

[32] A. K. Majhool, K. A. Sukkar, and M. A. Alsaffar, "Combining α-Al2O3 packing material and a ZnO nanocatalyst in an ozonized bubble column reactor to ıncrease the phenol degradation from wastewater," Processes, Vol. 11, Article 2416, 2023. [CrossRef]

[33] Y. Cheng, H. Sun, W. Jin, and N. Xu, "Photocatalytic degradation of 4-chlorophenol with combustion synthesized TiO2 under visible light irradiation," Chemical Engineering Journal, Vol. 128, pp. 127–133, 2007. [CrossRef]

[34] S. A. Abdulrahman, Z. Y. Shnain, S. S. Ibrahim, and H. S. Majdi, "Photocatalytic degradation of ciprofloxacin by uv light using n-doped tio2 in suspension and coated forms," Catalysts, Vol. 12, Article 1663, 2022. [CrossRef]

[35] F. S. Freyria, M. Armandi, M. Compagnoni, G. Ramis, I. Rossetti, and B. Bonelli, "Catalytic and photocatalytic processes for the abatement of n-containing pollutants from wastewater. part 2: Organic pollutants," Journal of Nanoscience and Nanotechnology, Vol. 17, pp. 3654–3672, 2017. [CrossRef]

[36] M. Compagnoni, G. Ramis, F. S. Freyria, M. Armandi, B. Bonelli, and I. Rossetti, "Photocatalytic processes for the abatement of n-containing pollutants from wastewater. Part 1: Inorganic pollutants," Journal of Nanoscience and Nanotechnology, Vol. 17(6), pp. 3632–3653, 2017. [CrossRef]

[37] N. Blangetti, F. S. Freyria, M. C. Calviello, N. Ditaranto, S. Guastella, and B. Bonelli, "Photocatalytic degradation of paracetamol under simulated sunlight by four TiO2 commercial powders: An insight into the performance of two sub-micrometric anatase and rutile powders and a nanometric brookite powder," Catalysts, Vol. 13(2), Article 434, 2023. [CrossRef]

[38] M.A. Al-Nuaim, A.A. Alwasiti, and Z.Y. Shnain, "The photocatalytic process in the treatment of polluted water," Chemical Papers, Vol. 77, pp. 677–701, 2023. [CrossRef]

[39] K.-H. Wang, Y.-H. Hsieh, C.-H. Wu, and C.-Y. Chang, "The pH and anion effects on the heterogeneous photocatalytic degradation of o-methylbenzoic acid in TiO2 aqueous suspension," Chemosphere, Vol. 40(4), pp. 389–394, 2000. [CrossRef]

[40] H.Y. Chen, O. Zahraa, and M. Bouchy, "Inhibition of the adsorption and photocatalytic degradation of an organic contaminant in an aqueous suspension of TiO2 by inorganic ions," Journal of Photochemistry and Photobiology A: Chemistry, Vol. 108(1), pp. 37–44, 1997. [CrossRef]

[41] J. P. Holmberg, E. Ahlberg, J. Bergenholtz, M. Hassellöv, and Z. Abbas, "Surface charge and interfacial potential of titanium dioxide nanoparticles: Experimental and theoretical investigations," Journal of Colloid Interface Science, Vol. 407, pp. 168–176, 2013. [CrossRef]

[42] N. Jallouli, K. Elghniji, H. Trabelsi, and M. Ksibi, "Photocatalytic degradation of paracetamol on TiO2 nanoparticles and TiO2/cellulosic fiber under UV and sunlight irradiation," Arabian Journal of Chemistry, Vol. 10(Suppl 2), pp. S3640–S3645. [CrossRef]

[43] T. M. A. Dalmázio, R. Alves, and R. Augusti, "An appraisal on the degradation of paracetamol by TiO2/UV system in aqueous medium. Product identification by gas chromatography–mass spectrometry," Journal of the Brazilian Chemical Society, Vol. 19(1), pp. 81–88, 2008. [CrossRef]

[44] A. Sclafani, L. Palmisano, and E. Davi, "Photocatalytic degradation of hydroxyethylcellulose in aqueous Pt TiO2 suspension," Journal of Photochemistry and Photobiology A: Chemistry, Vol. 56, pp. 399–406, 1991. [CrossRef]

[45] M. Fujihira, Y. Satoh, and T. Osa, "Photocatalytic degradation of organic water contaminants: Mechanisms involving hydroxyl radical attack," Bull Chem Soc 1982. [CrossRef]

[46] C. Kormann, D.W. Bahnemann, and M. R. Hoffmann, "Photolysis of chloroform and other organic molecules in aqueous titanium dioxide suspensions," Environmental Science & Technology, Vol. 25, pp. 494–500, 1991. [CrossRef]

[47] D. F. Ollis, C. Y. Hsiar, L. Budiman, and C. L. Lee, "Visible-light activation of TiO2 photocatalysts: Advances in theory and experiments," Journal of Photochemistry and Photobiology C: Photochemistry Reviews, Vol. 25, pp. 1–29, 2015. [CrossRef]

[48] C. Maillard-Dupuy, C. Guillard, and P. Pichat, "Kinetics and products of the TiO2 photocatalytic degradation of pyridine in water," Environmental Science & Technology, Vol. 28, pp. 2176–2183, 1994. [CrossRef]

[49] E. Mostafa, P. Reinsberg, S. Garcia-Segura, and H. Baltruschat, "Chlorine species evolution during electrochlorination on boron-doped diamond anodes: In-situ electrogeneration of Cl2, Cl2O and ClO2," Electrochimica Acta, Vol. 281, pp. 831–840, 2018. [CrossRef]

[50] A. Abdelhaleem, H. N. Abdelhamid, M. G. Ibrahim, and W. Chu, "Photocatalytic degradation of paracetamol using photo-Fenton-like metal-organic framework-derived CuO@C under visible LED," Journal of Cleaner Production, Vol. 379, Article 134571, 2022. [CrossRef]

[51] D. C. Sanches Gloria, C. H. Vieira Brito, T. A. Prado Mendonça, T. R. Brazil, R. A. Domingues, N. C. Silva Vieira, E. B. Santos, and M. Gonçalves. "Preparation of TiO2/activated carbon nanomaterials with enhanced photocatalytic activity in paracetamol degradation," Materials Chemistry and Physics, Vol. 305, Article 127947, 2023. [CrossRef]

Environ Res Tec, Vol. 6, Issue. 4, pp. 359–370, December 2023

Environmental Research and Technology
https://ert.yildiz.edu.tr - https://dergipark.org.tr/tr/pub/ert
DOI: https://doi.org/10.35208/ert.1353244

Environmental Research & Technology

Research Article

Investigation of land surface temperature heterogeneity in municipal landfills by satellite images

Sedat YALÇINKAYA*[1], Fatih DOĞAN[2]

[1]*Department of Environmental Engineering, Marmara University, İstanbul, Türkiye*
[2]*Department of Urban Regeneration, İzmir Katip Çelebi University, İzmir, Türkiye*

ARTICLE INFO

Article history
Received: 31 August 2023
Revised: 28 September 2023
Accepted: 17 October 2023

Key words:
GIS; Land surface temperature; Landfill; Satellite imagery; Waste management

ABSTRACT

With the increasing population and urbanization, the amount of municipal solid waste (MSW) is increasing day by day. As a result, problems such as odor, fire, and intense biogas formation originate from landfills. In order to detect and solve these problems, landfills should be monitored regularly. Geographic Information Systems (GIS) and Remote Sensing offer fast and practical solutions for the regular monitoring of landfills compared to field studies. In this study, Kömürcüoda landfill on the Anatolian side of İstanbul is monitored throughout 2022 with open source Landsat8/9 and Sentinel-2 satellite images. In this context, the surface temperature heterogeneity of the landfill was mapped by generating Land Surface Temperature (LST) images for the landfill from the Landsat thermal band. Points with statistically significant high - low LST values were determined with Hot Spot Analysis. The average annual LST for 2022 was calculated as 25.5 °C. It was observed that LST had the highest values during the summer season and the lowest values during the winter season. Additionally, it has been determined that there are persistent hot spots and cold spots in the landfill. This study presents a simple methodology using open source satellite data to monitor LST and detect LST abnormalities on landfills.

Cite this article as: Yalçınkaya S, Doğan F. Investigation of land surface temperature heterogeneity in municipal landfills by satellite images. Environ Res Tec 2023;6(4)359–370.

INTRODUCTION

Solid waste is solid materials with different contents that must be disposed of by being removed from people for social and environmental health. In Türkiye, the collection and management of municipal solid waste (MSW) is the responsibility of district municipalities. The management of MSW consists of the following steps: the generation of solid waste at its source and temporary storage at designated collection points, collection and transfer to the nearest transfer facility, transportation to the landfill, and landfilling [1–3].

The amount of waste produced is constantly increasing due to reasons such as population growth, industrialization - urbanization, and the composition of the waste produced is changing with technological developments and differentiating consumption habits [4]. Landfills have become an important problem in recent years due to the reasons such as creating an irritating odor, negatively affecting the ecological balance around it, polluting ground and surface waters, disrupting the aesthetics of the city, creating a breeding ground for insects, rodents and microbes that may threaten human health [5]. Also, previous studies have stated that waste fires constitute an important part of fire cases [6] and fires in some landfills continue for a long time [7]. MSW in Türkiye contains a significant amount of organic waste [8]. Organic wastes in landfills are biodegraded under an-

***Corresponding author.**
*E-mail address: sedat.yalcinkaya@marmara.edu.tr

aerobic conditions and cause biogas formation. Generally, 50–70% of biogas is Methane (CH_4) and Carbon Dioxide (CO_2), which are the main greenhouse gases [9]. Considering that 2.6% (14.7 million tons of CO_2 equivalent) of Türkiye's greenhouse gas emissions in 2021 are caused by waste management [10], landfills can be considered as important greenhouse gas sources. Consequently, the landfill monitoring emerges as a clear necessity for identifying and tracking warm biogas leakages and waste fires.

The regular landfill monitoring is possible with some in-situ measurements and field studies, but these approaches require time, cost and effort. At this point, Geographic Information Systems (GIS) – Remote Sensing based approaches are effective alternatives for regular monitoring of landfills [11]. Land Surface Temperature (LST), which can be produced from satellite or Unmanned Aerial Vehicle (UAV) data with a thermal sensor, is widely used in related studies. Faisal et al. [12] examined landfills in Kuwait and Canada, generating LST using Landsat satellite imagery from 2007–2008. They also converted LST images into contours, detecting 5 suspicious waste dumps in the densely overlapping regions of the Al-jleeb landfill in Kuwait. Additionally, a positive Methane (CH4) - LST correlation was found for the Trail Road landfill in Canada. Abu Qdais and Shatnawi developed an Artificial Neural Network (ANN) architecture to predict LST using variables such as ambient temperature, humidity, wind velocity, evaporation, emitted methane, waste amount in their study for a landfill in Jordan [13]. They also determined a significant correlation (r = 0.884) between the amount of waste stored in the landfill and the LST. Fjelsted et al. [14] used an Unmanned Aerial Vehicle (UAV) equipped with a thermal sensor to generate high-resolution LST for two landfills in Denmark. In the study, the landfill gas (LFG) - LST relationship is presented by making use of some methane (CH_4) and carbon dioxide (CO_2) measurements. Nazari et al. [15] generated LST from Landsat satellite imagery for the Bridgeton landfill in the United States, demonstrating that LST anomalies correspond to known subsurface fires within the landfill. Karimi et al. [16] examined the thermal zone distribution of 8 different landfills in Canada, highlighting that LST data could be a suitable indicator for determining landfill biothermal zones. In another study in the literature, a methodology to detect fugitive landfill gas hot spots using LST is presented for a Canadian landfill. In this context, a model that predicts high resolution LST was developed by combining Landsat 8 and Sentinel-2 satellite image bands. It was emphasized that high consistency was observed between the real LST and the predicted LST [17]. Grondona et al. [18] downscaled Landsat 8 LST with the MHUTS (Modified High-resolution Urban Thermal Sharpener) method by combining Landsat 8 and Sentinel-2 satellite data. The downscaled LST was used to detect heat islands in a Brazilian landfill. The authors confirm in the study that the downscaling method does not compromise the accuracy of LST data. Chavan et al. [19] studied a landfill in Delhi, examining waste properties, CO levels, and LST. The study revealed that older waste exhibits a higher propensity for spontaneous combustion compared to fresh waste. Mahmood et al. [20] conducted a study using LST as an indicator, presenting satellite-based bio-thermal impact insights into MSW open dumps. These literature findings underscore the availability of various satellite-based imaging and analysis methods to comprehend potential of landfills on the environment and monitor these impacts.

This study presents a detailed investigation conducted on the Kömürcüoda landfill in İstanbul. LST images obtained from Landsat 8 and Landsat 9 satellites were used to examine the seasonal and monthly variations in the study area. Additionally, Sentinel-2 satellite images were acquired to analyze the higher-resolution RGB images of the study area. The downloaded satellite images were selected to include representative samples from each month of the year 2022. Particularly in the LST images generated for the landfill area, significant high and low temperature values were identified using the hot spot analysis method. This analysis enables us to comprehend the thermal behavior of the landfill and estimate its potential environmental impacts.

MATERIALS AND METHODS

The steps followed in the study can be summarized as follows: 1) Data collection, 2) geodatabase design and generation, 3) LST calculation, 4) base map creation, and 5) hot spot analysis (Fig. 1).

Study Area

Located at the intersection of two continents (Asia and Europe), İstanbul is Türkiye's most populous city with a population of 15,907,901 [21]. 16,000 tons of MSW per day is stored in 2 landfills in İstanbul, excluding recycling and recovery processes. 10,500 tons of this waste is disposed in Silivri - Seymen Landfill on the European side, and 5,500 tons in Şile - Kömürcüoda Landfill on the Asian side [22]. In this study, the Kömürcüoda Landfill on the Asian side of İstanbul was determined as the study area (Fig. 2). The study area has a surface area of 2.11 km^2 and located within the borders of Şile district. It is located close to the Black Sea and surrounded by forests. Kömürcüoda Landfill has a MSW disposal area, a power generation facility utilizing the landfill gas, a leachate treatment facility, an industrial waste disposal area, a semi closed compost plant, and a biomethanization plant. The landfill has an electricity generation capacity of 39 MWh from landfill gas [23]. The city of İstanbul, where the study area is located, has a transitional climate between the Black Sea and the Mediterranean due to its geographical location. İstanbul's summers are hot and humid, and its winters are cold and rainy. In this city, the lowest temperature can drop to -11 °C at different times of the year, while the highest temperature can reach 40 °C. Rare snowfalls may occur between December and March. Since the study area is under the influence of humid air masses coming from the Black Sea, the annual average relative humidity is between 70% and 80%. Moreover, since its north faces the Black Sea, it is under the influence of northerly winds [24].

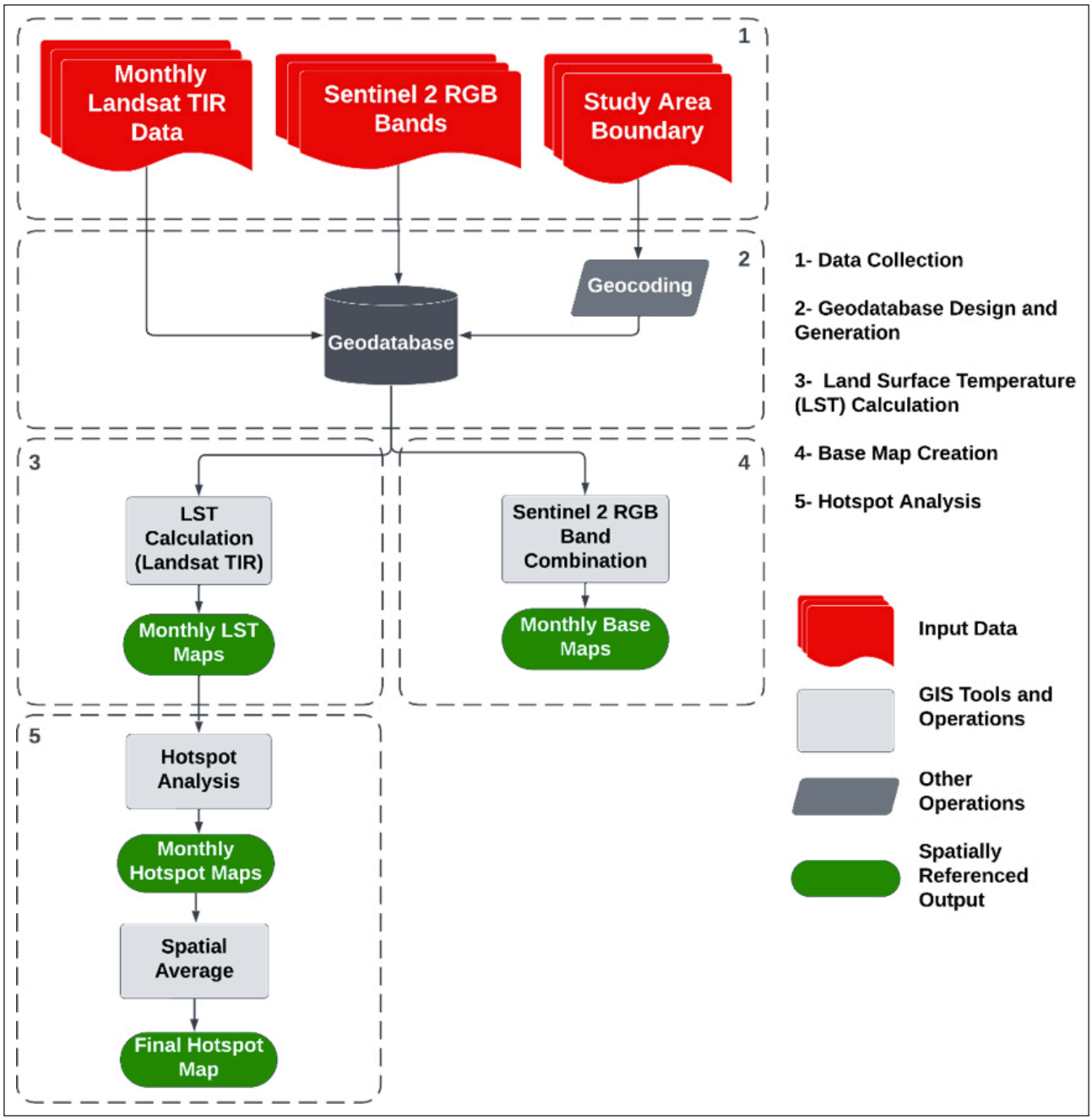

Figure 1. Stepwise methodology of the study.

Data Collection and Geodatabase Generation

The boundaries of the Kömürcüoda Landfill were manually extracted from the Google Earth Pro. The resulting KML file was transferred to the GIS environment. Landsat 8, Landsat 9 and Sentinel-2 satellite images were used in the study. An exemplary Landsat8/9 and a Sentinel-2 image were downloaded from each month of 2022. During this process, attention was paid to the temporal proximity of the Landsat and Sentinel images, to have the same path and row, and to have no cloudy images corresponding to the study area. In this context, cloud-free Sentinel and Landsat image dates were investigated for each month. If possible, Sentinel and Landsat images from the same day were downloaded. Otherwise, Landsat and Sentinel images with minimum temporal proximity among the options were paired and downloaded.

Landsat-8 and Lansat-9 satellites carry moderate resolution optical and thermal imaging systems. These systems, used to study the Earth's surface, can image the Earth's surface with a spatial resolution of up to 30 m and monitor atmospheric conditions, vegetation, oceans, glaciers, and various other land features [25]. United States Geological Survey (USGS) is responsible for managing and distributing the satellite data archive. Satellites complete their orbit around the earth approximately every 14 days and provide a new image for the same path-row coordinates every cycle. Landsat 8 and Landsat 9 contain 11 bands. First 9 bands are captured by Operational Land Imager (OLI) sensor. Bands 10 and 11 are captured by Thermal Infrared Sensor (TIRS) sensor. While 8 OLI bands have 30 m spatial resolution panchro-

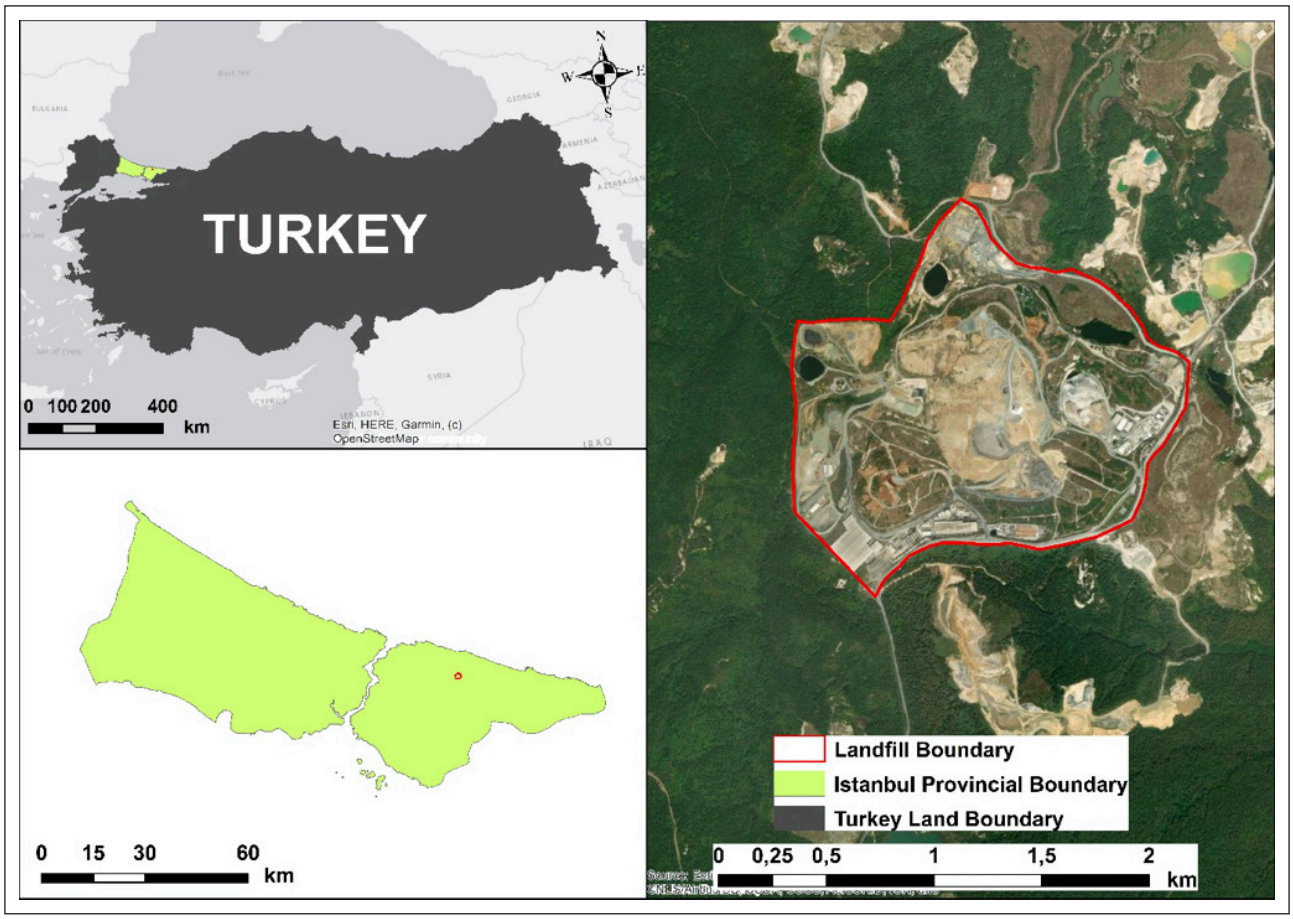

Figure 2. Study area.

matic (PAN) band has 15 m. The spatial resolution can be increased from 30 m to 15 m by pan-sharpening using the PAN band. Although TIR bands have a spatial resolution of 100 m, they are presented by resampling to 30 m. Since it is emphasized in the literature that band 11 has lower accuracy than band 10 [26], band 10 was used in LST calculations and hot spot analysis in the present study. The USGS's Earth Explorer website was used to download the Lansat-8 and Landsat-9 satellite images free of charge [27].

Sentinel-2A and Sentinel-2B are part of the Sentinel-2 satellites developed and operated by the European Space Agency (ESA). With the advanced remote sensing tools in the satellites, it can image the Earth's surface in a high resolution and multi-spectral manner. The images of these satellites can display the Earth's surface with a spatial resolution of up to 10 m. They were used in the base map creation step of the project, as they provide higher resolution and quality images compare to the Landsat images. Sentinel-2 satellites also have higher time resolution compared to Landsat satellites. They pass through an area on average every 10 days and produce an image. Sentinel satellite images were freely downloaded from the Copernicus Open Access Hub website [28]. Within the scope of the study, Landsat Collection 2 Level 2 and Sentinel Level 2A images were used, since Level 2 data products are preprocessed and do not require correction of atmospheric effects, geometric and radiometric calibrations. The satellite data list used in the study is presented in Table 1. All of the data were converted to the WGS 1984 UTM (Universal Traverse Mercator) Zone 35 N, which is the most suitable projected coordinate system for the study area and transferred to the GIS environment. Satellite image processing and spatial analyses were performed in Esri's ArcMap software.

Land Surface Temperature (LST) Calculation

"Additive Offset" and "Multiplicative Scale Factor" values given for Band-10 in Table 6.1 in the "USGS's Landsat 8–9 Collection 2 (C2) Level 2 Science Product (L2SP) Guide" [29], an equation to convert the reflectance values given in the raw data to LST in Kelvin (K°) degrees, were used. The equation was modified to output LST in Celsius (C°) degrees:

Surface Temperature (C^{o}) = 0,00341802 * Reflectance Value + 149,0 −273,15 Equation 1.

Raster calculation was performed to the satellite images using the Eq. 1. The reflectance values in every 30 m by 30 m of pixels were converted to LSTs (Fig. 3). Then, the area within the study area boundaries was extracted. This process was performed to the image of each month.

Hot Spot Analysis

After LST calculations, Hot spot Analysis was performed using previously created LST maps. For this reason, ArcMap's, "Hot Spot Analysis Getis Ord Gi*" Spatial Analysis Tool was

Table 1. Identifiers of the satellite data

Landsat 8/9 Data
LC09_L2SP_180031_20220120_20230430_02_T1
LC09_L2SP_180031_20220205_20230429_02_T1
LC09_L2SP_180031_20220325_20230424_02_T1
LC08_L2SP_180031_20220402_20220411_02_T1
LC09_L2SP_180031_20220512_20230417_02_T1
LC08_L2SP_180031_20220605_20220610_02_T1
LC08_L2SP_180031_20220723_20220802_02_T1
LC09_L2SP_180031_20220816_20230402_02_T1
LC08_L2SP_180031_20220909_20220914_02_T1
LC09_L2SP_180031_20221003_20230327_02_T1
LC09_L2SP_180031_20221104_20230323_02_T1
LC08_L2SP_180031_20221230_20230110_02_T1
Sentinel 2 Data
S2A_MSIL2A_20220117T090321_N0301_R007_T35TPF_20220117T120927
S2B_MSIL2A_20220211T090009_N0400_R007_T35TPF_20220211T111741
S2A_MSIL2A_20220325T084611_N0400_R107_T35TPF_20220325T120651
S2B_MSIL2A_20220402T085549_N0400_R007_T35TPF_20220402T123301
S2A_MSIL2A_20220514T084601_N0400_R107_T35TPF_20220514T133711
S2B_MSIL2A_20220601T085559_N0400_R007_T35TPF_20220601T120802
S2A_MSIL2A_20220723T084611_N0400_R107_T35TPF_20220723T131856
S2B_MSIL2A_20220817T084559_N0400_R107_T35TPF_20220817T102926
S2B_MSIL2A_20220909T085559_N0400_R007_T35TPF_20220909T103032
S2A_MSIL2A_20221001T084801_N0400_R107_T35TPF_20221001T132601
S2B_MSIL2A_20221105T085039_N0400_R107_T35TPF_20221105T114546
S2A_MSIL2A_20221230T085351_N0509_R107_T35TPF_20221230T131052

used. To use this tool, input data must be in point format. Therefore, before applying hot spot analysis to LST rasters were converted to point format. Then, the hot spot analysis was applied to the LST maps in point format (Fig. 4).

In Hot Spot Analysis, the Getis-Ord Gi* statistic is calculated for each component. Statistically significant high-low value clusters are determined with the obtained p-values and z-scores [30]. P-value represents the probability. During Hot Spot Analysis, p-value is used to determine whether the spatial distribution of events in a region is random. If the p value is statistically significantly lower, then the events in this region are unlikely to be random. Z-score is a statistical term that shows how far a data is from the mean value in standard deviation units [31]. Getis-Ord Gi* statistic can be formulated as:

$$G_i^* = \frac{\Sigma_{j=1}^{n} w_i x_j - \bar{x}\Sigma_{j=1}^{n} w_{i,j}}{s\sqrt{\frac{[\Sigma_{j=1}^{n} w_{i,j}^2 - (\Sigma_{j=1}^{n} w_{i,j})^2]}{n-1}}} \quad \text{Equation 2.}$$

Where; G_i^*= statistic z-score, x_j= attribute value for feature j, $w_{i,j}$= spatial weight between feature i and j, n=total number of features, $\overline{X}$=mean, S=standard deviation

$$\bar{X} = \frac{\Sigma_{j=1}^{n} x_j}{n} \quad \text{Equation 3.}$$

$$S = \sqrt{\frac{\Sigma_{j=1}^{n} x_j^2}{n} - (\bar{x})^2} \quad \text{Equation 4.}$$

In equation 2, weighted z-score calculations are made according to the distance between the points in vector format. In order to show them more meaningfully after z-score calculation, ArcMap's Getis-Ord Gi* tool separates z-score values according to specific z-score classification. This classification was calculated according to the determined confidence levels (90%, 95%, 99%). The principle of employing a fixed distance spatial relationship revolves around the evaluation of individual features in relation to their neighboring counterparts to identify spatial clusters of high or low LST. A feature with a high value may be intriguing, but it might not necessarily constitute a statistically significant hot spot. To qualify as a statistically significant hot spot, a feature must not only possess a high value but also be situated amidst other features that also exhibit high values. The local sum of a feature and its neighboring features is assessed in relation to the total sum of all features. When this local sum significantly deviates from the anticipated local sum, and this deviation

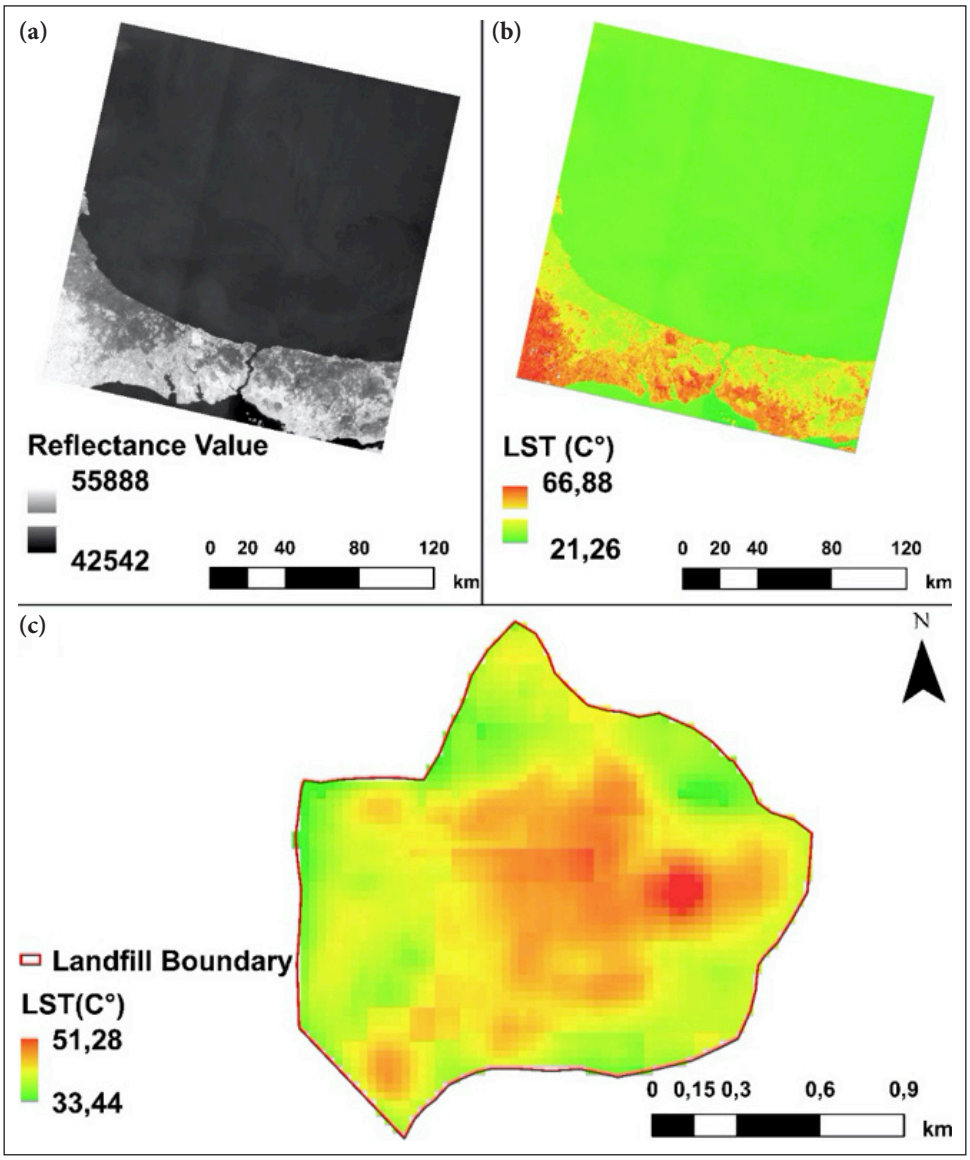

Figure 3. **(a)** Landsat thermal band, **(b)** calculated LST and **(c)** extracted landfill LST.

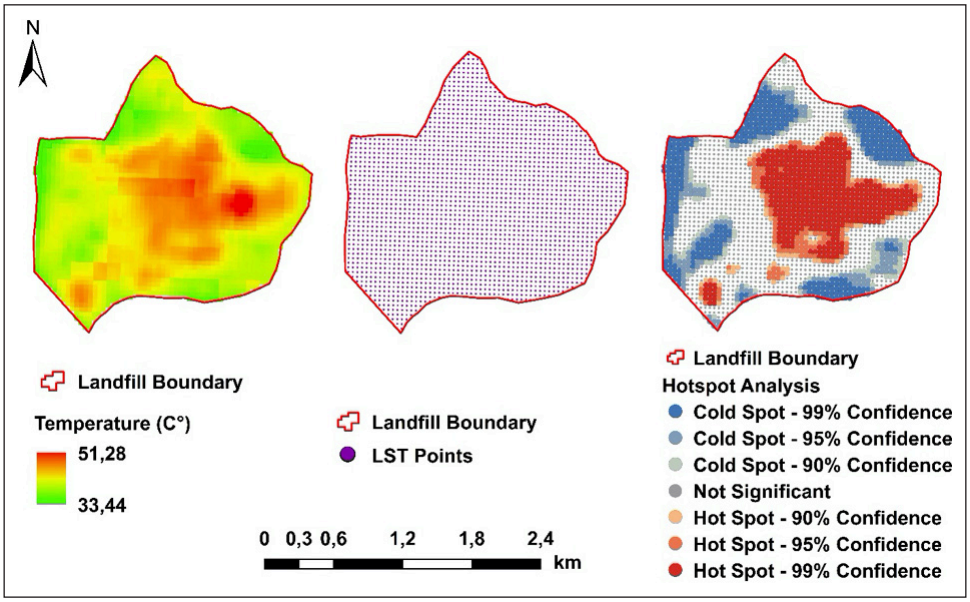

Figure 4. LST to hot spot analysis.

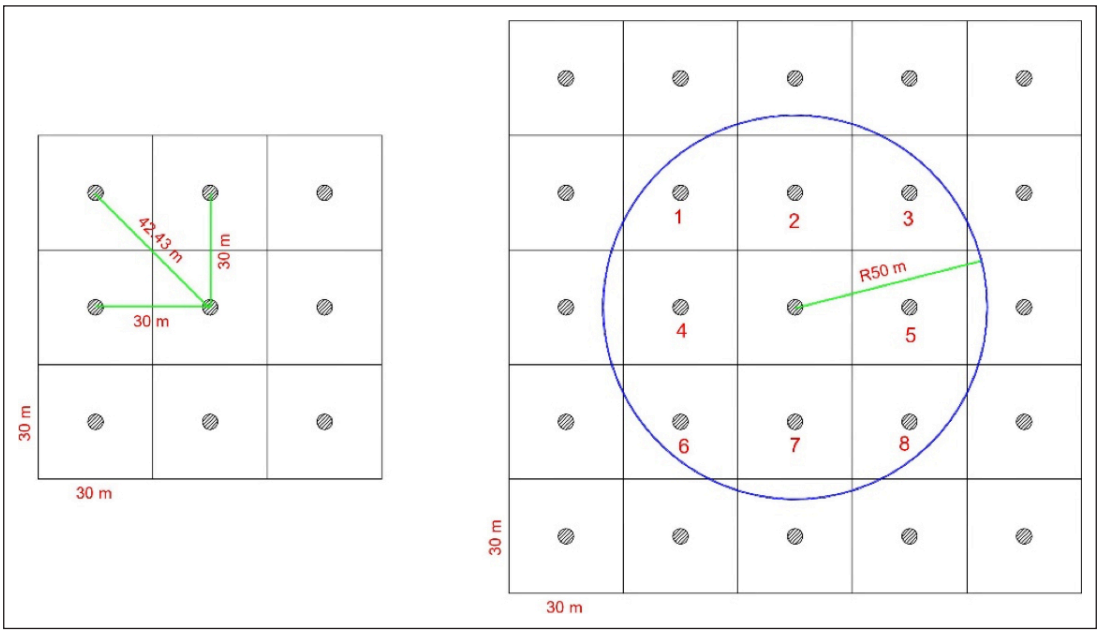

Figure 5. Schematic representation of the hot spot analysis application according to the threshold distance.

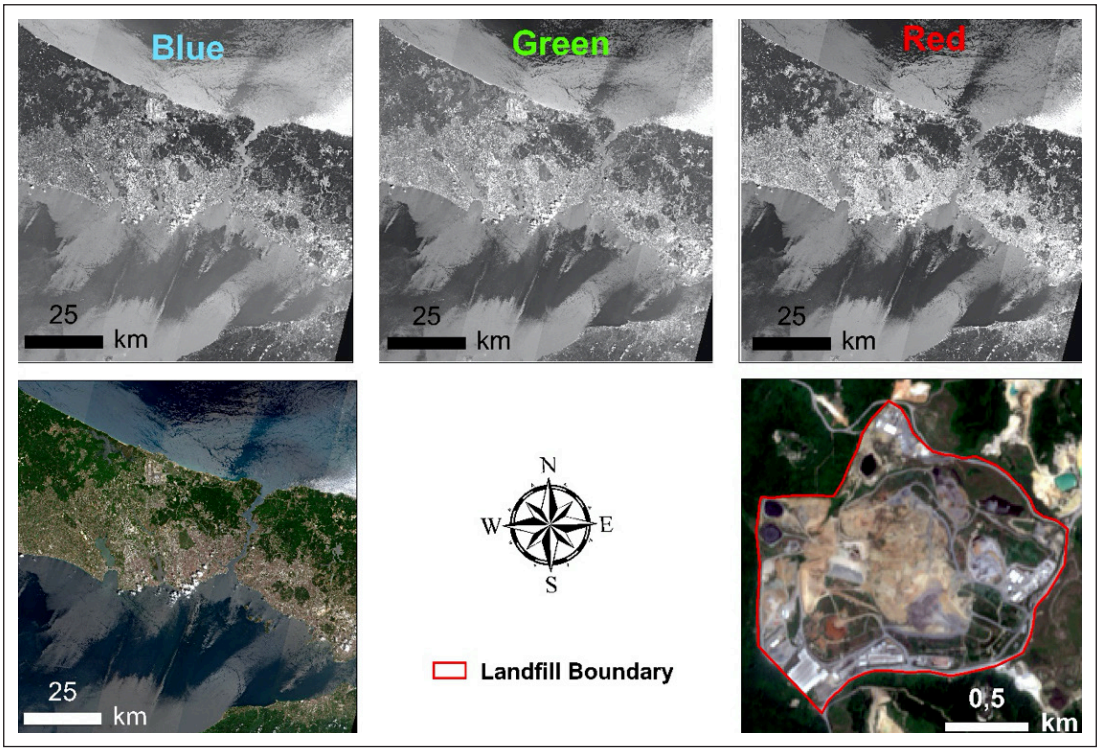

Figure 6. Base map creation process.

is too substantial to attribute to random chance, it yields a statistically significant z-score. Features situated within the designated threshold distance will carry a designated weight, consequently affecting computations pertaining to the target feature. On the other hand, neighboring features outside the threshold distance will receive a weight of zero and have no impact on computations related to the target feature. While performing the hot spot analysis, the spatial relationship was determined as fixed distance and the threshold value was entered as 50 m. Since the distance between the points obtained from the LSTs is 30 m, each target feature was analyzed with its 8 neighboring points (Fig. 5). 50 m threshold was used to include the surrounding eight neighbors. All hot spot analyses results were integrated into a single map, in terms of the z-values, to visualize the general trend in LST abnormalities.

Base Map Creation

To better understand what is happening in the hot spots and cold spots and what could cause the temperature difference there, base maps were created for each month from

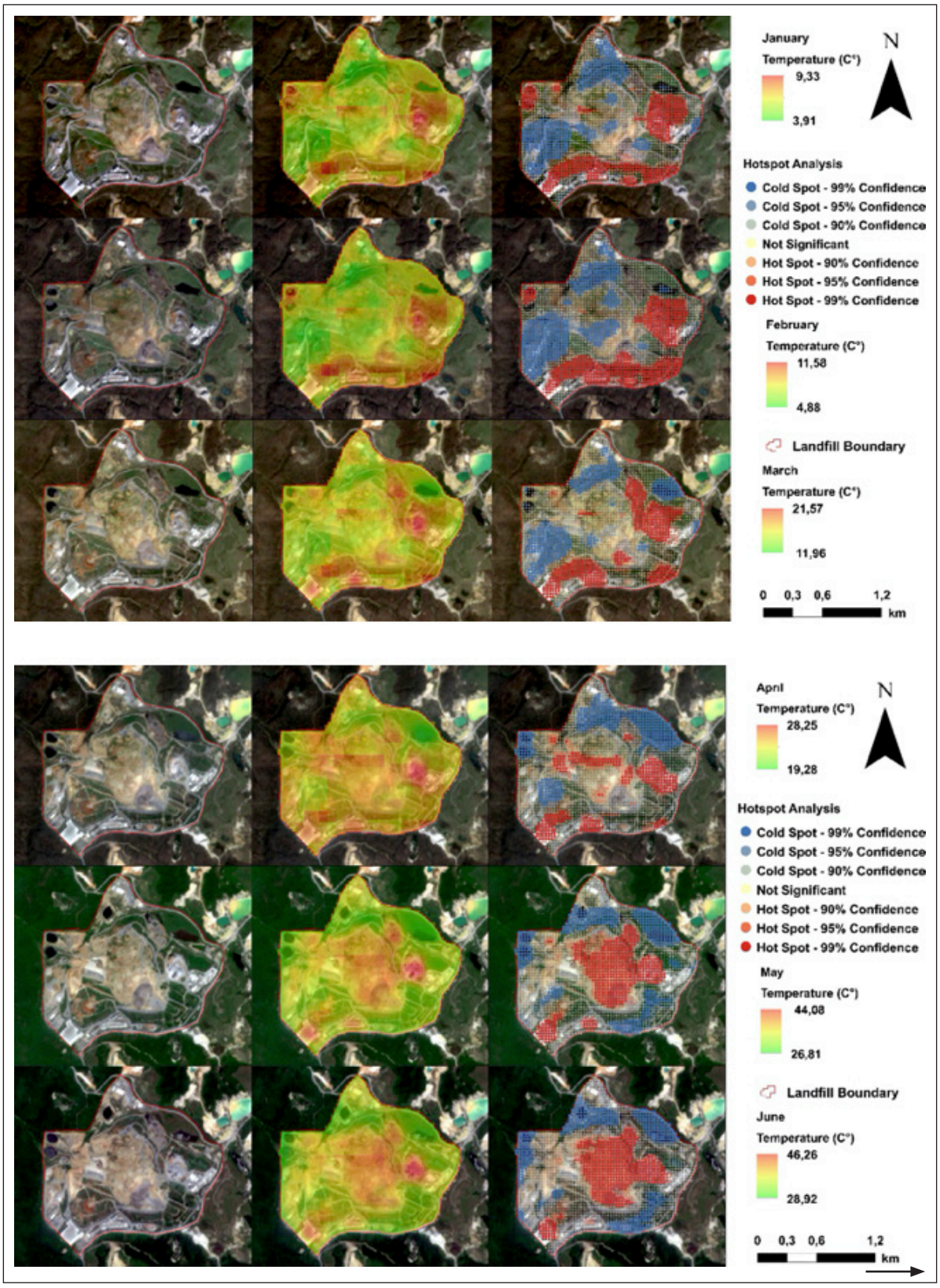

the Sentinel-2 satellite data of the closest or the same date to the Landsat satellite data which are used in LST calculation and Hot spot Analysis. For this purpose, Band 2 (blue), Band 3 (green), and Band 4 (red) from Sentinel-2 data were used as raw data. These 3 bands were combined and RGB images were produced. Area within the boundaries of the Kömürcüoda Landfill was extracted (Fig. 6). Sentinel's RGB band images (Band 2, Band 3, Band 4) were used to create the base map instead of Landsat's RGB band images, since Sentinel-2 has a higher resolution. Landsat provides 30 m x 30 m resolution images, while Sentinel has 10 m x10 m resolution images.

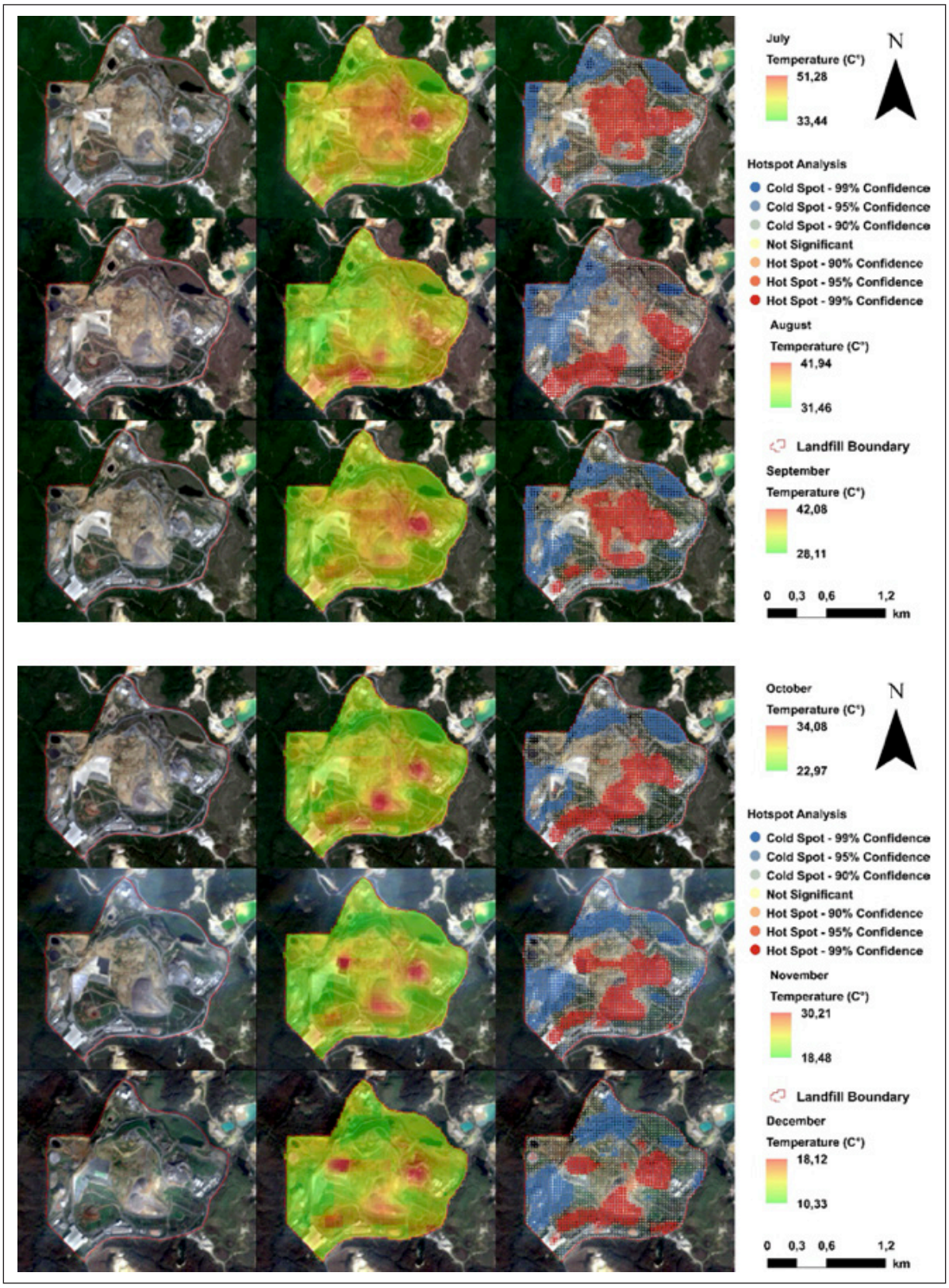

Figure 7. Base maps, land surface temperature maps and hot spot analysis result maps for 12 months of 2022.

RESULTS AND DISCUSSION

Within the scope of the study, base maps, LST and hot spot maps were produced for each month of 2022 (Fig. 7). Thus, the effect of seasonal conditions on LST was also considered. In LST rasters, low values are represented by green and high values by red. The month with the highest LST values was July, while the month with the lowest LST values was January. Significant difference between the minimum and maximum values were calculated for each

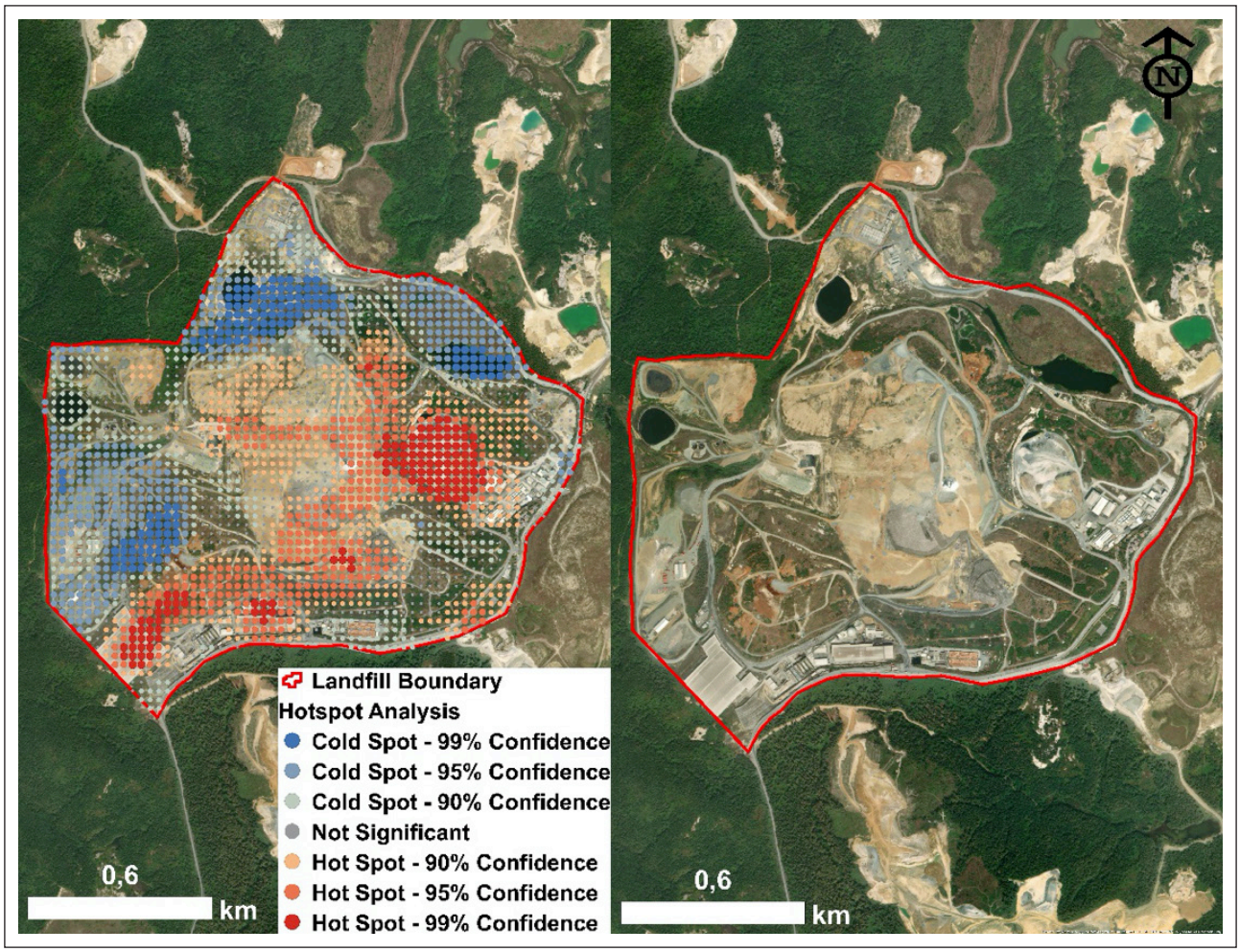

Figure 8. 12-month average hot spot analysis result map and base map.

month. The average temperature of the landfill in 2022 is calculated as 25.5 °C. Abu Qdais and Shatnawi calculated the average temperature of Al Akeedr landfill (Jordan) in 2016 as 32.4 °C [13]. This average temperature difference may be due to reasons such as the fact that the two landfills are located in regions with different climates, have different storage capacities, and are of different sizes. In addition, it has been observed that the seasonal and monthly changes of the Kömürcüoda landfill show a complex pattern. In winter, lower temperature values were observed due to the decrease in temperature and cold weather events. On the other hand, an increase in temperature was evident in the summer months, indicating an increase in thermal activity in the landfill. These findings clearly show the effect of seasonal changes on the thermal behavior of the landfill.

In the hot spot analysis results, the yellow dots are not statistically significant in terms of LST values in landfill. Red dots represent statistically significant high LST values, while blue dots represent statistically significant low LST values. These blue and red dots were classified in different confidence intervals according to the p-value and z-score values obtained as a result of the analysis. We are more interested in the LST abnormalities at high temperatures which may indicate biogas leakage.

High LST values and hot spots often determined in active landfill areas and specific areas where compost plant and co-generation plant. It has been observed that areas with vegetation on the edges of the landfill and leachate collection ponds are cold spot areas. This confirms the inverse relationship between LST and water - vegetation. The relationship of LST anomalies may be due to biogas leakage and/or underground bioconversion of organic fraction of municipal solid waste. Field studies are necessary to reach a certain conclusion.

12-month average hot spot results are presented in Figure 8. This is the holistic result of one year of LST observations for simple visualization. The presence of hot spots and cold spots spread over large areas shows that there are statistically significant high-low values that persist over one year. Nazari et al. [15] examined the Bridgeton landfill over a 17-year period and visualized locations based on the frequency of maximum or near-maximum LST values. In the current study, an approach based on spatial and statistical analysis is presented. This process provides a straightforward approach in identifying the continuous regions, as it is based on calculating the average of hot spot analysis results conducted for all months. Furthermore, applications such as trend analysis and emerging hot spot analysis can offer more detailed outcomes in determining the spatiotemporal patterns of the dataset [32].

The methodology developed in this study can be applied to any landfill for monitoring LST and detecting LST abnormalities. The study comes with certain limitations. For instance, the thermal band of the Landsat satellite with moderate resolution was utilized. It is likely that conducting a study that combines fieldwork with data from different satellites or sensors with higher sensitivity would yield more valuable results. Furthermore, only sample data from the year 2022 were used to assess the thermal behaviors of the landfill site. An investigation spanning a longer timeframe with data collected at more frequent intervals could provide a more comprehensive and reliable understanding of the thermal characteristics of the landfill. One of the most important limitations of the current study was that the satellite images contained cloudiness for many dates. In future studies on LST, the estimation of missing pixels due to cloudiness with modern approaches will be able to eliminate the problems regarding data frequency [33]. Lastly, the study examines the thermal behaviors of the Kömürcüoda landfill. Since the study area only encompasses the boundaries of the landfill, the thermal influence of the landfill to the surrounding area was not considered in this study.

CONCLUSION

The present study, which effectively utilizes open source multi temporal satellite data such as Landsat 8/9 and Sentinel-2, introduces a practical and sustainable approach for the regular monitoring of LST and LST abnormalities on landfills. Consequently, it is believed that the outcomes of this study and the applied methodology could serve as guidance for waste management authorities.

The study results reveal that LST does not exhibit a uniform structure at any given time. The relationship between LST anomalies and hot spots in the study area with phenomena like biogas leakage, sub-surface waste fires, and stored waste volume should be investigated through fieldwork and in-situ measurements. Moreover, the study area is adjacent to a forest, which prompts the examination of the thermal impact of landfill LST on the forest area in future research.

The continuous monitoring of landfills offers the potential to contribute to the resolution of issues stemming from landfill-related biogas emissions, fires, and odors. However, in order to comprehensively understand the thermal behaviors of landfills over an extended time frame, it is imperative to move beyond studies constrained by limited time periods and invest in automated, accurate, and continuously updated systems.

Averaging z-value may lose its significance for a general trend over the year. Averaging the LST value for each of the point and then performed Getis Ord Gi* analysis may be tried in the future studies. In addition, longer time periods may be studied to determine long time hot spots and evaluate inter-annual relationships.

In summary, this study's outcomes provide insights into the complexities of landfill thermal behaviors and emphasize the necessity of sustained monitoring practices, advanced technologies, and waste management strategies that align with sustainable principles.

DATA AVAILABILITY STATEMENT

The authors confirm that the data that supports the findings of this study are available within the article. Raw data that support the finding of this study are available from the corresponding author, upon reasonable request.

CONFLICT OF INTEREST

The authors declared no potential conflicts of interest with respect to the research, authorship, and/or publication of this article.

ETHICS

There are no ethical issues with the publication of this manuscript.

REFERENCES

[1] M. C. Höke, and S. Yalcinkaya, "Municipal solid waste transfer station planning through vehicle routing problem-based scenario analysis," Waste Management & Research, Vol. 39(1), pp. 185–196, 2021. [CrossRef]

[2] S. Yalcinkaya, "A spatial modeling approach for siting, sizing and economic assessment of centralized biogas plants in organic waste management," Journal of Cleaner Production, Vol. 255, Article 120040, 2020. [CrossRef]

[3] S. Yalcinkaya, and O. S. Kirtiloglu, "Application of a geographic information system-based fuzzy analytic hierarchy process model to locate potential municipal solid waste incineration plant sites: A case study of Izmir Metropolitan Municipality," Waste Management & Research, Vol. 39(1), pp. 174–184, 2021. [CrossRef]

[4] T. Bayram, Y. A. Arhun, and S. Tirink, "An Evaluation of Solid Waste Management in Turkey," Black Sea Journal of Engineering and Science, Vol. 2(3), pp. 88–91, 2019. [CrossRef]

[5] A. Sağlık, Y. S. Domaç, Ş. N. Reyhan, F. Avcı, F. Kartal, and D. Şenkuş, "Improvement and analysis of solid waste landfills example of Çanakkale Onsekiz Mart University," Academia Journal of Nature and Human Sciences, Vol 7(1), pp. 105–125, 2021.

[6] S. Yalçınkaya, F. Doğan, and H. İ. Kaleli, "Investigation of waste fires and spatial accessibility of fire stations in Izmir, Turkey," Urban Academy, Vol. 15(2), pp. 727–741, 2022. [CrossRef]

[7] J. Kret, L. Dalidowitz Dame, N. Tutlam, R. W. DeClue, S. Schmidt, K. Donaldson, R. Lewis, S. E. Rigdon, S. Davis, A. Zelicoff, C. King, Y. Wang, S. Patrick, and F. Khan, "A respiratory health survey of a subsurface smoldering landfill," Environmental Research, Vol. 166, pp. 427–436, 2018. [CrossRef]

[8] H. Şenol, E. A. Elibol, Ü. Açıkel, and M. Şenol, "Primary Biomass Sources for Biogas Production in Turkey," BEU Journal of Science, Vol. 6(2), pp. 81–92, 2017. [CrossRef]

[9] Y. Korkmaz, S. Aykanat, and A. Çil, "Biogas and energy production from organic wastes," SAÜ Fen Edebiyat Dergisi, SAU Journal of Science and Letters, Vol. 12, pp. 489–497, 2012.
[10] Turkish Statistical Institute, "Sera Gazı Emisyon İstatistikleri, 1990-2021," 2023. https://data.tuik.gov.tr/Bulten/Index?p=Sera-Gazi-Emisyon-Istatistikleri-1990-2021-49672 Accessed on Jul 16, 2023.
[11] L. G. Papale, G. Guerrisi, D. De Santis, G. Schiavon, and F. Del Frate, "Satellite data potentialities in solid waste landfill monitoring: Review and case studies," Sensors, Vol. 23(8), Article 3917, 2023. [CrossRef]
[12] K. Faisal, M. AlAhmad, and A. Shaker, "Remote sensing techniques as a tool for environmental monitoring," The International Archives of the Photogrammetry, Remote Sensing and Spatial Information Sciences, Vol. XXXIX-B8, pp. 513–518, 2012. [CrossRef]
[13] H. Abu Qdais, and N. Shatnawi, "Assessing and predicting landfill surface temperature using remote sensing and an artificial neural network," International Journal of Remote Sensing, Vol. 40(24), pp. 9556–9571, 2019. [CrossRef]
[14] L. Fjelsted, A. G. Christensen, J. E. Larsen, P. Kjeldsen, and C. Scheutz, "Assessment of a landfill methane emission screening method using an unmanned aerial vehicle mounted thermal infrared camera – A field study," Waste Management, Vol. 87, pp. 893–904, 2019. [CrossRef]
[15] R. Nazari, H. Alfergani, F. Haas, M. E. Karimi, M. G. Rabbani Fahad, S. Sabrin, J. Everett, N. Bouaynaya, and R. W. Peters, "Application of satellite remote sensing in monitoring elevated internal temperatures of landfills," Applied Sciences, Vol. 10(19), Article 6801,2020.
[16] N. Karimi, K. T. W. Ng, A. Richter, J. Williams, and H. Ibrahim, "Thermal heterogeneity in the proximity of municipal solid waste landfills on forest and agricultural lands," Journal of Environmental Management, Vol. 287, Article 112320, 2021.
[17] N. Karimi, K. T. W. Ng, and A. Richter, "Prediction of fugitive landfill gas hotspots using a random forest algorithm and Sentinel-2 data," Sustainable Cities & Society, Vol. 73, Article 103097, 2021.
[18] A. Grondona, L. P. Gomes, L. M. Schiavo, M. Caetano, and B. J. B. L. Barbosa, "Use of the downscalling method in satellite images for the analysis of heat islands in landfills," Remote Sensing Applications Society and Environment, Vol. 26, Article 100702, 2022.
[19] D. Chavan, G. S. Manjunatha, D. Singh, L. Periyaswami, S. Kumar, and R. Kumar, "Estimation of spontaneous waste ignition time for prevention and control of landfill fire," Waste Management, Vol. 139, pp. 258–268, 2022.
[20] K. Mahmood, F. Faizi, and F. Mushtaq, "Satellite based bio-thermal impact insights into MSW open dumps: a pair-unified proximity scenario," Geomatics, Natural Hazards & Risk, Vol. 13(1), pp. 667–685, 2022.
[21] Turkish Statistical Institute, "Adrese Dayalı Nüfus Kayıt Sistemi Sonuçları, 2022," 2023. https://data.tuik.gov.tr/Bulten/Index?p=Adrese-Dayali-Nufus-Kayit-Sistemi-Sonuclari-2022-49685 Accessed on Jul 22, 2023.
[22] Istanbul Metropolitan Municipality, "Düzenli Depolama," 2023. http://istac.ssplab.com/tr/temiz-istanbul/evsel-atiklar/duzenli-depolama Accessed on Jul 22, 2023.
[23] Istanbul Metropolitan Municipality, "Faaliyet Haritası," 2023.
[24] Istanbul Governorship, "İklim." http://www.istanbul.gov.tr/iklim-istanbul Accessed Sep 22, 2023.
[25] USGS, "Landsat Satellite Missions," 2023. https://www.usgs.gov/landsat-missions/landsat-satellite-missions Accessed on Jul 19, 2023.
[26] J. Guo, H. Ren, Y. Zheng, S. Lu, and J. Dong, "Evaluation of land surface temperature retrieval from landsat 8/TIRS images before and after stray light correction using the SURFRAD dataset," Remote Sensing, Vol. 12(6), Article 1023, 2020.
[27] USGS, "EarthExplorer," 2023. https://earthexplorer.usgs.gov/ Accessed on Jul 19, 2023.
[28] ESA, "Open Access Hub," 2023. https://scihub.copernicus.eu/ Accessed on Jul 21, 2023.
[29] USGS, "Landsat 8-9 Collection 2 Level 2 Science Product Guide," 2023. https://www.usgs.gov/media/files/landsat-8-9-collection-2-level-2-science-product-guide Accessed on Jul 24, 2023.
[30] ESRI, "How Hot Spot Analysis (Getis-Ord Gi*) works," 2023. https://pro.arcgis.com/en/pro-app/latest/tool-reference/spatial-statistics/h-how-hot-spot-analysis-getis-ord-gi-spatial-stati.htm Accessed on Jul 26, 2023.
[31] ESRI, "What is a z-score? What is a p-value?" https://pro.arcgis.com/en/pro-app/latest/tool-reference/spatial-statistics/what-is-a-z-score-what-is-a-p-value.htm Accessed on Sep 23, 2023.
[32] S. Yalcinkaya, and Y. Ruhbas, "Spatiotemporal analysis framework for identifying emerging hot spots and energy potential from livestock manure in Turkey," Renewable Energy, Vol. 193, pp. 278–287, 2022.
[33] S. Kartal, and A. Sekertekin, "Prediction of MODIS land surface temperature using new hybrid models based on spatial interpolation techniques and deep learning models," Environmental Science and Pollution Research, Vol. 29(44), pp. 67115–67134, 2022.

Environ Res Tec, Vol. 6, Issue. 4, pp. 371–382, December 2023

Environmental Research and Technology
https://ert.yildiz.edu.tr - https://dergipark.org.tr/tr/pub/ert
DOI: https://doi.org/10.35208/ert.1325106

Review Article

Synergies and potential of hybrid solar photovoltaic for enhanced desalination: A review of selected countries

Dwiprayogo WIBOWO[*1,2], Raldi Hendrotoro SEPUTRO KOESTOER[1]

[1]*School of Environmental Science, Universitas Indonesia, Jl. Salemba Raya Kampus UI Salemba, DKI Jakarta, Indonesia*
[2]*Department of Environmental Engineering, Universitas Muhammadiyah Kendari, Faculty of Engineering, Southeast Sulawesi, Indonesia*

ARTICLE INFO

Article history
Received: 22 July 2023
Revised: 23 August 2023
Accepted: 05 September 2023

Key words:
Desalination; Energy; Indonesia; Technology; Photovoltaic

ABSTRACT

In an effort to construct a desalination pilot plant, a study of several kinds of literature is needed to ensure Indonesia develops advanced and environmentally friendly desalination technology. This research aims to explore several research papers referenced in developing the desalination pilot plant to gain information on environmentally friendly and sustainable desalination technologies in selected countries such as Spain (Burriana), Mexico, Chile, the Philippines, and Iran (Kish Island), including in the Middle East and North Africa (MENA) region on the development of desalination technology for environmentally friendly and sustainable-based communities. This research used a systematic literature review (SLR) approach emphasizing secondary information from several studies based on selected countries to develop desalination technology. Each technology developed is examined for suitability with environmental conditions and desalination technology to be further applied in Indonesia. The main reason for building desalination plants in selected countries is to support sustainable development based on green energy and technology. They are combining desalination technology with photovoltaic (PV) electrical energy, which is a critical factor in promoting green technology through electrodialysis (ED) or reverse osmosis (RO) techniques. The developed desalination pilot plant can achieve 7–14 L/(m^2.h) productivity at approximately 0.36–0.78 USD/m^3. If implemented in Indonesia, it is necessary to prepare financial support to construct, operate, and maintain. Desalination technology in Indonesia should prioritize environmentally friendly technology. Indonesia's topographic region is a golden advantage to supporting sustainable green energy by utilizing PV-RO or PV-ED-RO to create fresh water from seawater.

Cite this article as: Wibowo D, Seputro Koestoer RH. Synergies and potential of hybrid solar photovoltaic for enhanced desalination: A review of selected countries. Environ Res Tec 2023;6(4)371–382.

INTRODUCTION

Desalination technology in various countries supports the sustainable development goals (SDGs) to reduce the clean water crisis and ensure proper sanitation for communities [1, 2]. In addition, it also commits to developing clean and renewable energy to ensure that it supports sustainable development [3, 4]. Aende et al. [5] reported that desalination plants worldwide have significantly increased to improve the quality and quantity of treated freshwater and anticipate the threat of climate change. In 2020 more than 22,000 desalination plants worldwide

***Corresponding author.**
*E-mail address: dwiprayogo@umkendari.ac.id

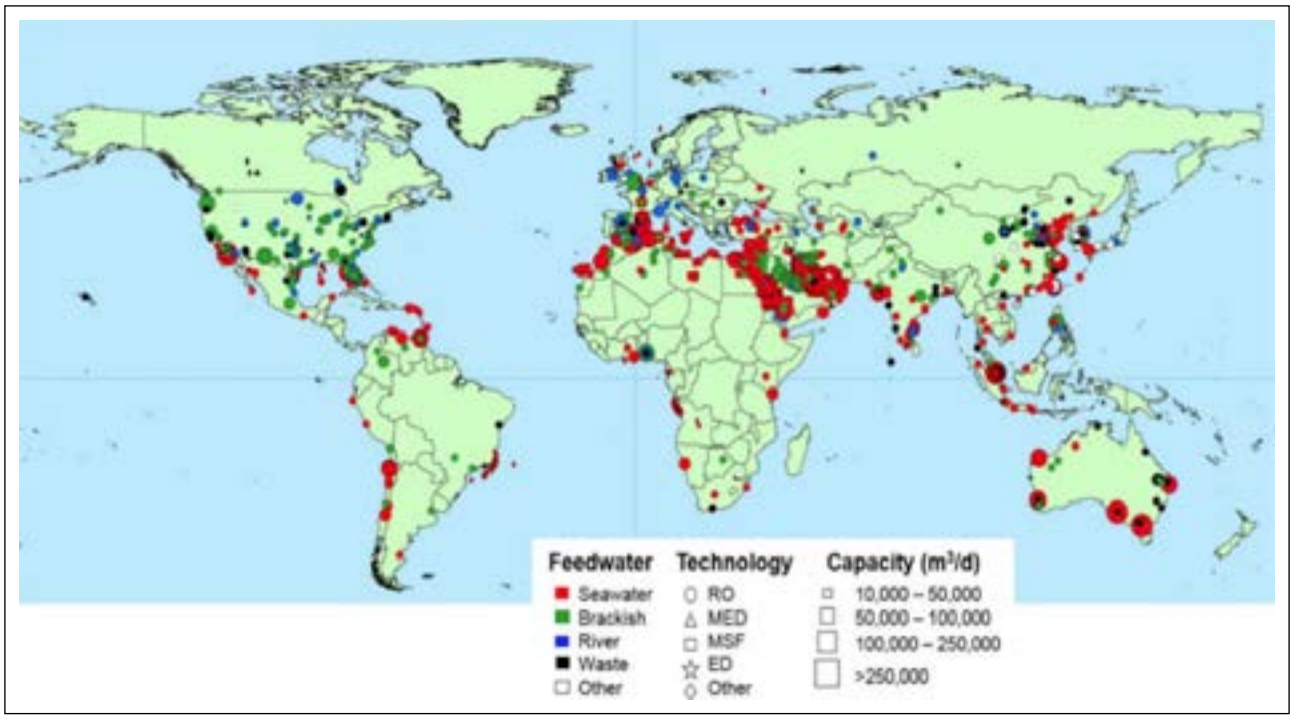

Figure 1. 2020 worldwide desalination plants reviewed by [11, 16].

were constructed and produced around 92 million m^3/day of fresh water, dominated by European and Middle East and North Africa (MENA) countries [6, 7]. These countries have innovated desalination technologies to reduce environmental impacts, such as applying renewable energy, minimizing waste and pollution, using environmentally friendly technologies, and paying attention to environmental sustainability [8, 9].

Environmentally sound desalination technology research from European and MENA countries can provide invaluable lessons for developing countries, particularly in Indonesia. The Indonesian government is also committed to encouraging the construction of desalination plants to build more efficient and environmentally friendly technologies [10, 11]. These will have a significant beneficial impact on taking lessons and some suggestions from desalination technologies developed in selected countries such as Spain (Burriana) [12], Mexico [13], Chile [11], Iran (Kish Island) MENA region [14], and the Philippines [15] to evaluate the feasibility of implementing desalination technologies in Indonesia.

Therefore, this paper aims to provide an overview of the development of desalination technology that has been implemented by researchers in selected countries so that it can be a lesson for Indonesia to start developing environmentally friendly and sustainable energy-based desalination technology. In line with the review of the progress of desalination technology applied, it can provide understanding for the community to support sanitation and technological advances jointly. Of course, this needs to be based on technological advances that will be developed to support environmental sustainability for the people of Indonesia.

MATERIALS AND METHODS

This research uses a systematic literature review (SLR) method by searching for several recent articles on desalination technology studies in various countries such as Spain (Burriana) [12], Mexico [13], Chile [11], Iran (Kish Island) in the MENA region [14], and the Philippines [15] are building desalination pilot plants. The selected countries as an example for review because they are strongly interested in developing desalination capabilities and addressing water scarcity issues. This is based on their geographical location, which experiences high evaporation rates, leading to increased droughts and clean water crises. They are interested in studying electrical efficiency and advancing desalination technology to gather information on environmentally friendly technologies. We explored several research papers referenced in developing the desalination pilot plant to gain information on environmentally friendly and sustainable desalination technologies. Figure 1 shows the distribution of desalination plants worldwide in 2020, reviewed by Cornejo-ponce et al. [11] and Jones et al. [16] are the main reasons why we studied the selected countries to examine the development of the technology.

Specifically, this SLR research observed and collected quantitative data from selected sources, such as articles, original reviews, and trusted websites. This method relied more on qualitative descriptions as we presented a study on the positive and negative impacts of the desalination technology they developed for implementation in Indonesia. An important factor in building desalination pilot plants in other countries is the model the Indonesian government can learn from to build desalination technology based on a sustainable environment.

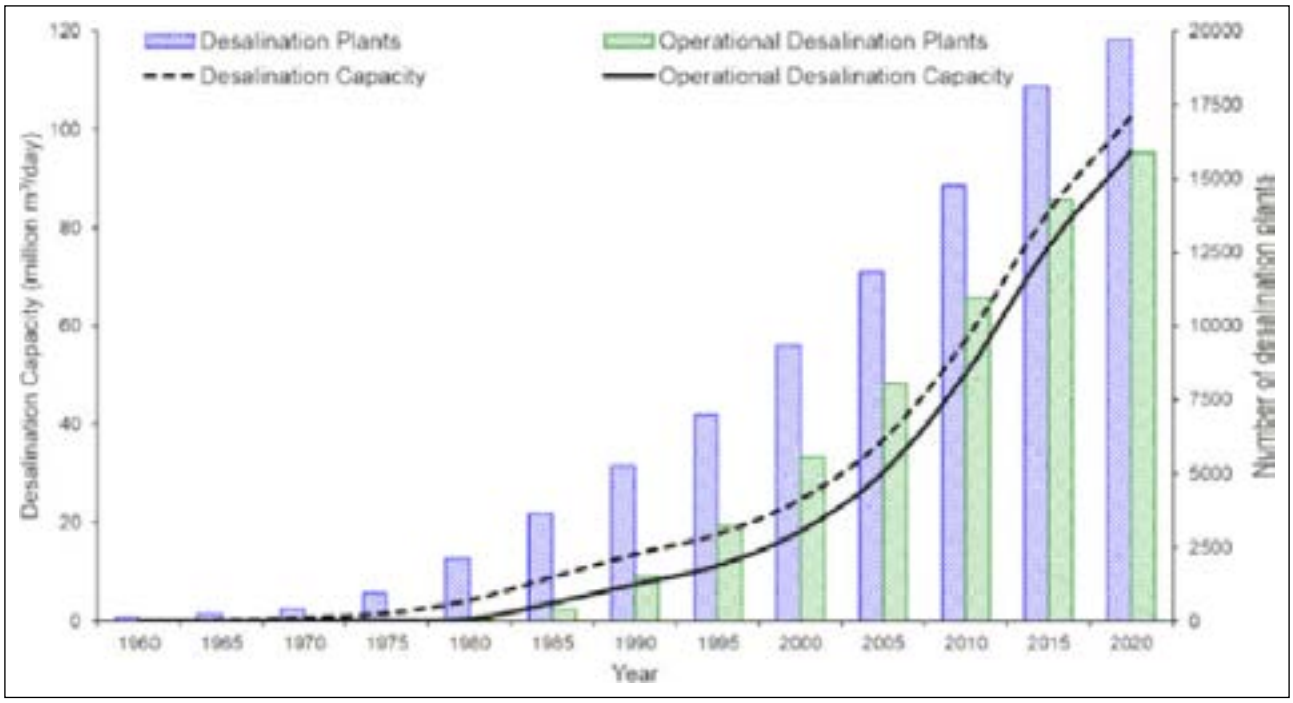

Figure 2. World desalination growth from 1960 to 2020 [5].

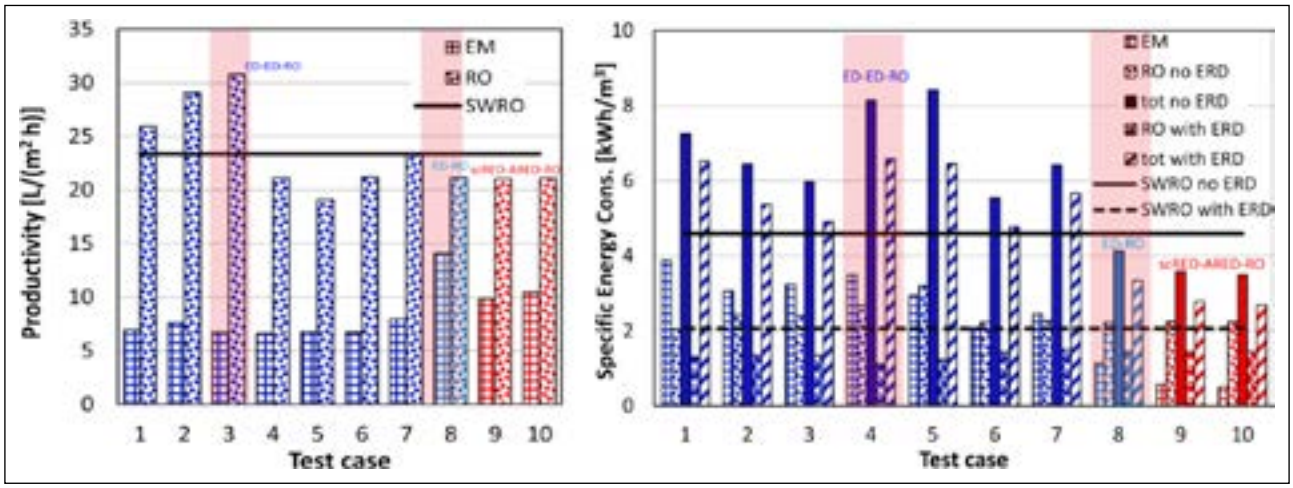

Figure 3. Results of desalination tests in Burriana (Spain) by [12]: (a) ED-ED-RO, (b) ED-RO, (c) scRED-ARED-RO, (a) Productivity comparison, and (b) Energy consumption.

RESULTS AND DISCUSSION

Review of Desalination Technology in Selected Countries

The development of desalination technology worldwide has continued to increase from 1960 to 2020 [5]. Desalination technology development focuses on the operational level, production capacity, and desalination capacity (Fig. 2). Some of the technologies developed depend highly on the type of technology used, the scale of production, and available resources such as energy and seawater used as raw materials [17]. The main objectives in establishing and developing pilot plant desalination technologies are low operational rates, requiring less energy, and having smaller production capacities than other desalination technologies [18]. In our review, the operational level, production capacity, and desalination capacity, the economic desalination technologies reverse osmosis (RO) and electrodialysis (ED) are widely developed because they are considered economical and environmentally friendly.

Technology developed in Spain (Burriana), the study conducted by Gurreri et al. [12] entitled "*Coupling of electromembrane processes with reverse osmosis for seawater desalination: Pilot plant demonstration and testing*" have designed a new innovative technology of seawater desalination pilot plant built inside a container (Fig. 4a) that aims to address the growing problem of freshwater access in the Spanish region. They created the desalination technology by combining ED-RO technology to optimize the process synergistically. In general, the energy consumption of the ED-RO integrated pilot plant is almost comparable to the performance of a seawater reverse osmosis (SWRO) system (Fig. 3a). The developed ED-ED-RO integrated system can produce better quality drinking

Figure 4. Desalination technologies installed and tested in several studies; **(a)** Burriana, Spain [12], and **(b)** Mexico [13].

water of 31 L/m^2.h at a reasonably high energy rate between 3.5–8.4 kWh/m^3. The disadvantage of this system is that ED technology increases electrical energy consumption compared to only the ED-RO system (Fig. 3b). The manuscript suggests that using ED-RO technology is sufficient to solve the water crisis by producing safe and clean drinking water from seawater in a more energy-efficient and affordable way [12]. Desalination water treatment processes are becoming more competitive in terms of consuming less energy and being less harmful to the environment [19]. However, Spain pays more attention to the context of water supply outcomes rather than resource management. Therefore, desalination technology in the Spanish state is constantly being improved to cater to a more excellent water supply.

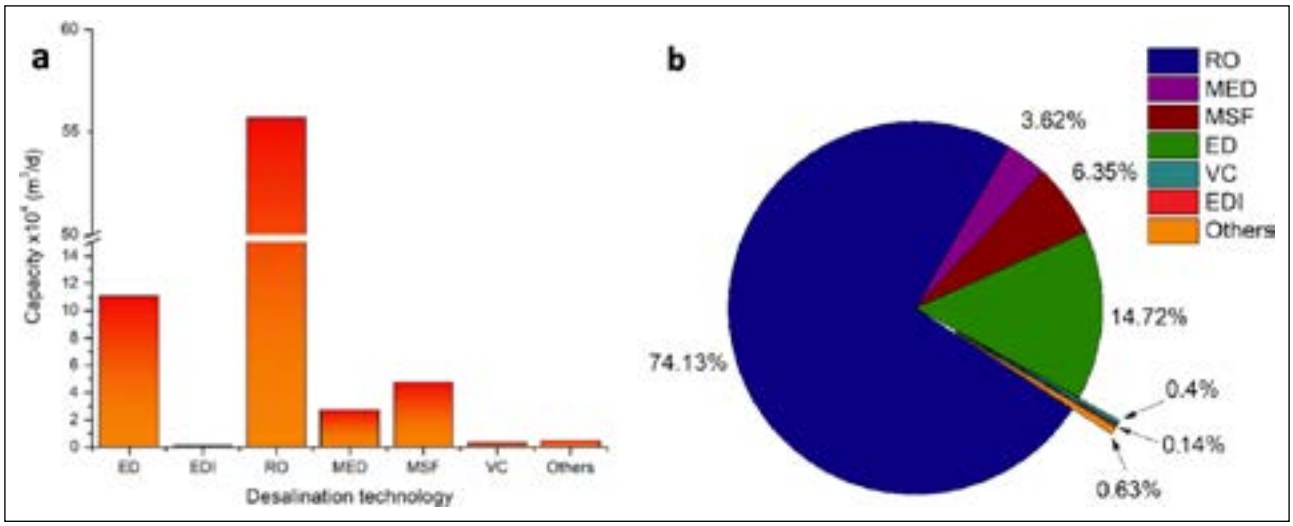

Figure 5. Desalination in Mexico; **(a)** Installed capacity per type in 2022 **(b)** Percentage of installed capacity by technology [23].

In a review study by Gurreri et al. [12], the ED process can reduce RO membrane fouling, extending RO membrane life and minimizing repair costs. However, Gurreri et al. [12] needed to explain the negative impacts of the developed technology and the strategic location for deploying the developed desalination technology. Although the developed technology is highly efficient and easily mobilization is strategically implemented, the community factor determines the sustainability of the developed desalination technology. Techno-economic factors that affect the reciprocal relationship between technology and the economy must also be explained. A limitation of the technology that has yet to be described is the cost of building a sophisticated desalination technology in a container (Fig. 4[a]). In addition, the source of electrical energy is not widely associated with environmentally friendly technologies [20]. Although the developed technology is excellent in that the average ED-RO productivity is 7–14 L/(m^2.h), it requires specialized space and adequate human resources to operate the desalination pilot plant. In addition, the negative impacts of implementing the desalination technology in Burriana are the high operational costs and space requirements for the location of the desalination plant have also not been considered if it is implemented in coastal areas and its very high maintenance.

In contrast, the desalination technology developed by Cervantes-rend et al. [13], entitled "*Rural Application of a Low-Pressure Reverse Osmosis Desalination System Powered by Solar-Photovoltaic Energy for Mexican Arid Zones*" has built a sustainable desalination energy by combining solar panels and reverse osmosis (PV-RO) that is low-cost and easy to operate (Fig. 4b). The desalination investment costs incurred by the researchers are proportional to the results obtained during one year of productivity. Cervantes-rend et al. [13] also recommended that low-pressure RO desalination systems produce lower energy consumption and higher water recovery rates. These systems can be developed by utilizing PV energy, a clean and renewable energy source abundant in arid zones. PV in desalination systems can be used independently to distribute electrical power and reduce dependence on fossil fuels [21, 22]. The potential desalination model developed by Cervantes-rend et al. [13] involves several steps including PV modules that are firmly installed to withstand the strong winds in the area that can reach 79 km/hour. Then, the PV-RO system is connected to hydraulic and electrical parts to drive the RO technology. The engineered desalination model developed by Cervantes-rend et al. [13] is very feasible to develop at low cost and suitable for coastal islands.

In Mexico, the application of RO technology has achieved an optimal capacity of clean water of 52×104 m^3/s (Fig. 5a) [13]. The Mexican government strongly supports innovations made by Cervantes-rend et al. [13] to continue innovating to reduce atmospheric gas emissions by utilizing PV as a driver for desalination technology. This is one of the main reasons why Mexico continues strengthening ways to get clean water using desalination technology. Some of the technologies used in desalination plants in Mexico (Fig. 5b) include reverse osmosis (RO), multiple effect distillation (MED), multi-stage flash (MSF), electrodialysis (ED), vapor compression (VC), electro-deionization (EDI), and others.

Cornejo-ponce et al. [11] also stated the same condition in their publication "*Small-Scale Solar-Powered Desalination Plants: A Sustainable Alternative Water-Energy Nexus to Obtain Water for Chile's Coastal Areas*" which examines small-scale desalination technology in coastal areas of Chile. Cornejo-ponce et al. [11] suggested increasing sustainable alternative energy to obtain clean water. The technology developed in Chile is more about applying RO technology to obtain fresh water. They also added PV as a source of electrical energy to power the electric pump (Fig. 10). Utilizing solar energy to reduce the impact of fossil energy dependence and the role of the community is also needed to support the sustainability of PV-RO to supply fresh water from seawater [21, 22]. In this context, saltwater becomes one of the essential non-conventional water resources to be developed in Chile. Research conducted by Cornejo-ponce

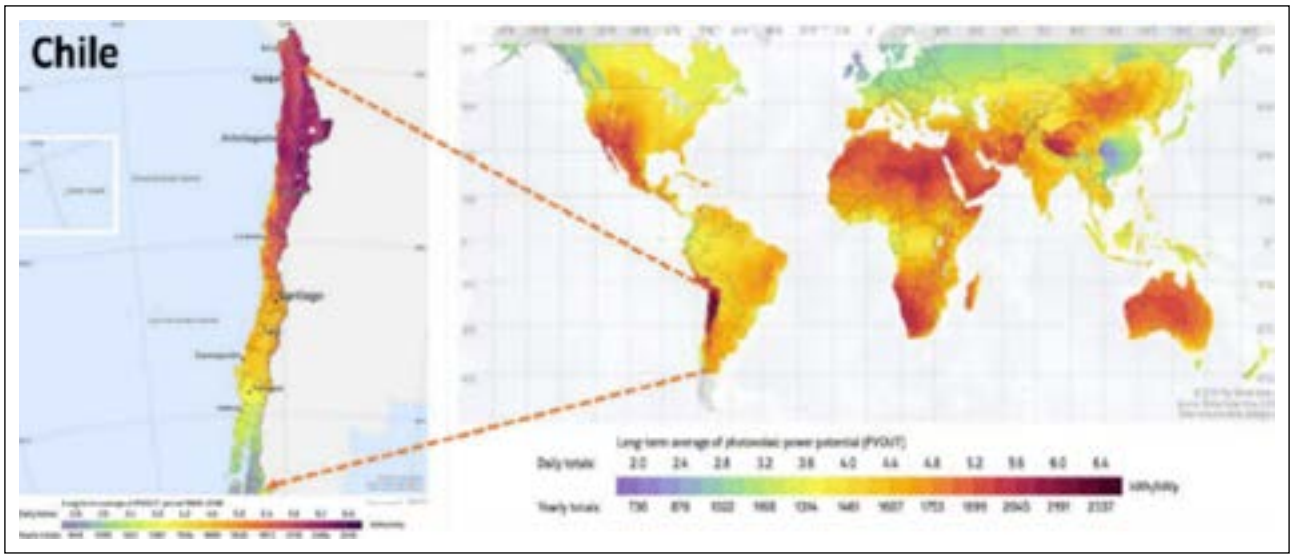

Figure 6. Map of solar photovoltaic resources in the world and Chile [11].

et al. [11] has simulated photovoltaic/desalination energy to harness solar power to build small-scale desalination plants in the coastal areas of Chile (Fig. 6).

The application of PV in Chile provides an average energy increase of 6.4 kWh/kWp per day to supply electrical energy to the desalination plant using solar energy (Fig. 6). This paper has yet to describe the model and long-term negative impacts of using PV for desalination applications on coastal communities. Given that small-scale desalination plants require maintenance and impact on the environment. The arid and hot northern region of Chile needs to review the feasibility study of the durability of the PV used.

Research conducted by Riyahi et al. [14] entitled "*Energy analysis and optimization of a hybrid system of reverse osmosis desalination system and solar power plant (case study: Kish Island)*" identified the integration of solar power plants with RO desalination systems to supply fresh water on Kish Island, Iran. Riyahi et al. [14] identified the energy and production and optimized the performance of a hybrid system compared to a conventional method using diesel-powered electrical energy. The study results explained that the optimal configuration of the developed system includes a solar power plant with a capacity of 2MW and an RO desalination system with a total of 10,000 m^3/day that can meet the water demand with an annual average solar fraction of 72% with a PV-RO construction cost of about $11.6 million, and when compared with the conventional system of diesel-powered electrical energy of $18.4 million. Based on the economic analysis, the hybrid system provides significant cost savings compared to a traditional diesel-powered system. The payback period for the hybrid system is about five years, while the payback period for the conventional method is about nine years. Overall, this study concludes that a combined PV-RO system is a viable and sustainable solution for supplying freshwater to Kish Island, with the potential to be applied in other coastal areas with similar conditions.

Suggestions include energy analysis and optimization by estimating energy requirements for desalination and planning a solar power plant that can provide electrical energy based on solar irradiation data [25]. Kish Island receives about 1900 kWh/m^2 of electrical energy per year from PV panels and it can support electrical power to RO technology (Fig. 7). Then build an RO desalination system with energy efficiency and optimize the PV-RO coupled system to maximize system efficiency and minimize costs. The strategic condition of Kish Island is the reason for the opportunity to develop desalination technology [26]. In addition, Kish Island is located in the Persian Gulf, where temperatures can reach 45°C during summer and water salinity is high. Therefore, the Iranian government supports high capability and determination to become a solid industrialized country; desalination technology has gradually become an important instrument to promote the country's development [27].Developing PV-RO technology is a practical study that integrates renewable energy to be sustainable. PV-RO can be considered as an economical technology where the desalination cost ranges from 0.883–2.14 $.$m^3$. In addition, this technology is also considered competitive for green energy as it does not rely on fossil fuel energy for its electrical energy supply [28].A study in a developing country such as the Philippines by Peter et al. [15] entitled "*A review of desalination technologies and its impact in the Philippines*" explained that the Philippines also started innovating desalination technology development. The beginning of the development of MED system desalination technology from 2012 to 2016 with a target of distributing clean water to 6 million people using simple flotation, filter, aeration, and ultrafiltration technologies. From 2017 until now, the Philippines developed RO and disinfection technology to optimize the need for clean water free of bacteria and harmful chemicals [15]. The study described by Peter et al. [15] the importance of assessing the potential impacts of desalination by discharging brine and other chemicals into the ocean and energy consumption. They explained that the

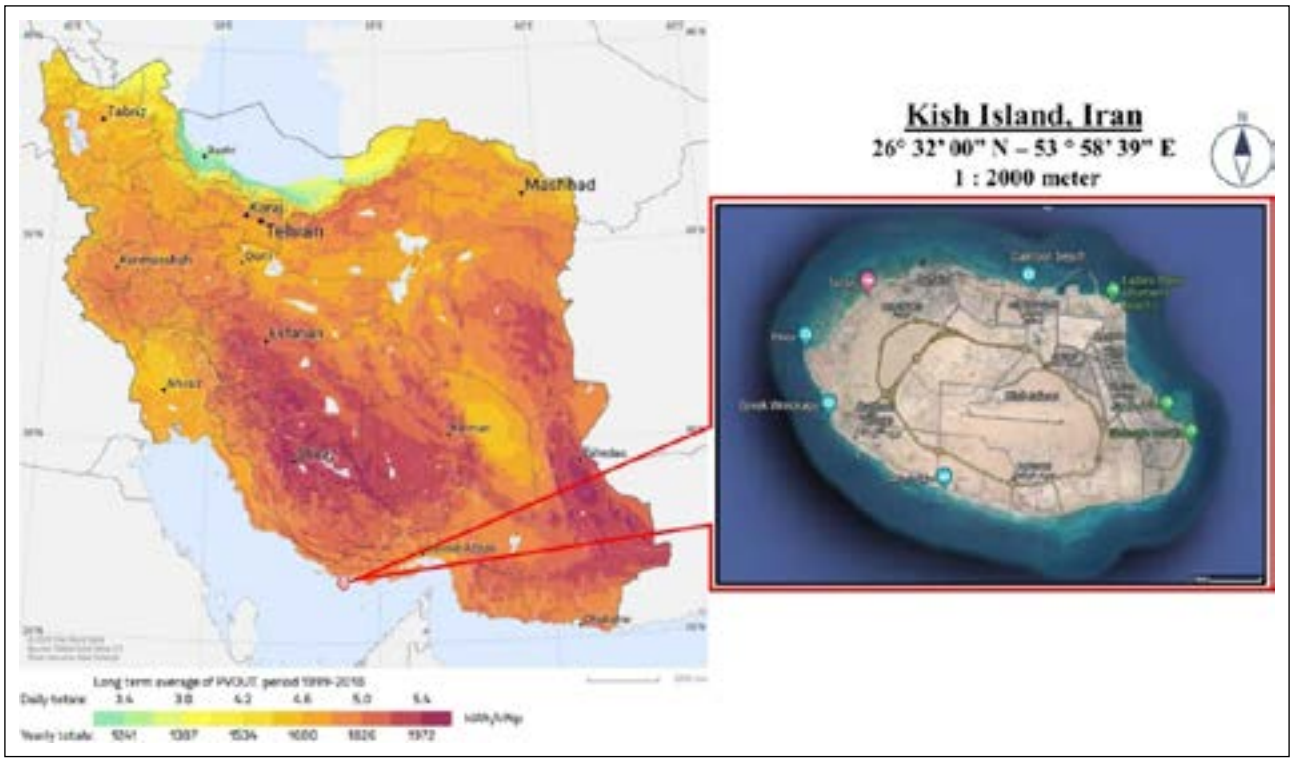

Figure 7. Location and intensity conditions of photovoltaic power potential of Kish Island (Iran) (Modified from [24]).

feasibility study of clean water after the desalination process should be identified physical, chemical, and biological parameters to be safe for use by local communities.

The paper emphasizes the need to carefully plan and manage desalination projects to minimize environmental impacts [15]. In 2021, the finalized desalination technology was developed in the Philippines and produced 1000 L/day using seawater. The suggested technologies utilized include thermal distillation and membrane processes. Thermal distillation involves boiling seawater and collecting the condensed vapor, while membrane processes use semipermeable membranes to filter out salts and other minerals [22, 29]. Even though desalination technology in the Philippines has yet to fulfill the need for clean water fully, it is a promising solution for communities experiencing water shortages and poor water quality. It is essential to carefully consider desalination's environmental, economic, and social implications to maximize its benefits and minimize its potential negative impacts.

Economic Feasibility and Mitigation Practices

Economic feasibility based on solar-powered desalination systems can be improved through several strategies. The PV modules combined desalination technology-based RO process performed well compared to other techniques. To improve the economic feasibility, firstly, reducing the cost of PV modules to provide an attractive option for renewable energy use in water treatment under simple desalination technology. When solar photovoltaic systems power RO desalination facilities, they can reduce the specific energy consumption from fossil energy by about 10%, reducing the total water cost [30]. Secondly, prospering site analysis, including the water storage or salinity issue, available resources (electricity, membranes, gas reservoirs, solar energy), and the requirement of desalination plants (small or large), should be performed in the area that needs fresh water [31, 32]. This will allow the introduction of area-specific efficient, and cost-effective desalination methods. Several of the largest desalination plants in the MENA region studied by Maftouh et al. [33] explore that the RO process has exhibited exemplary performance with low-cost efficiency for seawater as feedwater, with a daily production capacity of 540,000 m^3 and costs of \$0.585/m^3. In addition, studies conducted by Cai et al. [17] explain that the RO cost is relatively low due to small investment in RO equipment and low energy consumption (4–6 kWh/m^3). The cost of freshwater production for RO is about US \$0.45–1.72/m^3 [34]. This is lower than other methods, such as Multi-Stage Flash (MSF) and Low-Temperature Multi-Effect Distillation (LT-MED), mainly due to the small investment in RO equipment and relatively low energy consumption (e.g., 4–6 kW h/m^3). The large amount of electricity consumption in the desalination system is the main reason for the high cost. Therefore, to control the production costs of RO desalination, there is a need to reduce the cost of materials, increase the rate of water harvesting and freshwater production, and replace obsolete RO equipment promptly.

The other challenge is minimizing desalination's negative impacts and the prospect of sustainable and eco-friendly desalination. Current desalination approaches have moderate and non-negative environmental impacts. However, with proper mitigation and utilization of modern technol-

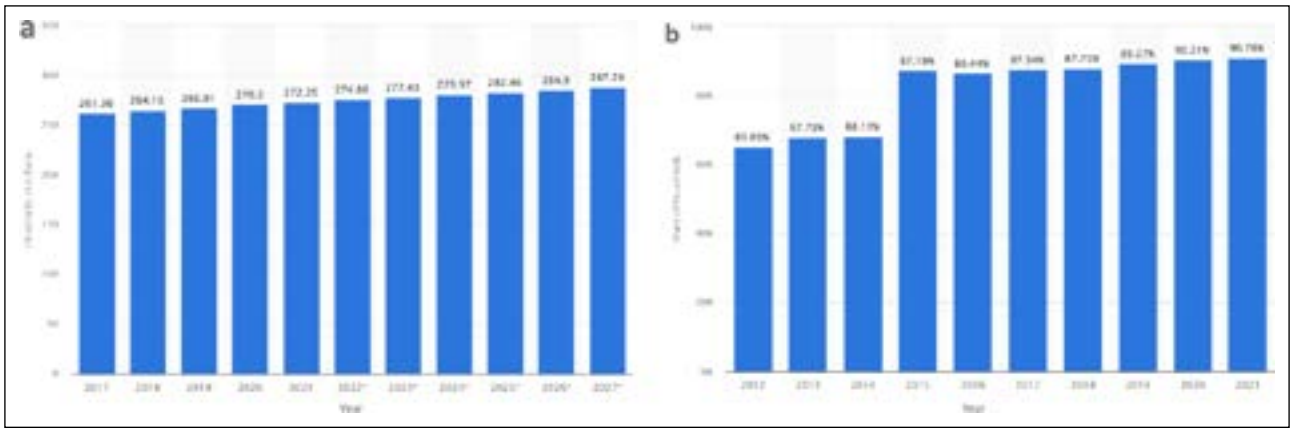

Figure 8. **(a)** Predicted population of Indonesia from 2017 to 2027, and **(b)** Drinking water consumption in Indonesia from 2012 to 2021 [37].

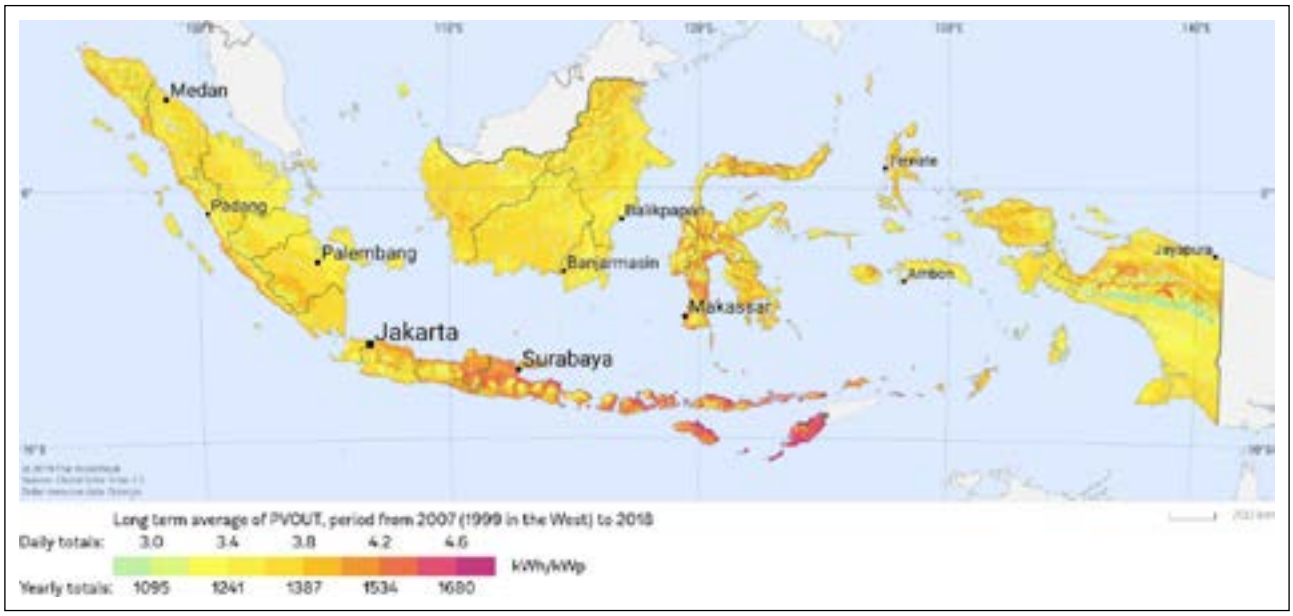

Figure 9. Potential for solar-powered in Indonesia [42].

ogies, these impacts can be reduced by using various beneficial techniques while reducing adverse impacts [35]. Recent advancements in desalination technology have also offered many alternative approaches that provide avenues to adapt to more environmentally friendly desalination. Based on the study results, Ihsanullah et al. [35] explained that the primary concern of SWRO is several environmental challenges that need to be considered, such as its potential impact on marine ecosystems and the disposal of saltwater waste. In addition, the effect of solid waste, such as corrosion and cleaning process chemicals, can also affect environmental pollution. Several mitigation measures and best practices can be implemented to address the ecological impacts of SWRO desalination, such as proper site selection, brine management, environmental monitoring, research, and innovation. High salinity brine discharge can be utilized for salt crystal production to open opportunities in national salt production into a sustainable circular economy study.

Lessons for Indonesia

Currently, desalination technology in Indonesia is similar to the Philippines. Indonesia focuses on providing fresh water for visiting tourists, where the background of desalination development is the same as Kish Island, which prioritizes tourists. Several desalination pilot plants in Indonesia have been built in Ancol (North Jakarta) and Labuan Bajo Island as tourist destinations for tourists visiting Indonesia [36]. Some of the roles of the Indonesian government in providing financial support and incentives for sustainable desalination projects contribute best to the availability of clean water in some remote islands. But this time, the Indonesian government has not 100% allocated financial support to build desalination projects due to the high cost, intensive maintenance, and unprepared human resources. The government only provides regulatory and administrative support to accelerate equitable development and welfare in some small islands. In Indonesia, many desalination projects are developed by private companies to support industrial develop-

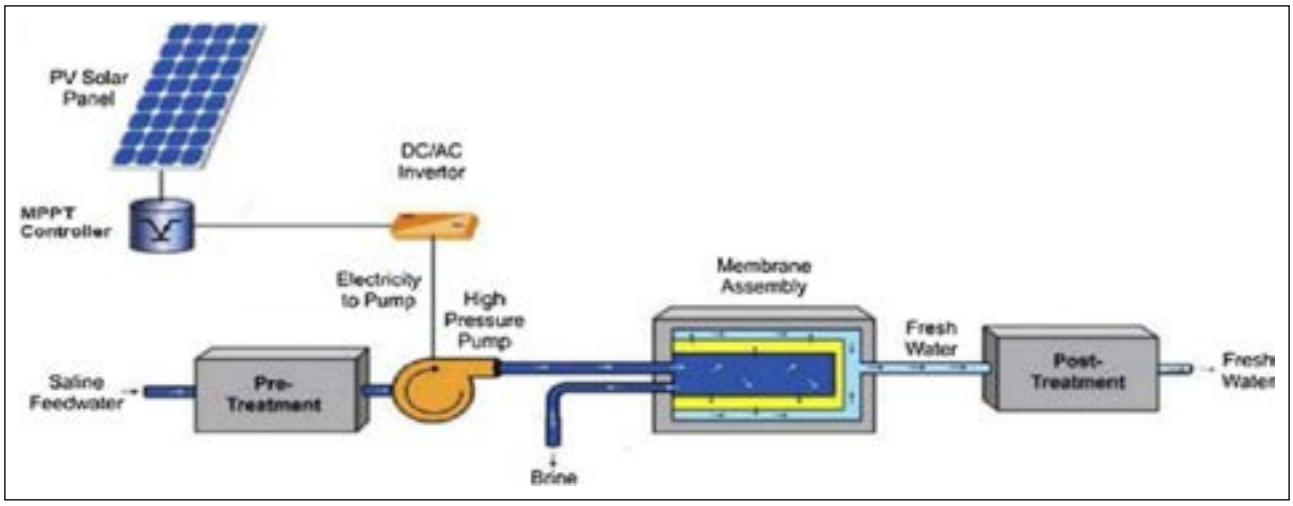

Figure 10. Schematic of reverse osmosis-direct photovoltaic connection system [14].

ment such as mining, logistics, and tourism. The last option is to provide clean water services to the community around the company as a form of corporate social responsibility.

Although Indonesia has abundant natural resources, the community still needs to meet fully the clean water condition. The Central Bureau of Statistics reports that the achievement of clean water access in Indonesia has only reached 72.55%, below the SDG's target of 100% [38]. The demand for clean water increases every year and is proportional to the increase in population (Fig. 8a). Currently, the estimated population of Indonesia is 277.43 million people, with a demand for clean water in 2020 of 90.21% and 2021 of 90.78%, resulting in an annual increase of 0.57% (Fig. 8b). In fact, Indonesia and the Philippines still rely on surface water and groundwater, resulting in land subsidence. Semarang and Jakarta are categorized as coastal cities experiencing land subsidence, one of which is caused by groundwater exploitation [39].Based on reviews from several researchers from other countries to reduce the use of fossil-fueled electrical energy to power desalination instrumentation, Indonesia should be able to utilize PV for renewable energy. Although, regulations in Indonesia have been stated in Government Regulation No. 79 of 2014 on National Energy Policy and Law No. 17 of 2007 on National Long-Term Plan 2005–2025 to support national energy growth. Indonesia has committed to supporting renewable energy at more than 23% of total energy consumption and reducing fossil fuels to less than 25% [40].

While desalination technology can solve water scarcity in Indonesia, its implementation should be sensitive to the social and cultural contexts of local communities and indigenous populations. Government Regulation under the Ministry of Marine and Fisheries of the Republic of Indonesia No. 1/PERMEN-KP/2020 also has committed to supporting the freshwater facilities in small islands that do not have clean water reserves to fulfill their daily needs. Desalination is a potential technology for helpful water scary by transforming seawater or brackish water into fresh water [31]. The potential impacts on local communities and indigenous populations might require land acquisition, changing the cultural habits, livelihoods, and ecology [41]. Moreover, to successfully implement decentralized desalination systems in rural and remote areas, a holistic approach is required including technical feasibility assessments, community engagement, capacity building, financial support, and considerations for long-term sustainability. Collaborative efforts involving local governments, non-governmental organizations (NGOs), technical experts, and communities are essential to navigate these challenges and unlock the potential benefits of decentralized desalination systems.

PV-RO technology developed in areas that have a high amount of light energy such as Indonesia has the potential to support sustainable desalination technology. Based on the intensity of sunlight to improve PV performance (Fig. 9), the total average daily photovoltaic power in Indonesia reaches 3.8 kWh/kWp. This condition can clearly drive desalination instrumentation with a daily requirement of 3.5–8.4 kWh, as researched by Gurreri et al. [12]. Schematic model of PV-RO installation as reviewed by Riyahi et al. [14] (Fig. 10), PV contributes electrical energy to drive the high-pressure pump in the RO system. The utilization of PV supports sustainable energy and technologies that do not expect fossil energy as a source of electrical energy.

Regarding desalination in Indonesia, Dewita et al. [40] also made a nuclear desalination concept that is very effective for driving desalination technology. Nuclear plays a role in increasing the temperature of seawater to start the evaporation process and stored in freshwater tanks. Unfortunately, nuclear-based energy is still debated by some people regarding the safety factor of nuclear reactors. Indonesia is a region that often experiences earthquakes, which can easily cause accidents and damage nuclear reactors. In addition, they also suggested that renewable energy for RO desalination technology could use wind energy or PV as a power source to drive the RO pump. The role of Indonesian government should take steps in preparing policies and budgets to start implementing desalination technology to provide improved sanitation and quality of life, especial-

Table 1. Summary of desalination technology recommendations from selected countries as lessons for Indonesia

No.	Selected country recommendations	Lessons for Indonesia
1	Need to increase environmental conservation efforts; desalination technology should prioritize ecological sustainability to reduce emissions.	Indonesia should slowly start developing desalination technology to achieve 23% of total energy consumption and reduce fossil fuels to less than 25% by 2025–2030.
2	Fossil-dependent electrical energy supply is slowly being replaced with PV to utilize solar energy as an environmentally friendly sustainable energy source.	In 2025–2030 Indonesia seeks to utilize energy from PV to power desalination instrumentation with a daily requirement of 3.5–8.4 kWh according to the intensity of PV sunlight.
3	The topographic region is critical in implementing sustainable energy as a renewable electrical power source. Sufficient sunlight irradiation can improve the high-performance of PV instruments.	Indonesia has a strategic topographic area between the equator with a 40–52% solar irradiation intensity, making it very suitable for PV electrical energy to be applied for desalination development.
4	The choice of desalination technology also affects the resulting freshwater product. In general, some countries apply ED, RO, and distillation technologies.	Desalination technology should be built in Indonesia, considering that 70% of Indonesia is an ocean. The selection of technology that can be applied in Indonesia using ED-RO technology is deemed to have low costs and easy operations.
5	They recommend that the government prioritize socio-economic issues in building desalination technology pilot plants. These include the community and the low cost of building a desalination plant.	The Indonesian government should be able to build a low-cost desalination plant that is applied to the community to improve clean water services by the Directorate General of Marine Spatial Management Regulation on Technical Guidelines for Distributing Government Assistance in the form of Seawater Desalination Facilities in 2017.
6	The development of large-scale desalination technology had a good impact on society to improve the quality of life.	The development of large or small-scale desalination technologies should consider the beneficial impacts to support sanitation and clean water sources for the community.

ly for people who need fresh water. Based on a review of desalination technologies developed in selected countries, the lessons learned for Indonesia if it wants to start and establish desalination technology are summarised in Table 1.

CONCLUSIONS

This paper presents a review of the current situation regarding the challenges of desalination technology development that has been developed by selected countries in the hope that it can serve as a basis for action for Indonesia to develop an environmentally sound and sustainable pilot desalination plant. Based on the reviewed articles, several countries have different backgrounds in developing desalination technology.

The main reasons for developing desalination technology are climate change conditions, population growth, depletion of surface and groundwater sources, and pollution of water resources due to mining and wastewater activities. The main challenges that must be considered to develop desalination technology are the cost of desalination technology construction, location of technology application, maintenance of desalination equipment, and sustainability of desalination technology.

The decisive factor in improving environmentally sound and sustainable desalination technology must consider PV-based electrical energy supply and allow it to be very suitable to be applied in Indonesia because PV can optimally absorb the intensity of solar energy with a power of ~3.8 kWh/kWp. The existence of an electrical energy source from PV makes it possible to build an efficient desalination technology based on ED and RO that is easy to implement in Indonesia.

Acknowledgements

The authors would like to thank the School of Environmental Science, Universitas Indonesia for providing facilities and literature.

DATA AVAILABILITY STATEMENT

The authors confirm that the data that supports the findings of this study are available within the article. Raw data that support the finding of this study are available from the corresponding author, upon reasonable request.

CONFLICT OF INTEREST

The authors declared no potential conflicts of interest with respect to the research, authorship, and/or publication of this article.

ETHICS

There are no ethical issues with the publication of this manuscript.

REFERENCES

[1] T. Salameh, P. P. Kumar, A. G. Olabi, K. Obaideen, E. T. Sayed, H. M. Maghrabie, and M. A. Abdelkareem, "Best battery storage technologies of solar photovoltaic systems for desalination plant using the results of multi optimization algorithms and sustainable development goals," Journal of Energy Storage, Vol. 55, Article 105312, 2022. [CrossRef]

[2] H. Saboori, and H. Mehrjerdi, "Tri-objective optimization of a synergistic wind-photovoltaic plant for water desalination addressing sustainable development goals," Sustainable Development, Vol. 30(6),

pp. 1811–1822, 2022. [CrossRef]
[3] S. Gelb, and A. Krishnan, "Technology, migration and the 2030 Agenda for Sustainable Development," London, UK: Overseas Development Institute, 2018.
[4] W. Leal Filho, S. K. Tripathi, J. Andrade Guerra, R. Giné-Garriga, V. Orlovic Lovren, and J. Willats, "Using the sustainable development goals towards a better understanding of sustainability challenges," International Journal of Sustainable Development & World Ecology, Vol. 26(2), pp. 179–190, 2019. [CrossRef]
[5] A. Aende, J. Gardy, and A. Hassanpour, "Seawater desalination: A review of forward osmosis technique, its challenges, and future prospects," Processes, Vol. 8(8), Article 901, 2020. [CrossRef]
[6] A. N. Angelakis, M. Valipour, K.-H. Choo, A. T. Ahmed, A. Baba, R. Kumar, G. S. Toor, and Z. Wang, "Desalination: From ancient to present and future," Water, Vol. 13(16), Article 2222, 2021. [CrossRef]
[7] E. T. Sayed, A. G. Olabi, K. Elsaid, M. Al Radi, R. Alqadi, and M. A. Abdelkareem, "Recent progress in renewable energy based-desalination in the Middle East and North Africa MENA region," Journal of Advanced Research, Vol. 45, pp. 125–156, 2022. [CrossRef]
[8] L. Ospina-Forero, G. Castañeda, and O. A. Guerrero, "Estimating networks of sustainable development goals," Information & Management, Vol. 59(5), Article 103342, 2022. [CrossRef]
[9] M. Ayaz, M. A. Namazi, M. Ammad, M. I. M. Ershath, A. Mansour, and M. Aggoune, "Sustainable seawater desalination: Current status, environmental implications and future expectations," Desalination, Vol. 540, Article 116022, 2022. [CrossRef]
[10] M. Elma, M. Mahmud, F. Ria Mustalifah, A. Akhbar, L. Suryani, A. E. Pratiwi, D. Rahmah, and N. Baity, "Evaluasi kinerja membran silika pektin untuk desalinasi air payau terhadap suhu kalsinasi membran," Vol. 7(1), pp. 56–65, 2021. [CrossRef]
[11] L. Cornejo-ponce, P. Vilca-Salinas, M. J. Arenas-Herrera, C. Moraga-Contreras, H. Tapia-Caroca, and S. Kukulis-Martínez "Small-scale solar-powered desalination plants: A sustainable alternative water-energy nexus to obtain water for chile's coastal areas," Energies, Vol. 15(23), Article 9245, 2022. [CrossRef]
[12] L. Gurreri, M. La Cerva, J. Moreno, B. Goossens, A. Trunz, and A. Tamburini, "Coupling of electromembrane processes with reverse osmosis for seawater desalination: Pilot plant demonstration and testing," Desalination, Vol. 526, Article 115541, 2022. [CrossRef]
[13] E. Cervantes Rendon, J. I. Bahena, L. E. Cervera-Gómez, R. J. Romero, J. Cerezo, A. Rodríguez-Martínez, and U. D. Carrasco," Rural application of a low-pressure reverse osmosis desalination system powered by solar – photovoltaic energy for Mexican Arid Zones," Sustainability, Vol. 14(17), Article 10958, 2022. [CrossRef]
[14] N. Riyahi, A. Saraei, A. Vahdat Azad, and F. Fazelpour, "Energy analysis and optimization of a hybrid system of reverse osmosis desalination system and solar power plant (case study: Kish Island)," International Journal of Energy and Environmental Engineering, Vol. 13(1), pp. 67–75, 2022. [CrossRef]
[15] N. Peter, P. M. L. Ucab, G. C. Dadol, L. M. Jabile, I. N. Talili, and M. T. I. Cabaraban, "A review of desalination technologies and its impact in the Philippines," Desalination, Vol. 534, Article 115805, 2022. [CrossRef]
[16] E. Jones, M. Qadir, M. T. H. van Vliet, V. Smakhtin, and S. Kang, "The state of desalination and brine production: A global outlook," Science of the Total Environment, Vol. 657, pp. 1343–1356, 2019. [CrossRef]
[17] Y. Cai, J. Wu, S. Q. Shi, J. Li, and K.-H. Kim, "Advances in desalination technology and its environmental and economic assessment," Journal of Cleaner Production, Vol. 397, Article 136498, 2023. [CrossRef]
[18] M. A. Rosen, and A. Farsi, "Sustainable energy technologies for seawater desalination," Academic Press, 2022. [CrossRef]
[19] Á. Morote, A. Rico, and E. Moltó, "Critical review of desalination in Spain: A resource for the future?" Geographical Research, 55(4), pp. 1–12, 2017. [CrossRef]
[20] A. Shokri, and M. S. Fard, "A sustainable approach in water desalination with the integration of renewable energy sources," Environmental Advances, Vol. 9, Article 100281, 2022. [CrossRef]
[21] J. Bundschuh, M. Kaczmarczyk, N. Ghaffour, and B. Tomaszewska, "State-of-the-art of renewable energy sources used in water desalination: Present and future prospects," Desalination, Vol. 508, Article 115035, 2021. [CrossRef]
[22] B. Anand, R. Shankar, S. Murugavelh, W. Rivera, K. Midhun Prasad, and R. Nagarajan, "A review on solar photovoltaic thermal integrated desalination technologies," Renewable and Sustainable Energy Reviews, Vol. 141, Article 110787, 2021. [CrossRef]
[23] G. E. Dévora-Isiordia, C. A. Cásares-de la Torre, J. A. Corona-Sánchez, and S. Islas, "State of the Art of Desalination in Mexico," Energies, Vol. 15(8434), pp. 1–23, 2022. [CrossRef]
[24] World Bank Group, "Solar resource maps of Iran," SolarGis, 2022. https://solargis.com/maps-and-gis-data/download/iran
[25] M. M. Rashidi, I. Mahariq, N. Murshid, S. Wongwises, O. Mahian, and M. A. Nazari, "Applying wind energy as a clean source for reverse osmosis desalination: A comprehensive review," Alexandria Engineering Journal, Vol. 61(12), pp. 12977–12989, 2022. [CrossRef]
[26] A. H. Shafaghat, M. Eslami, and M. Baneshi, "Techno-enviro-economic study of a reverse osmosis desalination system equipped with photovoltaic-thermal collectors," Applied Thermal Engineering, Vol. 218, Article 119289, 2023. [CrossRef]

[27] E. Mohi, G. H. J. Ghajar, and N. Kaynia, "State of desalination projects in Iran," Desalination, Vol. 23(1–3), pp. 465–470, 1977. [CrossRef]

[28] A. M. Ghaithan, A. Mohammed, and L. Hadidi, "Assessment of integrating solar energy with reverse osmosis desalination," Sustainable Energy Technologies and Assessments, Vol. 53, Article 102740, 2022. [CrossRef]

[29] F. A. Essa, "Thermal desalination systems: from traditionality to modernity and development," in Distillation Processes-From Conventional to Reactive Distillation Modeling, Simulation and Optimization. IntechOpen, 2022. [CrossRef]

[30] A. Kaya, M. E. Tok, and M. Koc, "A levelized cost analysis for solar-energy-powered sea water desalination in the Emirate of Abu Dhabi," Sustainability, Vol. 11(6), Article 1691, 2019. [CrossRef]

[31] D. Wibowo, F. Mustapa, S. Selviantori, M. Idris, A. Mahmud, M. Maulidiyah, M. Z. Muzakkar, A. A. Umar, and M. Nurdin "CA/PEG/Chitosan membrane incorporated with TiO2 nanoparticles for strengthening and permselectivity membrane for reverse osmosis desalination," Environmental Nanotechnology, Monitoring & Management, Vol. 20, Article 100848, 2023. [CrossRef]

[32] M. T. Ali, H. E. S. Fath, and P. R. Armstrong, "A comprehensive techno-economical review of indirect solar desalination," Renewable and Sustainable Energy Reviews, Vol. 15(8), pp. 4187–4199, 2011. [CrossRef]

[33] A. Maftouh, O. El Fatni, S. Bouzekri, F. Rajabi, M. Sillanpää, and M. H. Butt "Economic feasibility of solar-powered reverse osmosis water desalination: a comparative systemic review," Environmental Science and Pollution Research, Vol. 30(2), pp. 2341–2354, 2023. [CrossRef]

[34] A. Al-Karaghouli, and L. L. Kazmerski, "Energy consumption and water production cost of conventional and renewable-energy-powered desalination processes," Renewable and Sustainable Energy Reviews, Vol. 24, pp. 343–356, 2013. [CrossRef]

[35] I. Ihsanullah, M. A. Atieh, M. Sajid, and M. K. Nazal, "Desalination and environment: A critical analysis of impacts, mitigation strategies, and greener desalination technologies," Science of the Total Environment, vol. 780, p. 146585, 2021. [CrossRef]

[36] M. V. Nirwanda, "Analisis risiko sistem instalasi pengolahan air SWRO PT. Pembangunan Jaya Ancol Menggunakan Metode Failure Mode and Effects Analysis (FMEA)," Institut Teknologi Sepuluh Nopember Surabaya, 2022.

[37] Statista, "Indonesia: Total population from 217 to 2027," Statista, 2023. https://www.statista.com/statistics/294100/total-population-of-indonesia/

[38] R. D. Kurniawati, M. H. Kraar, V. N. Amalia, and M. T. Kusaeri, "Peningkatan akses air bersih melalui sosialisasi dan penyaringan air sederhana desa Haurpugur," Jurnal Pengabdian dan Peningkatan Mutu Masyarakat, Vol. 1(2), pp. 136–143, 2020. [CrossRef]

[39] J. Illigner, M. Haghshenas, K. Gisevius, and B. Braun, "Land subsidence in Jakarta and Semarang Bay – The relationship between physical processes, risk perception, and household adaptation," Ocean and Coastal Management, Vol. 211, Article 105775, 2021. [CrossRef]

[40] E. Dewita, T. Ariyanto, H. Susiati, and M. Pancoko, "Conceptual design of ındonesia experimental power reactor coupled with desalination unit," Journal of Physics: Conference Series, Vol. 1198(2), Article 022056, 2019. [CrossRef]

[41] S. D. Odell, "Desalination in Chile's mining regions: Global drivers and local impacts of a technological fix to hydrosocial conflict," Journal of Cleaner Production, Vol. 323, Article 129104, 2021. [CrossRef]

[42] World Bank Group, "Solar resource maps of Indonesia," SolarGis, 2022. [Online]. Available: https://solargis.com/maps-and-gis-data/download/indonesia

Environ Res Tec, Vol. 6, Issue. 4, pp. 383–390, December 2023

Environmental Research and Technology
https://ert.yildiz.edu.tr - https://dergipark.org.tr/tr/pub/ert
DOI: https://doi.org/10.35208/ert.1334434

Review Article

How body burden from exposure to endocrine disruptors effects accelerated aging?

Eunhye SON[1], Ki Han KWON[*2]

[1]Sungshin Women's University, Seoul, Republic of Korea
[2]College of General Education, Kookmin University, Seoul, Republic of Korea

ARTICLE INFO

Article history
Received: 29 July 2023
Revised: 17 September 2023
Accepted: 03 October 2023

Key words:
Accelerated aging; Aging; Body burden; Chronic disease; Endocrine disruptors

ABSTRACT

This paper reviewed various studies on the effects of endocrine disruptors on human health, focusing on accelerated aging in the younger generation. In particular, we analyzed how the modern lifestyle and ignorance of endocrine disruptors in the younger generation are accelerating aging, and how the concentration of endocrine disruptor exposure in the human body affects the body's burden. Based on existing papers, we conducted a systematic review using Web of Science, Google Scholar, and Scopus to comprehensively investigate and summarize the definition of endocrine disruptors, their effects on hormones, and the physical burden of continuous exposure to endocrine disruptors. Research has shown that persistent exposure to endocrine disruptors disrupts homeostasis in the body and creates oxidative stress that can lead to aging and chronic inflammation. These characteristics were also found to be significant in the observation of telomere length, which is a measure of aging. Therefore, in order to prevent accelerated aging in the younger generation, we can suggest ways to minimize exposure to endocrine disruptors and slow down normal aging in the entire public health, including the 3040s, in the long term.

Cite this article as: Son E, Kwon KH. How body burden from exposure to endocrine disruptors effects accelerated aging? Environ Res Tec 2023;6(4)383–390.

INTRODUCTION

Environmental pollutants typically consist of dozens of environmental chemicals that are harmful to human health. Many of these substances can interact with genetic and epigenetic mechanisms to alter the normal course of development [1]. One particularly harmful environmental factor is endocrine disrupting chemicals (EDCs). EDCs are widespread in the environment we live in. When exposed to EDCs, organisms are highly sensitive to perturbations by substances with hormone-like activity, which negatively affects their development [2, 3]. EDCs have been shown to interfere with endocrine system function, either by suppressing hormone production or by altering the way hormones move through the body, affecting the functions they regulate. Modern humans are exposed to EDCs because most EDCs are persistent or widely used substances in our environment, including synthetic chemicals such as dioxin-like compounds, dioxins, phthalates, polychlorinated biphenyls, pharmaceuticals, pesticides, and heavy metals [2–5]. Endocrine-disrupting chemicals (EDCs) disrupt the synthesis, metabolism, or function of hormones, leading to disturbances in the usual regulatory processes of the body or reproductive functions [6]. In both animal and human studies, early childhood exposure to EDCs has been shown to impede normal development and lead to negative health outcomes such as lifelong tumor development [7, 8]. Some EDCs have also been shown to interfere with epigenome programming [9]. The main focus of this review is on aging caused by EDC exposure. Studies report that continued exposure to EDCs

***Corresponding author.**
*E-mail address: kihan.kwon@kookmin.ac.kr

This paper has been presented at Sixth EurAsia Waste Management Symposium (EWMS 2022)/İstanbul, Türkiye / 24–26 October 2022.

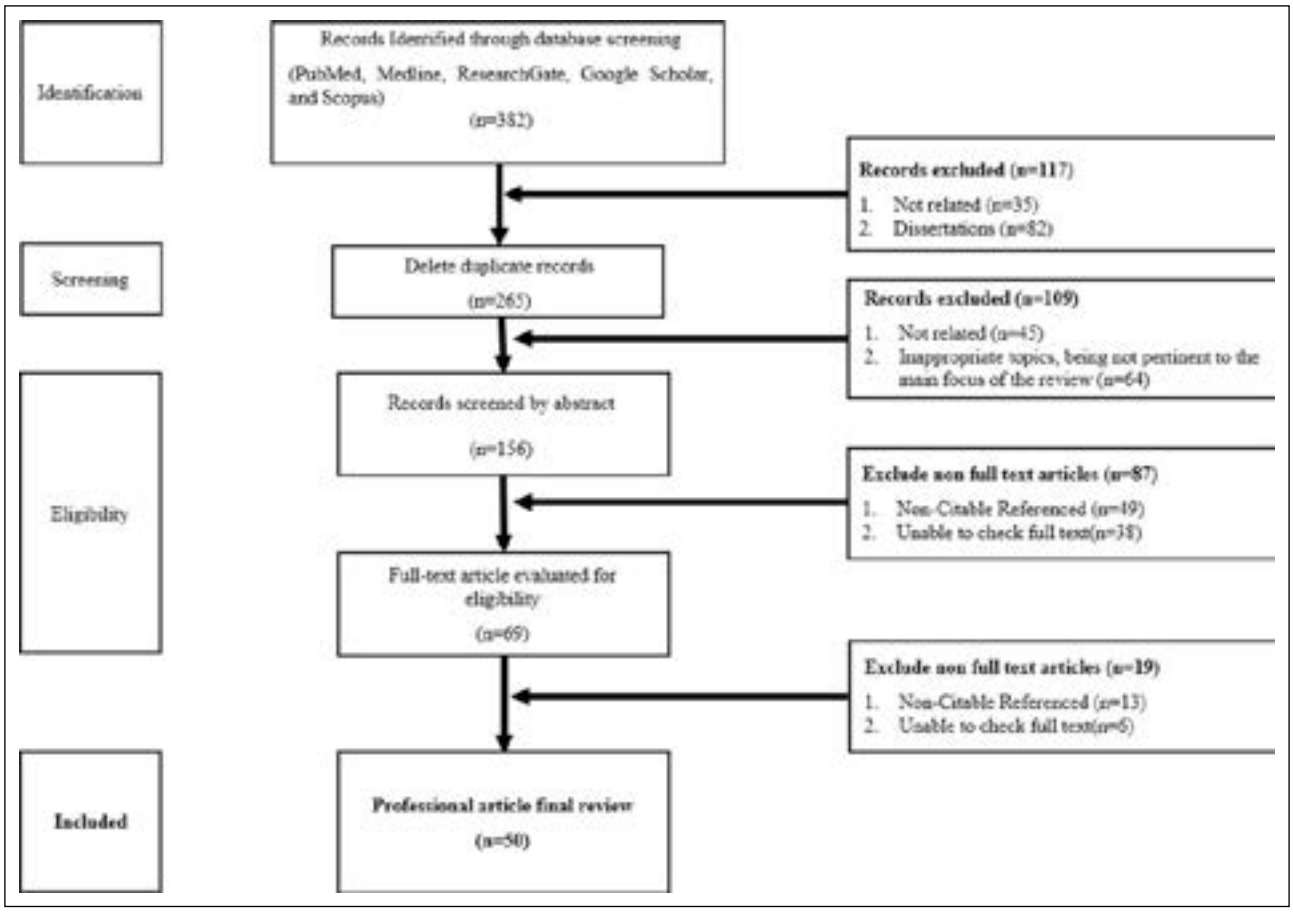

Figure 1. PRISMA flow chart for literature review search results.

may increase the risk of developing chronic diseases associated with aging, including obesity, cardiovascular disease, diabetes, and cancer, as well as several mental and behavioral disorders, such as schizophrenia and mood disorders [10]. Especially in recent years, the prevalence of chronic diseases such as hypertension, diabetes, and obesity has been increasing in the younger age group of 3040. This is associated with accelerated aging. In fact, in people who developed chronic inflammation and disease due to exposure to endocrine disruptors, mRNA levels of markers of aging (GLB1, p16, p21, p53) and inflammation (IL-6, TNF-α) were significantly higher, and telomere length was also shortened. From an epigenetic perspective, the key to the biological conditions that accelerate aging are lifestyle habits that create chronic inflammation and insulin resistance [11]. The purpose of this study is to review how continuous exposure to EDCs contributes to the total amount of EDCs in the body as a body burden. We provide a summary of recent research findings that indicate factors that may accelerate aging, especially in younger generations. We suggest lifestyle choices that may reduce the total amount of EDCs entering the body.

MATERIALS AND METHOD

Noting the increasing exposure to endocrine disruptors in modern society, this review aims to update the current state of research on endocrine disruptors, with a focus on whether they may play a role in accelerating ageing when absorbed by the body and added to the body's burden. Below we describe in detail our search strategy, article selection methods, and data synthesis procedures.

Search Strategy

For this review, we searched six databases in the natural sciences, biology, medicine, and health and wellbeing, following PRISMA flow guidelines: PubMed, Scopus, Medline, ResearchGate and Google Scholar using the keyword sets (a) 'endocrine disruptors' and 'endocrine system organs' (b) 'body burden' (c) 'accelerated ageing' and 'ageing agents' as search terms. Figure 1 is a flowchart showing the process of selecting studies for inclusion in this review.

Eligibility Criteria

Articles included in this review had to meet the eligibility criteria for this review, which included selecting studies related to the following: types of endocrine disruptors, characteristics of endocrine disruptors, endocrine disruptors and body burden, body burden and accelerated ageing, and ageing substances.

Screening and Data Extraction

The following articles were included in the corpus: (1) investigated the association between endocrine disruptors and body burden, (2) included increased body burden and

aging, (3) included post-absorptive properties of endocrine disruptors, (4) included the effects of endocrine disruptors on accelerated aging, (5) were peer-reviewed, and (6) were included in the corpus if they were journal articles or conference presentations.

We excluded articles that (1) did not investigate the nature of endocrine disruptors, (2) did not investigate the association between endocrine disruptors and body burden, or (3) did not investigate the effects of endocrine disruptors on aging.

We considered a range of article types, including original articles, full-text articles, internet articles, summary reports, and series, and did not impose restrictions on publication date or language. Exclusion criteria included inaccessible full text, full text without raw data, inappropriate topics, and doctoral dissertations; these articles were retrieved through the ProQuest Dissertations and Theses Global Database.

Study Selection and Data Extraction

We used a literature review approach. A total of 382 references were selected from the major journal search sites PubMed, Google Scholar, ResearchGate, Medline, and Scopus using the PRISMA flowchart. This resulted in a total of 50 articles that were finally selected. The PRISMA flowchart is shown in Figure 1.

ENDOCRINE DISRUPTORS

The role of the endocrine system is to regulate metabolism through carbohydrates, proteins, and fats to ensure that the body always has the energy it needs. Hormones play an important role in keeping blood sugar levels steady. They also store extra fuel when it's available and mobilize it when needed. Therefore, hormonal changes are dangerous because they can lead to metabolic imbalances [12]. An endocrine disrupting chemical (EDC) is an exogenous substance or mixture of substances that has an adverse effect on an organism's endocrine system. Typically, they act on the receptor to mimic the natural hormone, perturbing the receptor to activate the receptor and cause a response (agonistic effect), or they bind to the receptor and prevent the activation of the natural hormone (antagonistic effect) [13]. Humans and even wildlife are exposed to EDCs that adversely affect biological systems. Many of these substances have been detected in various environmental matrices, including water, sediments, soil, and lipid tissues of animals [14].

Types of Endocrine Disruptors and Routes of Exposure

Endocrine-disrupting chemicals (EDCs) are external compounds that disrupt the equilibrium and control of the body's endocrine system or that of its progeny. These substances typically exhibit chemical durability, resist easy degradation, accumulate within organisms, and exert adverse effects on their descendants [15]. Some EDCs occur naturally - phytoestrogens are an example - but most EDCs are synthetic chemicals that have been released into the environment by anthropogenic human activities with little or no impact or concern for ecosystems and human health. Humans are constantly exposed to chemicals in pesticides, herbicides, industrial and household plastics, detergents and flame retardants, and ingredients in personal care products, both indoors and out. These substances can enter the human body through a variety of routes, including oral, inhalation, and dermal absorption [16].

It describes the origins and endocrine disrupting actions of some of the most common and well-known endocrine disruptors that we are exposed to.

Bisphenol A and phthalates are substances used in the manufacture of plastics. Bisphenol A (BPA) has cross-linking properties and is used to make polycarbonate plastics and epoxy resins, which are now widely used in everyday consumer products such as water bottles, water pipe linings, food and beverage can coatings, thermal paper, and dental sealants [12]. Phthalates and other components utilized in plastics have been identified within human tissues, with these substances being emitted from plastic items [17, 18]. Phthalates serve as primary plasticizers employed to enhance flexibility, clarity, resilience, and lifespan. They find extensive application in the production of consumer goods, encompassing polyvinyl chloride (PVC), a multitude of adhesives, paints, packaging materials, children's toys, electronics, flooring, medical devices, personal care items, air fresheners, food packaging, pharmaceuticals, and textiles. In 2004, the OECD listed phthalates as a mass-produced chemical as a top endocrine disruptor [19, 20].

Polybrominated diphenyl ethers (PBDEs) and polybrominated biphenyls, which are currently detectable in human tissue, are the main ingredients in flame retardants [21]. Serum PBDE levels showed a significant positive correlation with certain thyroid hormones and antibodies, including free triiodothyronine (fT3), total triiodothyronine (tT3), total thyroxine (tT4), and thyroid peroxidase antibodies (TPO-Ab), which provides new evidence for the thyroid disruptive and hepatotoxic effects of PBDEs [22].

4-Nonylphenol is a commonly employed surfactant in both industrial manufacturing and everyday household items, such as detergents and plastics. Additionally, it has been documented to impact female fertility by either mimicking or inhibiting the activity of the estrogen receptor (ER) [23].

Parabens (alkyl esters of p-hydroxybenzoic acid) are used as antimicrobial agents for the preservation of personal care products, food, pharmaceuticals, and paper products. Parabens are widely present in human tissues, including breast tissue, and have estrogenic properties [24].

HOW ENDOCRINE DISRUPTORS AFFECT AGING?

Endocrine Disruptors and Chronic Inflammation

Plasticizers, synthetic compounds, are extensively utilized in various items such as children's toys, food packaging, construction materials, medical equipment, cosmetics, and inks. They have been associated with detrimental impacts

on human thyroid function and the development of allergic diseases. As the prevalence of plasticizer utilization rises, these substances are increasingly detected in the environment, within animals and humans, concurrently with a surge in the presence of plasticizer derivatives, a subgroup of endocrine-disrupting chemicals (EDCs) [25]. Previous studies have shown that the prevalence of allergic diseases has increased rapidly and dramatically in Westernized countries in recent decades and that persistent exposure to EDCs is associated with the development of allergic diseases. Various EDCs are considered to be key factors in the development of chronic inflammatory and allergic diseases across the lifespan, from prenatal to old age. What we've learned from test tube and animal studies is that most EDCs not only cause but also enhance allergic inflammation [26]. The dramatic increase in chronic inflammatory diseases, particularly asthma and allergies, is thought to be linked to the increased consumption of phthalates, which are used in PVC materials and many consumer products. For example, PVC flooring in the home has been implicated as a factor in increasing the risk of asthma and allergic rhinitis [27].

Endocrine-disrupting chemicals (EDCs) have the capacity to disrupt the production of cytokines, immunoglobulins, and inflammatory signaling molecules, thereby modifying the responses of T helper (Th) cells. For instance, the administration of nonylphenol (NP) and 4-octylphenol (OP) inhibits key Th1-associated chemokine IFN-ɣ-inducible protein-10 (IP-10) and Th2-associated chemokine macrophage-derived chemokine (MDC) induced by lipopolysaccharide, implying that EDCs might suppress Th1 responses against intracellular pathogens and Th2 responses to bacterial and parasitic infections. EDCs exert their influence on allergic diseases and inflammation by reshaping Th cell responses, potentially by inducing Th2 polarization through the modulation of antigen-presenting cells (APCs). This hypothesis gains support from observations involving benzophenone, p-octylphenol, and tributyltin chloride, which reduce IL-12 production by splenic APCs, elevate IL-10 levels, and skew the immune response towards the Th2 end of the spectrum. Furthermore, it has been demonstrated that EDC treatment leads to a significant reduction in glutathione levels within APCs, exacerbating airway inflammation [28]. Inflammation is a necessary process for normal tissue self-regulation and reproduction (e.g., implantation and parturition) and can be viewed as a host defense against pathogenic invasion. However, uncontrolled inflammation poses a serious health risk, because unresolved inflammation leads to impaired tissue function and the risk that the affected target tissue will develop cancer in the future. This misregulation of inflammation leads to accelerated aging, chronic disease, and dysfunction of all physiological systems and associated comorbidities [29].

Endocrine Disruptors and Hormones

Chemicals are an inevitable part of everyday life. However some chemicals classified as endocrine disruptors have adverse effects on the body's endocrine system, especially the hormonal system. Hormones, in trace amounts and at precise moments, regulate physical development and growth, reproduction and metabolism, and immunity. Endocrine disruptors in particular disrupt natural hormone systems, so exposure to EDCs can not only have lifelong effects on you, but can also affect the next generation [30].

To summarize the main mechanisms of action by which EDCs cause adverse health effects, they are as follows. (1) binding to hormone receptors to activate signaling pathways, (2) binding to hormone receptors to inhibit signaling pathways, (3) interaction with components of hormone signaling pathways downstream of the receptor, (4) stimulation or (5) inhibition of endogenous hormone biosynthesis, (6) binding to circulating hormone-binding proteins, (7) stimulation or inhibition of hormone-binding protein synthesis or degradation, (8) stimulate or (9) inhibition of hormone receptor expression [31].

EDCs also affect endogenous free active hormone concentrations. This may be associated with aging. EDCs are generally hydrophobic and compete for hormones and transport proteins from hydrophobic hormones (steroids and thyroid hormones) that contribute to aging. In summary, EDCs directly interfere with hormone-binding transport proteins in the body. Many EDCs compete for blood levels of endogenous hormones, and it has been shown that many EDCs interact with steroid hormone-binding protein (SHBG) or α-fetoprotein (AFP), which can interfere with the transport and blood levels of steroid hormones.

EDCs that exert their effects through this mechanism can compete for binding to hormone-binding transport proteins because they are structurally similar to the hormones [32, 33].

Accelerated Aging

Continued exposure to endocrine disruptors also accelerates the aging process. Inflammation and stress are important features of aging. They also cause telomeres to shorten faster. Inflammation and oxidative stress not only affect aging itself, but also contribute to the development of several diseases such as atherosclerosis, hypertension, or diabetes. In general, oxidative stress is caused by the overproduction of reactive oxygen species (ROS). ROS can damage a variety of tissues. The main source of ROS is the mitochondria, and the situation is exacerbated when mutant mitochondria inhibit mitophagy. In this case, pro-inflammatory changes are rapidly magnified [34].

There is ample research showing that endocrine disruptors cause inflammation in our bodies, and it is this inflammation that induces aging between our immune and central nervous systems [35]. This body burden of endocrine disruptors leads to overproduction of reactive oxygen species (ROS). ROS damage cells and create negative changes in macromolecular metabolism. A typical example is the development of aging phenotypes [36]. ROS-induced oxidative stress is also associated with telomere length [37]. Various factors, encompassing genetic, psychosocial, environmental, and behavioral elements, such as DNA damage, psychological stress, dietary habits and obesity, as well as

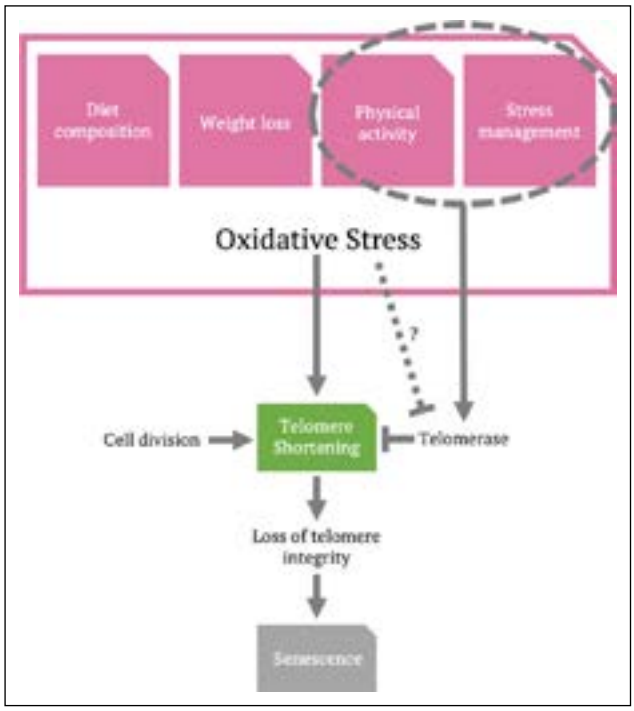

Figure 2. *Accelerated telomere shortening and aging due to endocrine disruptor accumulation. Excessive telomere shortening disrupts the integrity of telomeres, leading to cellular senescence, one of the hallmarks of organismal aging. The accumulation of senescent cells contributes to the loss of tissue homeostasis and the development of age-related pathologies* (Jorge D. Erusalimsky, Oxidative stress, telomeres and cellular senescence: What non-drug interventions might break, 2020).

tobacco smoking, have the potential to expedite the attrition of telomeres, ultimately culminating in premature cell aging and mortality [38] (Fig. 2).

Several cytokine-related effects are observed with aging. Characteristically, levels of anti-inflammatory cytokines decrease and pro-inflammatory cytokines (interleukin-1 (IL-1), IL-6, and tumor necrosis factor alpha (TNF-α)) increase. The combination of these changes and alterations in the innate immune response is called "inflammation." Subclinical inflammation is characterized by altered immune responses resulting from inflammatory diseases. Serum tests of aging subjects show only a slight increase in pro-inflammatory cytokine levels [39]. Inflammation is linked to the consequences of immune aging, implying an inadequate response of adaptive immunity to pathogen exposure and other types of chronic stress in aging subjects [40]. The onset and progression of reproductive aging are predominantly influenced by a combination of genetic and environmental factors. While most research has historically emphasized genetic predisposition, it is increasingly recognized that environmental hormones, particularly endocrine-disrupting chemicals (EDCs), may have a significant impact and potentially accelerate the process of reproductive aging, resulting in a shorter reproductive lifespan. Emerging studies suggest that exposure to EDCs during critical developmental phases, notably during prenatal and early childhood stages, can induce molecular and cellular alterations that ultimately affect the function of affected tissues in later life. This concept is referred to as the fetal/developmental basis of adult disease. Animal research has demonstrated that EDCs such as MXC, BPA, and dioxins can expedite the aging of the reproductive system. Recent epidemiological findings also indicate that exposure to environmental hormones during childhood, including diethylstilbestrol and perfluorocarbons, is associated with an accelerated onset of menopause. Additionally, BPA has been shown to promote oxidative stress and inflammation, potentially increasing the susceptibility of postmenopausal women to age-related health issues [41].

One of the biggest causes of accelerated aging is hidden in everyday life. From an epigenetic perspective, the key to the biological conditions that accelerate aging is a lifestyle that creates chronic inflammation and insulin resistance - a "hedonistic" environment that allows us to take it easy. Examples include a diet of ultra-processed foods, alcohol and tobacco use, lack of exercise, binge-watching TV shows, falling asleep late, and accumulating stress from worrying about an uncertain future. All of these causes of accelerated aging are prevalent in the 3040s and in society today.

Reduced Body Burden from Endocrine Disruptors

The danger of endocrine disrupting chemicals (EDCs), or environmental hormones, is that even at very low concentrations, they disrupt normal hormone action and cause adverse health effects [42]. Due to the pervasive presence of endocrine-disrupting chemicals (EDCs) in various consumer goods such as electronics, construction materials, cosmetics, medical equipment, and food packaging, individuals can encounter inadvertent exposures when these substances are released into the environment [43, 44]. However, public awareness and knowledge of endocrine disruptors is reported to be low. While a variety of studies exist on the risks of EDCs to human health, a qualitative study on the topic found that the majority of participants were unaware of endocrine disruptors. Even those who were aware of some specific endocrine disruptors, such as pesticides and BPA, were found to have poor awareness of the chemicals [45]. Suggestions for developing and implementing effective strategies to prevent exposure to EDCs are needed to prevent the acceleration of age-related health problems that are becoming increasingly prevalent in younger generations [42].

The best way to reduce chemical burden is to reduce EDC concentrations in the body, and the most effective strategy is to use alternative products and foods. Information transfer through counseling, interviews, and interactive education about endocrine disruptors, such as online games, is also needed. Interventions that include self-incentivization, phone calls, or encouragement have generally been shown to reduce EDC concentrations [46]. Dietary interventions to reduce canned foods and other plastic packaging known to contain environmental hormones focus on

using "fresh" organic foods without chemical packaging. We also avoid fast food and delivery as much as possible. When they do need to use containers, they are encouraged to use takeout containers such as stainless steel or glass rather than plastic. The dietary intervention studies that observed these changes all showed significant changes in BPA levels, even though they were designed to target only canned foods [47–49].

Aging has the property of compounding. Once it starts, the problems of aging pile up and get faster and faster. Eat fresh foods to avoid chronic inflammation and stay away from artificial, ultra-processed foods. You should also make it a habit to use natural cosmetics instead of artificial chemicals, and glass and stainless steel instead of plastic to reduce the total amount of endocrine disruptors that enter the body. Lastly, to slow down the rate of aging, we should do at least three sessions a week of moderate to vigorous cardio, strength training, and stretching [50].

CONCLUSION

Environmental exposure to endocrine disruptors is an ongoing threat to reproductive and population health, and should motivate further implementation and refinement of intervention strategies to address persistent exposure to these substances. Accelerated aging is occurring in younger populations, especially due to modernized lifestyles, with the current 3040 generation being the first generation to age faster than their parents. Endocrine disruptors have become unavoidable in personal care products, food and beverages, and indoor environments. The interventions presented in this review offer products and approaches to reduce exposure and body burden, along with awareness of endocrine disruptors, but there is still a dearth of data. Increasing the body of knowledge on the harmful effects of exposure to endocrine disruptors as a contributor to accelerated aging will enable the development of effective and targeted intervention strategies in the future. Novel approaches such as web-based or digital health interventions and educational tools, targeted alternative products, and personalized interactions are useful strategies for future interventions.

DATA AVAILABILITY STATEMENT

The authors confirm that the data that supports the findings of this study are available within the article. Raw data that support the finding of this study are available from the corresponding author, upon reasonable request.

CONFLICT OF INTEREST

The authors declared no potential conflicts of interest with respect to the research, authorship, and/or publication of this article.

ETHICS

There are no ethical issues with the publication of this manuscript.

REFERENCES

[1] V. Bollati, and A. Baccarelli, "Environmental epigenetics," Heredity (Edinb), Vol. 105(1), pp. 105–112, 2010. [CrossRef]

[2] R. L. Wong, and C. L. Walker, "Molecular pathways: environmental estrogens activate nongenomic signaling to developmentally reprogram the epigenome," Clinical Cancer Research, Vol. 19(14), pp. 3732–3737, 2013. [CrossRef]

[3] T. T. Schug, A. Janesick, B. Blumberg, and J. J. Heindel, "Endocrine disrupting chemicals and disease susceptibility," The Journal of Steroid Biochemistry and Molecular Biology, Vol. 127(3-5), pp. 204–215, 2011. [CrossRef]

[4] S. De Coster, and N. van Larebeke, "Endocrine-disrupting chemicals: associated disorders and mechanisms of action," Journal of Environmental and Public Health, Vol. 2012, Article 713696, 2012. [CrossRef]

[5] R. T. Zoeller, T. R. Brown, L. L. Doan, A. C. Gore, N. E. Skakkebaek, A. M. Soto, T. J. Woodruff, and F. S. Vom Saal, "Endocrine-disrupting chemicals and public health protection: a statement of principles from The Endocrine Society," Endocrinology, Vol. 153(9), pp. 4097–4110, 2012. [CrossRef]

[6] S. W. Santosh, "Chapter 3.1.2 - Focus on reproductive health and alterations in women," in Environmental Contaminants and Endocrine Health, 179–200, 2023. [CrossRef]

[7] A. Vaiserman, "Early-life exposure to endocrine disrupting chemicals and later-life health outcomes: An epigenetic bridge?," Aging and Disease, Vol. 5(6), pp. 419–429, 2014.

[8] M. B. Macon, and S. E. Fenton, "Endocrine disruptors and the breast: early life effects and later life disease," Journal of Mammary Gland Biology and Neoplasia, Vol. 18(1), pp. 43–61, 2013. [CrossRef]

[9] A. J. Bernal, and R. L. Jirtle, "Epigenomic disruption: the effects of early developmental exposures," Birth Defects Research Part A: Clinical and Molecular Teratology, Vol. 88(10), pp. 938–944, 2010. [CrossRef]

[10] M. Kundakovic, and F. A. Champagne, "Epigenetic perspective on the developmental effects of bisphenol A," Brain, Behavior, and Immunity, Vol. 25(6), pp. 1084–1093, 2011. [CrossRef]

[11] A. Soundararajan, P. Prabu, V. Mohan, Y. Gibert, and M. Balasubramanyam. "Novel insights of elevated systemic levels of bisphenol-A (BPA) linked to poor glycemic control, accelerated cellular senescence and insulin resistance in patients with type 2 diabetes," Molecular and Cellular Biochemistry, Vol. 458(1-2), pp. 171–183, 2019. [CrossRef]

[12] P. D. Darbre, "Endocrine disruptors and obesity," Current Obesity Reports, Vol. 6(1), pp. 18–27, 2017. [CrossRef]

[13] P. Arslan, S. C. Özeren, and B. Yurdakök Dikmen, "The effects of endocrine disruptors on fish," Environmental Research and Technology, Vol. 4(2), pp. 145–151, 2021. [CrossRef]

[14] O. Kuzukiran, A. Filazi, P. Arslan, B. Yurdakök Dikmen, and U. N. Yazgan Tavşanoğlu, "Determination of persistent organic pollutants in water and sediment samples from Kızılırmak River," Kocatepe Veterinary Journal, Vol. 12(4), pp. 430–436, 2019. [CrossRef]

[15] Z.-R. Tang, X.-L. Xu, S.-. Deng, Z.-X. Lian, and K. Yu, "Oestrogenic endocrine disruptors in the placenta and the fetus," International Journal of Molecular Sciences, Vol. 21(4), Article 1519, 2020. [CrossRef]

[16] P. D. Darbre, "Endocrine disruption and human health," Academic Press, pp. 390, 2015.

[17] S. Basak, M. K. Das, and A. K. Duttaroy, "Plastics derived endocrine-disrupting compounds and their effects on early development," Birth Defects Research, Vol. 112(17), pp. 1308–1325, 2020. [CrossRef]

[18] B. S. Rubin, "Bisphenol A: an endocrine disruptor with widespread exposure and multiple effects," The Journal of Steroid Biochemistry and Molecular Biology, Vol. 127(1-2), pp. 27–34, 2011. [CrossRef]

[19] P. Awasthi, and A. Dobhal, "Endocrine disruptors in food contact materials: A health threat," in Food Marketing Technology, 2021.

[20] P.-C. Huang, S.-H. Liou, I.-K. Ho, H.-C. Chiang, H.-I. Huang, S.-L. Wang, "Phthalates exposure and endocrinal effects: An epidemiological review," Journal of Food and Drug Analysis, Vol. 20(4), pp. 719–733, 2012.

[21] L. Bramwell, S. V. Glinianaia, J. Rankin, M. Rose, A. Fernandes, S. Harrad, T. Pless-Mulolli, "Associations between human exposure to polybrominated diphenyl ether flame retardants via diet and indoor dust, and internal dose: A systematic review," Environment International, Vol. 92-93, pp. 680–694, 2016. [CrossRef]

[22] X. Zhao, X. Yang, Y. Du, R. Li, T. Zhou, Y. Wang, T. Chen, D. Wang, Z. Shi," Polybrominated diphenyl ethers in serum from residents living in a brominated flame retardant production area: Occurrence, influencing factors, and relationships with thyroid and liver function," Environmental Pollution, Vol. 270, Article 116046, 2021. [CrossRef]

[23] F. T. Celino-Brady, C. K. Petro-Sakuma, J. P. Breves, D. T. Lerner, and A. P. Seale, "Early-life exposure to 17β-estradiol and 4-nonylphenol impacts the growth hormone/insulin-like growth-factor system and estrogen receptors in Mozambique tilapia, Oreochromis mossambicus," Aquatic Toxicology, Vol. 217, Article 105336, 2019. [CrossRef]

[24] P. D. Darbre, and P. W. Harvey, "Parabens can enable hallmarks and characteristics of cancer in human breast epithelial cells: a review of the literature with reference to new exposure data and regulatory status," Journal of Applied Toxicology, Vol. 34(9), pp. 925–938, 2014. [CrossRef]

[25] C. Bereketoglu, and A. Pradhan, "Plasticizers: negative impacts on the thyroid hormone system," Environmental Science and Pollution Research, Vol. 29, pp. 38912–38927, 2022. [CrossRef]

[26] C. H. Kuo, S. N. Yang, P.-L. Kuo, C.-H. Hung, "Immunomodulatory effects of environmental endocrine disrupting chemicals," The Kaohsiung Journal of Medical Sciences, Vol. 28(Suppl 7), pp. S37–S42, 2012. [CrossRef]

[27] M. Larsson, L. Hagerhed-Engman, B. Kolarik, P. James, F. C. Lundin, S. Janson, J. Sundell, C. G. Bornehag, "PVC-as flooring material-and its association with incident asthma in a Swedish child cohort study," Indoor Air, Vol. 20(6), pp. 494–501, 2010. [CrossRef]

[28] M.B. Zerdan, S. Moussa, A. Atoui, H. I. Assi, "Mechanisms of Immunotoxicity: Stressors and Evaluators," International Journal of Molecular Sciences, Vol. 22(15), Article 8242, 2021. [CrossRef]

[29] R. R. Dietert, "Misregulated inflammation as an outcome of early-life exposure to endocrine-disrupting chemicals," Reviews on Environmental Health, Vol. 27(2-3), pp. 117–131, 2012. [CrossRef]

[30] C. Monneret, "What is an endocrine disruptor?," Comptes Rendus Biologies, Vol. 340(9-10), pp. 403–405, 2017. [CrossRef]

[31] Y. Combarnous, and T. M. D. Nguyen, "Comparative overview of the mechanisms of action of hormones and endocrine disruptor compounds," Toxics, Vol. 7(1), Article 5, 2019. [CrossRef]

[32] I.A. Sheikh, R.F. Turki, A. M. Abuzenadah, G. A. Damanhouri, M. A. Beg "Endocrine disruption: computational perspectives on human sex hormone-binding globulin and phthalate plasticizers," PLoS One, vol. 11(3), Article e0151444, 2016. [CrossRef]

[33] H. Hong, W.S. Branham, H. W. Ng, C. L. Moland, S. L. Dial, H. Fang, R. Perkins, D. Sheehan, and W. Tong, "Human sex hormone-binding globulin binding affinities of 125 structurally diverse chemicals and comparison with their binding to androgen receptor, estrogen receptor, and alpha-fetoprotein," Toxicological Sciences, Vol. 143(2), pp. 333–348, 2015. [CrossRef]

[34] Y. E. Yegorov, A. V. Poznyak, N. G. Nikiforov, I. A. Sobenin, and A. N. Orekhov, "The link between chronic stress and accelerated aging," Biomedicines, Vol. 8(7), Article 198, 2020. [CrossRef]

[35] S. Salim, "Oxidative stress: a potential link between emotional wellbeing and immune response," Current Opinion in Pharmacology, Vol. 29, pp. 70–76, 2016. [CrossRef]

[36] M. El Assar, J. Angulo, J. A. Carnicero, S. Walter, F. J. García García, E. López-Hernández, J. M. Sánchez-Puelles, "Frailty is associated with lower expression of genes involved in cellular response to stress: Results from the toledo study for healthy aging," Journal of the American Medical Directors Association, Vol. 18(8), pp. 734–737, 2017. [CrossRef]

[37] J. D. Erusalimsky, "Oxidative stress, telomeres and cellular senescence: What non-drug interventions might break the link?," Free Radical Biology and Medicine, Vol. 150, pp. 87–95, 2020. [CrossRef]

[38] R. Rampersaud, G. W. Y. Wu, V. I. Reus, J. Lin, E. H. Blackburn, E. S. Epel, C. M. Hough, S. H. Mellon, and O. M. Wolkowitz, "Shorter telomere length predicts poor antidepressant response and poorer cardiometabolic indices in major depression," Scientific Reports, Vol. 13, Article 10238, 2023. [CrossRef]

[39] T. Fülöp, A. Larbi, and J. M. Witkowski, "Human inflammaging," Gerontology, Vol. 65(5), pp. 495–504, 2019. [CrossRef]

[40] J. J. Goronzy, and C. M. Weyand, "Successful and maladaptive T cell aging," Immunity, Vol. 46(3), pp. 364–378, 2017. [CrossRef]

[41] M. Kumar, D. K. Sarma, S. Shubham, M. Kumawat, V. Verma, A. Prakash, and R. Tiwari, "Environmental endocrine-disrupting chemical exposure: role in non-communicable diseases," Public Health, Vol. 8, Article 553850, 2020. [CrossRef]

[42] J. Park, H. Lee, and S. Lee., "Interventions on reducing exposure to endocrine disrupting chemicals in human health care context: A scoping review," Risk Management and Healthcare Policy, Vol. 15, pp. 779–791, 2022. [CrossRef]

[43] G. Delbes, M. Blázquez, J. I. Fernandino, P. Grigorova, B. F. Hales, C. Metcalfe, L. Navarro-Martín, L. Parent, B. Robaire, A. Rwigemera, G. Van Der Kraak, M. Wade, and V. Marlatt, "Effects of endocrine disrupting chemicals on gonad development: Mechanistic insights from fish and mammals," Environmental Research, Vol. 204, Article 112040, 2022. [CrossRef]

[44] A. Guart, F. Bono-Blay, A. Borrell, and S. LAcorte,"Migration of plasticizersphthalates, bisphenol A and alkylphenols from plastic containers and evaluation of risk," Food Additives & Contaminants: Part A, Vol. 28(5), pp. 676–685, 2011. [CrossRef]

[45] M. Kelly, L. Connolly, and M. Dean, "Public awareness and risk perceptions of endocrine disrupting chemicals: A qualitative study," International Journal of Environmental Research and Public Health, Vol. 17(21), Article 7778, 2020. [CrossRef]

[46] L. Martin, Y. Zhang, O. First, V. Mustieles, R. Dodson, G. Rosa, A. Coburn-Sanderson, C. D. Adams, & C. Messerlian, "Lifestyle interventions to reduce endocrine-disrupting phthalate and phenol exposures among reproductive age men and women: A review and future steps," Environment International, Vol. 170, Article 107576, 2022. [CrossRef]

[47] A. Szybiak, A. Rutkowska, K. Wilczewska, A. Wasik, J. Namieśnik, and D. Rachoń, "Daily diet containing canned products significantly increases serum concentrations of endocrine disruptor bisphenol A in young women Polish Archives of Internal Medicine, Vol. 127(4), pp. 278–280, 2017. [CrossRef]

[48] J. L. Carwile, X. Ye, Zhou X, A. M. Calafat, K. B. Michels, "Canned soup consumption and urinary bisphenol A: a randomized crossover trial," JAMA, Vol. 306(20), pp. 2218–2220, 2011. [CrossRef]

[49] R. A. Rudel, J. M. Gray, C. L. Engel, T. W. Rawsthorne, R. E. Dodson, J. M. Ackerman, J. Rizzo, J. L. Nudelman, and J. G. Brody, "Food packaging and bisphenol A and bis(2-ethyhexyl) phthalate exposure: findings from a dietary intervention," Environmental Health Perspectives, Vol. 119(7), pp. 914–920, 2011. [CrossRef]

[50] T. Hagobian, A. Smouse, M. Streeter, C. Wurst, A. Schaffner, and S. Phelan., "Randomized intervention trial to decrease bisphenol a urine concentrations in women: Pilot study," Journal of Women's Health, Vol. 26(2), pp. 128–132, 2017. [CrossRef]